Journal of the Serbian Chemical Society

*e*Version
*e*lectronic

Available on line at

СХД
1897

www.shd.org.rs/JSCS/

CONTENTS*

* For colored figures in this issue please see electronic version at the Journal Home Page: http://www.shd.org.rs/JSCS/

Theoretical evaluation of pectin therapeutic potential in relation to degree of methylation

JELENA B. MARTINOV NESTOROV[1], GORAN V. JANJIĆ[2]
and MARIJA M. PETKOVIĆ BENAZZOUZ[3]*

[1]*University Clinical Centre of Serbia, Clinic for Gastroenterology and Hepatology, School of Medicine, University of Belgrade, Belgrade, Serbia,* [2]*University of Belgrade – Institute of Chemistry, Technology and Metallurgy, National Institute of the Republic of Serbia, Njegoševa 12, Belgrade, Serbia and* [3]*University of Belgrade – Faculty of Physics, Studentski trg 12–16, Belgrade, Serbia*

Abstract: Pectin is the focus of scientific interest due to both its physicochemical and biochemical properties, as well as its non-toxic nature. Methylation of pectin is a natural process that exists as part of the cell wall defence system against various pathogens. In this study the docking analysis was conducted to predict if methylation o affects the anticancer and antimicrobial properties of pectin and what extent. Four pectin derivatives with varying degrees of methylation and two sets of biomolecules were used. The first set included enzymes responsible for anticancer activity (HMGR, the AGE receptors, tumour protein p53 and oncogenic phosphatase SHP2), while the second set included those for antimicrobial activity (*Salmonella Typhi* TtsA, *Pseudomonas aeruginosa* Earp, *Streptococcus mutans* MetE and *Staphylococcus aureus* Cas9). The results indicated that the degree of methylation does not play a decisive role in the mentioned activities. because all bind to the same sites with similar binding energies. Additionally, it was shown that pectin derivatives have a higher binding affinity towards DNA than towards enzymes. Only the fully methylated derivative exhibited different behaviour, binding to a different binding site in the case of *Streptococcus mutans* MetE.

Keywords: docking study; anticancer properties; antimicrobial properties.

INTRODUCTION

More recently, numerous studies have showed significant health benefits of pectin. Pectin represents soluble dietary fibre, have potential prebiotic, hypoglycemic, hypolipidemic, immunostimulating and anticancer properties.[1] It is believed that part of the positive effect of pectin is due to its influence in modul-

---

137

ating the composition and activity of the intestinal microbiota. Pectin inhibits the growth of pathogenic bacteria and stimulates the growth of beneficial bacteria and act as potential prebiotic.[1–3] Pectin is hydrolysed in colon by intestinal bacteria[3] and most important products of its fermentation are short-chain fatty acids (SCFA). The prebiotic properties of pectin-oligosaccharides (POS) from apple, citrus and sugar beet have been evaluated using fecal fermented cultures and these sugars are able to increase the number of Bifidobacteria and Lactobacillus and reduce the number of Bacteroides and Clostridies.[2] The anti-infective properties of pectin are mainly associated with the improvement of the composition of intestinal microbiota in the colon, inhibiting the adhesion of pathogens to epithelial cells, inhibiting bacterial colonization and binding bacterial toxins.[4] Citrus oligogalacturonides exhibited antibacterial activity and bactericidal effect against selected food pathogens including *S. typhimurium*, *S. aureus*, *L. monocytogenes* and *P. aeruginosa*.[5] Pectin derivatives, prepared by the chemical modification of polysaccharides with natural fatty acids, are promising and effective antimicrobial agents against the two most common food pathogens, *E. coli* and *S. aureus*, which can find further application in the field of food packaging.[6] Pectin is the most promising biocompatible natural anticarcinogenic product, because many *in vitro* and *in vivo* studies have demonstrated that pectin-derived compounds affect cancer progression. It inhibits cell growth and cancerous cell proliferation and promotes apoptosis.[7] Modified pectin, especially citrus pectin, is highly effective in preventing the growth and spread of cancers such as breast and colon cancer. Studies suggest that low molecular weight pectin fragments, rich in galectins, may bind to carbohydrate recognition domains (CRD) on the pro-metastatic protein Gal-3 (galectin-3) and thus inhibits cell-cellular tumour interaction, aggregation of cancer cells with each other and with healthy cells and inhibit metastatic lesions.[8] Pectin derivatives (modified with a maleoyl group) are much more effective than pure or unmodified pectin in inhibiting colon cell cancer growth.[9] The development of foods enriched with pectin might open new avenues regarding the management of colorectal cancer. Pectin has been reported to exhibit antioxidant and anti-inflammatory properties, making it a potentially interesting candidate in the prevention and management of carcinogenesis. In this study, the theoretical impact of pectin esterification (methylation of carboxyl groups) on their antimicrobial and antitumor (anticancer) activity will be predicted through the inhibition of respective biomolecules.

METHODOLOGY

For the purpose of investigating the effect of pectin methylation on its biological activities, four pectin derivatives (Scheme 1) were selected as model compounds, each containing three sugar units (α-1,4-linked D-galacturonic acid). In the first derivative, all three units are D-galacturonic acid (TRIGAL). The other three derivatives have one methylated carboxyl group (1Me-pectin), two methylated groups (13dMe-pectin), or all three groups methylated

(123tMe-pectin). The examined pectin derivatives are negatively charged ($pK_a \approx 3.5$) due to their negatively charged carboxyl groups, except for the fourth derivative (123tMe-pectin), which lacks a carboxyl group as all three groups are esterified, rendering this derivative neutral. The structures of the investigated compounds were optimized at the wb97xd-def2tzvp level of theory.
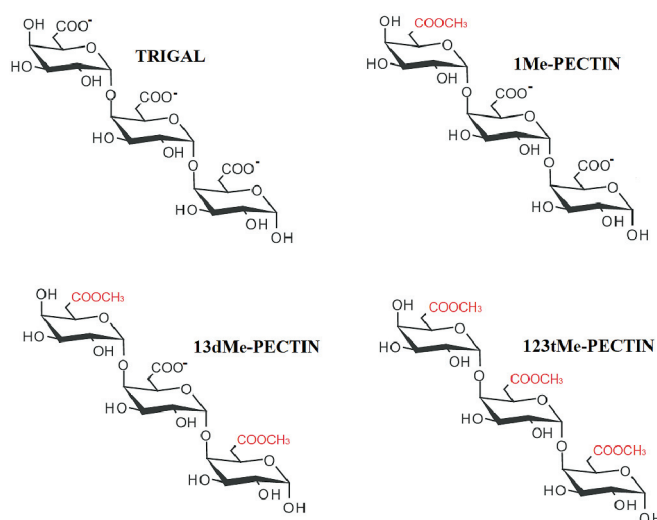
Scheme 1. Illustration of the structures of the investigated pectin derivatives.

The anti-tumour efficacy of pectin derivatives was evaluated *via* docking analyses employing crystallographic structures obtained from the Protein Data Bank (PDB). For these purposes, the structures of encompassing HMG-CoA reductase (HMGR, pdb code: 1DQ8),[10] receptor for the advanced glycation endproducts (RAGE, pdb code: 6XQ1),[11] oncogenic phosphatase SHP2 (pdb code: 5IBS)[12] and human p53 DNA-binding domain (PDB code: 6GGB)[13] were extracted.

To assess antimicrobial potential, docking studies were performed on various enzymes, the crystal structures of which were also retrieved from the PDB. These enzymes include the crystal structures of *Pseudomonas aeruginosa* Earp in complex with TDP (pdb code: 6J7L),[14] *Salmonella typhi* TtsA (pdb code: 6V40),[15] *Staphylococcus aureus* Cas9 (pdb code: 5CZZ),[16] and *Streptococcus mutans* MetE (pdb code: 3T0C).[17]

The structures of ligands (pectin derivatives) and targets were prepared in AutoDockTools program, while the docking calculations were performed in the AutoDock program.[18] A grid box, encompassing the rigid structure of targets, was employed to accommodate the investigated pectin derivatives. The Lamarckian genetic algorithm served as the search method, applying 100 runs for each virtual screening. The analysis and graphical presentation of the docking study results were performed using the Discovery Studio software (BIOVIA Software product).[19]

RESULTS AND DISCUSSION

Pectin is the focus of increasing attention as a potential antioxidant because of its unique physicochemical properties and low toxicity. Pectins have a notable

ability to scavenge free radicals and their efficiency depends on the D-galacturonic acid (GalA) content.[20] In addition to radical mechanisms, it is known that pectins also possess inhibitory capabilities. To ascertain whether esterification (methylation in this case) significantly impacts the inhibitory potential of pectins, the docking studies were conducted on two sets of target proteins. For the first set of targets, the anticancer potential of pectin derivatives was investigated, while for the second set of targets, the antimicrobial activity of the tested pectin derivatives is predicted. The following four enzymes were selected as targets for testing anticancer potential.

Docking study on HMG-CoA reductase (HMGR)

HMGR serves as a catalyst in the initial step of cholesterol biosynthesis, thereby regulating a pivotal factor in cardiovascular diseases. Pectin is used as an agent to mitigate total blood cholesterol levels.[21] Moreover, HMGR inhibitors are explored as potential anticancer agents against malignant neoplasms in women.[22] To ascertain whether the investigated pectin derivatives possess inhibitory potential against HMGR, a docking study was conducted. The natural ligand of the enzyme (coenzyme A) and the drug atorvastatin were employed as control compounds (further detailed in Supplementary material to this paper). Docking results demonstrated that coenzyme A binds to the active sites of enzyme with binding energies of –30.12 kJ/mol (Fig. 1a). Atorvastatin also binds to both active sites, albeit with slightly higher binding energy (–30.96 kJ/mol), affirming its inhibitory activity. None of the four pectin derivatives bind to the active sites but instead occupy a nearby binding pocket, exhibiting similar binding energies (ranging from –30.96 to –31.38 kJ/mol) and significant conformational flexibility. By binding to this adjacent binding pocket, predominantly through hydrogen bonds with Glu559, Gly560, Asn658, Gly756, Leu862 or Ser865 (Fig. S-1 of the Supplementary material), pectin derivative impedes the approach of coenzyme A to the active site, indicative of noncompetitive inhibition. Furthermore, as all four derivatives bind to the same pocket with similar binding energies, it can be inferred that methylation does not influence the inhibitory activity of pectin.

Docking study on AGE receptor (RAGE)

The receptor for the advanced glycation end products (RAGE) is a ubiquitously expressed transmembrane immunoglobulin-like receptor with multiple isoforms, engaging in binding with a diverse array of endogenous extracellular ligands and intracellular effectors. Due to its involvement in various pathological conditions such as cancer, diabetes, cardiovascular diseases and neurodegeneration, RAGE has emerged as an appealing therapeutic target for inhibitors targeting both its extracellular and intracellular domains.[23] The detailed description

of the receptor and its binding sites are provided in the Supplementary material. To ascertain the inhibitory capabilities of the investigated pectin derivatives against the AGE receptor, a docking study was conducted, employing tranilast as a test compound. The receptor structure encompasses only the V and C1 domains from the extracellular portion and docking was performed on both domains. The results of docking revealed that the control compound (tranilast) binds to site 2 located on the V domain (Fig. 1b), with a binding energy of –27.20 kJ/mol. All four investigated pectin derivatives bind to the same binding site (site 3) on the V domain. Their binding to the same site indicates that methylation does not influence the activity of these derivatives. Additionally, besides sharing the same binding site, their binding energies are highly similar (ranging from –21.76 to –22.59 kJ/mol). The binding site of pectin derivatives aligns with that of galacturonic acid, as determined from the docking study.[24] Discrepancies in the binding site between the control compound and pectin derivatives result from the presence of aromatic rings in the control compound, as well as a significantly higher number of donor and acceptor groups for the conventional hydrogen bonding in pectin derivatives. Specifically, tranilast forms classical hydrogen bonds with Lys110 and Asn112, as well as π–aromatic interactions with Ala21, Ala23 and Arg98. Conversely, pectin derivatives predominantly form a larger number of hydrogen bonds in the most stable binding site, involving residues Gln24, Thr27, Glu32, Pro33, Val35 or Tyr118 (Fig. S2). The results of docking suggest the inhibitory capabilities of pectin derivatives, consistent with some previous experimental findings on this subject. It is noteworthy that pectic oligosaccharides from orange peel (OPOs) and pectin polysaccharides from Arabica coffee husks have been reported to exhibit inhibitory capacities against AGEs.[24,25]

Docking results on tumor protein p53

Pectin exhibits anticancer properties, which have been demonstrated to impede tumor development and proliferation across a diverse range of cancer cell types.[26] Notably, modified pectin (MP) shows promise in mitigating the progression and metastasis of colon and breast cancers. Furthermore, beyond its role as a soluble dietary fibre, MP demonstrates beneficial effects on malignancy by activating tumour-suppressor protein p53.[27] This activation subsequently triggers apoptosis pathways and induces cell cycle arrest, contributing to the suppression of tumour progression. The extended description of the structure and function of the tumour protein p53 is provided in the Supplementary material (SM3). The docking results indicate that all four derivatives of pectin bind to the same site (Fig. 1c), which does not correspond to the DNA-binding site. The binding energies are highly similar (ranging from –24.27 to –25.52 kJ/mol), suggesting that methylation does not affect the binding site and thus, the mechanism of enzyme inhibition. All four derivatives bind to the beta-sheet structure of the

enzyme, primarily through hydrogen bonds with amino acid residues. The derivatives predominantly form conventional hydrogen bonds with Phe113, Tyr126 and Asn131. In addition to the conventional and weak hydrogen bonds of the C–H/O type, derivatives also engage in π-aromatic interactions with Arg110 and Trp146 (Fig. S-3 of the Supplementary material). It is evident that a competitive mechanism is not at play and the binding of pectin to the region of the protein with a beta-sheet structure induces conformational changes, resulting in alterations in the conformation of the DNA-binding site (non-competitive mechanism).
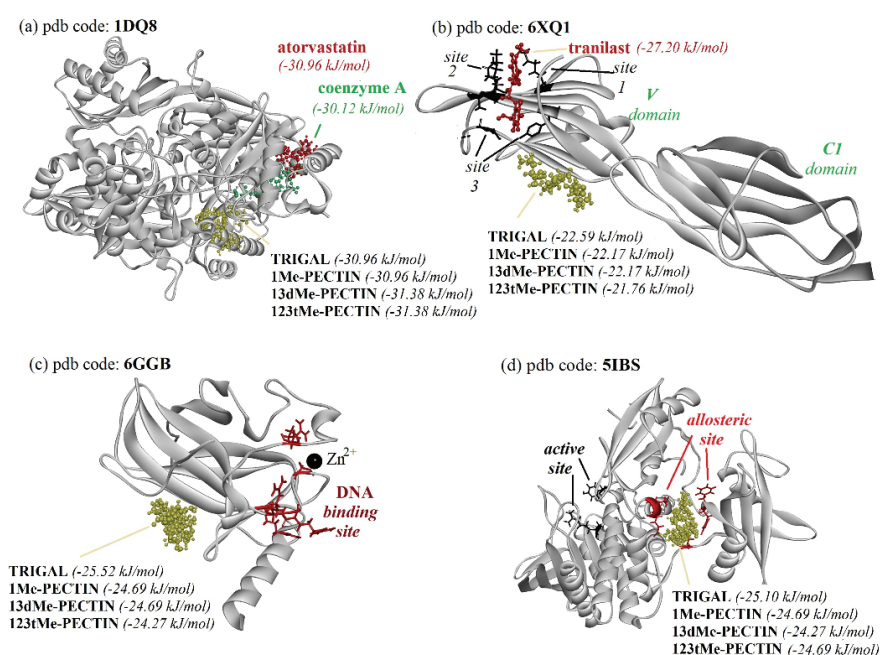
Fig. 1. Binding sites and binding energies of the investigated compounds for HMGR (a), the AGE receptors (b), p53 cancer mutant (c) and oncogenic phosphatase SHP2 (d).

Docking study on the oncogenic phosphatase SHP2

The Src homology 2-containing protein tyrosine phosphatase 2 (SHP2) is a non-receptor protein tyrosine phosphatase widely expressed, predominantly within the cytoplasm of various tissues. Src homology region 2-containing protein tyrosine phosphatase 2 (SHP2) is implicated in breast cancer, leukaemia, lung cancer, liver cancer, gastric cancer, laryngeal cancer, oral cancer and other malignancies.[28] Germline mutations in SHP2 lead to developmental disorders, while somatic mutations are observed in both childhood and adult cancers, contributing to leukaemia in murine models. SHP2 presents as a promising therapeutic target due to its involvement in numerous biological processes. For further details on the structure and function of the protein, refer to Supplementary

material. The docking results indicate non-competitive inhibition, as all four derivatives bind to an allosteric site on SHP2 (Fig. 1d). Binding energies are similar for all four tested compounds, ranging from –24.27 to –25.10 kJ/mol, suggesting that the degree of methylation does not play a significant role in recognition at the binding site on SHP2. The classical hydrogen bonds are responsible for the binding of derivatives to SHP2, although contributions are also made by carbon–hydrogen bonds and hydrophobic interactions. The formation of hydrogen bonds primarily includes Thr108, Glu110, His114, Thr218, Glu 232 and Arg229 (Fig. S-4 of the Supplementary material).

The radical mechanism is present in the protective mechanism of derivatized pectins from apples, citrus fruits and polygalacturonic acid, which reduce the growth of *Escherichia coli* and *Staphylococcus aureus*.[20] However, the antimicrobial action of pectins is not solely achieved through the radical mechanism but also by inhibiting relevant biomolecules. For this purpose, four targets were selected, which play a crucial role in antimicrobial activity.

Docking study on the Salmonella Typhi *TtsA*

S. Typhi TtsA is a protein crucial for secreting typhoid toxin, a virulence factor of *S. Typhi*. TtsA aids in transporting the toxin across the peptidoglycan layer of the bacterial cell wall, essential for its release into the *Salmonella*-containing vacuole.[29] A detailed description of the structure and function of the enzyme is given in the Supplementary material. To determine whether the investigated pectin derivatives possess inhibitory capabilities, a docking study was conducted, in which azithromycin (Supplementary material) was used as the test compound. Azithromycin and pectin derivatives are bound at the same site, between the amino-terminal catalytic domain (1–92) and carboxy-terminal substrate binding domain (93–180) of TtsA (Fig. 2a), forming hydrogen bonds mainly with the N-terminal histidine-epitope (Fig. S-5 of the Supplementary material). Pectin derivatives have higher binding energies (in the range of –30.12 to –30.96 kJ/mol) than azithromycin (–28.87 kJ/mol), which indicates a more pronounced inhibitory potential of derivatives. Stronger binding energies are due to a larger number of hydrogen bonds of pectin derivatives (about 4 bonds, Fig. S-5) than azithromycin (only 1 bond, Fig. S-5).

Docking study of Pseudomonas aeruginosa *Earp*

Protein glycosylation, the most widespread posttranslational modification in nature, significantly influences protein structure and function. Arginine glycosylation was reported as an L-rhamnosylation modification on a specific arginine residue within bacterial translation elongation factor P (EF-P). *P. aeruginosa* EarP may provide a platform for the development of new narrow-spectrum antibacterial agents to combat infections from *P. aeruginosa* and other EarP-con-

taining pathogenic bacteria. A detailed description of the structure and function of the Earp is given in the Supplementary material. Thymidine-5'-diphosphate (TDP) was used as a control compound (the structures of target and TDP were extracted from the crystal structure with the pdb code 6J7L).[30] The control compound is as expected docked on active site (Asp12, Asp16 and Glu272) with high binding energy –37.66 kJ/mol. The findings indicate that all four examined pectin derivatives demonstrate binding affinity to the same site (Fig. 2b), but with significantly lower binding energies (in the range of –28.45 to –28.87 kJ/mol). One can conclude that pectin derivatives possess inhibitory properties and methylation exerts minimal influence on the activity of these derivatives, by binding to this adjacent binding pocket, predominantly through hydrogen bonds with Asn13, Asp16, Thr296 and Lys300 (Fig. S-6 of the Supplementary material).
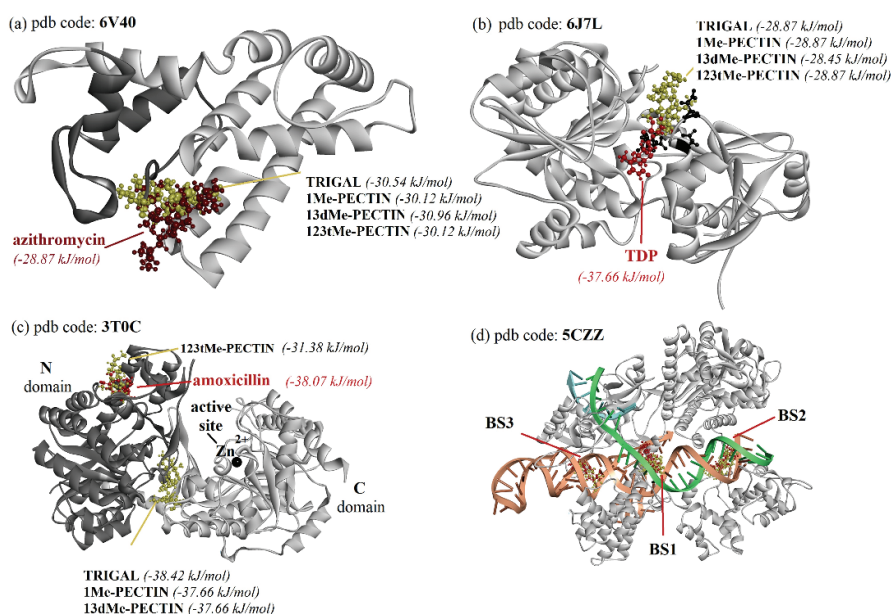
Fig. 2. The binding sites and binding energies of investigated compounds for *Salmonella typhi* TtsA (a), *Pseudomonas aeruginosa* Earp (b), *Streptococcus mutans* MetE (c) and *Staphylococcus aureus* Cas9 (d).

Docking results on Streptococcus mutans *MetE*

S. mutans MetE is an enzyme found in the bacterium *S. mutans*. Specifically, MetE is involved in the biosynthesis of methionine, an essential amino acid. *S. mutans* is primarily known for its role in dental caries (tooth decay) and dental plaque formation. However, it can also cause other oral health issues such as gingivitis and periodontitis when conditions favour its growth and colonization in the oral cavity. Additionally, *S. mutans* has been implicated in infective endo-

carditis, a serious infection of the heart valves, particularly in individuals with underlying heart conditions or compromised immune systems. A detailed description of the structure and function of the MetE is given in the Supplementary material.[31] Amoxicillin (AMX) is one of the most prescribed antibiotics globally, which for the purposes of this study is used as a control compound. Not one molecule from derivatives of neither pectin nor amoxicillin is docked on the active site where Zn is coordinated (Fig. 2c). Amoxicillin was docked for a site located in the N domain, with the binding energy of –38.07 kJ/mol), indicating its allosteric mechanism of inhibition. The 123tMe-PECTIN derivative was bound to the same site, forming hydrogen bonds with Arg43, Phe63, Leu65, Asp71, Il90, Asn131 and Asn132 (Fig. S-7 of the Supplementary material), with a significantly lower binding energy of –31.38 kJ/mol. It is obvious that the binding of these two compounds causes conformational changes in the N-domain, which are transmitted to the C-domain, interfering with the binding of the substrate to the active site. The remaining three pectin derivatives bind near the α-helix that connects two domains, with significantly higher binding energies (in range from –37.66 to –38.49 kJ/mol) compared to the 123tMe-pectin derivative. It is possible that the docked derivatives may act as an allosteric modulator inducing conformational changes that affect enzyme activity. The conventional hydrogen bonds with the Arg287, Asn288, His321 and Asn549 are mainly responsible for the binding of mentioned derivatives (Fig. S-7 of the Supplementary material).

Docking results on Staphylococcus aureus *Cas9*

S. aureus Cas9 (SaCas9) is an RNA-guided endonuclease derived from the bacterium *S. aureus*. The bacterial protein from *S. aureus* is associated with various human infections, including skin and soft tissue infections, pneumonia, bloodstream infections and others.[32] The RNA-guided DNA endonuclease Cas9 cleaves double-stranded DNA targets with a protospacer adjacent motif (PAM) and complementarity to the RNA guide. For the purposes of docking studies, the target structure of *S. aureus* Cas9 in a complex with sgRNA and its DNA targets was selected.[16] The cleavage site in the target DNA strand (the phosphodiester linkage between dC3 and dA4) is distant from the active site of the HNH domain (Asn580) and RuvC domain (Asp10), indicating that the present structure represents the inactive state. Triterpenoids, such as betulinic acid (BA), show promising antimicrobial properties and are a promising candidate for combating biofilm-associated infections.[33] The results of docking studies showed the existence of three binding sites (BS1, BS2 and BS3) of betulinic acid and pectin derivatives (Fig. 2d), with similar binding energies and number of conformations. However, all three places are not located on the enzyme, but in parts representing double helicoidal structures. The first binding site is located close to the cleavage site. All this leads to the conclusion that pectin derivatives and betulinic acid stabilize

the structure of the DNA double helix, thus preventing the DNA cleavage. The binding energy in the cleavage site (BS1) of betulinic acid (–47.70 kJ/mol) is higher than the binding energy of pectin derivatives (in range from –41.84 to –45.19 kJ/mol).

CONCLUSION

The present study investigated whether the esterification of pectin, particularly the methylation of carboxyl groups, affects the inhibitory potential of pectins, with a focus on their antimicrobial and anticancer properties. The results of docking analyses indicate that pectin derivatives exhibit binding affinities to target proteins in some extend especially in microbial infection. The results of calculations have revealed the minimal influence of methylation on chosen target set and mostly in allosteric mechanism of actions. It is also detected that pectin derivatives exhibit more affinity towards DNA compared to enzymes and that may unlock the potential for further investigation and therapeutically application.

SUPPLEMENTARY MATERIAL

Additional data and information are available electronically at the pages of journal website: https://www.shd-pub.org.rs/index.php/JSCS/article/view/12903, or from the corresponding author on request.

И З В О Д

ТЕОРИЈСКА ЕВАЛУАЦИЈА ТЕРАПИЈСКОГ ПОТЕНЦИЈАЛА ПЕКТИНА У ФУНКЦИЈИ СТЕПЕНА МЕТИЛОВАЊА

ЈЕЛЕНА Б. МАРТИНОВ НЕСТОРОВ[1], ГОРАН В. ЈАЊИЋ[2] и МАРИЈА М. ПЕТКОВИЋ БЕНАЗЗОУЗ[3]

[1]Универзитетски клинички ценар Србије, Клиника за гастроентерологију и хепатологију, Медицински факултет Универзитета у Београду, Београд, [2]Универзитета у Београду – Институт за хемију, технологију и металургију, Институт од националног значаја за Републику Србију, Његошева 12, Београд и [3]Универзитет у Београду – Физички факултет, Студентски трг 12–16, Београд

Пектин је у фокусу научних интересовања како због својих физичко-хемијских и биохемијских особина, тако и због своје ниске токсичности. Метиловање пектина је природан процес који постоји као део одбрамбеног система ћелијског зида од напада различитих патогена. У овом раду урађена је докинг студија са циљем да се предвиди да ли метиловање и у ком степену утиче на антиканцерогене и антимикробне особине пектина. Коришћена су 4 деривата пектина са различитим степеном метиловања и два сета биомолекула. У првом сету су ензими одговорни за антиканцерогено дејство (HMG-CoA редуктаза, AGE рецептор, туморни протеин p53, онкогена фосфатаза SHP2) а у другом су ензими одговорни за антимикробно дејство (*Salmonella Typhi* TtsA, *Pseudomonas aeruginosa* Earp, *Streptococcus mutans* MetE и *Staphylococcus aureus* Cas9). Резултати докинга су указали да степен метиловања не игра одлучујућу улогу у поменутим активностима, јер се сва четири деривата везују на иста места са сличним енергијама везивања. Такође, показано је да деривати пектина имају већи афинитет везивања према ДНК него према

ензимима. Једино је потпуно метиловани дериват показао различито понашање, везу-јући се на другом везивном месту у случају *S. mutans* MetE.

REFERENCES

1. A. Dambuza, P. Rungqu, A. Omowunmi Oyedeji, G. Miya, A. Oluwabunmi Oriola, Y. Yiseyon Sunday Hosu, O. Oyehan Oyedeji, *Molecules* **29** (2024) 896 (https://doi.org/10.3390/molecules29040896)
2. N. Koropatkin, E. Cameron, E. Martens, *Nat. Rev. Microbiol.* **10** (2012) 323 (https://doi.org/10.1038/nrmicro2746)
3. K. Shinohara, Z. Ohashi, K. Kawasumi, A. Terada, T. Fujisawa, *Anaerobe* **16** (2010) 410 (https://doi.org/10.1016/j.anaerobe.2010.03.005)
4. R. Ciriminna, A. Fidalgo, F. Meneguzzo, A. Presentato, A. Scurria, D. Nuzzo, R. Alduina, L. M. Ilharco, M. Pagliaro, *ChemMedChem* **15** (2020) 2228 (https://doi.org/10.1002/cmdc.202000518)
5. M. C. Wu, H. C. Li, P. H. Wu, P. H. Huang, Y. T. Wang, *J. Food Sci*. **79** (2014) 1541 (https://doi.org/10.1111/1750-3841.12526)
6. E. Calce, E. Mignogna, V. Bugatti, M. Galdiero, V. Vittoria, S. De Luca, *Int. J. Biol. Macromol*. **68** (2014) 28 (https://doi.org/10.1016/j.ijbiomac.2014.04.011)
7. T. B. Emran, F. Islam, S. Mitra, S. Paul, N. Nat, Z. Khan, R. Das, D. Chandran, R. Sharma, C. M. Gonçalves Lima, A. A. Al Awadh, I. A. Almazni, A. H. Alhasaniah, R. P. F. Guinéet, *Molecules* **27** (2022) 7405 (https://doi.org/10.3390/molecules27217405)
8. V. V. Glinsky, *Carbohydr. Res*. **344** (2009) 1788 (https://doi.org/10.1016/j.carres.2008.08.038)
9. E. A. Almeida, S. P. Facchi, A. F. Martins, S. Nocchi, I. T. A. Schuquel, C. V. Nakamura, A. F. Rubira, E. C. Muniz, *Carbohydr. Polym*. **115** (2015) 139 (https://doi.org/10.1016/j.carbpol.2014.08.085)
10. E. S. Istvan, M. Palnitkar, S. K. Buchanan, J. Deisenhofer, *EMBO J.* **19** (2000) 819 (https://doi.org/10.1093/emboj/19.5.819)
11. N. Kozlyuk, B. A. Gilston, L. E. Salay, R. D. Gogliotti, P. P. Christov, K. Kim, M. Ovee, A. G. Waterson, W. J. Chazin, *Proteins* **89** (2021) 1399 (https://doi.org/10.1002/prot.26162)
12. J. R. LaRochelle, M. Fodor, X. Xu, I. Durzynska, L. Fan, T. Stams, H. M. Chan, M. J. LaMarche, R. Chopra, P. Wang, P. D. Fortin, M. G. Acker, S. C. Blacklow, *Biochemistry* **55** (2016) 2269 (https://doi.org/10.1021/acs.biochem.5b01287)
13. M. R. Bauer, R. N. Jones, R. K. Tareque, B. Springett, F. A. Dingler, L. Verduci, K. J. Patel, A. R. Fersht, A. C. Joerger, J. Spencer, *Future Med. Chem*. **11** (2019) 2491 (https://doi.org/10.4155/fmc-2019-0181)
14. He, N. Liu, F. Li, X. Jia, H. Peng, Y.Liu, Y.Xiao, *J. Bacteriol.* **201** (2019) 1 (https://doi.org/10.1128%2FJB.00128-19)
15. T. Geiger, M. Lara-Tejero, Y. Xiong, J. E. Galán, *eLife* **9** (2020) e53473 (https://doi.org/10.7554/eLife.53473)
16. H. Nishimasu, L. Cong, W. X. Yan, F. A. Ran, B. Zetsche, Y.Li, A.Kurabayashi, R. Ishitani, F. Zhang, O. Nureki, *Cell* **162** (2015) 1113 (https://doi.org/10.1016/j.cell.2015.08.007)
17. T.-M. Fu, J. Almqvist, Y.-H. Liang, L. Li, Y. Huang, X.-D- Su, *J. Mol. Biol.* **412** (2011) 688 (https://doi.org/10.1016/j.jmb.2011.08.005)

18. G. M. Morris, R. Huey, W. Lindstrom, M. F. Sanner, R. K. Belew, D. S. Goodsell, A. J. Olson, *J. Comput. Chem.* **30** (2009) 2785 (https://doi.org/10.1002/jcc.21256)
19. D. Biovia, H. Berman, J. Westbrook, Z. Feng, G. Gilliland, T. Bhat, T. J. T. J. o. C. P. Richmond, *Dassault Systèmes BIOVIA, Discovery Studio Visualizer, v. 17.2.0.16349*, Dassault Systèmes, San Diego, CA, 2016, 10 (2000) 0021-9991
20. J. Martinov, M. Krstić, S. Spasić, S. Miletić, J. Stefanović-Kojić, A. Nikolić-Kokić, D. Blagojević, I. Spasojević, M. B. Spasić, *Food Res. Int.* **100** (2017) 132 (https://doi.org/10.1016/j.foodres.2017.08.040)
21. H. S. Park, J. S. Choi, K. H. Kim, *Nutr. Res.* **20** (2000) 1783 (https://doi.org/10.1016/S0271-5317(00)00269-4)
22. A. Markowska, M. Antoszczak, J. Markowska, A. Huczyński, *Pharmaceuticals* **13** (2020) 422 (https://doi.org/10.3390/ph13120422)
23. S. Bongarzone, V. Savickas, F. Luzi, A. D. Gee, *J. Med. Chem.* **60** (2017) 7213 (https://doi.org/10.1021/acs.jmedchem.7b00058)
24. Z. Li, B. Zhou, T. Zheng, C. Zhao, Y. Gao, W. Wu, Y. Fan, X. Wang, M. Qiu, J. Fan, *Foods* **12** (2023) 423 (https://doi.org/10.3390/foods12020423)
25. H. Yan, X. Zhang, L. Yang, Y. Shen, L. Liu, *Food Chem.* **398** (2023) 133886 (https://doi.org/10.1016/j.foodchem.2022.133886)
26. T. B. Emran, F. Islam, S. Mitra, S. Paul, N. Nath, Z. Khan, R. Das, D. Chandran, R. Sharma, C. M. G. Lima, A. A. Al Awadh, I. A. Almazni, A. H. Alhasaniah, R. P. F. Guiné, *Molecules* **27** (2022) 7405 (https://doi.org/10.3390/molecules27217405)
27. L. Delphi, H. Sepehri, *Biomed. Pharmacother.* **84** (2016) 637 (https://doi.org/10.1016/j.biopha.2016.09.080)
28. J. Zhang, F. Zhang, R. Niua, *J. Cell. Mol. Med.* **19** (2015) 2075 (https://doi.org/10.1111/jcmm.12618)
29. J. P. Skittrall, D. Levy, C. Obichukwu, A.Gentle , M. A. Chattaway , D. Hayns , C. Etheridge, C. M. Parry, V. Wong, J. Whitehorn, *Clin. Infect. Pract.* **10** (2021) 100069 (https://doi.org/10.1016/j.clinpr.2021.100069)
30. C. He, N. Liu, F. Li, X. Jia, H. Peng, Y. Liu, Y. Xiao, *J. Bacteriol.* **201** (2019) (https://doi.org/10.1128/JB.00128-19)
31. T.-M. Fu, J. Almqvist, Y.-H. Liang, L. Li, Y. Huang, X. D. Su, *J. Mol. Biol.* **412** (2011) 688 (https://doi.org/10.1016/j.jmb.2011.08.005)
32. W. Chen, Y. Zhang, W.S. Yeo, T. Bae, Q. Ji, *J. Am. Chem. Soc.* **139** (2017) 3790 (https://doi.org/10.1021/jacs.6b13317)
33. G. Hamion, W. Aucher, A. Mercier, F. Tewes, M. Menard, J. Bertaux, M. Girardot, C. Imbert, *Int. J. Antimicrob. Agents* **63** (2024) 107166 (https://doi.org/10.1016/j.ijantimicag.2024.107166).

Journal of the Serbian Chemical Society

Theoretical evaluation of pectin therapeutic potential in relation to degree of methylation

JELENA B. MARTINOV NESTOROV[1], GORAN V. JANJIĆ[2]
and MARIJA M. PETKOVIĆ BENAZZOUZ[3]∗

[1]*University Clinical Centre of Serbia, Clinic for Gastroenterology and Hepatology, School of Medicine, University of Belgrade, Belgrade, Serbia,* [2]*University of Belgrade – Institute of Chemistry, Technology and Metallurgy, National Institute of the Republic of Serbia, Njegoševa 12, Belgrade, Serbia and* [3]*University of Belgrade – Faculty of Physics, Studentski trg 12–16, Belgrade, Serbia*

SM1. DOCKING STUDY ON HMG-COA REDUCTASE

Coenzyme A, serving as the control compound, was tested in its neutral state, considering its neutrality under gastrointestinal tract conditions ($pKa_1 = 4.0$ (adenine NH_3^+) and $pKa_2 = 9.6$ (thiol)). The pH gradient in the gastrointestinal tract gradually rises from pH 6 in the small intestine to approximately pH 7.4 in the terminal ileum. Subsequently, the pH decreases to 5.7 in the caecum, followed by a gradual increase to pH 6.7 in the rectum. The dissolved pectin exhibits a negative charge at neutral pH, approaching neutrality at low pH, with a pKa value of approximately 3.5. Atorvastatin, belonging to the class of medications known as HMG-CoA reductase inhibitors (statins), functions by inhibiting the synthesis of cholesterol in the body, thereby reducing the accumulation of cholesterol on arterial walls and mitigating the risk of arterial blockage, particularly in vital organs such as the heart and brain. In the gastrointestinal tract, atorvastatin bears a negative charge due to its pKa value of 4.46.

∗ Corresponding author. E-mail: marijapetkovic@ff.bg.ac.rs

Coenzyme A

Atorvastatin
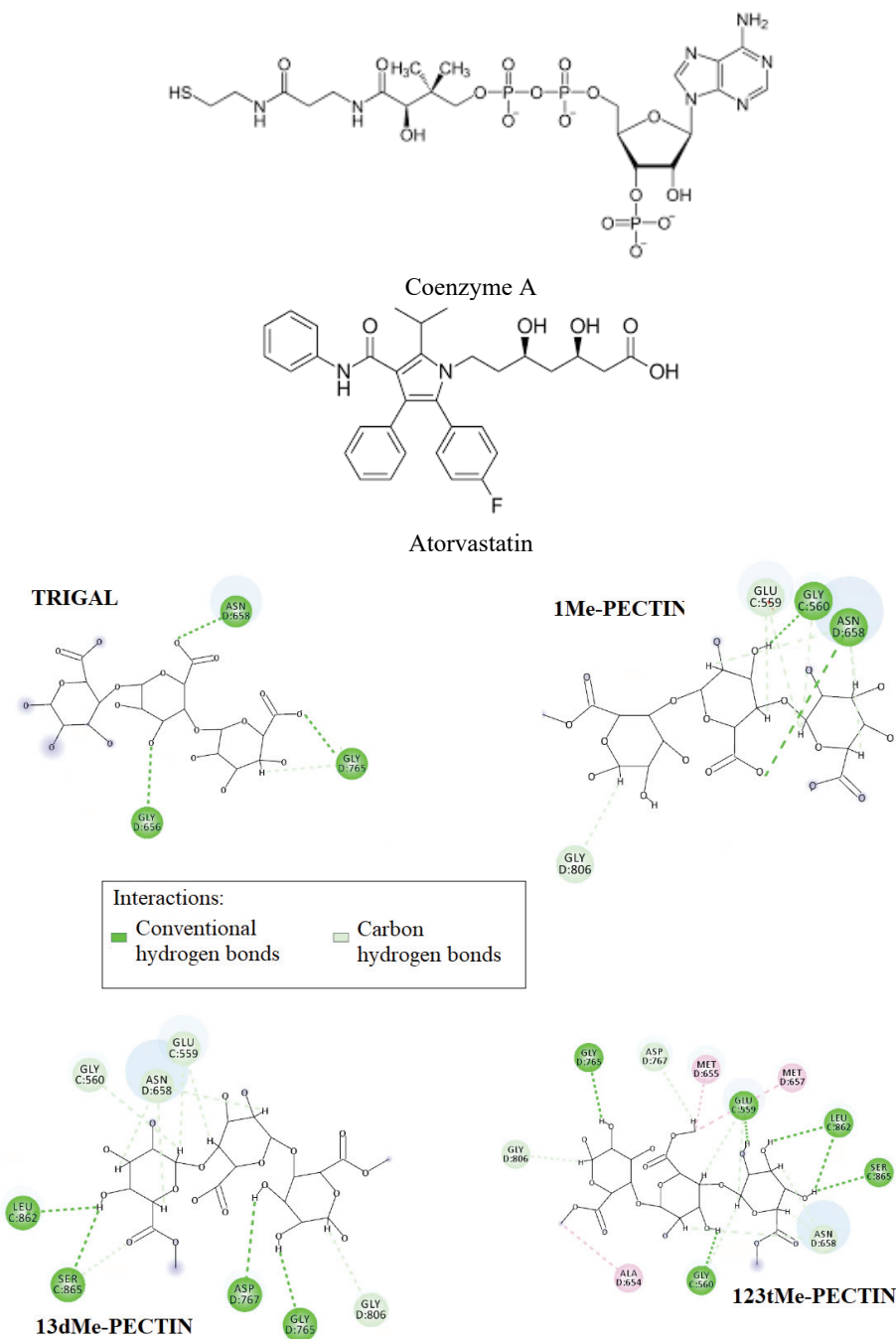
Fig. S-1. Amino acid environment of the investigated pectin derivatives for HMG-CoA Reductase, in the binding site with the highest binding energy.

SM2. DOCKING STUDY ON AGE RECEPTORS (RAGE)

The binding of ligands to the extracellular domain of RAGE initiates a multifaceted intracellular signalling cascade, triggering the generation of reactive oxygen species (ROS), immunoinflammatory responses, cellular proliferation, or apoptosis, along with the upregulation of RAGE itself. Human RAGE is composed of three main domains: an extracellular region (residues 23–342), a hydrophobic transmembrane region (residues 343–363) and a cytoplasmic region (residues 364–404). The extracellular structure of RAGE comprises three immunoglobulin-like domains: a variable (V) domain (residues 23–116) and two constant C1 (residues 124–221) and C2 (residues 227–317) domains. Within the V domain, eight strands (A′, B, C, C′, D, E, F and G) are connected by six loops, forming two β-sheets linked by a disulfide bridge between *Cys38* and *Cys99*.[23] Specifically, residues showing chemical shift perturbations (CSPs) in the V domain correspond to crucial residues in the binding surface, such as *Glu50, Ly52, Arg98, Gln100, Ala101, Lys110 and Asn112* (which are key ligand interaction residues for sites 1 and 2). The further analysis of this structure has revealed details about the interactions in a newly identified "site 3," including a strong interaction with *Lys39* and an additional contact with *Tyr113*. These residues are of particular interest, as some initial hit fragments caused CSPs in these residues, suggesting their potential as starting points for incorporating the new site 3 into future inhibitor designs.[SM1] Tranilast, anti-allergic drug molecule that significantly inhibits the binding interactions of V-domain of RAGE, was used as a control compound.
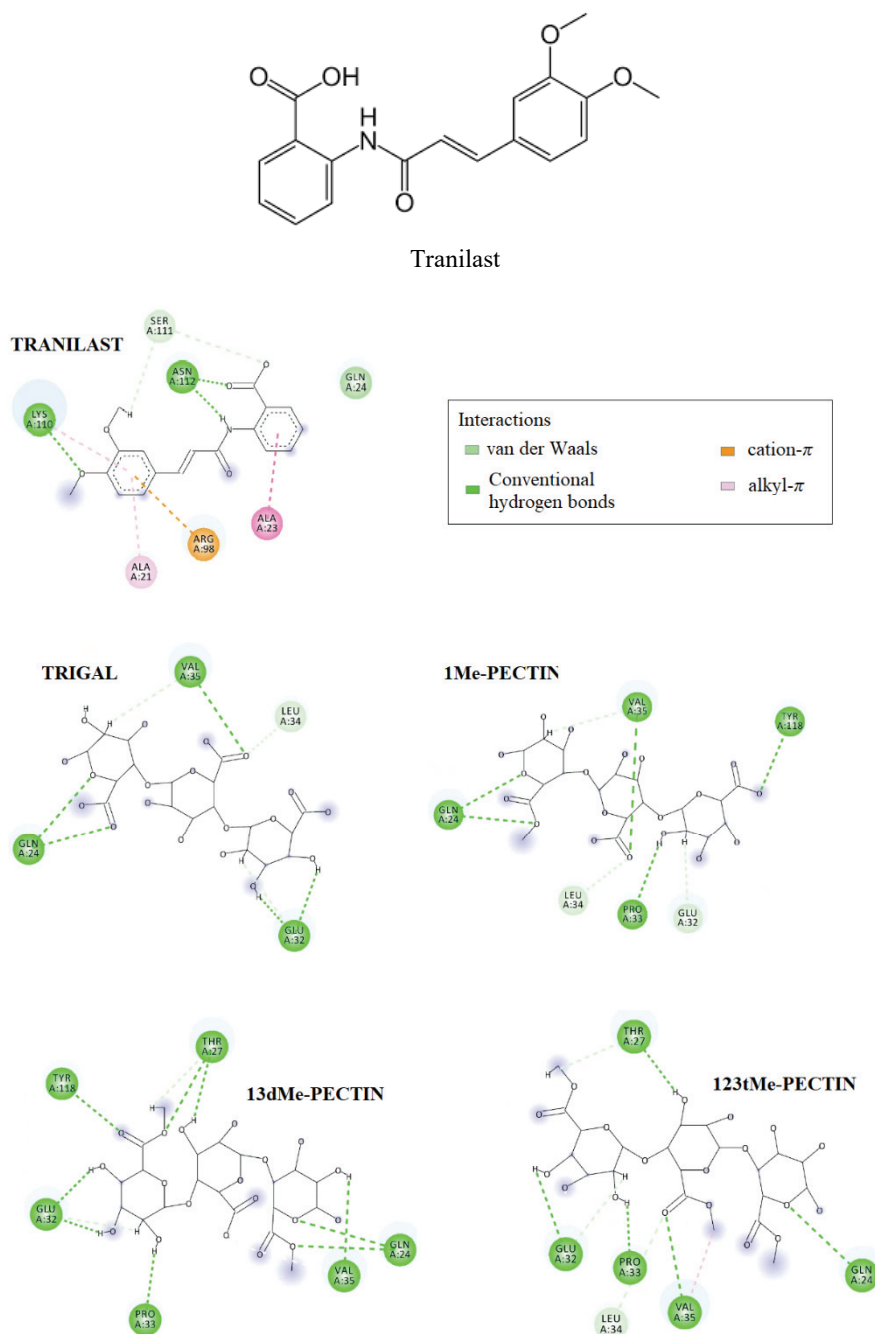
Tranilast

Fig. S-2. Amino acid environment of drug tranilast and the investigated pectin derivatives for the AGE receptors (RAGE), in the binding site with the highest binding energy.

SM3. DOCKING STUDY ON TUMOR PROTEIN P53

The p53 tumour suppressor gene plays a pivotal role in triggering apoptosis and is commonly known as the guardian of the genome.[SM1] In approximately half of human cancers, the mutations in the p53 tumour suppressor gene are observed, often manifesting as missense substitutions in its core domain, specifically the DNA-binding core domain (CD) (residues 94–312). The p53-Y220C mutant serves as a notable model for developing drugs intended to stabilize mutant p53 proteins.[SM1] Mutations affecting DNA contacts within the core DNA-binding domain can result in the loss of function of the p53 tumour suppressor protein. Nevertheless, this functionality can be reinstated through second-site suppressor or rescue mutations.[SM2] Six residues within p53 are identified as the hotspots for tumorigenic mutations, all localized within the DNA-binding substructure. These mutations may disrupt DNA contacts or induce structural alterations, leading to local conformational instability or global denaturation. Four "structural" hotspots (*Arg175, Gly245, Arg249 and Arg282*) predominantly exhibit a single substitution, while two "DNA-contact" hotspots, *Arg248* and *Arg273*, are distinguished.[SM3]
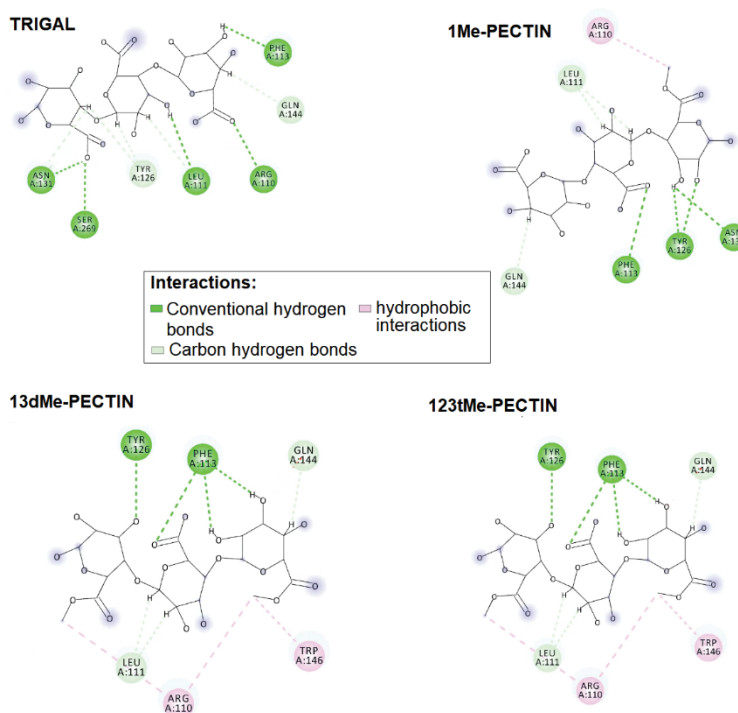
Fig. S-3. Amino acid environment of investigated pectin derivatives for the p53 cancer mutant, in the binding site with the highest binding energy.

SM4. DOCKING STUDY ON THE ONCOGENIC PHOSPHATASE SHP2

SHP2 is a 68 kDa protein comprising 593 amino acid residues, which include two tandem SH2 domains (N-SH2 and C-SH2) spanning residues 1–120, a catalytic protein tyrosine phosphatase domain (PTP domain residues 237-525) and a disordered C-terminal tail (residues 526–593) containing phosphorylation sites at *Tyr542* and *Tyr580*.[SM4] In its inactive state, SHP2 is autoinhibited by residues located on the catalytic surface of the PTP domain and the N-SH2 domain, thereby suppressing the protein's activity and restricting substrate access to its catalytic site. Activation by growth factors induces intramolecular "dissociation" upon phosphopeptide binding, releasing the N-SH2 domain from the PTP domain. In the case of catalytic site obstruction, the N-terminal SH2 domain promptly obstructs its active site.

Traditionally, the inhibition of SHP2 catalytic activity would necessitate targeting the PTP domain. Historically, various selective SHP2 inhibitors have been investigated in the context of leukemia-associated SHP2 mutants; however, many of these compounds still face challenges related to low bioavailability or permeability.[SM5] Targeting the PTP active site requires the development of highly selective molecules and efforts to discover compounds with specific binding to this site are ongoing. Moreover, the positively charged environment of the PTP catalytic pocket poses unique challenges for drug discovery, as most catalytic site inhibitors require multiple ionizable functional groups to inhibit the enzyme. The key residues within the PTP catalytic cleft include *Cys459*, serving as the catalytic nucleophile; *Arg465*, contributing to the "phosphate binding cradle"; and *Asp425*, acting as the general acid in catalysis.[SM5]

Fig. S-4. Amino acid environment of the investigated pectin derivatives for the Oncogenic Phosphatase SHP2, at the binding site with the highest binding energy.

SM5. DOCKING STUDY ON THE *SALMONELLA TYPHI* TTSA

Salmonella Typhi TtsA -This enzyme, represented by PDB code 6V40 with four chains (A, B, C, D), exhibits muramidase activity vital for traversing the peptidoglycan layer. Muramidases like TtsA catalyze the hydrolysis of bonds in peptidoglycan, facilitating the passage of toxin-containing vesicles through the cell wall and contributing to bacterial cell lysis. The enzyme contains from 4 chains A, B, C, D. In the protein's structure, the amino terminal domain hosts the lysozyme-like catalytic triad positioned beneath a 'flap' structure formed by a loop. This loop is tethered to the domain through interactions with three short helices. Conversely, the carboxy-terminal substrate-binding domain comprises six anti-parallel α-helices that assemble into a helix bundle arrangement. This helix bundle serves as a scaffold for a platform housing a central groove, which, in conjunction with the catalytic triad-containing flap, adopts a ring-like

configuration. For the purposes of the docking study, only A chain was taken as the target.

Presently, ceftriaxone, ciprofloxacin and azithromycin have garnered recommendation as primary antibiotics for the clinical management of Salmonella infection, particularly those precipitated by S. Typhimurium.[SM6] Azithromycin [9-deoxo-9a-aza-9a-methyl-9a-homoerythromycin] is a part of the azalide subclass of macrolides. Azithromycin functions by impeding bacterial proliferation, thereby augmenting the host immune response against infection.

Azithromycin

This pharmaceutical agent is frequently prescribed to address an assortment of bacterial afflictions,[SM6] including but not limited to respiratory conditions such as bronchitis, pneumonia and sinusitis. Additionally, azithromycin finds its use in treating certain sexually transmitted infections (STIs) such as chlamydia and gonorrhoea, alongside other bacterial infections like dermatological and otological conditions.[SM6]
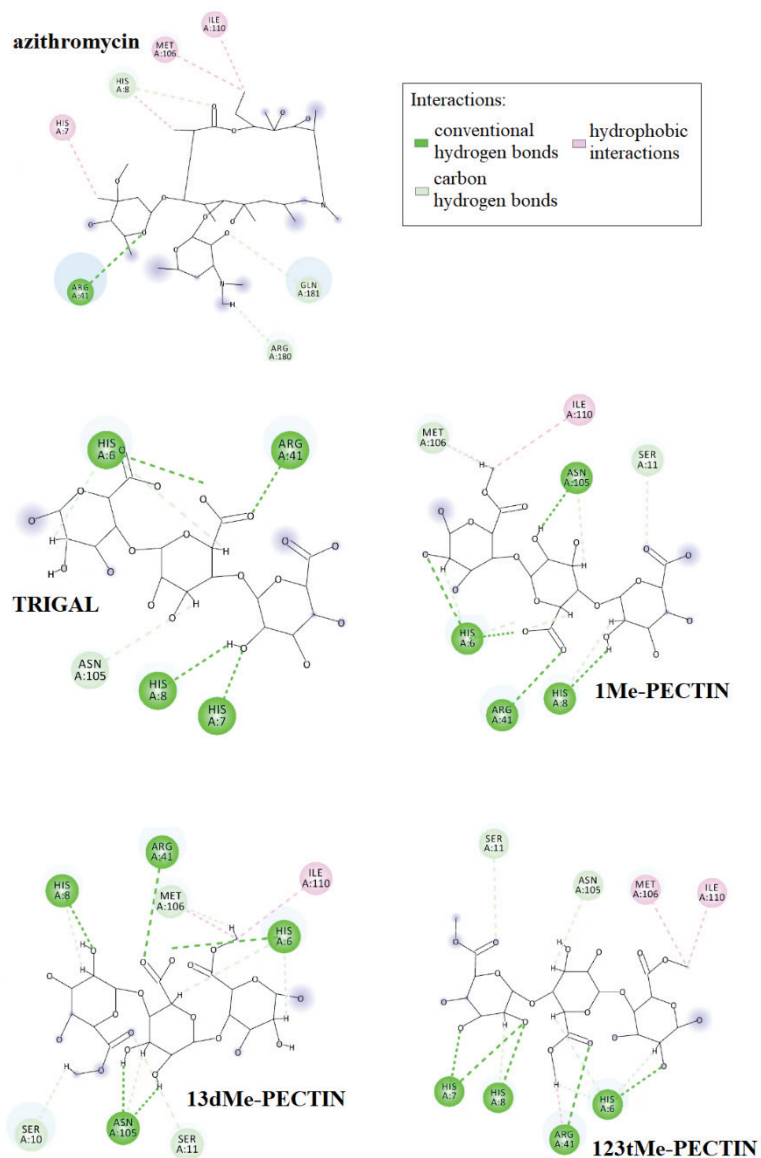
Figure S-5. Amino acid environment of the investigated pectin derivatives for *Salmonella Typhi* TtsA, at the binding site with the highest binding energy.

SM6. DOCKING STUDY OF *Pseudomonas aeruginosa* EARP

Protein glycosylation, the most widespread posttranslational modification in nature, significantly influences the protein structure and function. Initially thought to be exclusive to eukaryotes, it's now evident that bacteria, including

pathogens, possess both O- and N-linked glycosylation pathways, exhibiting similarities and unexpected variations compared to their eukaryotic counterparts.[SM7] N-linked protein glycosylation typically targets Asn residues within Asn-X-Ser/Thr sequences, with X representing any amino acid except proline. Notably, the type III secretion effector NleB from attaching/effacing pathogens has been found to catalyse rare N-glycosylation of arginine residues on host proteins with N-acetylglucosamine (GlcNAc), thereby inhibiting antibacterial and inflammatory host responses. Pseudomonas aeruginosa EarP exhibits a distinctive structure consisting of two Rossmann-like domains separated by a deep cleft. The N-terminal domain (NTD features a four-stranded parallel β-sheet at its core flanked by α-hairpins, surrounded by helices.[SM7] Contrary to that, the C-terminal domain (CTD) comprises a five-stranded parallel β-sheet with an antiparallel strand on one side, encircled by helices. The interdomain contacts are maintained by a C-terminal helix extending from the CTD and connecting loops between the domains. The active site is located in a cavity in the cleft between the NTD and the CTD (Figure 1B). TDP-Rha" stands for "thymidine diphosphate-L-rhamnose." It is a nucleotide sugar molecule consisting of thymidine diphosphate (TDP) bound to L-rhamnose. TDP-Rha serves as a substrate in various biological processes, particularly in glycosylation reactions, where the rhamnose moiety is transferred to acceptor molecules, such as proteins, lipids, or other carbohydrates, by glycosyltransferase enzymes.[SM7] This modification plays critical roles in various cellular functions, including cell wall biosynthesis, protein glycosylation and the biosynthesis of secondary metabolites. The docking study was obtained using crystal structure of Pseudomonas aeruginosa Earp (pdb code: 6J7L). For the control compound we docked the cleared enzyme with thymidine-5'-diphosphate (TDP).
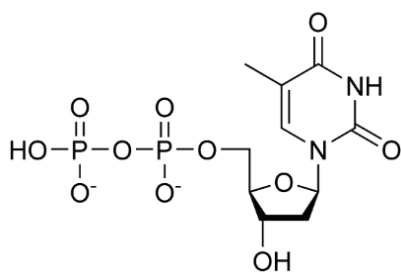
thymidine-5'-diphosphate (TDP)
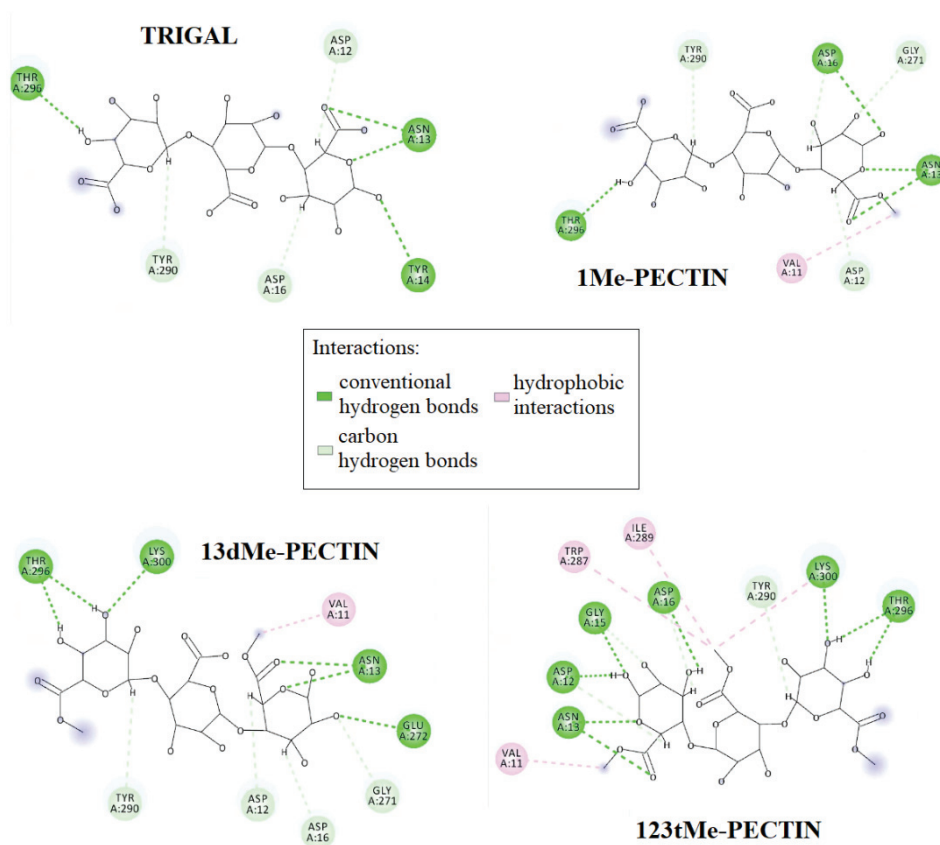
Figure S-6. Amino acid environment of the investigated pectin derivatives for *Pseudomonas aeruginosa* Earp, at the binding site with the highest binding energy.

SM7. DOCKING RESULTS ON *Streptococcus mutans* MetE

Streptococcus mutans MetE is an enzyme found in the bacterium *Streptococcus mutans*. Specifically, MetE is involved in the biosynthesis of

methionine, an essential amino acid. In S. mutans, methionine biosynthesis is crucial for various cellular processes, including protein synthesis and metabolism.[SM7] *S. mutans* is primarily known for its role in dental caries (tooth decay) and dental plaque formation. However, it can also cause other oral health issues such as gingivitis and periodontitis when conditions favour its growth and colonization in the oral cavity. Additionally, *S. mutans* has been implicated in infective endocarditis, a serious infection of the heart valves, particularly in individuals with underlying heart conditions or compromised immune systems. MetE has two domains, N and C, The N-domain is made up of residues 1–359, while the C-domain contains residues 398–745. each folded into (βα)8 barrels, joined by a helix linker. The active site, housing a zinc atom, lies at their interface. The two domains are positioned with the two barrels facing each other in a head-to-head alignment. A deep groove is formed with the active site of MetE at the domain interface. The deep groove between the two domains also provides a solvent-accessible path leading to the active site. The zinc atom is situated at the active site (Figure 1) and regulates enzyme function and can impact cellular processes. Amoxicillin (AMX) is one of the most prescribed antibiotics globally. The high absorption rate of AMX into the bloodstream reduces side effects and increases serum concentrations, making it desirable as an oral treatment.
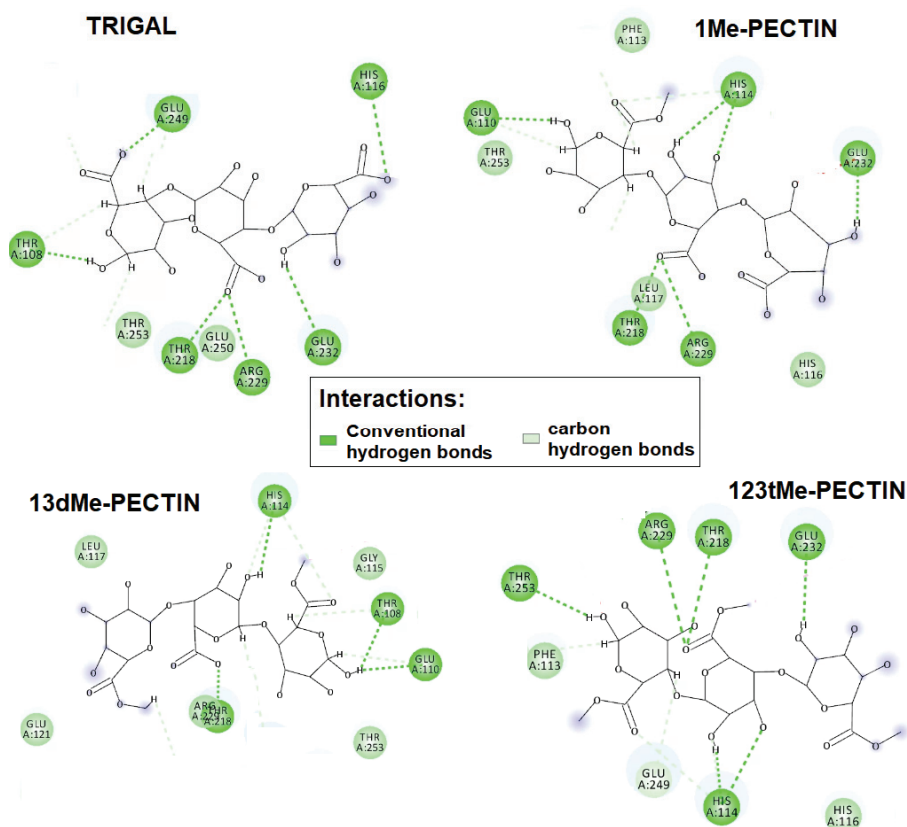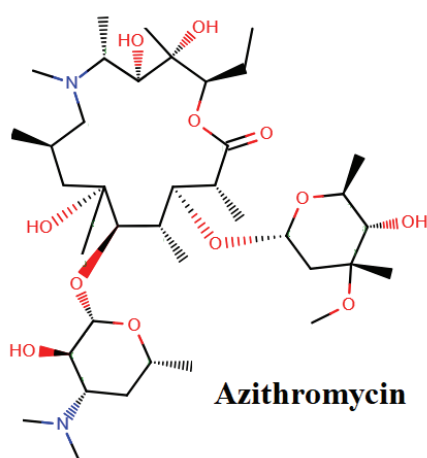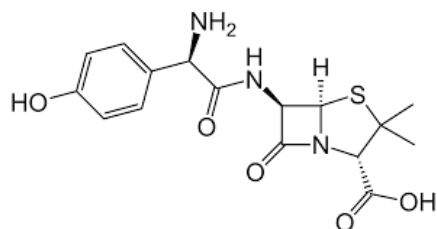
Amoxicillin
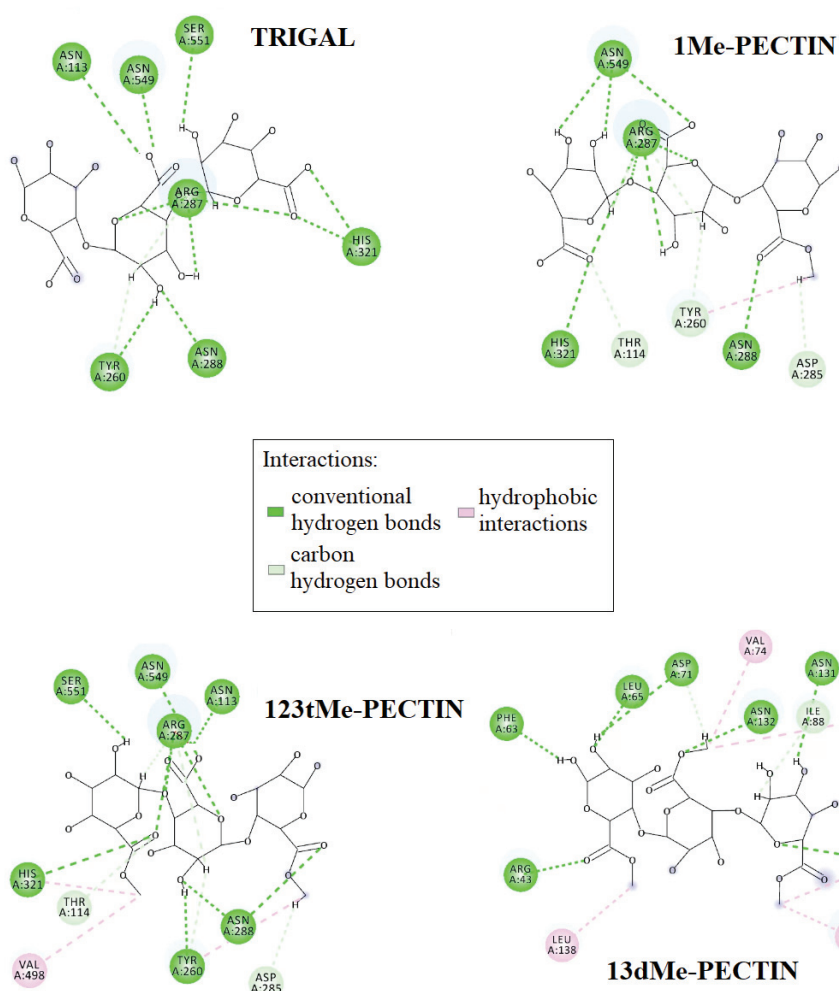
Figure S-7. Amino acid environment of the investigated pectin derivatives for *Streptococcus mutans* MetE, at the binding site with the highest binding energy.

REFERENCES

SM1. M. C. N. Picot-Allain, V. S. Neergheen, *Heliyon* **9** (2023) e22236 (https://doi.org/10.1016/j.heliyon.2023.e22236)

SM2. B. Kamaraj, A. Bogaerts, *PLoS One* **10** (2015) e0134638 (https://doi.org/10.1371/journal.pone.0134638)

SM3. A. N. Bullock, J. Henckel, A. R. Fersht, *Oncogene* **19** (2000) 1245 (https://doi.org/10.1038/sj.onc.1203434)

SM4. D. Bajia, K. Derwich, *Pharmaceuticals* **16** (2023) 926 (https://doi.org/10.3390/ph16070926)

SM5. P. Hof, S. Pluskey, S. Dhe-Paganon, M. J. Eck, S. E. Shoelson, *Cell* **92** (1998) 441 (https://doi.org/10.1016/s0092-8674(00)80938-1)

SM6. O. Steingrimsson, J. H. Olafsson, H. Thorarinsson, R. W. Ryan, R. B. Johnson, R. C. Tilton, J. *Antimicrob. Chemother.* **25** (1990) 109 (https://doi.org/10.1093/jac/25.suppl_a.109)

SM7. B. Sperandio, C. Gautier, S. McGovern, D.S. Ehrlich, P. Renault, I. Martin-Verstraete, E. Guédon, *J. Bacteriol.* **189** (2007) 7032 (https://doi.org/10.1128/jb.00703-07).

Synthesis and *in vitro* study of redox properties of pyrrole and halogenated pyrrole derivatives

MILOŠ R. PETKOVIĆ[1]*, JELENA M. KOTUR-STEVULJEVIĆ[2], PREDRAG M. JOVANOVIĆ[1], MILOŠ D. JOVANOVIĆ[1], NIKOLA M. MITROVIĆ[1], MILENA R. SIMIĆ[1], GORDANA D. TASIĆ[1] and VLADIMIR M. SAVIĆ[1]

[1]*University of Belgrade-Faculty of Pharmacy, Department of Organic Chemistry, Belgrade, Serbia and* [2]*University of Belgrade-Faculty of Pharmacy, Department of Medical Biochemistry, Belgrade, Serbia*

Abstract: The redox balance plays a crucial role in maintaining biological processes under normal conditions. Antioxidants inhibit and reduce harmful oxidation processes, while pro-oxidants can act as anti-cancer agents by promoting ROS-mediated cell death. The aim of this study is to compare the redox properties of seven newly synthesised tribromopyrrole derivatives with three novel and four previously synthesized non-halogenated analogues in an *in vitro* model (in human serum) and with exogenously induced oxidative stress. The obtained values of their oxy scores (OS) were compared and the result showed that four non-halogenated pyrrole derivatives with secondary amide group **M2**, **M10**, **M11** and **M12** have lower OS values than Trolox, a water-soluble analogue of vitamin E with proven antioxidant properties. All four compounds show strong resistance to oxidative stress, which is reflected in the maintenance of negative OS values when exposed to exogenous oxidative stress using TBH in the reaction mixture. This capability to resist invading ROS should be expected also in an endogenous environment, where constant prooxidant production takes place at a low, homeostatic level, but even more so in pathological conditions. The tribrominated derivative **M15** showed prooxidant activity with a significantly higher OS value than all other compounds tested. The comparison of the dose-response of Trolox and the five compounds with the lowest OS also shows that compounds **M2**, **M7** and **M10** have better antioxidant activity than Trolox.

Keywords: oxidative stress; antioxidant; prooxidant; synthesis; pyrroles.

149

INTRODUCTION

In the complex web of cell biology, oxidative processes play a crucial role in maintaining homeostasis and regulating various physiological functions. A central role in this complicated network is played by reactive oxygen species (ROS), a class of highly reactive species that serve both as important signaling molecules and potential indicators of cell damage. While ROS are essential components of various cellular processes, an imbalance in their production and elimination can lead to oxidative stress, a disorder that plays a role in a variety of pathological conditions, including cancer. Reactive oxygen species include a number of molecules, *e.g.*, superoxide anions, hydrogen peroxide and hydroxyl radicals ($^\bullet$OH), which are produced during normal cellular metabolism. These species are involved in important cellular signaling pathways such as redox signaling, but also pose a threat as they can cause oxidative damage to biomolecules such as proteins, lipids and nucleic acids.[1,2]

Oxidative stress occurs when the cellular antioxidant defense mechanisms are overwhelmed, leading to an accumulation of ROS that exceeds the cell's ability to neutralise them. This imbalance can have various causes, including metabolic disorders. Importantly, the consequences of oxidative stress extend beyond the immediate cellular environment. Persistent oxidative stress can trigger genomic instability and promote mutagenesis, creating a favorable environment for tumour development and progression. Cancer cells develop mechanisms to keep high oxidative stress under control. This enables the involvement of ROS in the angiogenesis, invasiveness and metastatic capacity of cancers. At each stage of cancer development, cancer cells are adapted to high levels of ROS, which enables their survival in conditions unbearable for normal cells.[3,4] Furthermore, the intricate interplay between prooxidant activities and cellular antioxidant defense mechanisms contributes to an even more complex understanding of redox dynamics in cancer biology.[5,6]

Pyrrole is a heterocyclic compound whose derivatives show diverse pharmacological properties. The flat, electron-rich ring of pyrrole is highly susceptible to electrophilic attack and can bind to numerous biomolecules through hydrogen bonding and π–π stacking interactions.[7] This essential structural element is found in various naturally occurring structures such as chlorophyll, haemoglobin, myoglobin, cytochromes, vitamin B12 and bile pigments such as bilirubin and biliverdin.[8] The pyrrole subunit can be considered as privileged structure in medicinal chemistry extensively used as a key structural element in antifungals,[9] antimicrobials,[10] anti-inflammatory agents,[11] HMG-CoA reductase inhibitors[12] and antitumour agents.[13] There are some commercially available drugs such as ketorolac (**1**), tolmetin (**2**) and zomepirac (**3**), which are trisubstituted pyrrole derivatives used as non-steroidal anti-inflammatory drugs (Fig. 1).

Due to the considerable reactivity of pyrroles with electrophiles, halogenated derivatives of pyrroles are widespread in nature. The enzymatic incorporation of halogens into the biosynthesis of natural compounds allows fine-tuning of electronic and steric properties, which influence the affinity and selectivity of a molecule's interactions with its biological target. The antibiotic properties of certain natural halogenated pyrroles, such as pentabromopseudilin (**4**), pyoluteorin (**5**) and pyrrolnitrin (**6**, Fig. 1), have long been recognized.[14] This class of compounds also has some anticancer and antifungal activity and inhibits cholesterol biosynthesis. Pyrrolomycines (**7**), polyhalogenated pyrrole metabolites isolated from the fermentation broth of Actinosporangium and *Streptomyces* species, also show antibiotic activity.
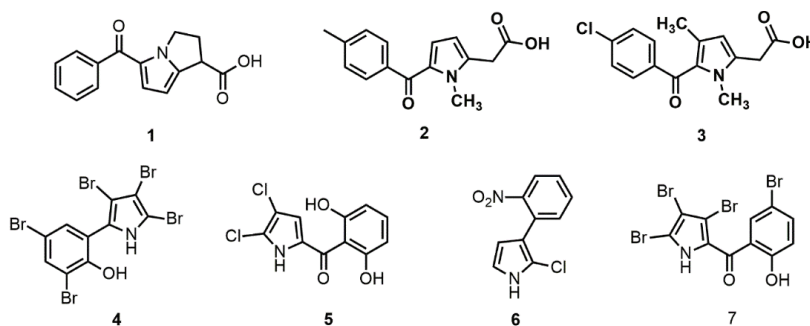
Fig. 1. Structures of some important pyrrole derivatives.

Typical antioxidants such as polyphenols neutralize oxygen radicals by a process that usually involves the transfer of hydrogen atoms (HAT) and results in a stabilized phenolic radical that does not continue the oxidative chain process. It has been shown that pyrroles, which have an N–H bond, also act as hydrogen atom donors and have antioxidant activity.[15] The antioxidant activity of various pyrrole derivatives, such as pyrrole-2-carbaldehydes,[16] pyrrole-2,5-diones,[17] pyrrole-based dihydropyrimidines,[18] hydrazides[19] and formazans,[20] has been demonstrated. Also, our previous study of substituted coumarins and the related isocoumarins and phthalides also showed the positive effect of azolyl substituents on the antioxidant/prooxidant balance of these compounds.[21]

Exploration of the antioxidant properties of pyrazole derivatives, revealed that the introduction of a chlorine atom into the aromatic ring increases the antioxidant capacity of these derivatives compared to non-halogenated ones.[22] Bearing in mind this fact, we envisioned to explore antioxidant/prooxidant potential of a series of newly synthesized tribromopyrrole derivatives in comparison with non-halogenated analogues in biological medium (serum pool of healthy volunteers). The unique pyrrole derivatives used in this study are easily accessible via chemistry that we have recently reported and further developed.[23]

EXPERIMENTAL

General

All chemicals used for the synthesis were obtained from commercial sources and were of reagent grade purity or better (Merck, Sigma Aldrich, Fluka, Fisher Scientific, *etc.*). ^{1}H- and ^{13}C-nuclear magnetic resonance (NMR) spectra were recorded at 400 and 101 MHz, respectively, using a Bruker Ascend 400 (400 MHz) spectrometer. Deuterochloroform was used as the solvent and chemical shifts are reported in ppm (δ) downfield from tetramethylsilane as the internal standard. Mass spectral data were recorded using an Orbitrap XL. Flash chromatography used a silica gel 60 (230–400 mesh), while thin-layer chromatography (TLC) was carried out using alumina plates with a 0.25 mm silica layer (Kieselgel 60 F254 Merck). The compounds were visualized by staining with potassium permanganate solution. Synthetic procedures are listed in the Supplementary data.

Sample collection

A serum pool was formed from samples of healthy individuals remaining after routine laboratory procedures. The use of patient data is excluded in this study. The selected samples included individuals whose key biochemical parameters were within the reference ranges for metabolites, which served as confirmation of their overall good health. The aliquots of the serum pool were frozen at −80 °C and used several months after the first collection. The substances to be analyzed, dissolved in DMSO at an initial concentration of 10 mmol/L, were mixed with the aliquots of the serum pool at a ratio of 1:9, thereby restricting sample dilution to 10 % and preserving the biomatrix. The final concentration for all tested substances was maintained at 1 mmol/L. This was followed by a two-hour incubation at 37 °C and the analyses were performed in duplicate, both alone and in combination with the exogenously added prooxidant *tert*-butyl hydroperoxide (TBH) at a concentration of 0.25 mmol/L, in an equivolume ratio.

Evaluation of biochemical parameters

The study involved the analysis of four redox status parameters using already published spectrophotometric methods. Two parameters defined prooxidant properties, total oxidative status (TOS) and prooxidant–antioxidant balance (PAB), while the other two, total antioxidant status (TAS) and total sulfhydryl groups (SHG), described antioxidant potential.

Serum TOS, a sum of lipid hydroperoxides and H_2O_2 concentrations, was determined by Erel's method modified in our laboratory. This involves the oxidation of ferrous ion in the *o*-dianisidine complex to ferric ion by oxidants present in the sample. The intensity of the color is proportional to the total amount of oxidant molecules in the sample. Calibration was performed with an aqueous solution of hydrogen peroxide (2–200 μmol/L) and the results are expressed as μmol H_2O_2 equivalent/L.[26,27]

Serum PAB is a measure of H_2O_2 concentration in an antioxidant environment measured by a previously published method.[28] The method involves the simultaneous reaction of 3,3'--5,5'-tetramethylbenzidine (TMB) with hydrogen peroxide and antioxidants such as uric acid. The reaction of hydrogen peroxide and chromogen is enzymatically catalyzed by peroxidase, whereas the reaction of serum antioxidants and chromogen is a non-enzymatic chemical process. The standard solutions were prepared by combining different proportions (0–100 %) of 1 mmol/L H_2O_2 with 6 mmol/L uric acid. The absorbance was measured at 450 nm and the PAB values are expressed in arbitrary units corresponding to the percentage of H_2O_2 in the standard solution. All measurements were performed using the micro-plate reader SPECTROstar Nano Microplate Reader (BMG Labtech, Ortenberg, Germany).

TAS represents the total concentration of all reductive substances in the blood and was measured using Erel's method, which was further optimized in the laboratory.[27] The assay involves the oxidation of reduced 2,2-azino-bis(3-ethylbenz-thiazoline-6-sulfonic acid) (ABTS) with hydrogen peroxide in an acidic medium. The antioxidants in the serum cause a discoloration of the reagent and the extent of the discolouration is proportional to their concentration.[29] Calibration was performed with Trolox, a water-soluble analogue of vitamin E, in the measuring range of 200–2000 µmol/L and the absorbance measured at 660 nm. The assay results are given in micromole Trolox equivalents/L.

SHG values were measured using a modification of the Ellman method by Kotur-Stevuljevic *et al*. The method used 10 mM 5,5'-dithiobis(2-nitrodithiobenzoic acid) (DTNB) as a reagent.[27] In a basic environment (pH 9.0), DTNB reacts with aliphatic thiol compounds to produce 1 mole of *p*-nitrophenol anion per mole of thiol. The absorbance was measured at 412 nm and the calibration used reduced glutathione as a standard in the concentration range of 0.01–4.0 mM.

Prooxidant score, antioxidant score and oxy score

The oxy score (OS) is calculated as the difference between the prooxidant score (average *Z*-scores of the measured prooxidants and their products, including TOS and PAB) and the antioxidant score (average *Z*-scores of the measured antioxidants, such as TAS and SHG). The *Z*-score is calculated as the difference between the original value and the control value divided by the standard deviation (*SD*) of the control samples' value. A higher oxy score indicates a poorer redox status (weaker antioxidant protection and a higher content of prooxidants).

Statistical analysis

Data are presented as median values (25th–75th percentile values). For the inter-groups comparison Kruskal–Wallis ANOVA and post-hoc Mann–Whitney U test were used. The *P* value below 0.05 was considered as statistically significant.

RESULTS AND DISCUSSION

Recently, we reported a novel method for the selective arylation of pyrrole derivatives in which the arylation agent fulfils a dual function: protection of the NH moiety and C(2) arylation.[23] During our mechanistic insight into this reaction, we found that treatment of acylpyrrole **1** with $Pd(OAc)_2$/PPh_3 and K_3PO_4 as a base in refluxing acetonitrile gives a tricyclic compound **2** (Scheme 1). The electrophilic aromatic substitution of the pyrrole ring with Br_2 in CCl_4 led to the formation of a tribrominated pyrrole derivative **3**, a structural motif found in several biologically active compounds. The subsequent ring opening of **2** or **3** with primary and secondary amine nucleophiles produces pyrrole derivatives **M1**–**M6**, **M10**–**M15** which are subjected to examination in antioxidant assays (Scheme 2). If an amine is used as a solvent, the reaction proceeds very quickly. After heating to 100 °C for 5 min, amides are formed in 72–96 % yields. An alternative with 3 equivalents of amine in acetonitrile as solvent gave comparable yield of product, but in this case overnight heating in boiling solvents is required. Furthermore, ring opening of compounds **2** and **3** with 1,2-diaminoethane, followed by reductive amination of the primary amino group with vanillin (3-hydroxy-4-methoxy-benzaldehyde), led to compounds **M7** and **M8**, in which the structures of pyrrole

are combined with a phenolic ring with proven antioxidant activity. In order to investigate the significance of the pyrrole ring for antioxidant activity, a compound without the pyrrole ring, **M9**, was also synthesized, which was achieved by reductive amination of benzylamine and vanillin.[25]
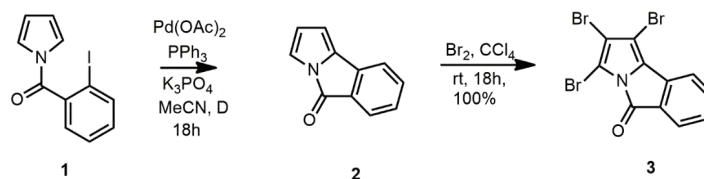
Scheme 1. Synthesis of tricyclic pyrrole derivatives.
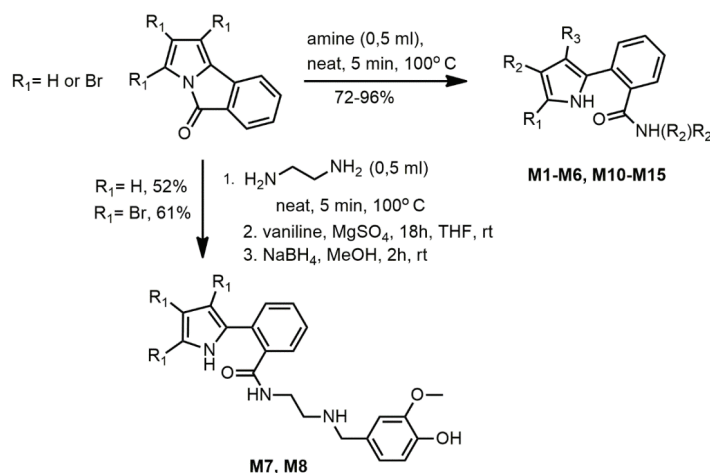
Scheme 2. Synthesis of pyrrole derivatives for the investigation of redox properties.

In order to estimate antioxidant potential of newly synthesized bromopyrrole derivatives and their non-halogenated analogues, we measured two prooxidant (TOS and PAB) and two antioxidant (TAs and SHG) parameters (data presented in the Supplementary material to this paper). The experiments were performed without or with externally added *t*-butyl hydroperoxide to mimic the conditions prevailing during the development of pathological processes. The main objective of this analysis is the calculation of three redox scores (without and with the addition of TBH), as their value indicates the level of prooxidant/antioxidant activity in the biological medium (serum pool). Typically, a low oxy score is associated with significant antioxidant capabilities of the compounds tested. Oxy scores, when considering the addition of TBH, reflect the capacity of the system to resist the effects of exogenous prooxidant.

The structures of all tested compounds are outlined in Fig. 2 and their redox scores are listed in Table I.
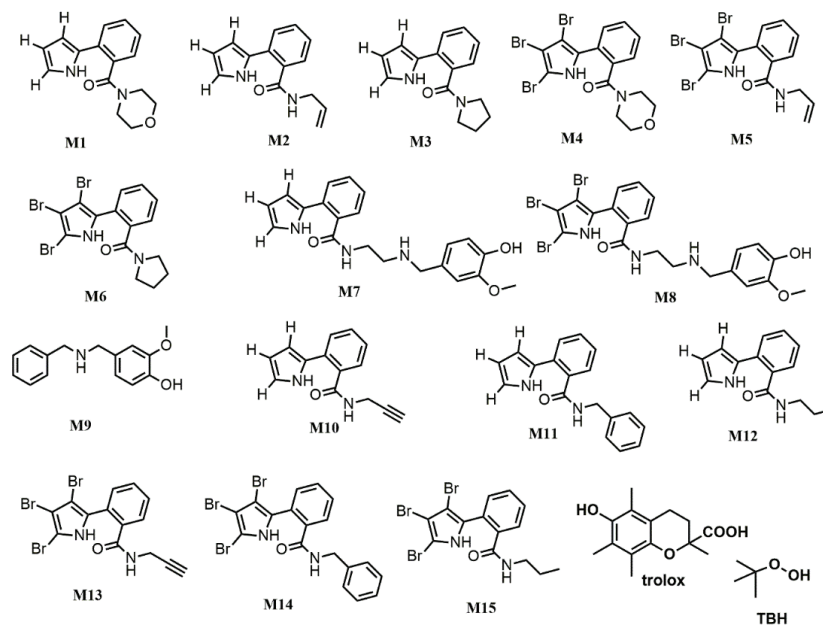
Fig. 2. Structures of tested compounds, Trolox and TBH.

TABLE I. Calculated values of prooxy, antioxy and oxy score of tested compounds; data presented as medians and 25th–75th percentile values in brackets; entries **a**–**o**: samples without TBH; entries **a′**–**o′**: samples with TBH

Entry	Compound	Prooxy score	Antioxy score	Oxy score
–	blank (0)	–3.3 (–5.9–0.0)	–0.4 (–2.2–0.6)	–1.1 (–4.2–0.0)
a	M1	–8.7 (–9.2–(–)8.1)	7.0 (6.9–7.1)	–15.7 (–16.1–(–)15.3)
b	M2	–18.3 (–19.3–(–)17.3)	8.6 (8.0–9.2)	–26.9 (–27.3–(–)26.5)
c	M3	–11.1 (–11.4–(–)10.9)	6.1 (6.0–6.2)	–17.2 (–17.5–(–)16.9)
d	M4	–7.9 (–8.5–(–)7.3)	7.2 (4.9–9.6)	–15.1 (–18.1–(–)12.2)
e	M5	–1.5 (–2.5–(–)0.5)	3.6 (3.6–3.6)	–5.1 (–6.1–(–)4.1)
f	M6	–1.3 (–1.4–(–)1.2)	4.8 (4.7–4.9)	–6.1 (–6.3–(–)6.0)
g	M7	–14.7 (–15.4–(–)13.9)	11.8 (11.2–12.4)	–26.4 (–26.6–(–)26.3)
h	M8	–2.6 (–3.2–(–)2.0)	8.0 (8.0–8.0)	–10.6 (–11.2–(–)10.0)
i	M9	–3.0 (–3.4–(–)2.5)	8.4 (8.3–8.5)	–11.4 (–12.0–(–)10.8)
j	M10	–18.5 (–21.3–(–)15.6)	4.9 (0.3–9.5)	–23.4 (–25.2–(–)21.6)
k	M11	–26.4 (–27.5–(–)25.4)	–2.4 (–3.6–(–)1.2)	–24.1 (–24.2–(–)23.9)
l	M12	–34.2 (–36.4–(–)32.0)	–6.1 (–6.8–(–)5.3)	–28.1 (–29.6–(–)26.7)
m	M13	–12.7 (–13.9–(–)11.6)	–11.6 (–12.7–(–)10.5)	–1.1 (–3.3–1.1)
n	M14	–12.4 (–14.7–(–)10.1)	5.9 (2.8–9.1)	–18.4 (–19.3–(–)17.5)
o	M15	14.3 (11.7–16.9)	2.7 (0.9–4.5)	11.6 (7.2–16.0)
a′	M1+TBH	6.0 (5.6–6.4)	2.8 (2.5–3.2)	3.2 (2.5–3.9)
b′	M2+TBH	–2.5 (–2.6–(–)2.5)	3.5 (3.2–3.8)	–6.1 (–6.4–(–)5.7)
c′	M3+TBH	4.0 (–0.6–8.7)	1.6 (0.2–3.0)	2.5 (–3.6–8.5)
d′	M4+TBH	6.6 (6.5–6.7)	1.7 (1.4–1.9)	4.9 (4.6–5.2)
e′	M5+TBH	9.5 (8.5–10.4)	1.2 (0.8–1.5)	8.3 (7.0–9.6)

TABLE I. Continued

Entry	Compound	Prooxy score	Antioxy score	Oxy score
f′	M6+TBH	12.6 (12.5–12.7)	–0.6 (–1.0–(–)0.2)	13.1 (12.8–13.4)
g′	M7+TBH	1.7 (1.0–2.5)	–1.2 (–9.6–7.1)	3.0 (–6.2–12.1)
h′	M8+TBH	10.3 (9.5–11.0)	3.5 (2.7–4.3)	6.8 (5.2–8.3)
i′	M9+TBH	10.2 (8.3–12.1)	1.8 (0.5–3.1)	8.3 (5.1–11.5)
j′	M10+TBH	–26.5 (–27.8–(–)25.2)	–4.6 (–5.8–(–)3.5)	–21.9 (–24.3–(–)19.5)
k′	M11+TBH	–20.3 (–21.6–(–)19.0)	–7.5 (–9.6–(–)5.4)	–12.8 (–16.2–(–)9.3)
l′	M12+TBH	–13.7 (–19.0–(–)8.4)	4.6 (1.1–8.0)	–18.3 (–27.1–(–)9.5)
m′	M13+TBH	2.5 (0.7–4.2)	–3.9 (–5.5–(–)2.3)	6.3 (3.0–9.7)
n′	M14+TBH	4.8 (–0.4–9.9)	–11.7 (–12.8–(–)10.7)	16.5 (10.3–22.7)
o′	M15+TBH	3.2 (1.6–4.8)	–11.0 (–11.2–(–)10.9)	14.2 (12.8–15.6)
–	Trolox+serum	–7.2 (–20.5–6.1)	13.1 (13.0–13.3)	–20.3 (–33.8–(–)6.8)
–	DMSO+serum	–5.4 (–10.7–0.5)	0.0 (–5.5–4.2)	–3.7 (–5.4–(–)3.4)
–	TBH+serum	10.2 (0.7–21.5)	–4.4 (–10.3–0.1)	(11.0–21.4)

Most of the substances had a negative oxy score, lower then blank serum, which indicates their antioxidant potential. Compounds **M2** (*OS* –26.9, entry **b**, Table I), **M7** (*OS* –26.4, entry **g**), **M10** (*OS* –23.4, entry **j**)**,** **M11** (*OS* –24.1, entry **k**) and **M12** (*OS* –28.1, entry **j**) had lower oxy score than Trolox (*OS* –20.3), water--soluble analogue of vitamin E with proven antioxidant activity. As an exception, the brominated pyrrole derivative **M15** (*OS* 11.6, entry **o**) stands out with a positive oxy score and may exhibit prooxidant properties, which may be a useful protective function like cytostatic, bacteriostatic and antivirotic.[30] When comparing non-halogenated and halogenated pyrrole derivatives, the non-halogenated analogues showed lower OS values for all matching pairs. The investigation of the antioxidant activity mechanism of N–H pyrroles revealed that the pyrrolyl radical adopts the 5π electron system after hydrogen atom transfer (HAT), the stability of which largely depends on the electronic properties of the substituents on the aromatic ring. It was shown that the electron-donating groups on the benzene ring of 2-arylpyrroles stabilise the generated radical and increase the antioxidant activity of the compound.[15] From this it can be concluded that the electron-accepting properties of the three bromine atoms could destabilise the pyrrolyl radical and negatively influence the antioxidant activity. Further SAR analysis demonstrated some additional facts. Non-halogenated pyrrole derivatives with tertiary amide group **M1** (*OS* –15.7, entry **a**) and **M3** (*OS* –15.7, entry **c**)**,** obtained in the reaction with secondary amines, had less negative *OS* values than derivatives **M2** (*OS* –26.9, entry **b**), **M10** (*OS* –23.4, entry **j**), **M11** (*OS* –24.1, entry **k**) and **M12** (*OS* –28.1, entry **l**) obtained in reactions with primary amines. This is not surprising considering that in a study on the antioxidant activity of carboxamide it was shown that the N–H bond of the amide can also be a site for the abstraction of the H atom.[31] It was also interesting to compare the OS values for amides with propyl, propenyl and propynil groups. For the non-halogenated

pyrrole derivatives **M12** (*OS* –28.1, entry **l**), **M2** (*OS* –26.9, entry **b**) and **M10** (*OS* –23.4, entry **j**), the values were comparable, while for the brominated derivatives, the compound with saturated propyl group **M15** (*OS* 11.6, entry **o**) showed prooxidant activity, with a significantly higher positive OS value compared to the propenyl and propynyl derivatives **M5** (*OS* –5.1, entry **e**) and **M13** (*OS* –1.1, entry **m**). Clear evidence for the essential role of the pyrrole ring is provided by the comparison of two compounds obtained by reductive amination with vanillin, an aldehyde with a phenolic ring with proven antioxidant activity.[32] The vanillin derivative **M7** (*OS* –26.4, entry **g**), which has a pyrrole ring, showed better antioxidant properties than the benzyl derivative **M9** (*OS* –11.4, entry **i**).

OS was also determined in the presence of *t*-butyl hydroperoxide, indicating the potential of the compounds to resist oxidative stress. Preserved negativity of the *OS* in samples containing compounds **M2** (*OS* –6.1, entry **b′**), **M10** (*OS* – 21.9, entry **i′**), **M11** (*OS* –12.8, entry **j′**) and **M12** (*OS* –18.3, entry **k′**) is a sign of its antioxidant strength, even in the presence of prooxidants. The change in *OS* towards positive values in other samples speaks in favor of its lower ability to respond to oxidative stress.

Oxy scores (*OS*) for all compounds are also outlined in Fig. 3 which summaries the results from both experiments (without and with TBH) after 2 h incubation at 37 °C in comparison with Trolox used as standard.
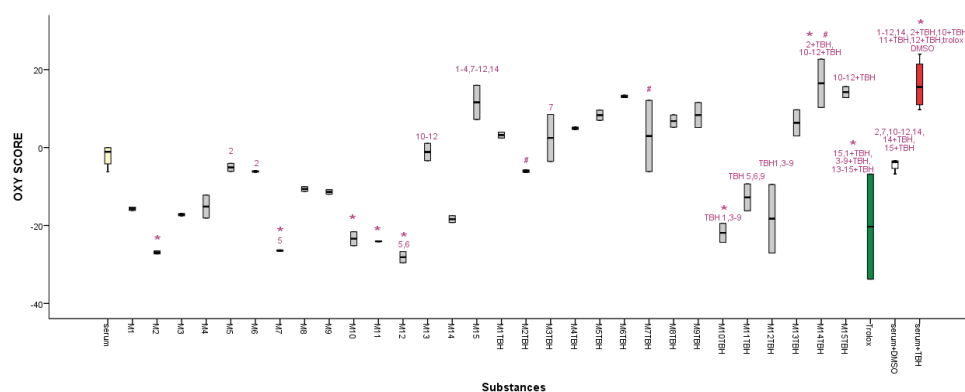
Fig. 3. Oxy score (OS) in tested substances with and without TBH, along with native serum, serum with Trolox (2000 μmol/L) and serum with TBH (0.25 mM); * – $P < 0.05$, *vs*. native serum; # – $P < 0.05$, *vs*. the same substance sample without TBH; numbers: statistically significant difference *vs*. distinct substance without or with TBH.

The lowest *OS*, observed in samples **M2**, **M7** and **M10**–**12** was the reason why we continued the dose-response analyses with these 5 samples. A water-soluble analogue of vitamin E (Trolox) was prepared in 5 concentrations: 2000,

1000, 500, 250 and 125 μmol/L in water. In addition, 3 dilutions of compounds **M2**, **M7** and **M10**–**M12** (0.5, 0.25 and 0.125 mmol/L from starting 1 mmol/L) were prepared in DMSO. The oxy scores were calculated and a graphical representation is shown in Fig. 4. A concentration dependence can be observed for all tested substances (the compounds show lower antioxidant activity, which is indicated by higher *OS* in samples with lower concentrations). A comparison of the *OS* shows that compound **M2** is a better antioxidant than compound **M7**, although both compounds have excellent antioxidant properties.
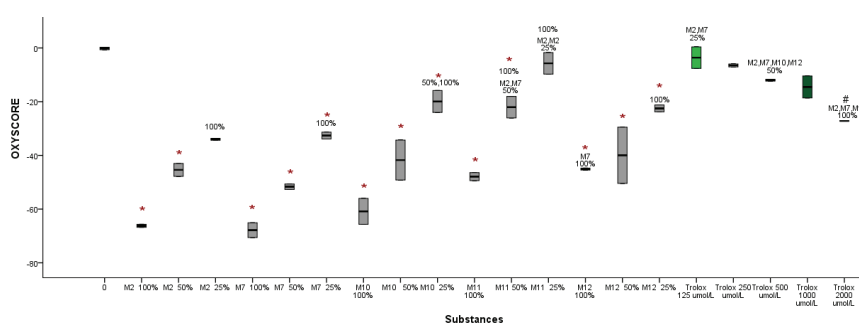
Fig. 4. Oxy score in three different concentrations of M2, M7, M10, M11 and M12 samples, so as in samples with Trolox (125–2000 μmol/L); *– *P* < 0.05 *vs.* native serum (blank); 100 %, 50 %: *P* < 0.05 *vs.* sample of the same substance with different concentration; Mx, My…Mi %: *P* < 0.05 *vs.* indicated sample of a specific dilution; # – *P* < 0.05 *vs.* Trolox (125 μmol/L).

In the case of Trolox, a concentration dependence is also observed, *i.e.*, the *OS* is significantly lower in serum samples with higher concentrations of Trolox. However, compared to samples containing compounds **M2**, **M7** and **M10**, its antioxidant activity is less pronounced (higher *OS* values, although still negative).

CONCLUSION

In this work, we have described an efficient and simple method for the preparation of tribrominated and non-halogenated analogue pyrrole derivatives. Our investigation of the redox properties of the synthesized compounds shows that the tribrominated derivative **M15** exhibits strong prooxidant activity. The four non-halogenated compounds with a secondary amide group, namely **M2**, **M10**, **M11** and **M12**, have lower oxy score (*OS*) values than Trolox, an analogue of vitamin E with proven antioxidant activity. In addition, all four compounds show strong resistance to oxidative stress. A comparison of the dose-response of compounds **M2**, **M7** and **M10** with Trolox shows that the synthesized compounds exhibit better antioxidant activity than Trolox. Therefore, they can be further developed as effective antioxidants.

SUPPLEMENTARY MATERIAL

Additional data and information are available electronically at the pages of journal website: https://www.shd-pub.org.rs/index.php/JSCS/article/view/12931, or from the corresponding author on request.

ИЗВОД

СИНТЕЗА И *IN VITRO* СТУДИЈА РЕДОКС ОСОБИНА ХАЛОГЕНОВАНИХ И НЕХАЛОГЕНОВАНИХ ДЕРИВАТА ПИРОЛА

МИЛОШ Р. ПЕТКОВИЋ[1], ЈЕЛЕНА М. КОТУР-СТЕВУЉЕВИЋ[2], ПРЕДРАГ М. ЈОВАНОВИЋ[1], МИЛОШ Д. ЈОВАНОВИЋ[1], ГОРДАНА Д. ТАСИЋ[1], МИЛЕНА Р. СИМИЋ[1] и ВЛАДИМИР М. САВИЋ[1]

¹Универзитет у Београду – Фармацеутски факултет, Катедра за органску хемију, Војводе Степе 450, 11221 Београд и ¹Универзитет у Београду – Фармацеутски факултет, Катедра за медицинску биохемију, Војводе Степе 450, 11221 Београд

Редокс равнотежа игра кључну улогу у одржавању биолошких процеса у нормалним условима. Антиоксиданси инхибирају и смањују штетне процесе оксидације, док прооксиданси могу деловати као антиканцерски агенси промовишући ћелијску смрт посредовану реактивним кисеоничним врстама. Циљ овог рада је да се упореде редокс својства седам новосинтетисаних деривата трибромопирола и нехалогенованих аналога (три новосинтетисана и четири претходно синтетисана) у *in vitro* моделу (у хуманом серуму) и са егзогено индукованим оксидативним стресом. Упоређене су добијене вредности њихових окси скорова (*OS*) и резултат је показао да четири нехалогенована деривата пирола са секундарном амидном групом **M2**, **M10**, **M11** и **M12** имају ниже вредности *OS* од Тролокса, аналога витамина E растворљивог у води са доказаним антиоксидативним својствима. Сва четири једињења показују јаку отпорност на оксидативни стрес, што се огледа у одржавању негативних вредности *OS* када су изложене егзогеном оксидативном стресу коришћењем ТВН у реакционој смеши. Ову способност да се одупиру ROS треба очекивати и у ендогеном окружењу, где се константна производња прооксиданата одвија на ниском, хомеостатском нивоу, али још више у патолошким стањима. Трибромовани дериват **M15** је показао прооксидативну активност са значајно вишом *OS* вредношћу од свих осталих тестираних једињења. Такође, упоредне анализе доза-одговор тестираних пет једињења са најнижим *OS* и Тролокса показују да Тролокс има слабију антиоксидативну активност од једињења **M2**, **M7** и **M10**.

(Примљено 15. маја, ревидирано 20. јуна, прихваћено 2. септембра 2024)

REFERENCES

1. T. Finkel, *J. Cell Biol.* **194** (2011) 7 (https://doi.org/10.1083/jcb.201102095)
2. M. Valko, D. Leibfritz, J. Moncol, M. T. D. Cronin, M. Mazur, J. Telser, *Int. J. Cell Biol.* **39** (2007) 44 (https://doi.org/10.1016/j.biocel.2006.07.001)
3. S. Arfin, N. K. Jha, S. K. Jha, K. K. Kesari, J. Ruokolainen, S. Roychoudhury, B. Rathi, D. Kumar, *Antioxidants* **10** (2021) 642 (https://doi.org/10.3390/antiox10050642)
4. J. D. Hayes, A. T. Dinkova-Kostova, K. D. Tew, *Cancer Cell* **38** (2020) 167 (https://doi.org/10.1016/j.ccell.2020.06.001)

5. D. Trachootham, W. Lu, M. A. Ogasawara, N. R.-D. Valle, P. Huang, *Antioxid. Redox Signal.* **10** (2008) 1343 (https://doi.org/10.1089/ars.2007.1957)
6. S. Toyokuni, *Arch. Biochem. Biophys.* **595** (2016) 46 (https://doi.org/10.1016/j.abb.2015.11.025)
7. S. Ahmad, O. Alam, Mohd. J. Naim, M. Shaquiquzzaman, M. M. Alam, M. Iqbal, *Eur. J. Med. Chem.* **157** (2018) 527 (https://doi.org/10.1016/j.ejmech.2018.08.002)
8. N. Jeelan Basha, S. M. Basavarajaiah, K. Shyamsunder, *Mol. Divers* **26** (2022) 2915 (https://doi.org/10.1007/s11030-022-10387-8)
9. R. H. Abd El-Hameed, A. I. Sayed, S. Mahmoud Ali, M. A. Mosa, Z. M. Khoder, S. S. Fatahala, *J. Enzyme Inhib. Med. Chem.* **36** (2021) 2183 (https://doaj.org/article/f1c9b4360a3c4baead207ed8f7344c44)
10. P. Rawat, R. N. Singh, A. Ranjan, A. Gautam, S. Trivedi, M. Kumar, *J. Mol. Struct* **1228** (2021) 129483 (https://doi.org/10.1016/j.molstruc.2020.129483)
11. A. R. Pandey, S. P. Singh, P. Joshi, K. S. Srivastav, S. Srivastava, K. Yadav, R. Chandra, A. C. Bisen, S. Agrawal, S. N. Sanap, R. S. Bhatta, R. Tripathi, M. K. Barthwal, K. V. Sashidhara, *Eur. J. Med. Chem.* **254** (2023) 115340 (https://doi.org/10.1016/j.ejmech.2023.115340)
12. J. A. Pfefferkorn, Y. Song, K.-L. Sun, S. R. Miller, B. K. Trivedi, C. Choi, R. J. Sorenson, L. D. Bratton, P. C. Unangst, S. D. Larsen, T.-J. Poel, X.-M. Cheng, C. Lee, N. Erasga, B. Auerbach, V. Askew, L. Dillon, J. C. Hanselman, Z. Lin, G. Lu, A. Robertson, K. Olsen, T. Mertz, C. Sekerke, A. Pavlovsky, M. S. Harris, G. Bainbridge, N. Caspers, H. Chen, M. Eberstadt, *Bioorg. Med. Chem. Lett.* **17** (2007) 4538 (https://doi.org/10.1016/j.bmcl.2007.05.096)
13. E. Mateev, M. Georgieva, A. Zlatkov, *J. Pharm. Pharm. Sci.* **25** (2022) 24 (https://doi.org/10.18433/jpps32417)
14. S. Cascioferro, M. Raimondi, M. Cusimano, D. Raffa, B. Maggio, G. Daidone, D. Schillaci, *Molecules* **20** (2015) 21658 (https://doi.org/10.3390/molecules201219797)
15. P. D. MacLean, E. E. Chapman, S. L. Dobrowolski, A. Thompson, L. R. C. Barclay, *J. Org. Chem.* **73** (2008) 6623 (https://doi.org/10.1021/jo8005073)
16. S. Matsugo, Y. Nakamura, *Molecules* **28** (2023) 2599 (https://pubmed.ncbi.nlm.nih.gov/36985566/)
17. G. Mallikarjuna Reddy, A. Camilo, J. Raul Garcia, *Bioorg. Chem.* **106** (2021) 104465 (https://doi.org/10.1016/j.bioorg.2020.104465)
18. A. Khalilpour, S. Asghari, *Med. Chem. Res.* **27** (2018) 15 (https://doi.org/10.1007/s00044-017-2041-4)
19. D. Tzankova, D. Aluani, M. Kondeva-Burdina, M. Georgieva, S. Vladimirova, L. Peikova, V. Tzankova, *Pharm. Chem. J.* **55** (2022) 1310 (https://doi.org/10.1007/s11094-022-02577-3)
20. J. D. Bhosale, A. R. Shirolkar, U. D. Pete, C. M. Zade, D. P. Mahajan, C. D. Hadole, S. D. Pawar, U. D. Patil, R. Dabur, R. S. Bendre, *J. Pharm. Res.* **7** (2013) 582 (https://doi.org/10.1016/j.jopr.2013.07.022)
21. M. Simic, J. Kotur-Stevuljevic, P. Jovanovic, M. Petkovic, M. Jovanovic, G. Tasic, V. Savic, *J. Serb. Chem. Soc.* **88** (2023) 589 (https://doi.org/10.2298/JSC221221017S)
22. S. Shetty, B. Kalluraya, *Pharma Chem.* **7** (2015) 26 (https://www.derpharmachemica.com/pharma-chemica/design-and-synthesis-of-hydrazone-incorporated-pyrazoles-and-triazoles-aspossible-antioxidants.pdf)
23. M. Petkovic, M. Jovanovic, P. Jovanovic, M. Simic, G. Tasic, V. Savic, *Synth.* **54** (2022) 2839 (https://doi.org/10.1055/a-2201-9951)

24. M. Simic, G. Tasic, P. Jovanovic, M. Petkovic, V. Savic, *Org. Biomol. Chem.* **16** (2018) 2125 (https://doi.org/10.1039/c8ob00260f)
25. M. Scipioni, G. Kay, I. Megson, P. Kong Thoo Lin, *Eur. J. Med. Chem.* **143** (2018) 745 (https://doi.org/10.1016/j.ejmech.2017.11.072)
26. O. Erel, *Clin. Biochem.* **38** (2005) 1103 (https://doi.org/10.1016/j.clinbiochem.2005.08.008)
27. J. Kotur-Stevuljevic, N. Bogavac-Stanojevic, Z. Jelic-Ivanovic, A. Stefanovic, T. Gojkovic, J. Joksic, M. Sopic, B. Gulan, J. Janac, S. Milosevic, *Atherosclerosis* **241** (2015) 192 (https://doi.org/10.1016/j.atherosclerosis.2015.05.016)
28. O. Erel, *Clin. Biochem.* **37** (2004) 277 (https://doi.org/10.1016/j.clinbiochem.2003.11.015)
29. D. H. Alamdari, K. Paletas, T. Pegiou, M. Sarigianni, C. Befani, G. Koliakos, *Clin. Biochem.* **40** (2007) 248 (https://doi.org/10.1016/j.clinbiochem.2006.10.017)
30. R. Sotler, B. Poljšak, R. Dahmane, T. Jukić, D. Pavan Jukić, C. Rotim, P. Trebše, A. Starc, *ACC* **58** (2019) 726 (https://doi.org/10.20471/acc.2019.58.04.20)
31. M. Cindrić, I. Sović, M. Mioč, L. Hok, I. Boček, P. Roškarić, K. Butković, I. Martin-Kleiner, K. Starčević, R. Vianello, M. Kralj, M. Hranjec, *Antioxidants* **8** (2019) 477 (https://doi.org/10.3390/antiox8100477)
32. A. Tai, T. Sawano, F. Yazama, H. Ito, *Biochim. Biophys. Acta* **1810** (2011) 170 (https://doi.org/10.1016/j.bbagen.2010.11.004).

SUPPLEMENTARY MATERIAL TO

Synthesis and *in vitro* study of redox properties of pyrrole and halogenated pyrrole derivatives

MILOŠ R. PETKOVIĆ[1]*, JELENA M. KOTUR-STEVULJEVIĆ[2], PREDRAG M. JOVANOVIĆ[1], MILOŠ D. JOVANOVIĆ[1], NIKOLA M. MITROVIĆ[1], MILENA R. SIMIĆ[1], GORDANA D. TASIĆ[1] and VLADIMIR M. SAVIĆ[1]

[1]*University of Belgrade-Faculty of Pharmacy, Department of Organic Chemistry, Belgrade, Serbia and* [2]*University of Belgrade-Faculty of Pharmacy, Department of Medical Biochemistry, Belgrade, Serbia*

CONTENTS

* Corresponding author. E-mail: milosp@pharmacy.bg.ac.rs

Synthetic procedures

5H-pyrrolo[2,1-a]isoindol-5-one (2) The mixture of (2-iodophenyl)(1H-pyrrol-1-yl)methanone **1** (1 mmol, 1 eq), K$_3$PO$_4$ (1.5 mmol, 1.5 eq), Pd(OAc)$_2$ (0,1 mmol, 0,1 eq) and PPh$_3$ (0,2 mmol, 0,2 eq) in acetonitrile (5 ml) was heated in a nitrogen atmosphere at reflux for 16 h. After completion of the reaction, the mixture was cooled to room temperature and the solvent was removed under reduced pressure. The crude mixture was purified by flash chromatography to afford the product. Flash chromatography (SiO2, 9:1 v/v petroleum ether–diethyl ether) afforded the product (281.2 mg, 81%) as a yellow solid, mp 62–63 °C.

^{1}H NMR (400 MHz, CDCl3) δ 7.55 (d, J = 7.2 Hz, 1H), 7.34 (t, J = 7.2 Hz, 1H), 7.19 (d, J = 7.2 Hz, 1H), 7.09 (t, J = 7.0 Hz, 1H), 6.93 (s, 1H), 6.10 (d, J = 12.7 Hz, 2H);

^{13}C NMR (101 MHz, CDCl3) δ 163.0, 136.4, 135.6, 134.4, 132.1, 127.1, 125.8, 119.5, 117.1, 116.6, 107.3;

The spectral data are consistent with those reported in the literature.[24]

1,2,3-tribromo-5H-pyrrolo[2,1-a]isoindol-5-one (3) 5H-pyrrolo[2,1-a]isoindol-5-one (2) (0.5 mmol, 1 eq) was dissolved in CCl$_4$ (10 mL) and bromine (4 mmol, 8 eq) was added dropwise. After 16 hours at room temperature, the reaction mixture was diluted with CH$_2$Cl$_2$ (15 mL) and the organic solvent was washed with 10% Na$_2$S$_2$O$_3$ (20 mL) and brine (20 mL). After drying with anhydrous Na$_2$SO$_4$, the organic solvent was evaporated to obtain the product (195.3 mg, 97%) as an orange solid, mp 207-208 °C.

^{1}H NMR (400 MHz, CDCl3) δ 7.70 (d, J = 7.4 Hz, 1H), 7.57-7.51 (m, 2H), 7.31-7.26 (m, 1H).

^{13}C NMR (101 MHz, CDCl3) δ 160.7, 135.3, 134.1, 133.6, 129.5, 128.4, 126.7, 119.6, 111.3, 102.1, 100.2.

General procedure for the synthesis of the amides *M1-M6 and M10-M15*

Compound **2** or **3** (0.1 mmol, 1 eq) was dissolved in amine (0.5 mL) and heated at 100º C for 5 minutes. After cooling, the excess amine was removed under reduced pressure. The crude mixture was dissolved in CH$_2$Cl$_2$ (15 mL), washed with 2M HCl (10 mL) and brine (10 mL). After drying with anhydrous Na$_2$SO$_4$, the organic solvent was evaporated under reduced pressure to obtain the product.

General procedure for the synthesis of the amides *M7-M8*

Compound **2** or **3** (0.1 mmol, 1 eq) was dissolved in ethylendiamine (0.5 mL) and heated at 100º C for 5 minutes. After cooling, the excess amine was removed under reduced pressure. To a solution of the crude mixture in THF (10 mL), vanillin (0.1 mmol, 1 eq) and MgSO$_4$ (0.5 mmol, 5 eq) were added and the mixture was stirred overnight. After filtration, the solvent was evaporated and the crude mixture was dissolved in MeOH (5 mL) and NaBH$_4$ (0.2 mmol, 2 eq) was added. The mixture was stirred for 2 hours at room temperature and, after evaporation of the solvent under reduced pressure, subjected directly to flash chromatography to obtain the product.

4-((benzylamino)methyl)-2-methoxyphenol (9) To a solution of benzylamine (0.1 mmol, 1 eq) in THF (10 mL), vanillin (0.1 mmol, 1 eq) and MgSO$_4$ (0.5 mmol, 5 eq) were added and the mixture was stirred overnight. After filtration, the solvent was evaporated and the crude mixture was dissolved in MeOH (5 mL) and NaBH$_4$ (0.2 mmol, 2 eq) was added. The mixture was stirred for 2 hours at room temperature and, after evaporation of the solvent under reduced pressure, subjected directly to flash chromatography. Flash chromatography (SiO2, EtOAc) afforded the product (133.7 mg, 55%) as a white, amorphous solid.

^{1}H NMR (400 MHz, CDCl3) δ 7.33 (d, J = 4.4 Hz, 4H), 7.25 (t, J = 4.2 Hz, 1H), 6.88 (s, 1H), 6.83 (d, J = 8.0 Hz, 1H), 6.78 (d, J = 8.0 Hz, 1H), 3.84 (s, 3H), 3.80 (s, 2H), 3.73 (s, 2H).

^{13}C NMR (101 MHz, CDCl3) δ 146.7, 144.8, 140.2, 132.0, 128.4, 128.2, 126.9, 121.0, 114.3, 110.9, 55.8, 53.1, 53.0.

The spectral data are consistent with those reported in the literature.[25]

Morpholin-4-yl -[2-(1H-pyrrol-2-yl)-phenyl]-methanone (M1)

Compound **M1** (17.9 mg, 70%) was synthesized following the general procedure, as a beige solid, mp: 162-163°C.

^{1}H NMR (400 MHz, CDCl₃) δ 9.20 (s, 1H), 7.54 (d, *J* = 7.8 Hz, 1H), 7.44 – 7.36 (m, 1H), 7.30 – 7.21 (m, 2H), 6.85 (d, *J* = 1.4 Hz, 1H), 6.41 (s, 1H), 6.27 (dd, *J* = 5.9, 2.7 Hz, 1H), 4.05 (dd, *J* = 12.9, 2.3 Hz, 1H), 3.76 – 3.69 (m, 1H), 3.50 – 3.36 (m, 3H), 3.14 – 3.06 (m, 1H), 2.99 – 2.91 (m, 1H), 2.81-2-76 (m, 1H).

^{13}C NMR (101 MHz, CDCl₃) δ 171.3, 132.6, 130.4, 130.4, 129.5, 128.2, 126.6, 126.5, 119.4, 109.6, 108.4, 66.6, 66.6, 47.6, 42.4.

The spectral data are consistent with those reported in the literature.[23]

N-Allyl-2-(1H-pyrrol-2-yl)-benzamide (M2)

Compound M2 (16.0 mg, 71%) was synthesized following the general procedure, as a brown, amorphous solid.

^{1}H NMR (400 MHz, CDCl₃) δ 10.14 (s, 1H), 7.63 (d, *J* = 7.9 Hz, 1H), 7.42 (t, *J* = 8.0 Hz, 2H), 7.29 – 7.21 (m, 1H), 6.85 (d, *J* = 1.5 Hz, 1H), 6.48 (s, 1H), 6.26 (d, *J* = 2.6 Hz, 1H), 5.91 (s, 1H), 5.87 – 5.75 (m, 1H), 5.21 – 5.08 (m, 2H), 4.00 (s, 2H).

^{13}C NMR (101 MHz, CDCl₃) δ 171.9, 133.4, 133.3, 131.3, 130.7, 130.4, 129.0, 127.9, 126.0, 119.4, 117.0, 109.2, 108.6, 42.6.

The spectral data are consistent with those reported in the literature.[23]

Pyrrolidin-1-yl-[2-(1H-pyrrol-2-yl)-phenyl]-methanone (M3)

Compound **M3** (19.7 mg, 82%) was synthesized following the general procedure as a light-brown solid, mp: 146-147°C.

^{1}H NMR (400 MHz, CDCl₃) δ 9.72 (s, 1H), 7.59 (d, *J* = 8.0 Hz, 1H), 7.42 – 7.34 (m, 1H), 7.29 – 7.20 (m, 2H), 6.82 (d, *J* = 1.5 Hz, 1H), 6.46 (s, 1H), 6.24 (d, *J* = 3.2 Hz, 1H), 3.59 (t, *J* = 6.6 Hz, 2H), 3.02 (bs, 2H), 1.85 (dd, *J* = 13.7, 6.8 Hz, 2H), 1.71 (bs, 2H).

^{13}C NMR (101 MHz, CDCl₃) δ 171.2, 133.8, 130.8, 130.0, 129.4, 128.4, 126.7, 126.1, 119.4, 109.1, 107.8, 48.6, 45.8, 25.8, 24.5.

The spectral data are consistent with those reported in the literature.[23]

Morpholino(2-(3,4,5-tribromo-1H-pyrrol-2-yl)phenyl)methanone (M4)

Compound **M4** (40.2 mg, 82%) was synthesized following the general procedure as a beige solid, mp: 221-222°C.

^{1}H NMR (400 MHz, CDCl₃) δ 9.98 (s, 1H), 7.63 (d, *J* = 7.8 Hz, 1H), 7.45 (t, *J* = 7.6 Hz, 1H), 7.37 (t, *J* = 7.5 Hz, 1H), 7.25 (d, *J* = 7.3 Hz, 1H), 3.96 (d, *J* = 13.2 Hz, 1H), 3.75 (dd, *J* = 9.5, 5.9 Hz, 1H), 3.57 – 3.49 (m, 1H), 3.48 – 3.40 (m, 1H), 3.38 – 3.29 (m, 1H), 3.16 – 3.08 (m, 1H), 3.01 – 2.90 (m, 2H).

^{13}C NMR (101 MHz, CDCl₃) δ 170.1, 134.6, 130.5, 129.3, 129.1, 128.6, 127.2, 126.6, 102.8, 100.9, 98.9, 66.7, 66.7, 47.5, 42.3.

HRMS (ESI) m/z calcd. for $[C_{15}H_{13}Br_3N_2O_2-H]^-$ 488.84544; found, 488.84533.

N-allyl-2-(3,4,5-tribromo-1H-pyrrol-2-yl)benzamide (M5)

Compound **M5** (38.2 mg, 83%) was synthesized following the general procedure as a light-brown solid, mp: 171-172°C.

^{1}H NMR (400 MHz, CDCl$_3$) δ 11.00 (bs, 1H), 7.67 (d, *J* = 7.6 Hz, 1H), 7.47 (t, *J* = 8.0 Hz, 2H), 7.32 (t, *J* = 7.6 Hz, 1H), 5.83 – 5.65 (m, 2H), 5.11 (dd, *J* = 18.3, 13.7 Hz, 2H), 3.87 (t, *J* = 5.8 Hz, 2H).

^{13}C NMR (101 MHz, CDCl$_3$) δ 170.1, 135.2, 132.9, 131.3, 130.3, 129.1, 128.4, 128.3, 128.1, 117.4, 102.5, 101.1, 98.8, 42.6.

HRMS (ESI) m/z calcd. for [C$_{14}$H$_{11}$Br$_3$N$_2$O -H]$^-$ 458.83487; found, 458.83470.

Pyrrolidin-1-yl(2-(3,4,5-tribromo-1H-pyrrol-2-yl)phenyl)methanone (M6)

Compound **M6** (45.5mg, 96%) was synthesized following the general procedure as a light-brown solid, mp: 161-162°C.

^{1}H NMR (400 MHz, CDCl$_3$) δ 10.41 (s, 1H), 7.74 (d, *J* = 7.8 Hz, 1H), 7.44 (t, *J* = 7.6 Hz, 1H), 7.36 (t, *J* = 7.3 Hz, 1H), 7.30 (d, *J* = 7.1 Hz, 1H), 3.54 (t, *J* = 7.0 Hz, 2H), 3.07 (s, 2H), 1.88 (dd, *J* = 13.8, 6.9 Hz, 2H), 1.80 – 1.73 (m, 2H).

^{13}C NMR (101 MHz, CDCl$_3$) δ 170.0, 136.0, 130.6, 129.2, 129.1, 128.1, 127.1, 126.6, 102.6, 100.7, 98.3, 48.9, 45.9, 25.8, 24.4.

HRMS (ESI) m/z calcd. for [C$_{15}$H$_{13}$Br$_3$N$_2$O -H]$^-$ 472.85052; found, 472.85027.

N-(2-((4-hydroxy-3-methoxybenzyl)amino)ethyl)-2-(1H-pyrrol-2-yl)benzamide (M7)

Compound **M7** was synthesized following the general procedure. Flash chromatography (SiO2, 1:1 v/v petroleum ether–EtOAc) afforded the product (19.0 mg, 52%) as an orange amorphous solid.

^{1}H NMR (400 MHz, CDCl$_3$) δ 10.37 (s, 1H), 7.59 (d, *J* = 8.1 Hz, 1H), 7.38 (d, *J* = 7.3 Hz, 2H), 7.19 (t, *J* = 7.4 Hz, 1H), 6.79 (d, *J* = 8.5 Hz, 3H), 6.71 (d, *J* = 8.1 Hz, 1H), 6.51 (s, 1H), 6.45 (s, 1H), 6.23 (s, 1H), 3.75 (s, 3H), 3.67 (s, 2H), 3.45 (d, *J* = 4.8 Hz, 2H), 2.75 (t, *J* = 5.5 Hz, 2H).

^{13}C NMR (101 MHz, CDCl$_3$) δ 171.9, 146.7, 145.0, 133.2, 131.2, 130.6, 130.3, 129.0, 128.1, 126.1, 121.3, 119.4, 114.4, 110.9, 109.2, 108.6, 55.8, 53.2, 47.7, 39.3.

HRMS (ESI) m/z calcd. for [C$_{21}$H$_{23}$N$_3$O$_3$-H]$^-$ 364.16667; found, 364.16636.

N-(2-((4-hydroxy-3-methoxybenzyl)amino)ethyl)-2-(3,4,5-tribromo-1H-pyrrol-2-yl)benzamide (M8)

Compound **M8** was synthesized following the general procedure. Flash chromatography (SiO2, 1:2 v/v petroleum ether–EtOAc) afforded the product (36.5 mg, 61%) as a light-brown solid, mp: 85-86°C.

^{1}H NMR (400 MHz, CDCl$_3$) δ 10.40 (s, 1H), 7.74 (d, J = 7.7 Hz, 0.23H, rotamer a), 7.69 (d, J = 7.7 Hz, 0.77H, rotamer b), 7.47 (dd, *J* = 15.5, 7.6 Hz, 2H), 7.34 (t, *J* = 7.6 Hz, 1H), 6.88 – 6.79 (m, 1H), 6.77 (s, 1H), 6.73 (d, *J* = 8.0 Hz, 1H), 6.47 (bs, 0.6H, rotamer b), 6.37 (bs, 0.4H, rotamer a), 3.81 (s, 3H), 3.66 (d, *J* = 5.8 Hz, 2H), 3.42 – 3.32 (m, 2H), 2.74-2.68 (m, 2H).

^{13}C NMR (101 MHz, CDCl$_3$) δ 170.6, 170.2, 146.6, 146.6, 145.2, 135.4, 131.5, 130.3, 129.7, 129.1, 128.6, 128.4, 128.2, 128.1, 121.6, 118.4, 114.3, 111.3, 100.7, 62.8, 55.9, 53.1, 50.8, 47.5, 47.3, 39.0, 29.7.

HRMS (ESI) m/z calcd. for [C$_{21}$H$_{20}$Br$_3$N$_3$O$_3$-H]$^-$ 597.89820; found, 597.89785.

N-(prop-2-yn-1-yl)-2-(1H-pyrrol-2-yl)benzamide (M10)

Compound **M10** (16.8 mg, 75%) was synthesized following the general procedure as a brown solid, mp: 91-92°C.

^{1}H NMR (400 MHz, CDCl₃) δ 10.05 (s, 1H), 7.61 (d, *J* = 7.8 Hz, 1H), 7.42 (dd, *J* = 9.7, 7.9 Hz, 2H), 7.23 (dd, *J* = 13.9, 6.4 Hz, 1H), 6.85 (s, 1H), 6.47 (s, 1H), 6.26 (d, *J* = 2.8 Hz, 1H), 6.07 (s, 1H), 4.13 (dd, *J* = 5.2, 2.5 Hz, 2H), 2.23 (t, *J* = 2.4 Hz, 1H).

^{13}C NMR (101 MHz, CDCl₃) δ 171.4, 132.3, 131.4, 130.7, 130.4, 129.1, 128.1, 126.1, 119.6, 109.3, 108.8, 78.8, 72.1, 29.9.

HRMS (ESI) m/z calcd. for [C₁₄H₁₂N₂O -H]⁻ 223.08769; found, 223.08765.

N-Benzyl-2-(1H-pyrrol-2-yl)-benzamide (M11)

Compound **M11** (21.0 mg, 76%) was synthesized following the general procedure as a beige solid, mp: 109-110°C.

^{1}H NMR (400 MHz, CDCl₃) δ 10.10 (s, 1H), 7.61 (d, *J* = 7.8 Hz, 1H), 7.49 – 7.36 (m, 2H), 7.34 – 7.24 (m, 3H), 7.20 (t, *J* = 7.9 Hz, 3H), 6.81 (s, 1H), 6.47 (s, 1H), 6.26 (d, *J* = 2.6 Hz, 1H), 6.13 (s, 1H), 4.54 (d, *J* = 5.7 Hz, 2H).

^{13}C NMR (101 MHz, CDCl₃) δ 171.8, 137.4, 133.2, 131.3, 130.6, 130.4, 129.0, 128.8, 127.8, 127.7, 127.7, 126.0, 119.5, 109.2, 108.6, 44.3.

The spectral data are consistent with those reported in the literature.[23]

N-propyl-2-(1H-pyrrol-2-yl)benzamide (M12)

Compound **M12** (16.9 mg, 74%) was synthesized following the general procedure as a beige solid, mp: 109-110°C.

^{1}H NMR (400 MHz, CDCl₃) δ 10.21 (s, 1H), 7.61 (d, *J* = 8.3 Hz, 1H), 7.40 (dd, *J* = 7.2, 5.0 Hz, 2H), 7.21 (t, *J* = 7.5 Hz, 1H), 6.84 (d, *J* = 1.3 Hz, 1H), 6.47 (s, 1H), 6.26 (dd, *J* = 5.5, 2.7 Hz, 1H), 5.87 (s, 1H), 3.33 (dd, *J* = 13.5, 6.7 Hz, 2H), 1.53 (dd, *J* = 14.6, 7.3 Hz, 2H), 0.90 (t, *J* = 7.4 Hz, 3H).

^{13}C NMR (101 MHz, CDCl₃) δ 172.1, 133.6, 131.2, 130.8, 130.2, 128.9, 127.8, 125.8, 119.4, 109.1, 108.4, 41.9, 22.6, 11.3.

HRMS (ESI) m/z calcd. for [C₁₄H₁₆N₂O -H]⁻ 227.11899; found, 227.11897.

N-(prop-2-yn-1-yl)-2-(3,4,5-tribromo-1H-pyrrol-2-yl)benzamide (M13)

Compound **M13** (40.3 mg, 88%) was synthesized following the general procedure as a beige solid, mp: 179-180°C.

^{1}H NMR (400 MHz, CDCl₃) δ 10.79 (s, 1H), 7.68 (d, *J* = 7.6 Hz, 1H), 7.50 (t, *J* = 7.2 Hz, 2H), 7.35 (t, *J* = 7.5 Hz, 1H), 5.93 (s, 1H), 4.06 (dd, *J* = 5.1, 2.4 Hz, 2H), 2.25 (d, *J* = 2.2 Hz, 1H).

^{13}C NMR (101 MHz, CDCl₃) δ 169.7, 134.5, 131.5, 130.6, 128.9, 128.5, 128.4, 128.2, 102.7, 101.2, 99.1, 78.4, 72.3, 30.0.

HRMS (ESI) m/z calcd. for [C₁₄H₉Br₃N₂O H]⁻ 456.81922; found, 456.81911.

N-benzyl-2-(3,4,5-tribromo-1H-pyrrol-2-yl)benzamide (M14)

Compound **M14** (37.2 mg, 73%) was synthesized following the general procedure as a light-brown solid, mp: 160-161°C.

^{1}H NMR (400 MHz, CDCl₃) δ 10.89 (s, 1H), 7.67 (d, *J* = 7.7 Hz, 1H), 7.52 – 7.44 (m, 2H), 7.36 – 7.27 (m, 4H), 7.12 (d, *J* = 7.0 Hz, 2H), 6.04 (s, 1H), 4.44 (d, *J* = 5.6 Hz, 2H).

^{13}C NMR (101 MHz, CDCl₃) δ 170.2, 136.9, 135.4, 131.3, 130.2, 129.1, 128.9, 128.4, 128.3, 127.9, 127.8, 127.6, 102.6, 101.0, 98.9, 44.4.

HRMS (ESI) m/z calcd. for [C₁₈H₁₃Br₃N₂O -H]⁻ 508.85052; found, 508.85041.

N-propyl-2-(3,4,5-tribromo-1H-pyrrol-2-yl)benzamide (M15)

Compound **M15** (40.2 mg, 87%) was synthesized following the general procedure as a brown solid, mp: 147-148°C.

^{1}H NMR (400 MHz, CDCl$_3$) δ 11.28 (s, 1H), 7.65 (d, *J* = 7.7 Hz, 1H), 7.50 – 7.41 (m, 2H), 7.31 (t, *J* = 7.6 Hz, 1H), 5.71 (s, 1H), 3.19 (dd, *J* = 13.4, 6.7 Hz, 2H), 1.40 (dd, *J* = 14.5, 7.3 Hz, 2H), 0.83 (t, *J* = 7.4 Hz, 3H).

^{13}C NMR (101 MHz, CDCl$_3$) δ 170.1, 135.5, 131.2, 130.1, 129.3, 128.4, 128.2, 128.2, 102.3, 101.0, 98.7, 41.9, 22.6, 11.2.

HRMS (ESI) m/z calcd. for [C$_{14}$H$_{13}$Br$_3$N$_2$O -H]$^-$ 460.85052; found, 460.85051.
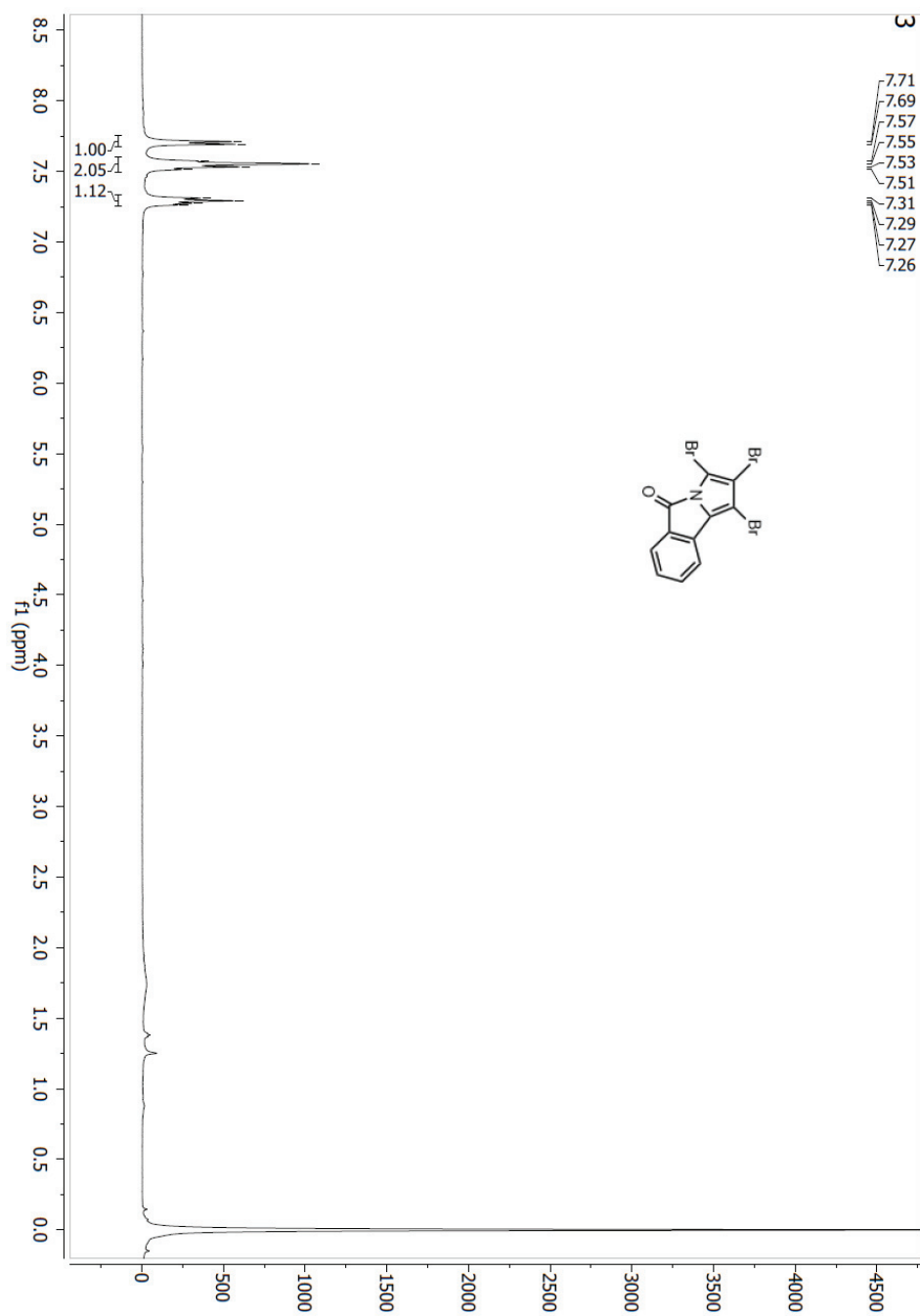
Fig S1. Compound **3** - ^{1}H NMR spectrum (400 MHz, CDCl$_3$)
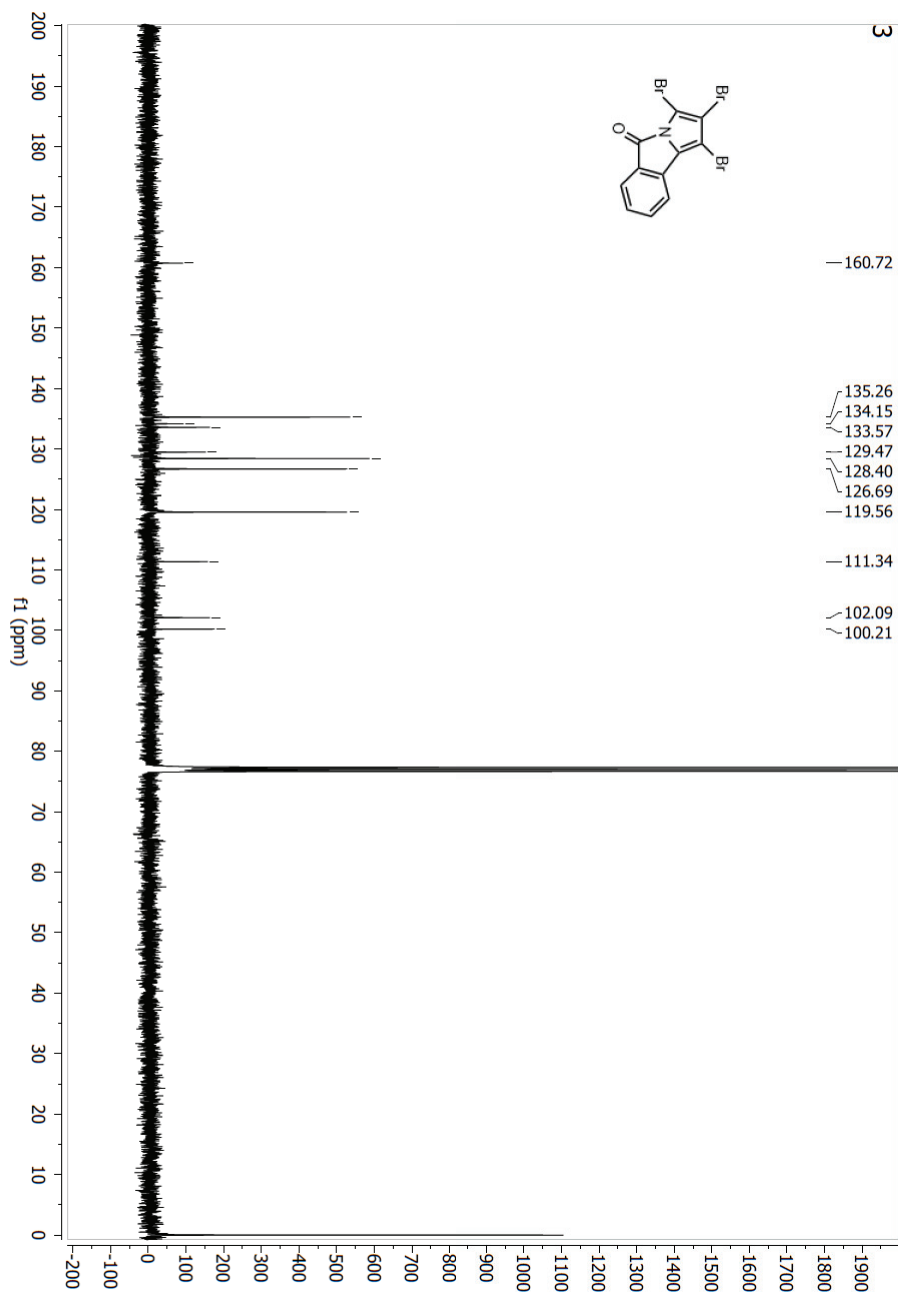
Fig S2. Compound **3** - ^{13}C NMR spectrum (101 MHz, CDCl$_3$)

PETKOVIĆ *et al.*
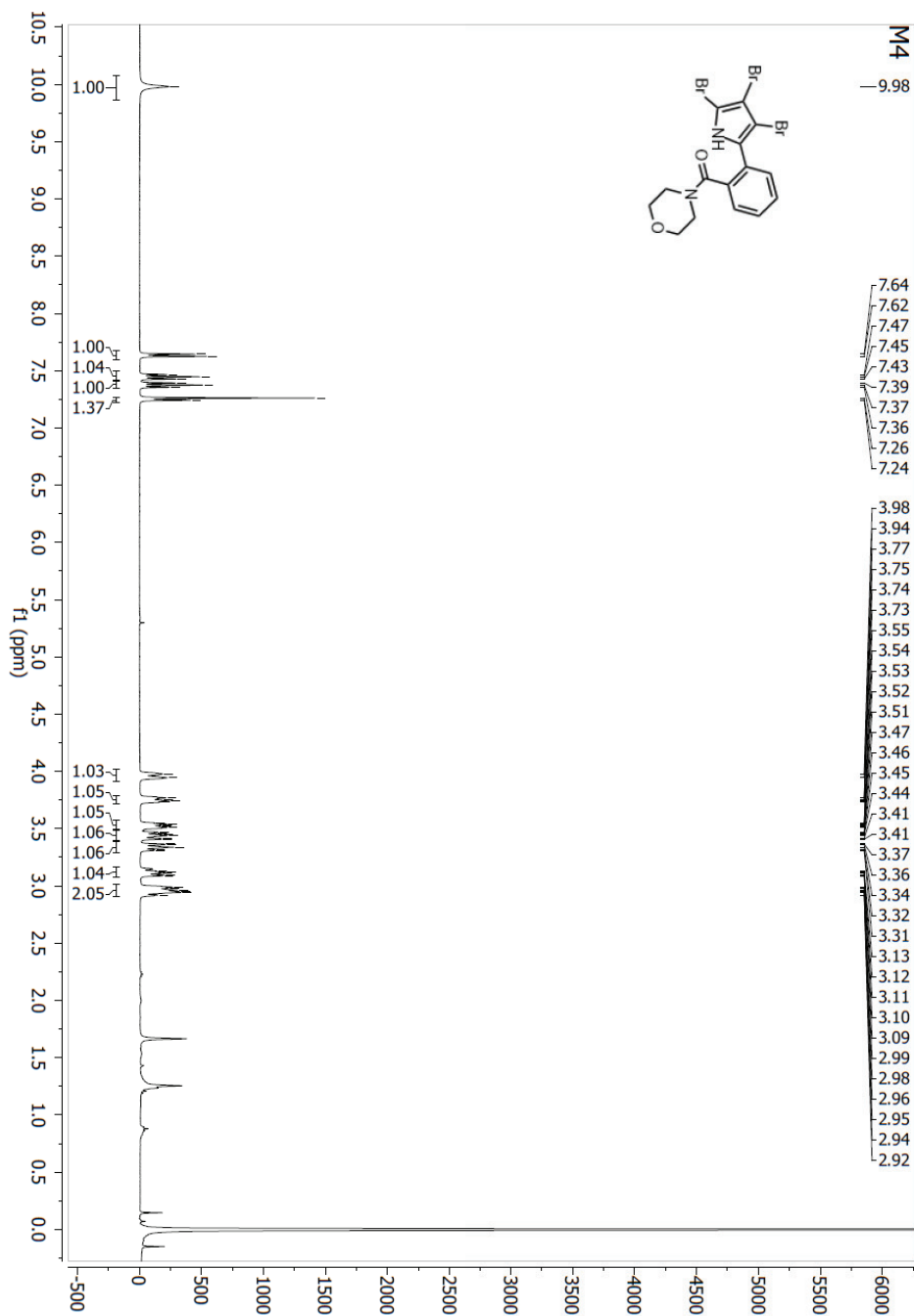
Fig S3. Compound **M4** - ^{1}H NMR spectrum (400 MHz, CDCl₃)
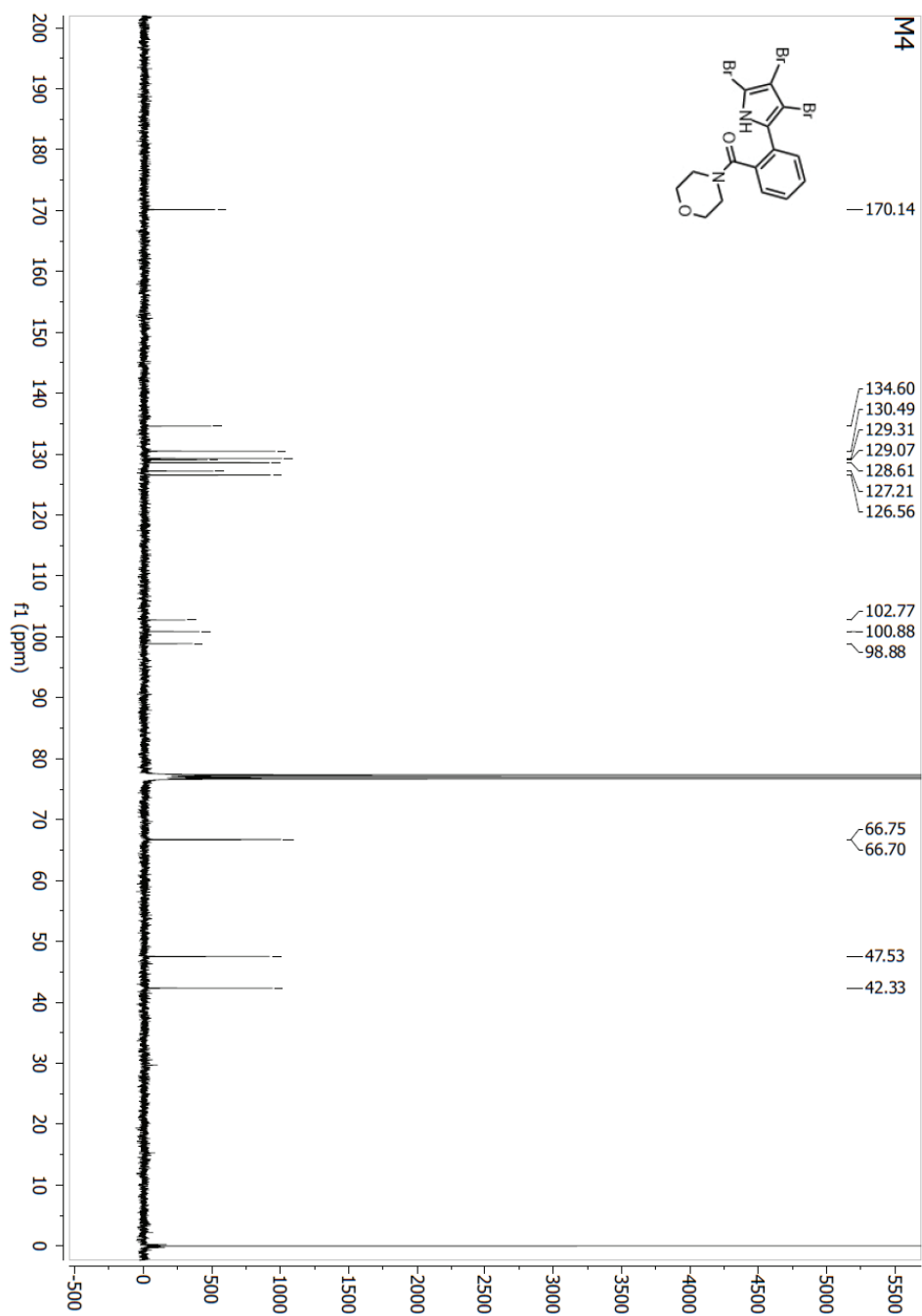
Fig S4. Compound **M4** - ^{13}C NMR spectrum (101 MHz, CDCl$_3$)
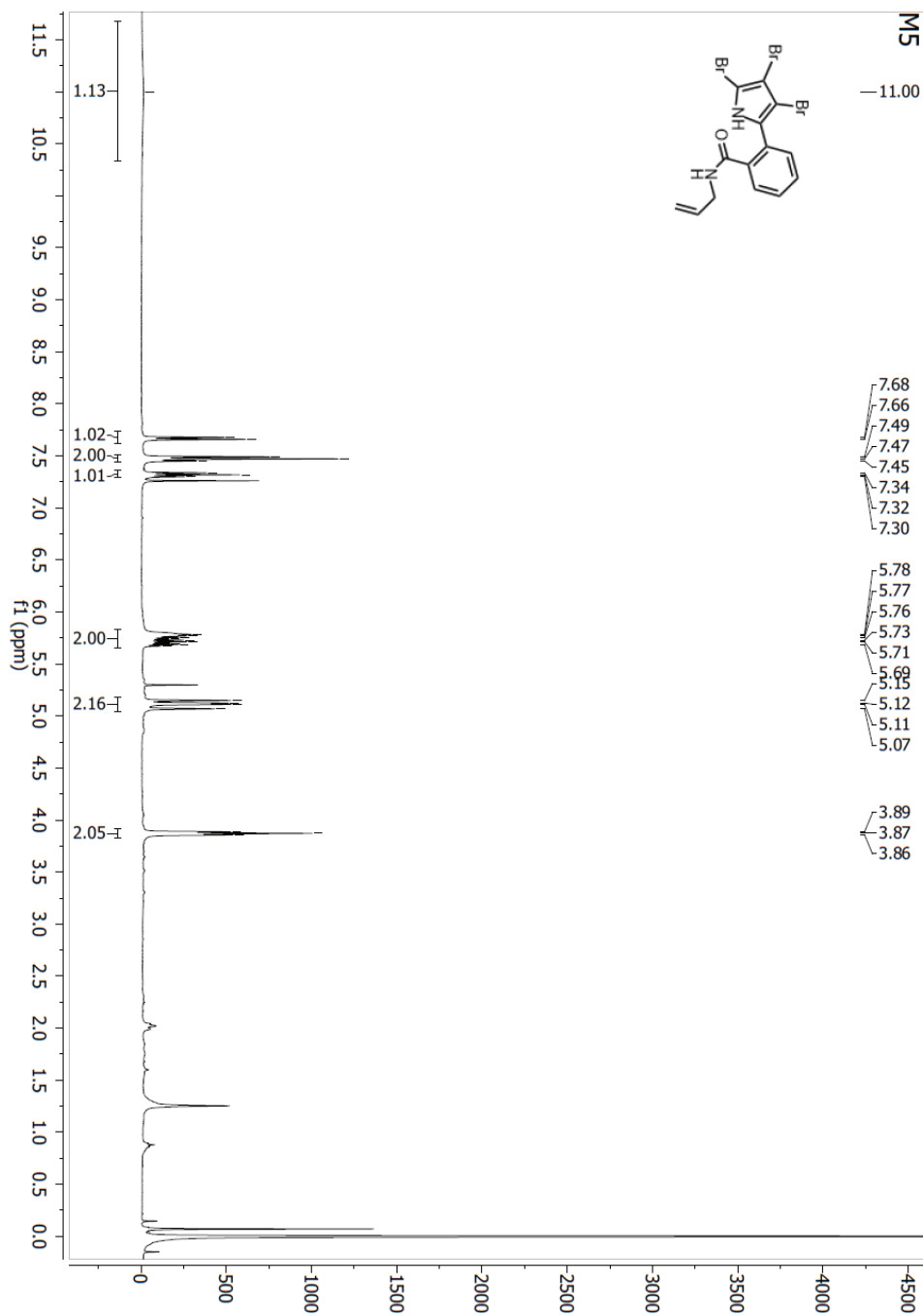
Fig S5. Compound **M5** - ^{1}H NMR spectrum (400 MHz, CDCl$_3$)
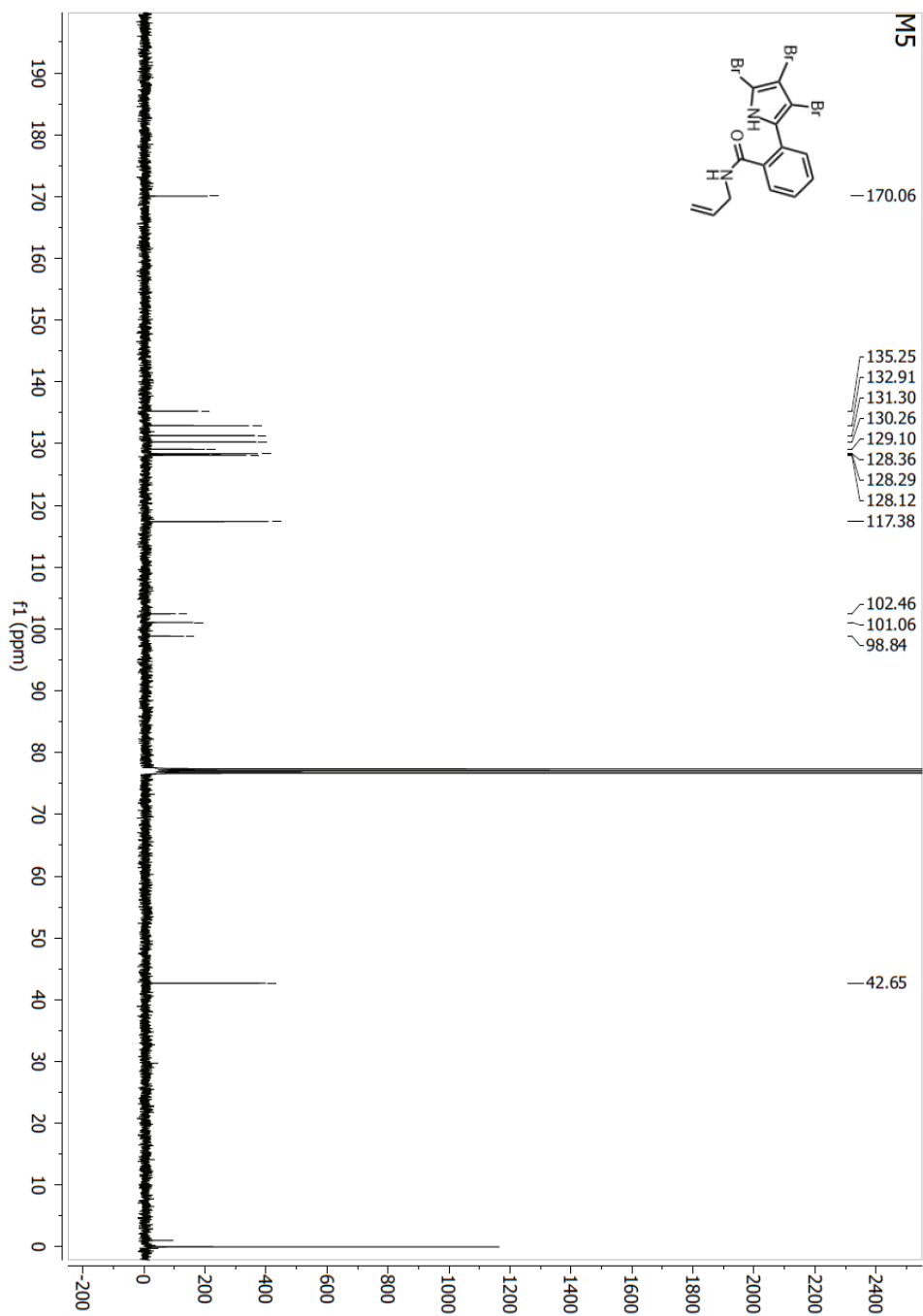
Fig S6. Compound **M5** - ^{13}C NMR spectrum (101 MHz, CDCl$_3$)

M6

—10.41

7.75
7.73
7.46
7.44
7.42
7.37
7.36
7.34
7.31
7.29

3.56
3.54
3.53

—3.07

1.91
1.89
1.87
1.86
1.79
1.77
1.76

1.00

1.00
1.04
1.09
1.00

2.05

1.95

2.07
2.34

f1 (ppm)
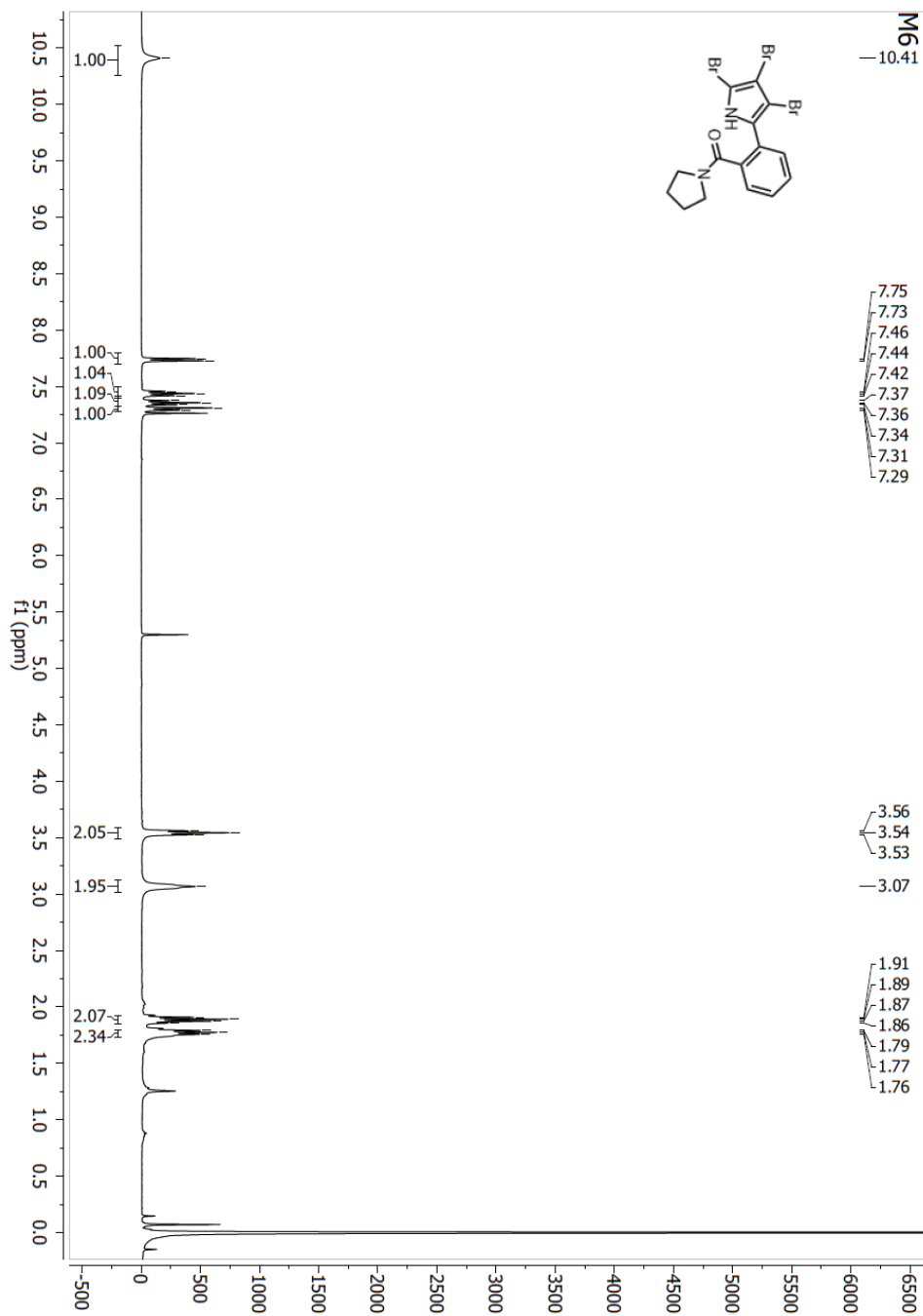
Fig S7. Compound **M6** - ^{1}H NMR spectrum (400 MHz, CDCl₃)
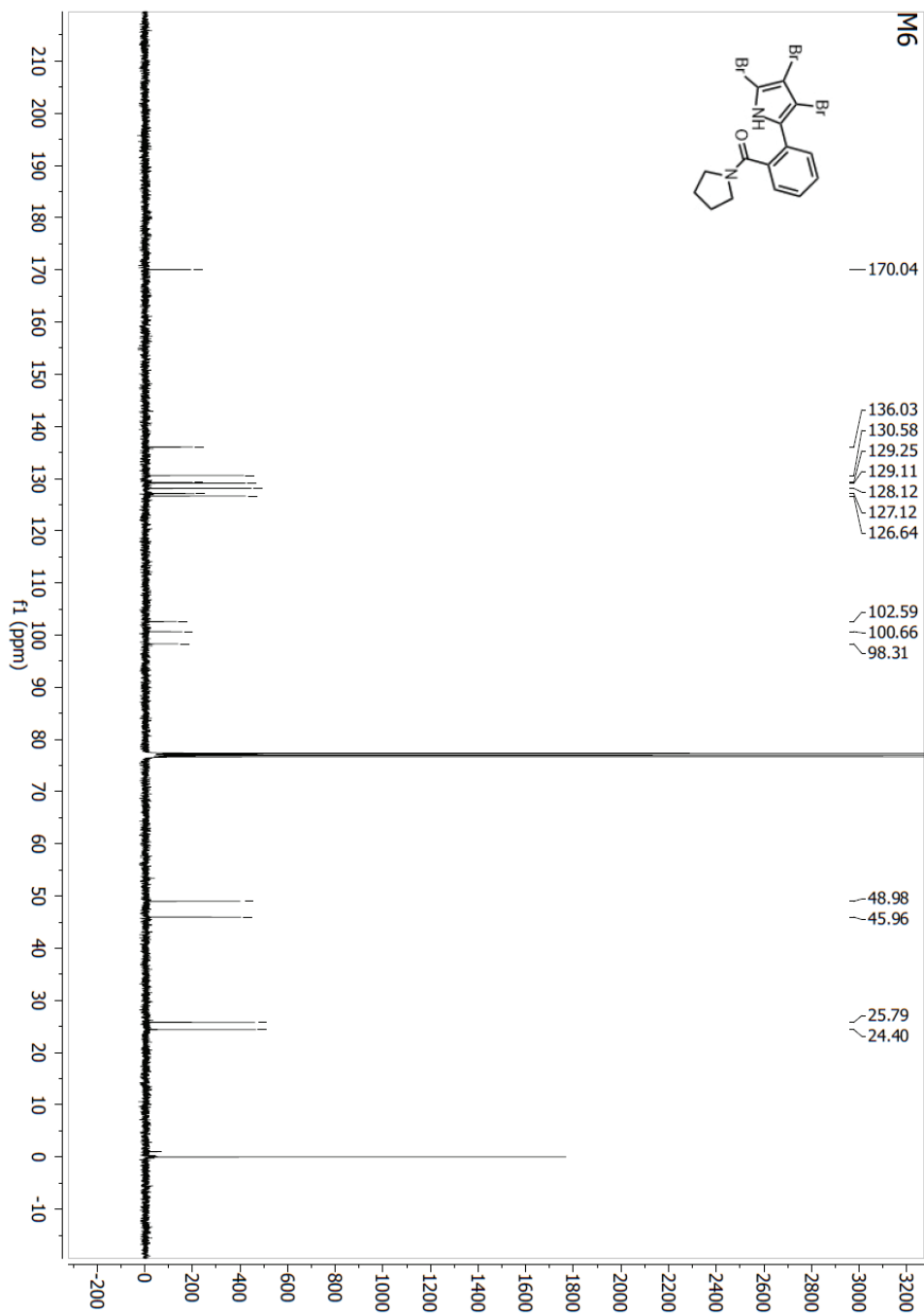
Fig S8. Compound **M6** - ^{13}C NMR spectrum (101 MHz, CDCl$_3$)
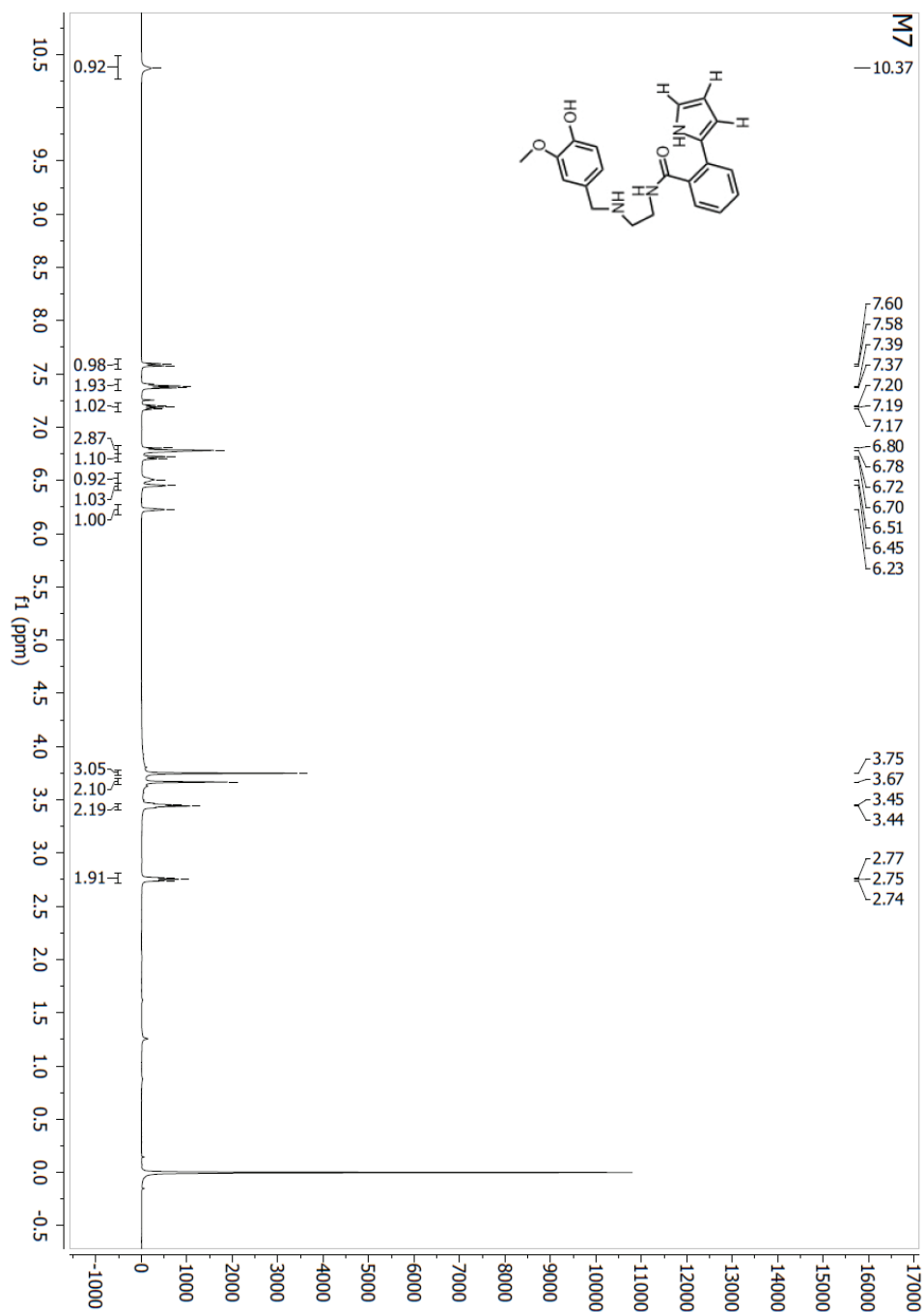
Fig S9. Compound M**7** - ^{1}H NMR spectrum (400 MHz, CDCl$_3$)
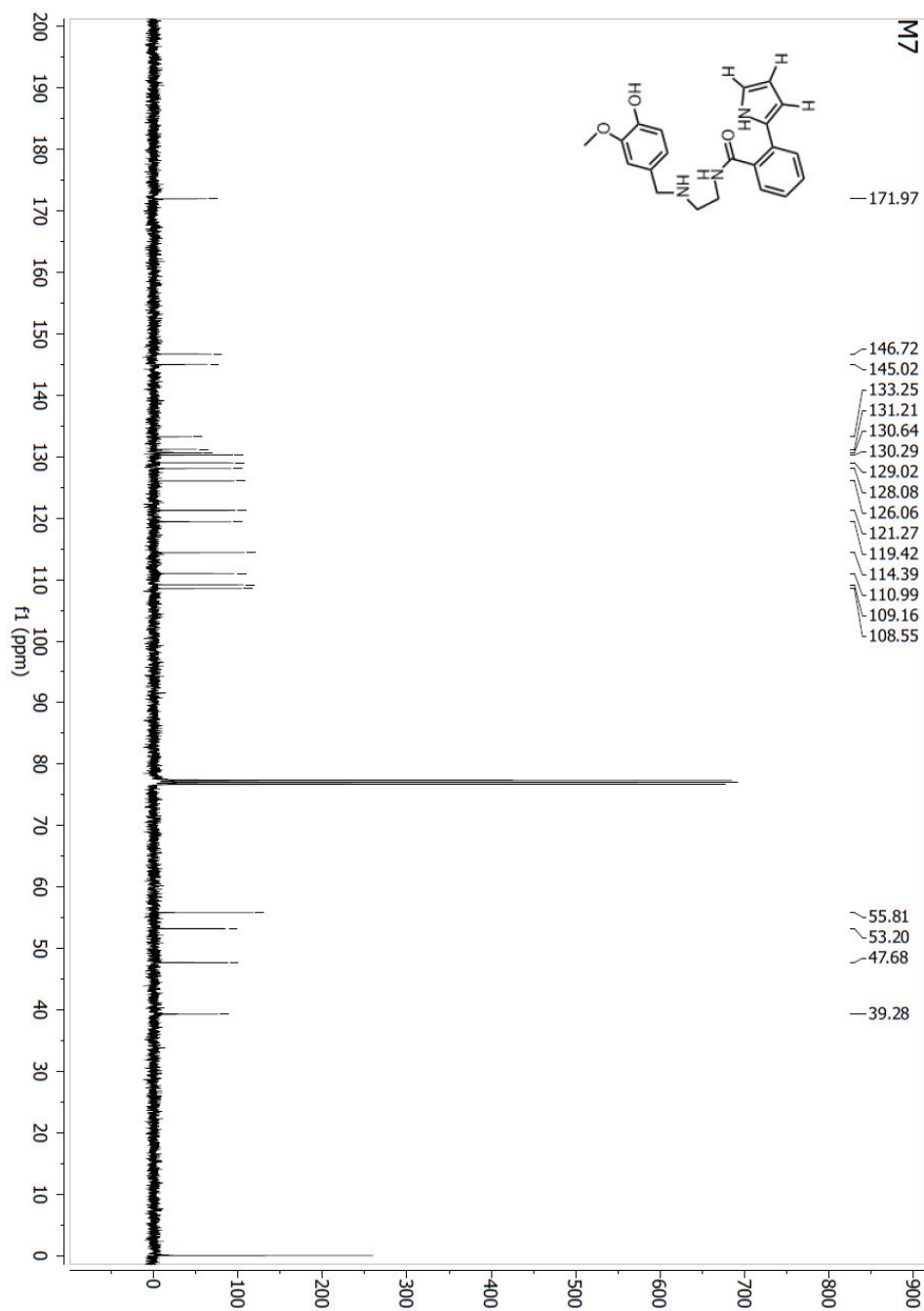
Fig S10. Compound M7 - ^{13}C NMR spectrum (101 MHz, CDCl$_3$)

M8

—10.40

7.75
7.73
7.70
7.68
7.50
7.48
7.46
7.44
7.36
7.34
7.32

6.84
6.83
6.82
6.77
6.74
6.72
6.47
6.37

3.81
3.66
3.65
3.38
3.37

2.74
2.73
2.71

0.84

0.23
0.78
1.93
1.00

1.09
0.95
1.03
0.63
0.41

2.96
1.97
2.02

2.02

f1 (ppm)
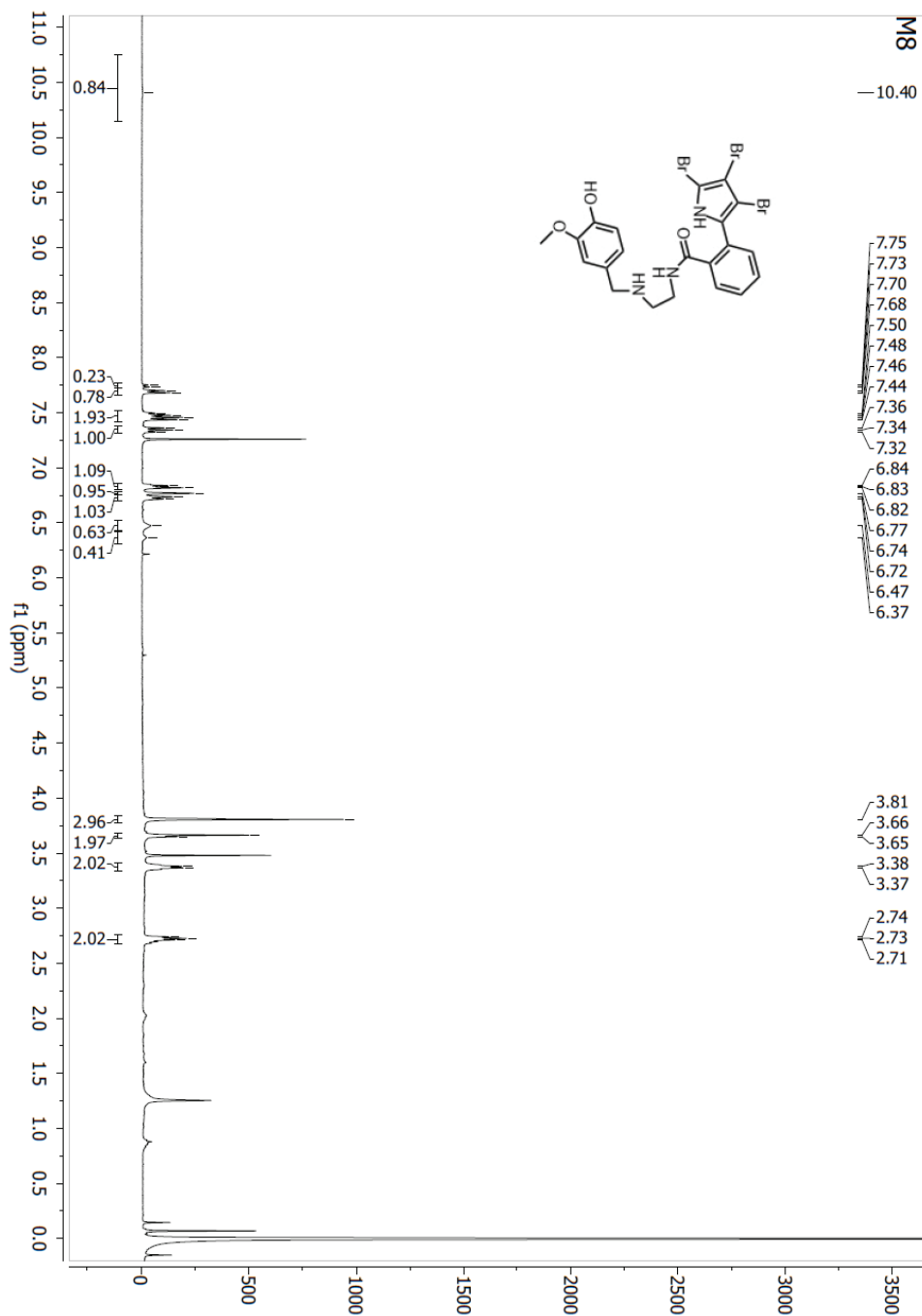
Fig S11. Compound **M8** - ¹H NMR spectrum (400 MHz, CDCl₃)
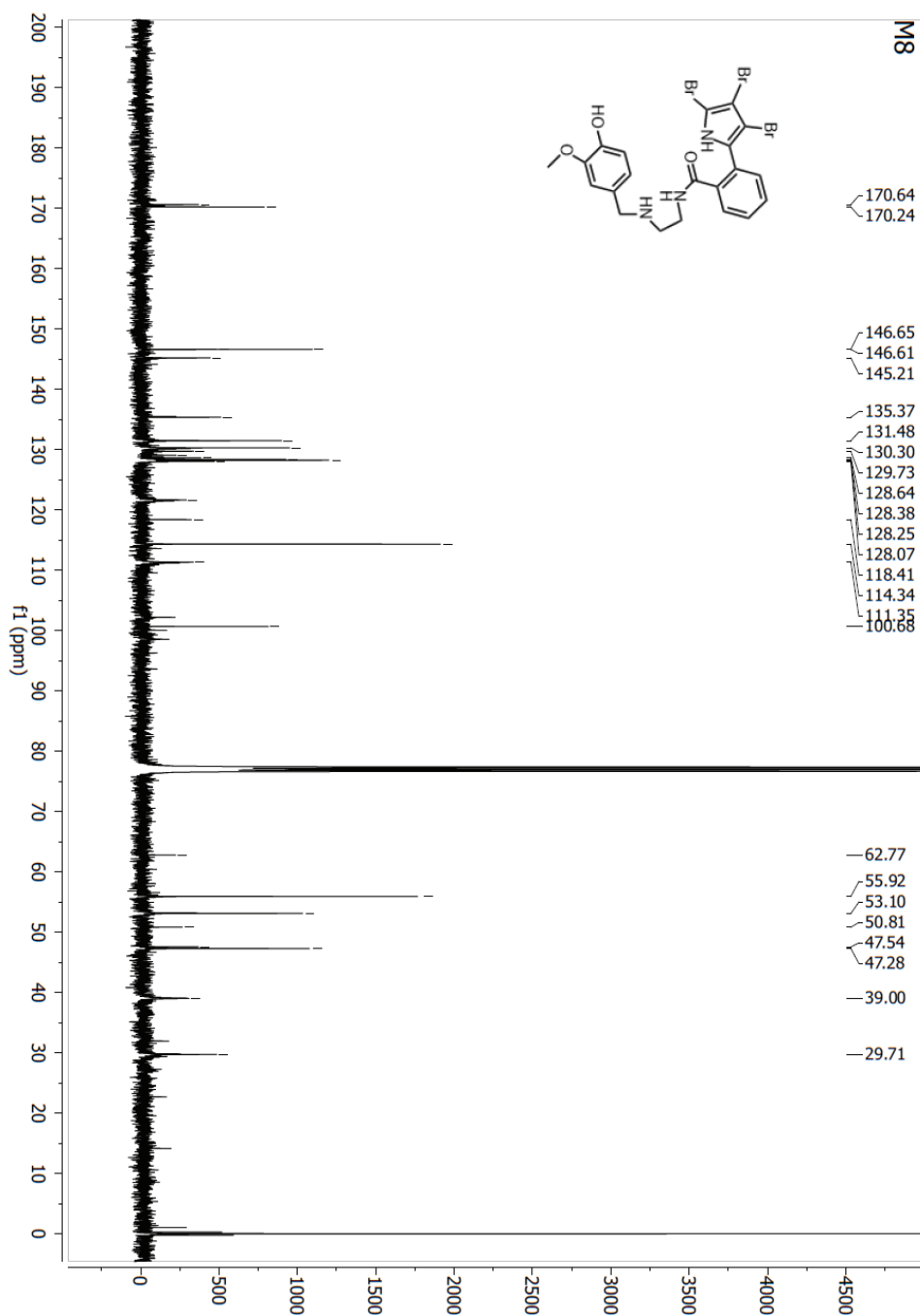
Fig S12. Compound **M8** - ^{13}C NMR spectrum (101 MHz, CDCl$_3$)
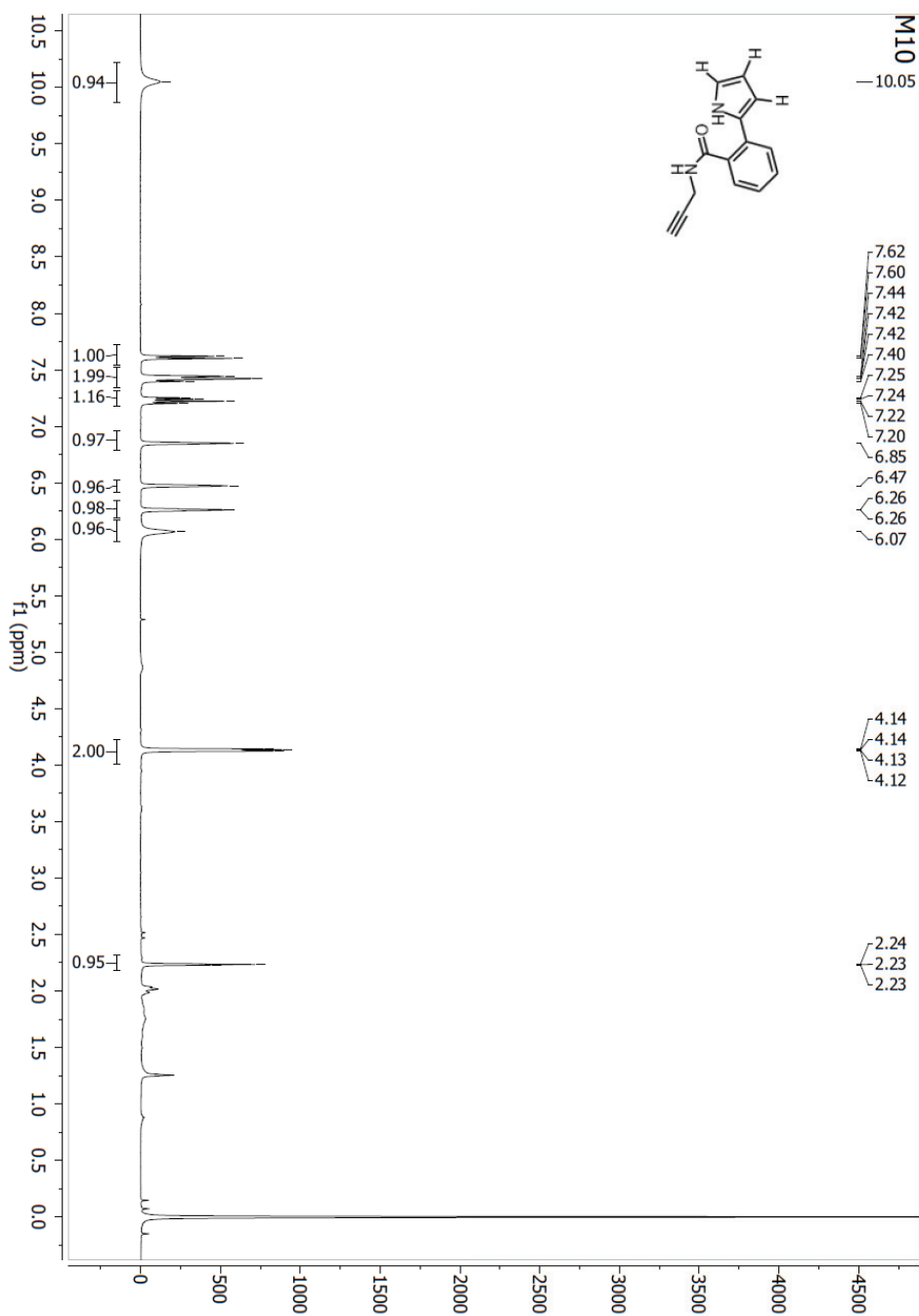
Fig S13. Compound **M10** - ^{1}H NMR spectrum (400 MHz, CDCl$_3$)
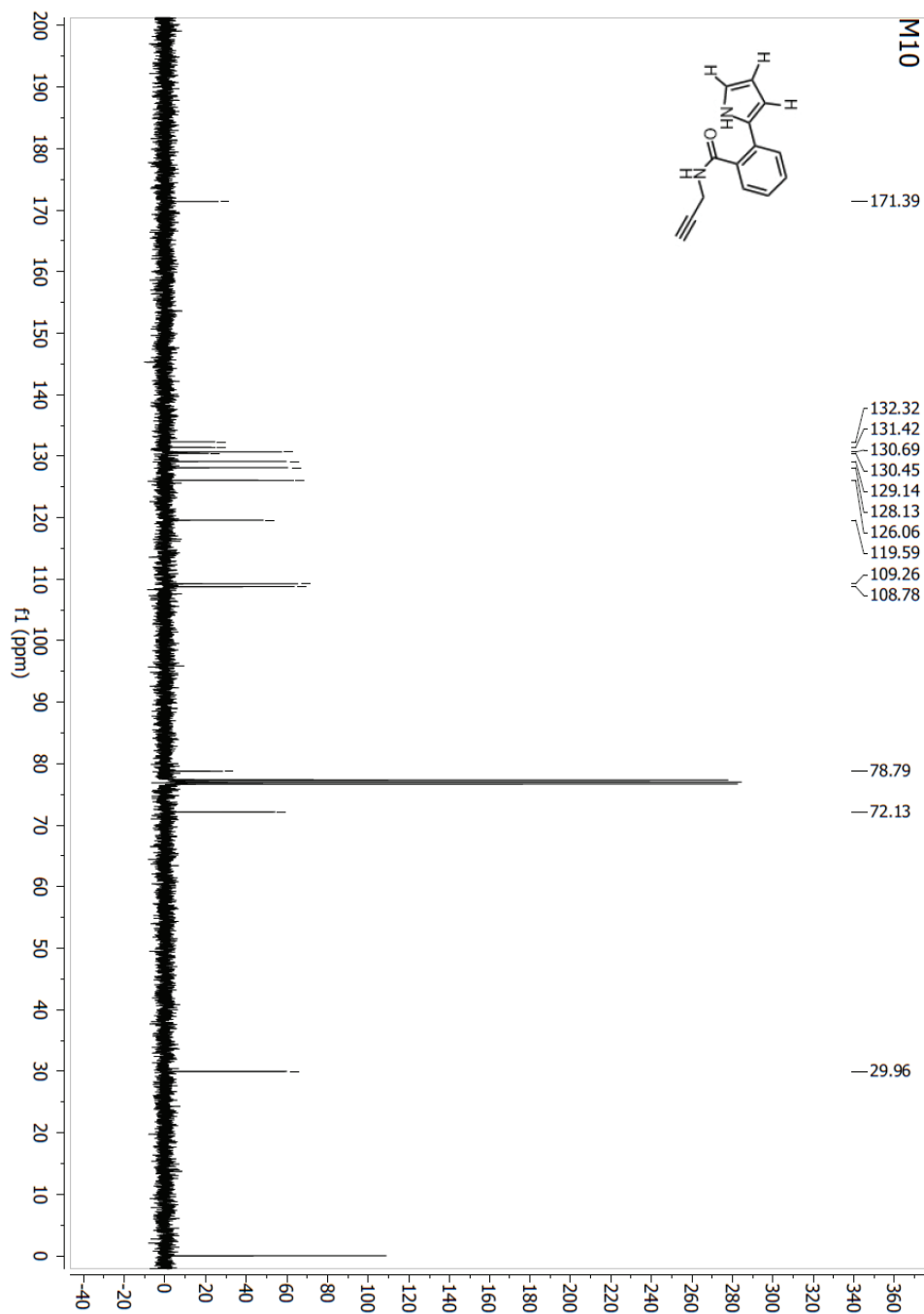
Fig S14. Compound **M10** - ^{13}C NMR spectrum (101 MHz, CDCl$_3$)

M12

— 10.21

7.62
7.60
7.42
7.41
7.40
7.39
7.23
7.21
7.19
6.85
6.84
6.47
6.27
6.26
6.25
6.24
5.87

3.35
3.33
3.32
3.30

1.56
1.54
1.52
1.50
0.92
0.90
0.88

0.93
1.03
2.02
1.03
1.00
1.01
1.00
0.94
2.01
2.12
3.10

f1 (ppm)
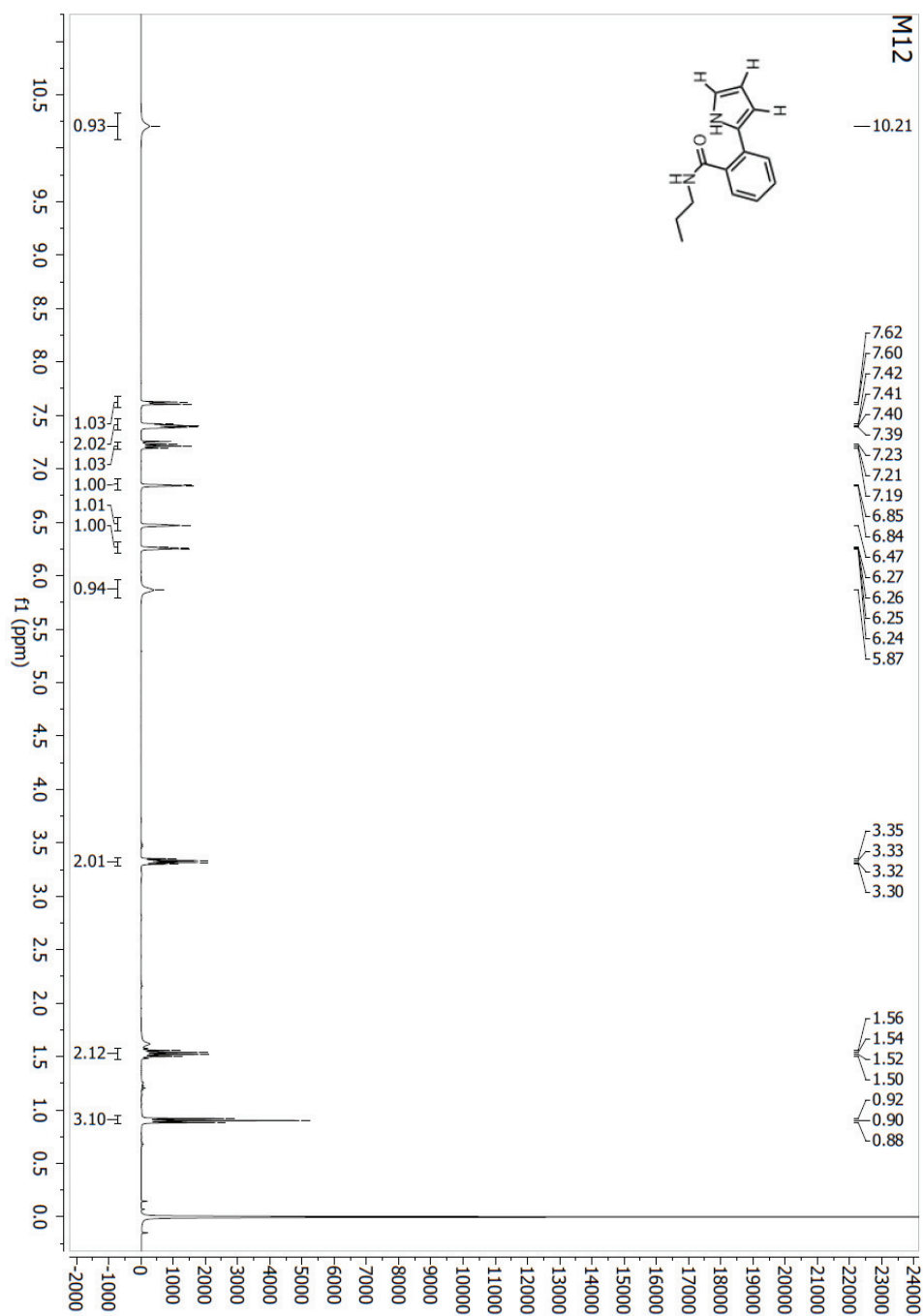
Fig S15. Compound **M12** - ^{1}H NMR spectrum (400 MHz, CDCl$_3$)
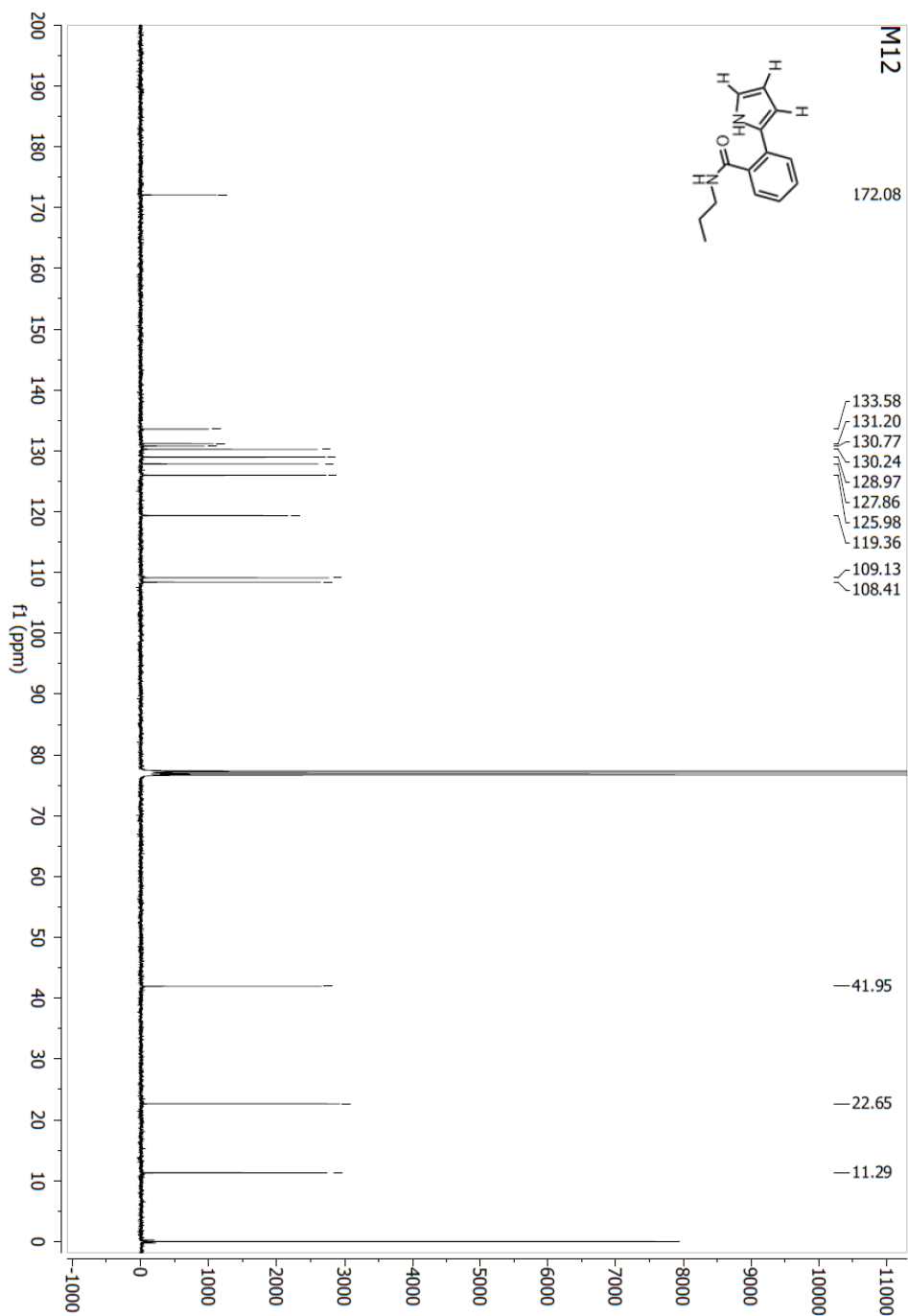
Fig S16. Compound **M12** - ^{13}C NMR spectrum (101 MHz, CDCl₃)
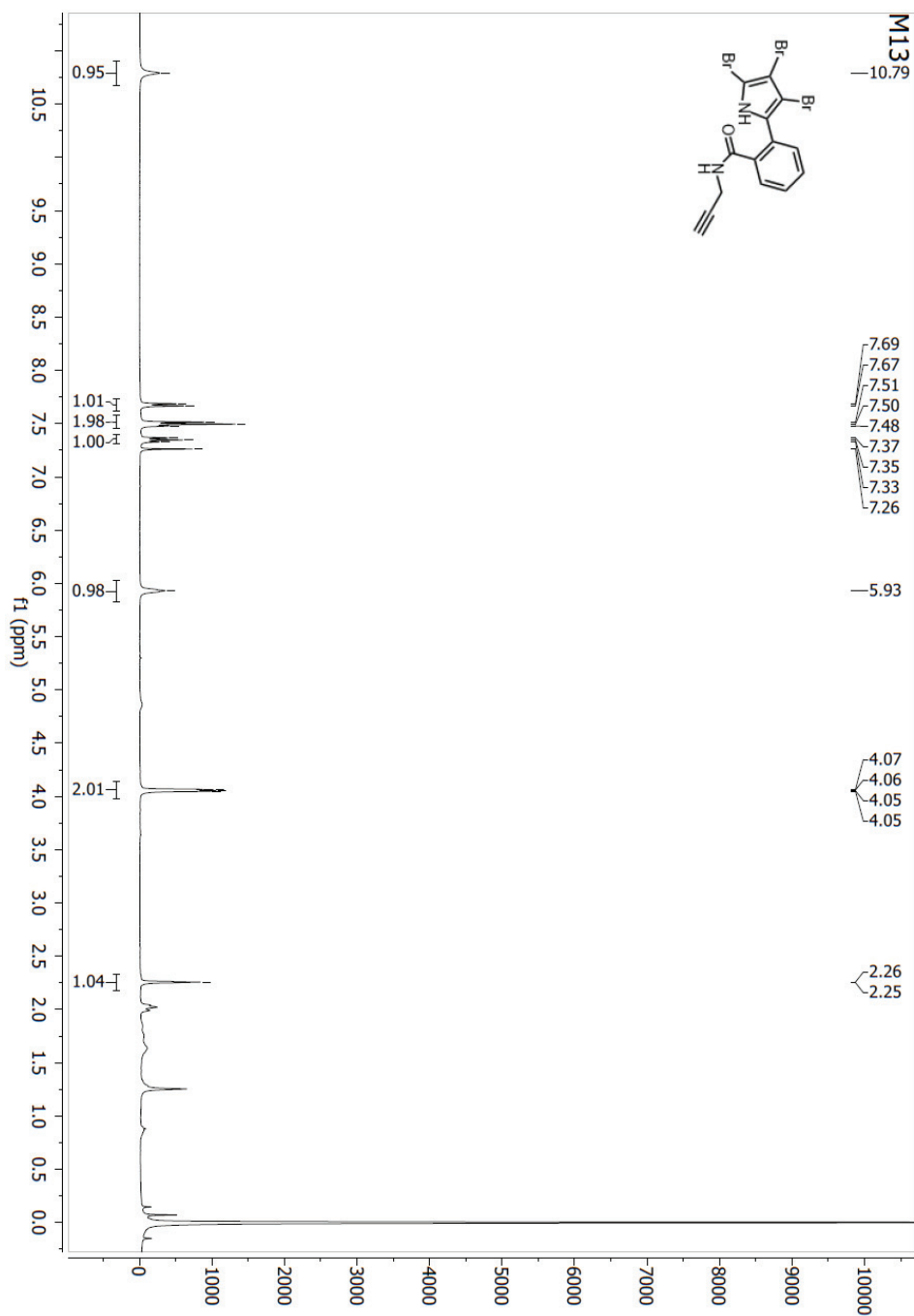
Fig S17. Compound **M13** - ^{1}H NMR spectrum (400 MHz, CDCl$_3$)
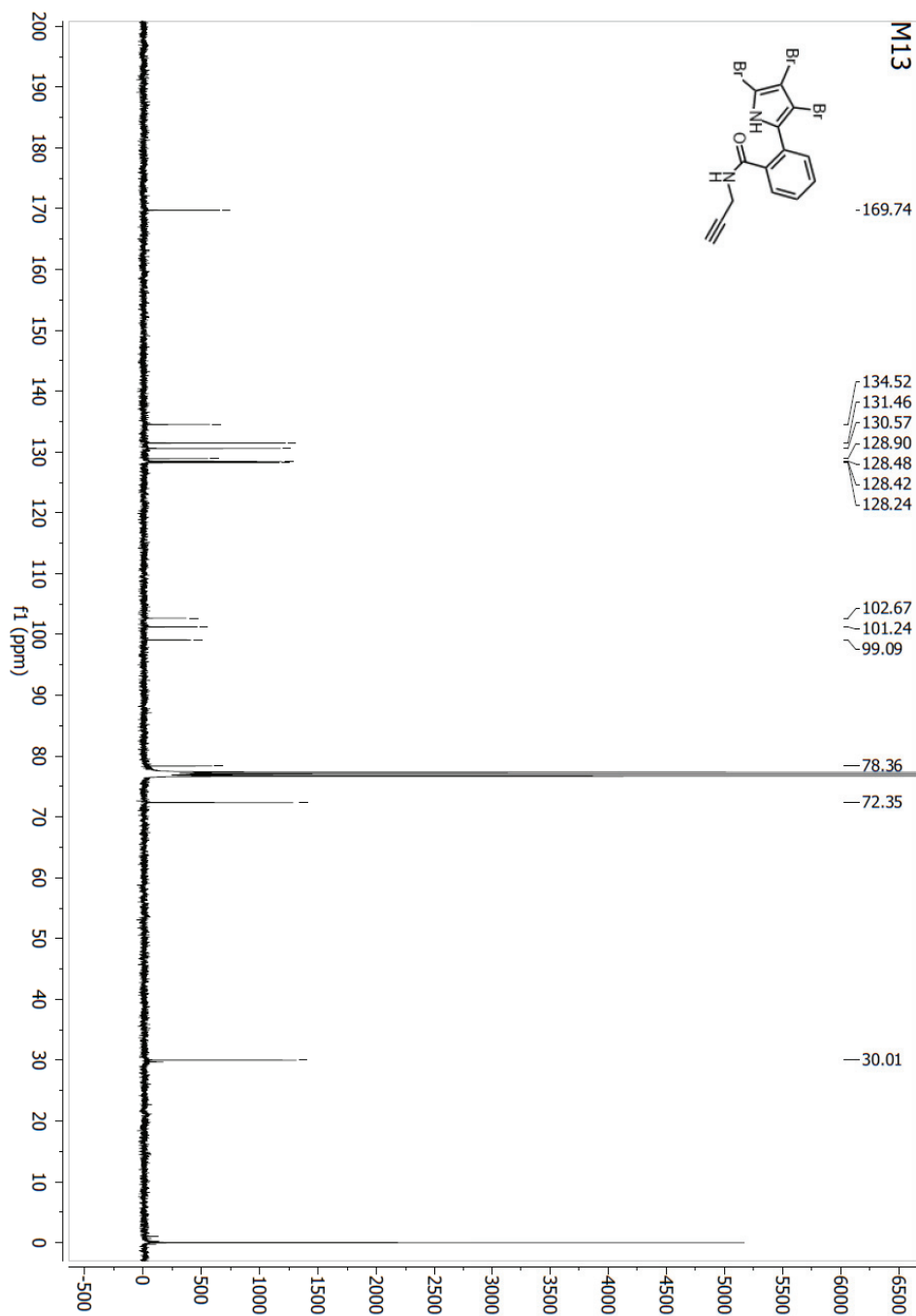
Fig S18. Compound **M13** - ^{13}C NMR spectrum (101 MHz, CDCl$_3$)
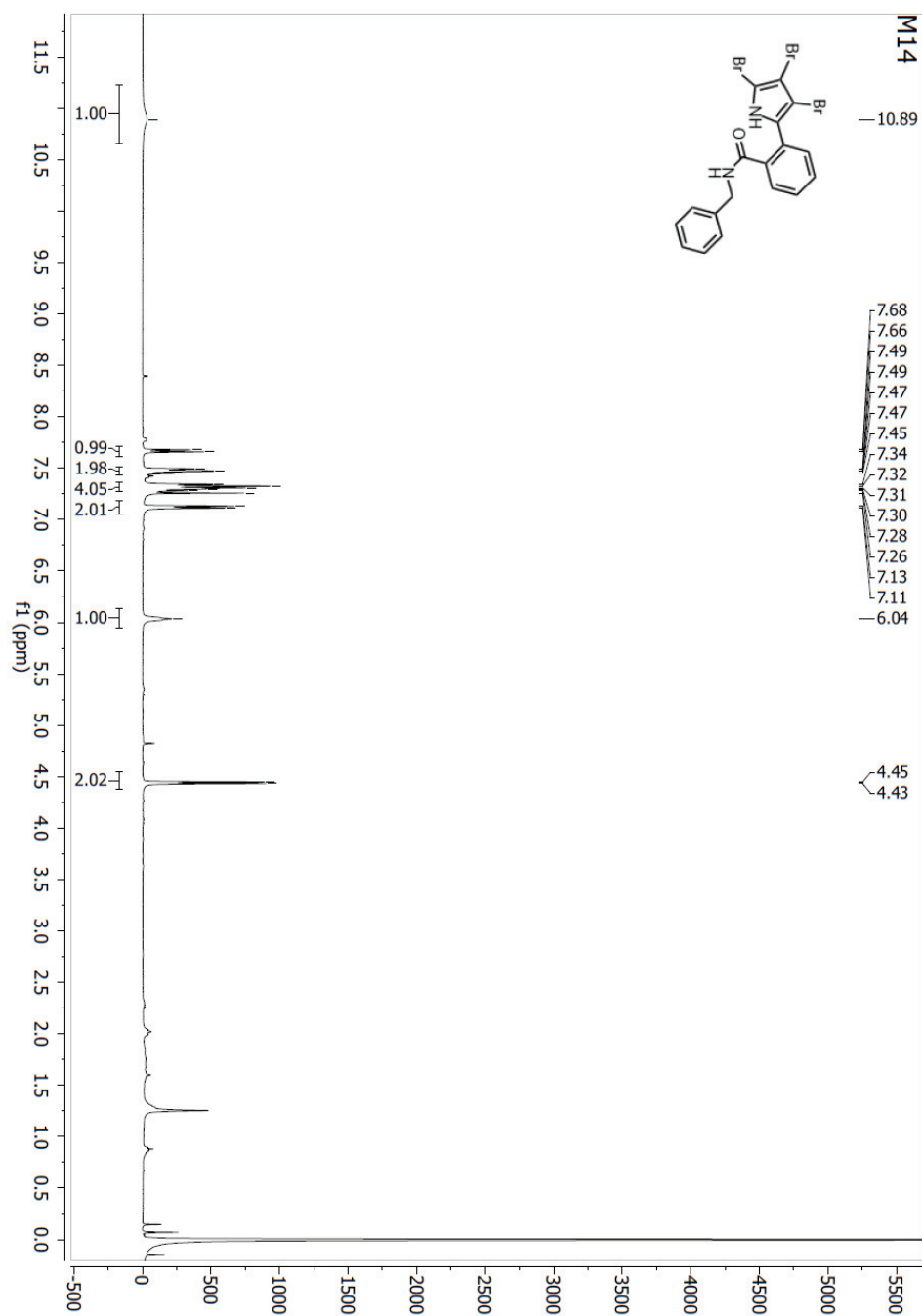
Fig S19. Compound **M14** - ¹H NMR spectrum (400 MHz, CDCl₃)
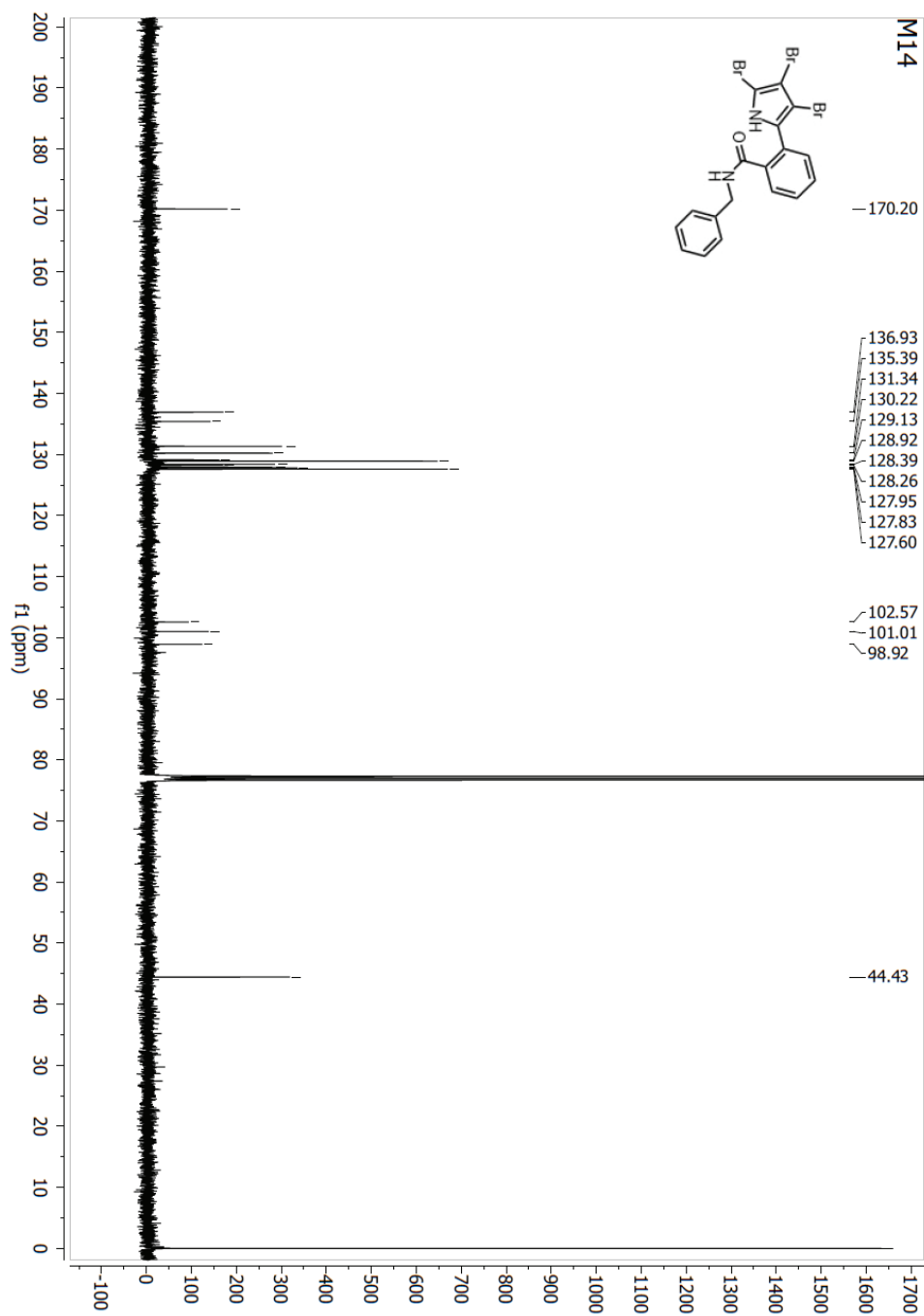
Fig S20. Compound **M14** - ^{13}C NMR spectrum (101 MHz, CDCl$_3$)
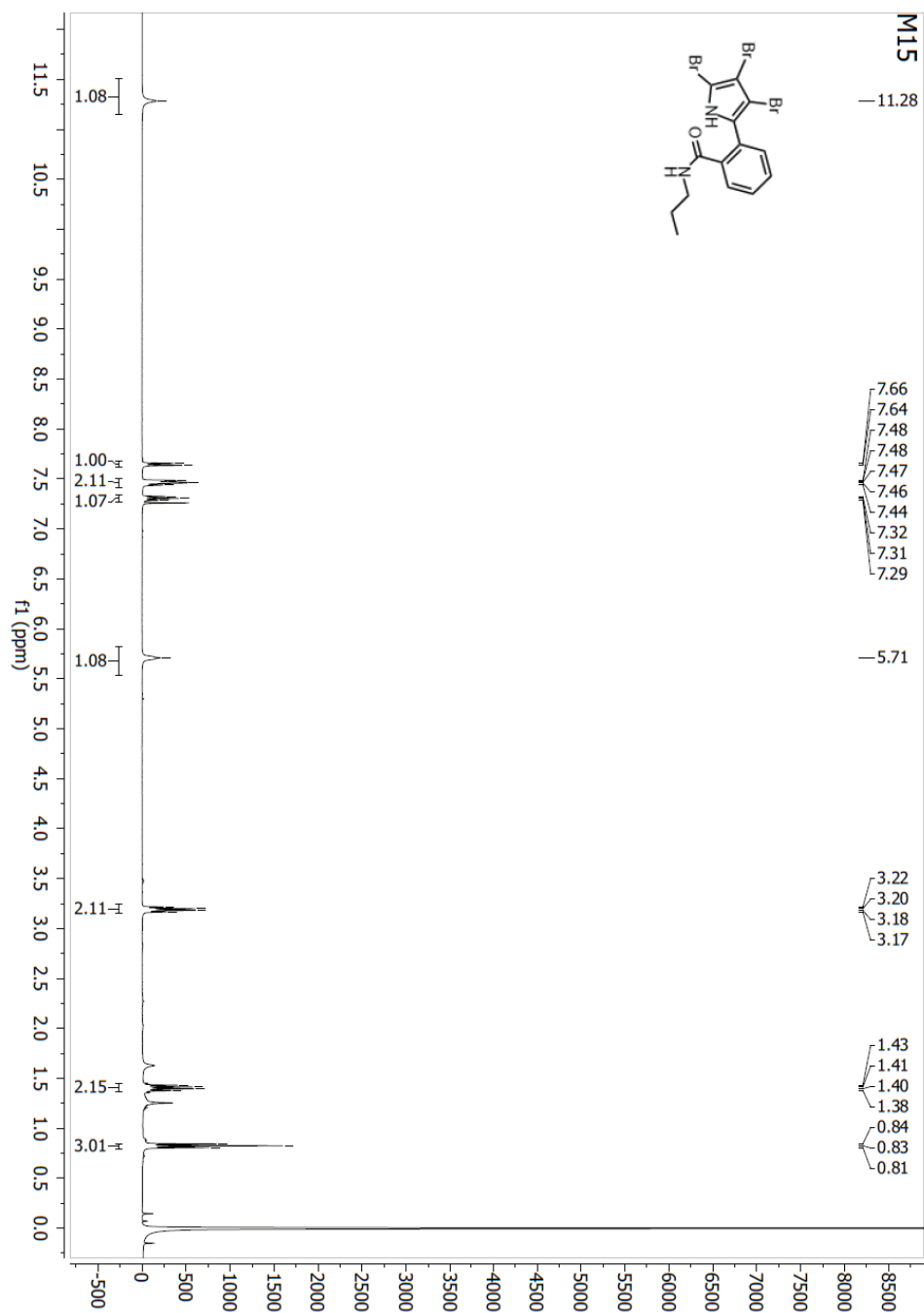
Fig S21. Compound **M15** - ^{1}H NMR spectrum (400 MHz, CDCl₃)
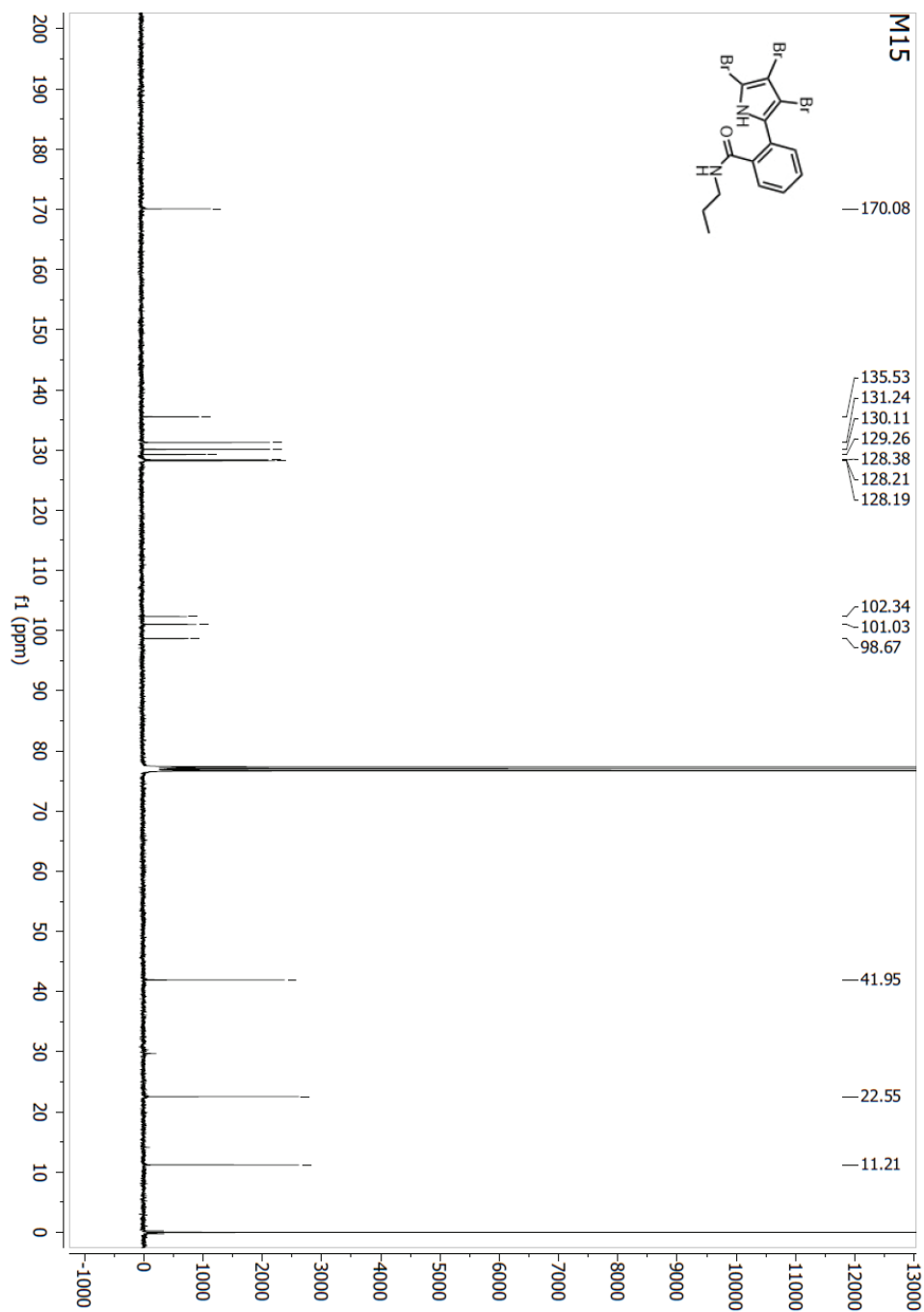
Fig S22. Compound **M15** - ^{13}C NMR spectrum (101 MHz, CDCl$_3$)

Table SI. Redox status parameters in serum pool after incubation with 15 new substances with or without TBH

Sample	PAB (U/L)	TOS (umol/L)	TAS (μmol/L)	SHG (mmol/L)
Blank (serum + H₂O)	100.7 ± 10.7	36.2±19.8	633±80	0.179±0.035
M1	66.8 ± 1.0*	23.5±3.1	923±29	0.280±0.012
M2	27.2 ± 1.5* M1	22.5±5.5	1030±23*	0.273±0.022
M3	63.0 ± 0.7* M2	18.7±0.7	896±8	0.260±0.006
M4	77.2 ± 1.2* M2, M4	18.4±1.8	852±23	0.334±0.117 *
M5	97.2 ± 1.2 M1,M2,M3	23.8±3.5	755±33	0.252±0.021
M6	96.1 ± 1.8 M1,M2,M3	25.0±1.8	734±35	0.312±0.028
M7	44.6 ± 4.2* M5,M6	21.2±0.4	1262±28* M3,M4,M5,M6	0.251±0.053
M8	95.1 ± 0.1 M1,M2,M3,M7	21.8±2.6	1070±18*	0.224±0.013
M9	96.9 ± 1.9 M1,M2,M3,M7	19.4±3.3	1051±19*	0.252±0.004
M10	43.0 ± 3.7* M4,M5,M6,M8, M9	82.5±14.6* M1,M2,M3, M4,M5,M6, M7,M8,M9	646±67 M2,M7,M8 M9	0.330±0.121 *
M11	40.9 ± 3.5* M4,M5,M6,M8, M9	65.3±8.3	492±93 M1,M2,M3, M4,M7,M8 M9	0.282±0.053
M12	41.0 ± 5.2* M4,M5,M6,M8, M9	45.8±1.2	405±12 M1,M2,M3 M4,M5,M7 M8,M9	0.268±0.046
M13	79.7 ± 4.0 M2,M7,M10,M11 M12	51.0±1.0	280±37* M1,M2,M3 M4,M5,M6, M7,M8,M9 M10	0.241±0.004
M14	82.3 ± 3.3 M2,M7,M10,M11 M12	48.5±12.1	727±69 M7,M8	0.270±0.057
M15	85.1 ± 1.1 M2,M7,M10, M11,M12	111.9±7.8* M1,M2,M3, M4,M5,M6,	533±28 M2,M3,M7 M8,M9	0.388±0.107 *

		M7,M8,M9, M12,M13, M15		
M1+TBH	91.0 ± 1.0	51.5±1.0	858±28	0.153±0.001
M2+TBH	54.4 ± 0.7*,# M1TBH	51.5±0.3	919±30	0.141±0.003
M3+TBH	88.4 ± 0.1 M2TBH	62.3±0.9	822±56	0.127±0.042
M4+TBH	88.6 ± 0.3 M2TBH	55.1±0.1	776±25	0.160±0.001 #
M5+TBH	106.9 ± 0.2 M2TBH	50.6±4.4	757±1	0.152±0.018
M6+TBH	108.1 ± 1.1 M2TBH	59.3±0.4	703±7	0.117±0.018 #
M7+TBH	72.3 ± 0.8*,# M5TBH,M6TBH	51.9±2.8	1142±39 M4TBH,M5TBH M6TBH	0.131±0.009
M8+TBH	105.9 ± 0.2 M2TBH, M7TBH	53.7±3.4	931±14	0.132±0.037
M9+TBH	106.1 ± 1.0 M2TBH, M7TBH	53.3±7.6	842±82	0.123±0.021
M10+TBH	47.7 ± 1.0* M1TBH,M3TBH , M4TBH, M5TBH, M6TBH, M7TBH, M8TBH, M9TBH	56.6±3.3	546±25 M2TBH,M7TBH M8TBH	0.155±0.022 #
M11+TBH	62.6 ± 10.7* M1TBH, M4TBH, M5TBH, M6TBH, M8TBH, M9TBH	53.6±8.7	470±97 M1TBH,M2TBH M3TBH,M7TBH M8TBH,M9TBH	0.152±0.018
M12+TBH	65.9 ± 8.0* M5TBH, M6TBH, M8TBH, M9TBH	65.9±9.0	770±165# M7TBH	0.181±0.037
M13+TBH	100.3 ± 1.6 M2TBH,M7TBH , M10TBH, M11TBH, M12TBH	63.3±8.2	570±47 M2TBH,M7TBH M8TBH	0.150±0.016

M14+TBH	101.2 ± 2.7 M2TBH, M7TBH, M10TBH,M11TBH, M12TBH	67.9±21.4	361±39[#] M13,M1TBH M2TBH,M3TBH M4TBH,M5TBH M7TBH,M8TBH M9TBH,M12TBH	0.147±0.002
M15+TBH	96.6 ± 2.6 M2TBH, M10TBH, M11TBH, M12TBH	69.8±8.8	355±19 M1TBH,M2TBH M3TBH,M4TBH M5TBH,M6TBH M7TBH,M8TBH M9TBH,M12TBH	0.174±0.028[#]
Trolox+serum	71.9 ± 5.5* M2,M7,M10,M11, M12,M5TBH, M6TBH, M8TBH, M9TBH, M12TBH	74.6±40.2 M1,M2,M3, M4,M5,M6, M7,M8,M9	960±5* M11,M12,M13, M15,M10TBH M13TBH,M14TBH M15TBH	0.227±0.012
DMSO+serum	96.6 ± 13.0 M1,M2,M3, M10,M11,M12 M2TBH, M7TBH, M10TBH, M11TBH, M13TBH, M14TBH,TROLOX	35.7±15.5 M10,M15	615±167 M1,M2,M7 M8,M9,M13 M2TBH,M7TBH M8TBH,M11TBH, TROLOX	0.241±0.046 M15
TBH+serum	104.6 ± 12.2 M1,M2,M3,M4, M7,M10,M11, M12,M13,M14 M2TBH, M7TBH, M10TBH, M11TBH M11TBH, M12TBH,TROLOX	74.1±11.9* M1,M2,M3, M4,M6,M7, M8,M9,DMSO	579±186 M1,M2,M3 M7,M8,M9 M13,M2TBH, M7TBH,M8TBH TROLOX	0.121±0.011 M1,M2,M4, M10,M11 M12,M14,M15
P	<0.001	<0.001	<0.001	<0.001

P from ANOVA; post hoc Tukey test with letters indicate significant differences with distinct substances
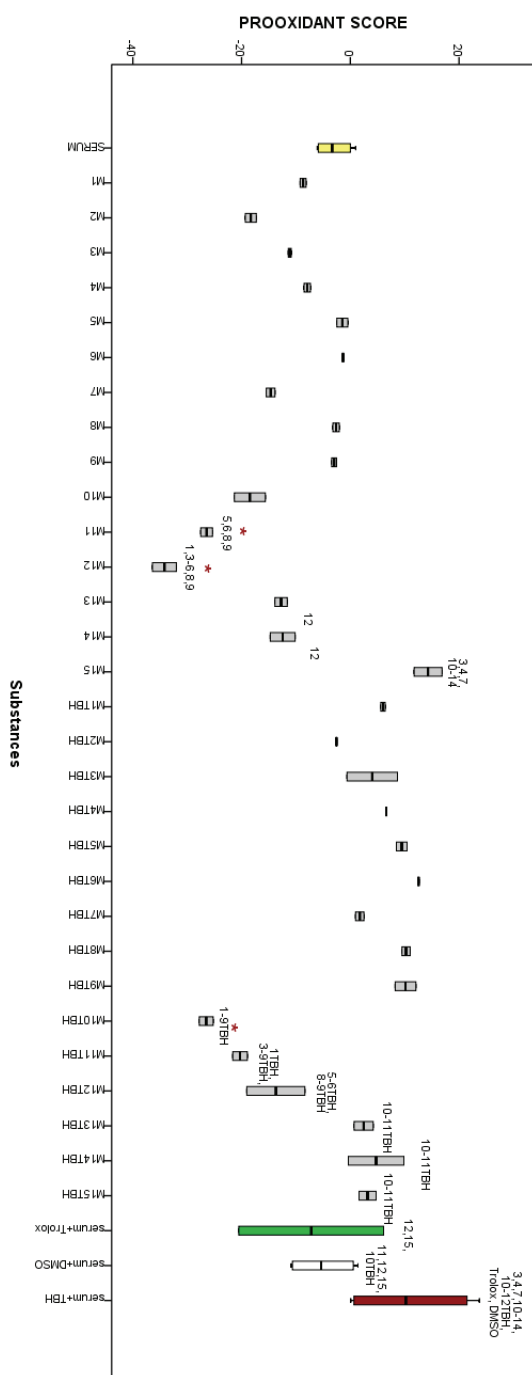
Fig S23. Prooxidant score (PS) in tested substances with and without TBH, along with native serum, serum with Trolox (2000 µmol/L) and serum with TBH (0,25 mM)

*P<0,05, *vs.* native SERUM; # P<0,05, *vs.* the same substance sample without TBH; numbers: statistically significant difference vs. distinct substance without or with TBH.

PETKOVIĆ *et al.*
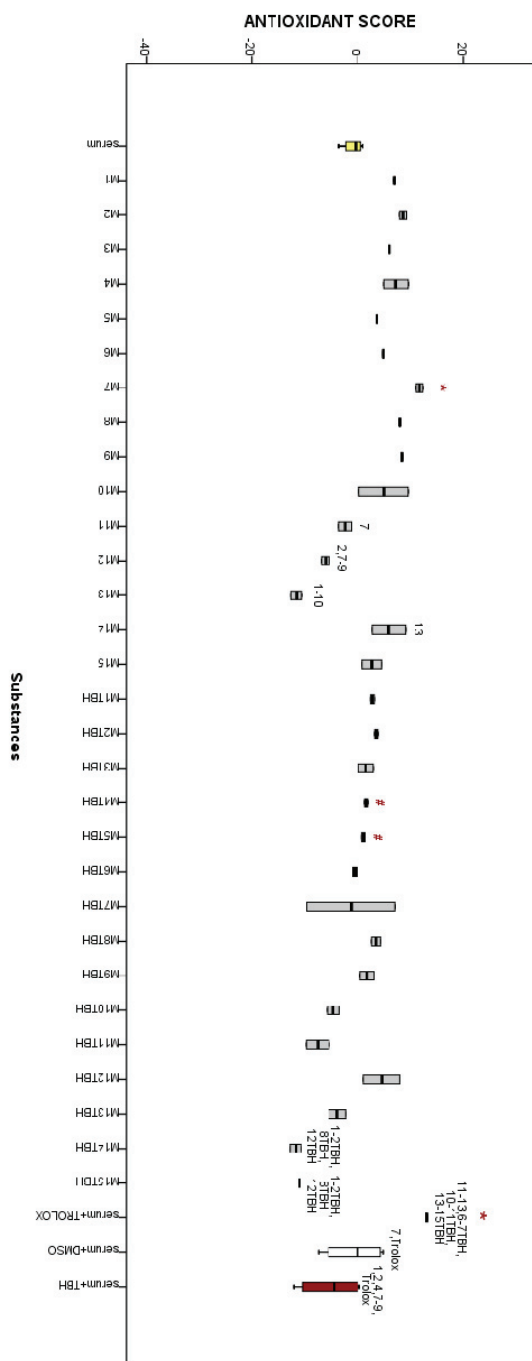
Fig S24. Antioxidant score (AS) in tested substances with and without TBH, along with native serum, serum with Trolox (2000 μmol/L) and serum with TBH (0,25 mM)

*P<0,05, *vs.* native SERUM; # P<0,05, *vs.* the same substance sample without TBH; numbers: statistically significant difference vs. distinct substance without or with TBH.
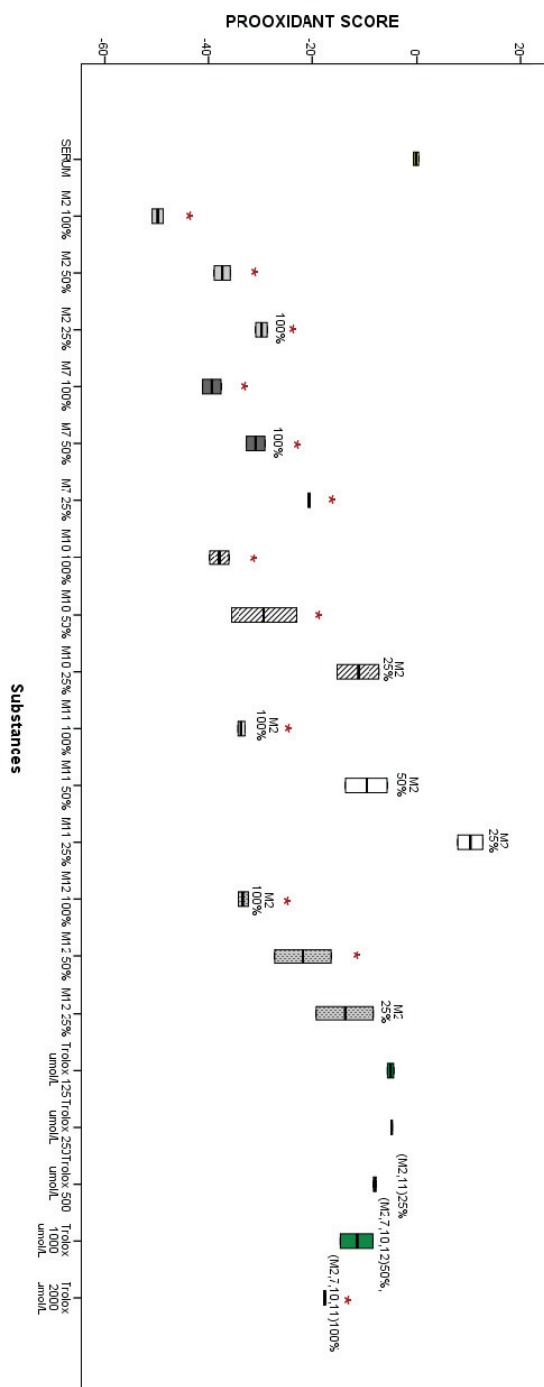
Fig S25. Prooxidant score in three different concetrations of M2, M7, M10, M11 i M12 samples, so as in samples with Trolox (125-2000 µmol/L)

*P<0.05 *vs.* native serum (blank);

100%, 50%: P<0.05 *vs.* sample of the same substance with different concentration;

Mx, My…Mi %: P<0.05 *vs.* indicated sample of a specific dilution;

#P<0.05 *vs.* Trolox (125 µmol/L).
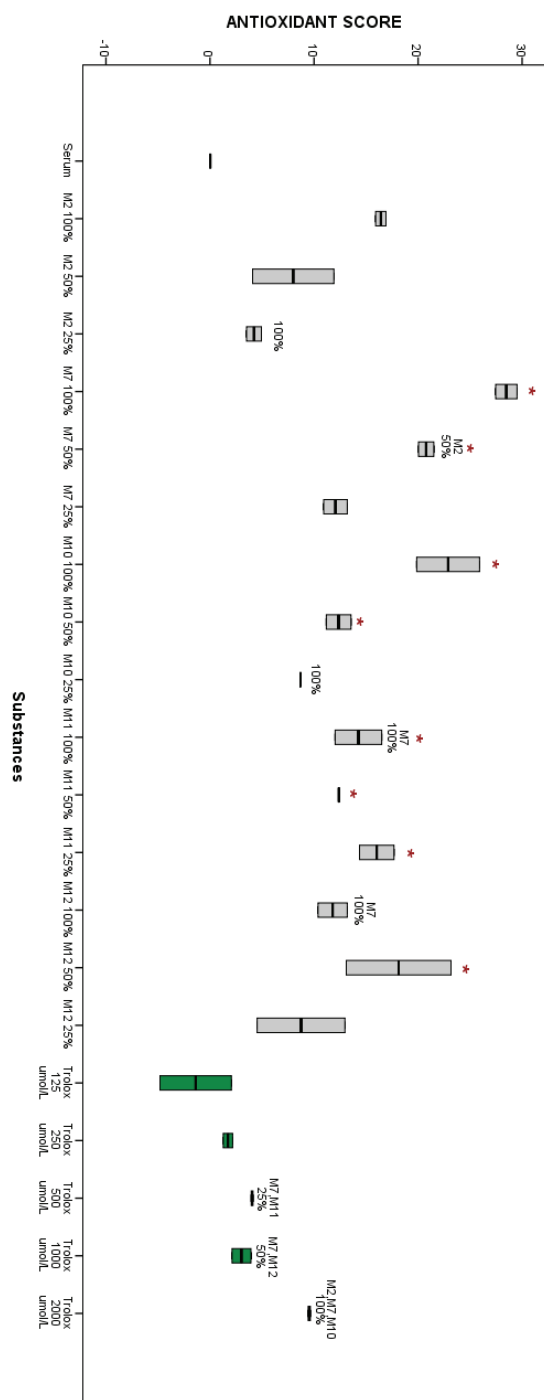
Figure S26. Antioxidant score in three different concentrations of M2, M7, M10, M11 i M12 samples, so as in samples with Trolox (125-2000 µmol/L)

*P<0.05 *vs.* native serum (blank);

100%, 50%: P<0.05 *vs.* sample of the same substance with different concentration;

Mx, My…Mi %: P<0.05 *vs.* indicated sample of a specific dilution;

#P<0.05 *vs.* Trolox (125 µmol/L).

Table S2. Calculated values of prooxy, antioxy and oxy score of tested compounds in three different concentrations

Samples	Prooxi score	Antioxi score	Oxy score
Serum	-0.2 (-0.7 - 0.3)	0.0 (0.0 - 0.0)	-0.2 (-0.7 - 0.3)
M2-100%	-49.8 (-50.9 - -48.8)	16.4 (15.9- 16.9)	-66.2 (-66.8 - -65.7)
M2-50%	-37.4 (-38.9 - -35.9)	8.0 (4.1- 11.9)	-45.4 (-47.8 - -43.0)
M2-25%	-29.8 (-30.9 - -28.7)	4.2 (3.5- 4.9)	-34.0 (-34.4 - -33.6)
M7-100%	-39.4 (-41.1 - -37.6)	28.5 (27.5 - 29.5)	-67.8 (-70.6 - -65.1)
M7-50%	-30.9 (-32.6 - -29.1)	20.8 (20.0 - 21.5)	-51.7 (-52.7 - -50.6)
M7-25%	-20.6 (-20.7 - -20.4)	12.1 (10.9 - 13.2)	-32.6 (-33.9 - -31.4)
M10 100%	-38.0 (-39.8 - -36.2)	22.9 (19.9 - 25.9)	-60.8 (-65.7 - -56.0)
M10 50%	-29.4 (-35.6 - -23.1)	12.4 (11.2 - 13.6	-41.7 (-49.2 - -34.3)
M10 25%	-11.2 (-15.3 - -7.2)	8.7 (8.6-8.8)	-19.9 (-24.0 - -15.8)
M11 100%	-33.7 (-34.4 - -32.9)	14.3 (12.0 - 16.5	-47.9 (-49.4 - -46.4)
M11 50%	-9.7 (-13.7 - -5.6)	12.4 (12.3-12.5)	-22.0 (-26.0 - -18.0)
M11 25%	10.3 (8.0 - 12.7)	16.0 (14.4 - 17.7)	-5.7 (-9.7 - -1.7)
M12 100%	-33.3 (-34.4 - -32.3)	11.8 (10.4 - 13.2)	-45.1 (-45.5 - -44.7)
M12 50%	-21.8 (-27.3 - -16.4)	18.1 (13.1 - 23.2)	-40.0 (-50.4 - -29.5)
M12 25%	-13.8 (-19.2 - -8.3)	8.8 (4.5 - 13.0)	-22.5 (-23.8 - -21.2)
E 2.0	-17.6 (-17.8 - -17.5)	9.5 (9.4 - 9.6)	-27.2 (-27.2 - -27.1)
E 1.0	-11.5 (-14.7 - -8.3)	3.0 (2.1 - 3.9)	-14.5 (-18.6 - -10.4)
E 0.500	-8.0 (-8.2 - -7.7)	4.0 (3.9 - 4.1)	-12.0 (-12.3 - -11.7)
E 0.250	-4.8 (-4.9 - -4.7)	1.7 (1.3 - 2.2)	-6.5 (-7.0 - -5.9)
Serum+Trolox 0.125	-5.0 (-5.6 - -4.4)	-1.4 (-4.8 - 2.1)	-3.6 (-7.6 - 0.4)

Chlorogenic acid with cytotoxic activity and other constituents from *Anacyclus valentinus* from Algeria

BAKHTA RAMLI[1], MOHAMED RABIE MOKRED[1], ABDELKADER HAMIANI[1],
SALIMA BELLAHOUEL BENZINE[1], CHOUKRY KAMEL BENDEDDOUCHE[1], MARIA
TERESA LAO[2], MARIE-LAURE FAUCONNIER[3] and NADIA KAMBOUCHE BOUZIDI[1]*

[1]*Organic Synthesis Laboratory, Department of Chemistry, Faculty of Exact and Applied Sciences, Oran 1 Ahmed Ben Bella University, Oran, Algeria,* [2]*Agronomy Department, Research Center for Mediterranean Intensive Agrosystems and Agri-Food Bio-Technology CIAMBITAL, Agrifood Campus of International Excellence ceiA3, University of Almeria, Almeria, Spain and* [3]*Laboratory of Chemistry of Natural Molecules, Gembloux Agro-Bio Tech. University of Liège, Passage des Déportés 2, Gembloux, Belgium*

Abstract: *Anacyclus valentinus* is a Saharan plant belonging to the Asteraceae family. This study identified and determined the structure of isolated compounds obtained from unrefined extract of *A. valentinus*. Their cytotoxic effects on two human cancer cell lines were examined. The extract of the aerial part of *A. valentinus* was fractioned by solid phase extraction (SPE). The fractions obtained were analysed by NMR spectroscopy and HPLC-DAD–MS. This is the first cytotoxic investigation of *A. valentinus*. The extracts of the plant were prepared, and their cytotoxic effects on two human cancer cell lines (A549, human lung adenocarcinoma; HepG2, hepatocellular carcinoma) were examined using the MTT assay. Several compounds have been identified. The results illustrated two newly identified compounds: chlorogenic acid and the *β*-glucosides derivative. In addition, C-glycosides (2 isomers of apigenin) were detected in the genus *Anacyclus*. The IC_{50} values of unrefined extracts of the aerial parts of *A. valentinus* against the A549 cell line were determined as 19.79 µg/mL. The values for the HepG2 cell line were 32.63 µg/mL. Chlorogenic acid was showed the highest cytotoxic activities on the A549 and HepG2 cell lines with IC_{50} values of 13.59 and 12.84 µg/mL, respectively.

Keywords: *Anacyclus valentinus*; chlorogenic acid; cytotoxic activity; flavonoids; *β*-glucosides; HPLC-DAD–MS.

163

INTRODUCTION

The healing potential of plant has been known for thousands of years. Plants produce a whole series of different compounds, which are not of particular significance for primary metabolism, but can have a remarkable effect to other plants, microorganisms and humans. Currently, due to their effectiveness with low side effects, medicinal plants have a growing demand in the prevention and treatment of diseases as natural remedies. These organic compounds are defined as biologically active substances[1] and include polyphenols and essential oils.[2]

Anacyclus valentinus L. Aiton (*Asteraceae*), called "Guertoufa" in Arabic, is an annual plant restricted to the Mediterranean region, well represented in the western Mediterranean Basin, including Algeria[3] and Spain,[4] its distribution is related to annual mean temperature (BIO 1) and the precipitation of the coldest quarter (BIO 19). Nevertheless, *A. valentinus* presents a high degree of intergeneric hybridization that makes its collection difficult. This plant is known for its anti-diabetic[5] and antifungal[6] effects. It is also used in some parts of the country as a food condiment.

The phytochemical constituents of *A. valentinus* revealed the presence of essential oil[7,8] which has a potential for use as a safe biocontrol agent to prevent food crops from fungal diseases and improve product quality and safety.[9]

Currently, have been identified by gas chromatography/mass spectrometry (GC/MS) analysis, 29 components of which δ-3-carene (31 %), spathulenol (14.2 %), were the major compounds of this oil. The methanol extract of *A. valentinus* has been reported to contain quercetin, myricetin, kaempferol, luteolin and apigenin.[10,11]

The aim of this study was to identify and determine the structures of compounds isolated from different fractions of *A. valentinus*, using spectroscopic methods, to determine their potential cytotoxic activities.

In the present study, phytochemical analysis of *A. valentinus*, revealed the presence of other phenolic acid and flavonoid compounds.

Thus, flavonoids display various bioactive effects, including anti-inflammatory, cardioprotective, antidiabetic, antiviral and anticancer effects.

Drugs isolated from plants and microorganisms, or synthesized after isolation, constitute a significant proportion of anticancer agents used in cancer treatment.[12] Plants are a good source of antitumor compounds; indeed, some compounds initially derived from plants[13–16] show good potential as primary sources of chemotherapeutic drugs. Some chemotherapeutic agents, such as vinca alkaloids for leukaemia, paclitaxel for breast cancer and flavopiridol for colorectal cancer, have been derived from medicinal plants.[17]

Several studies have shown that herbal medicine may prevent tumour growth and exhibit cytotoxic activities on tumour cells, without negative effects on normal cells.[18–20]

EXPERIMENTAL

Vegetal material

Anacyclus valentinus was collected during the period (April–May) in Tiaret region, the plant material was identified and validated by Prof. Dr. Hadjadj-Aoul (Botany Department, Oran 1, Algeria). The plant was cleaned, washed with tap water and dried in the shade. Then it was weighed, coarsely ground and collected in clean bags. Voucher specimens were identified and deposited in the herbarium of the Agricultural Institute in Algeries, Algeria.

Chemicals

Formic acid and HPLC grade methanol were purchased from Sigma–Aldrich. All chemicals: acetone, methanol and ammonium formiate were purchased from Sigma–Aldrich.

Sample preparation of the extracts

The following extracts were prepared: 25, 50,100 and 200 mg of the aerial parts of the plant were macerated with 4 mL of two solvents: A) formic acid and methanol (99/1 volume ratio) and B) formic acid, acetone and water (60/39/1 volume ratio). The solutions were subjected to agitation by an extractor (Precelly® 24, Bertin Technologies S.A.S, France) according to the parameters 5100-3×40-040, during 10 min and 3 times, the liquid phase was evaporated.[21] Reagents were purchased from Sigma–Aldrich.

HPLC-DAD–MS analysis

The chromatographic and mass analysis of the samples were carried out on a chain UPLC Waters, coupled with a mass spectrometer (Brucker) by liquid chromatography with ultra-high performance with ionization by atmospheric pressure and an ionic trap door, in order to obtain three levels of fragmentation.[22] The HPLC analysis was carried out on a Waters 2690 HPLC system equipped with a Waters 996 DAD (Waters Corp., Milford, MA) and Empower software (Waters).[23]

The column used is C18, 1.7μm. The solvents were 1 % aqueous formic acid (solvent A) and water/formic acid (98:1, solvent B). The states of gradient conditions were as follows: from 0 to 6 min 98 % A, in 7 min 82 % A, in 12 min at the 14 min 70 % A and 30 % B and at 27 min 25 % A and 75 % B and in 32 min 95 % B with a flow of 0.08 mL/min. The volume of injection was the 0.5 μL and detection was carried out between 210 and 650 nm. Experiments were performed in negative and positive ion mode. The desolvation temperature was 300 °C. High spray voltage was set at 5000 V. Nitrogen was used as the dry gas at a flow rate of 75 mL min^{-1}. MS was carried out using helium as target gas. The identifications were achieved on the basis of the molecular ion mass, fragmentation, UV–Vis spectra and relative retention times or co-injection with standards.[24]

Breaking-up by cartouche SPE

The methanolic extract was dissolved in water (9 ml), filtered and fractionated by SPE using a Waters-SPE-PakRvac 20cc TC 18-5g cartridge. After cleaning with 5 mL of a solution of water/formic acid (99/1 volume ratio), 5 mL of methanol/formic acid (99/1 volume ratio) and with a preconditioning with 5 ml of water/formic acid (99/1 volume ratio), the cartridge was loaded with the sample (2 ml). The analysts were eluted three times with 5 ml of methanol/water/formic acid (15/84/1 volume ratio), three times with 5 ml of methanol/water/formic acid (25/74/1 volume ratio), three times with 5 ml of methanol/water/formic acid (30/69/1 volume ratio), three times with 5 ml of methanol/water/formic acid (60/39/1 volume ratio). The protocol was repeated with 2 ml of sample until exhaustion. The fractions were combined and evaporated with a rotary evaporator.

The SPE makes it possible to extract and preconcentrer the sample in a liquid matrix, because is an adequate method for the preparation of samples.[25] The SPE is then followed of a chromatographic method of analysis.

Cytotoxic assay

Cell lines and culture medium. The following cancer cell lines were used in this study: A549 (human lung adenocarcinoma) and HepG2 (hepatocellular carcinoma). Cells were obtained from the National Cell Bank of Algiers (Pasteur Institute, Algiers).

MTT assay. The cytotoxic activity of crude extracts of the aerial parts of *A. valentinus* and chlorogenic acid compound was determined using an MTT colorimetric assay (3-[4,5-dimethylthiazol-2-yl]-2,5-diphenyl tetrazolium bromide assay).

Cell viability was quantified using an MTT colorimetric assay (3-[4,5-dimethylthiazol-2--yl]-2,5-diphenyl tetrazolium bromide assay).[26] Cells were seeded into 96-well plates were incubated for 72 h at 37 °C in a 5 % CO_2 incubator. After that, the chlorogenic acid compound and the plant extracts at different concentrations 0.005, 0.01, 0.02,0,03 and 0.04 mg/mL were dissolved in 10 % DMSO and added to the cell culture to be tested against cell lines. The cells were incubated for 24, 48, and 72 h to evaluate dose and time responsiveness.

Subsequently, 10 μL phosphate-buffered saline containing 5 mg/mL MTT was added to each well. After 4 h of incubation, the medium was discarded, and formazan blue crystals formed in the cells were dissolved in 100 mM DMSO. Reduced MTT concentrations were quantified using a microplate reader (Thermo Scientific Multiscan Spectrum) at 540 nm absorbance. The cytotoxic effects of the tested extracts were determined by comparing the optical density of the treated cells with that of the untreated cells. The cytotoxicity relative to controls was calculated using the following formula:[27]

$$\text{Cytotoxicity (\%)} = 100((A_c - A_t)/A_c)) \qquad (1)$$

where A_c and A_t are the mean absorbances of the control and test wells, respectively.

Statistical analysis

The data were analysed using SPSS software (Microsoft Corp., Chicago, IL, USA). The multiple treatment comparisons were performed using one-way analysis of variance and Student's *t*-test. The differences were considered statistically significant at *$p < 0.05$, *$p < 0.01$ and *$p < 0.005$. The data are presented as the mean ± standard deviation of three replicates.

RESULTS AND DISCUSSION

Identification of chromatographic HPLC-DAD–MS peaks

The analysis of each of these fractions showed several compounds eluting throughout the chromatographic profiles.

The profiles of the fractions appeared to be quite different, and most of the compounds were recovered in only one of them (Fig. 1). Moreover, some compounds eluting at the same retention time in the fractions showed different UV––Vis properties.

The methanolic fraction presents the highest content of polyphenols and flavonoids in this study.

The molecular structure of the compounds found is the following: Fig. 2 shows the structures of derivative *β*-glucosides and his dimer (A) and (B).

Fig. 1. Chromatogram of HPLC-DAD–MS of the methanolic extracted of the plant *A. valentinus*.
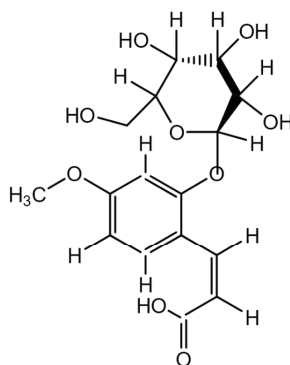
Derivative β-glucosides
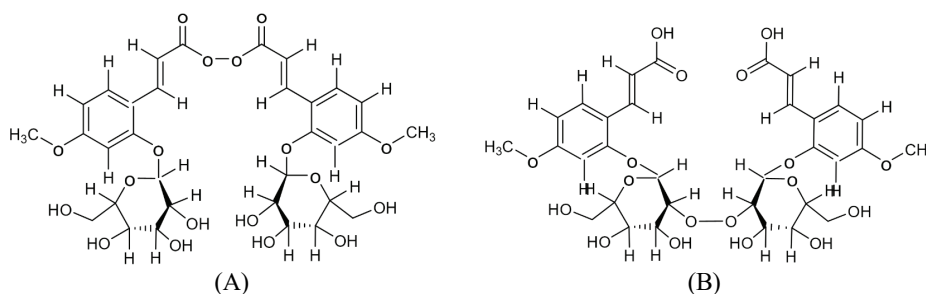
Fig. 2. Structures of derivative *β*-glucosides and its dimers (A) and (B).

The phenolic acid and flavonoid compounds are given in Table I.

TABLE I. Phenolic components detected in *A. valentinus* aerial part in methanolic extract by HPLC-DAD–MS

Rt min	UV λ_{max}	Mol. ion [M–H] (*m/z*)	Fragmentation	Identified compound
10.8	289	711	355 (100), 193 (100), 149 (23)	Derivative *β*-glucosides
13.3	300	353	191 (100), 178 (9)	Chlorogenic acid
14.3	293-305	711	355 (100), 549 (37), 369 (32), 271 (18)	Dimer of derivative *β*-glucosides
14.4	271-336	593	472 (100), 353 (42), 503(36), 575 (19), 383 (27)	6,8-Di-*C*-glucopyra-nosyl apigenin
16.2	295-319	711	355 (100), 193 (100), 149 (23)	Dimer of derivative *β*-glucosides
17.7	269-340	431	311 (100), 431 (40), 413 (9)	Vitexin derivatives

Fig. 3 shows major compounds chlorogenic acid, identified with a retention time of 13.3 min with absorption wavelength peak at 300 nm, while mass spectrum 593 had a retention time of 14.4 min with two absorption wavelength peaks (271 and 336 nm) and corresponds to flavone, 6,8-di-*C*-glucopyranosyl apigenin (Fig. 4).
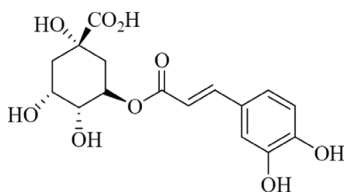
Fig. 3. Structure of chlorogenic acid.
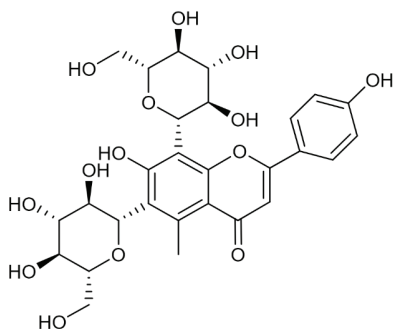
Fig. 4. Structure of 6,8-di-*C*-glucopyranosyl apigenin.

Peaks with the retention time of 10.08 and 16.2 min correspond to the same mass 711 with the same fragmentation (355, 193, 149). The molecule is symmetric it would give only set of NMR signals as the monomer (results no showed), which explains that they are isomers.

The last pic at 17.7 min, spectrum UV with 2 absorption wavelengths peaks (269 and 340 nm), and her mass spectrum 431 corresponds to flavone, derived from the vetexin (Fig. 5).

(A)   (B)
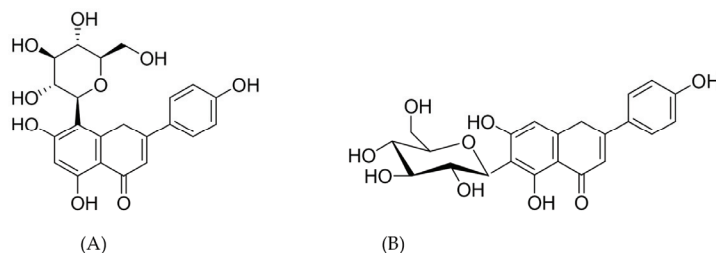
Fig. 5. Structures of 8-*C*-glucosylapigenin (vitexin) (A) and 6-*C*-glucosylapigenin (isovitexin) (B).

Cytotoxic assay

As shown in graphs 1 and 2 of Figs. 6 and 7, the IC_{50} values of crude extracts of the aerial parts of *A. valentinus* against the A549 cell line were determined as 19.79 µg/mL. The values for the HepG2 cell line were 32.63 µg/mL.

The different extracts showed dose-dependent cytotoxic effects on the cancer cell lines. Chlorogenic acid exhibited the best cytotoxic effects on the A549 and HepG2 cell lines with IC_{50} values of 13.59 and 12.84 µg/mL, respectively.
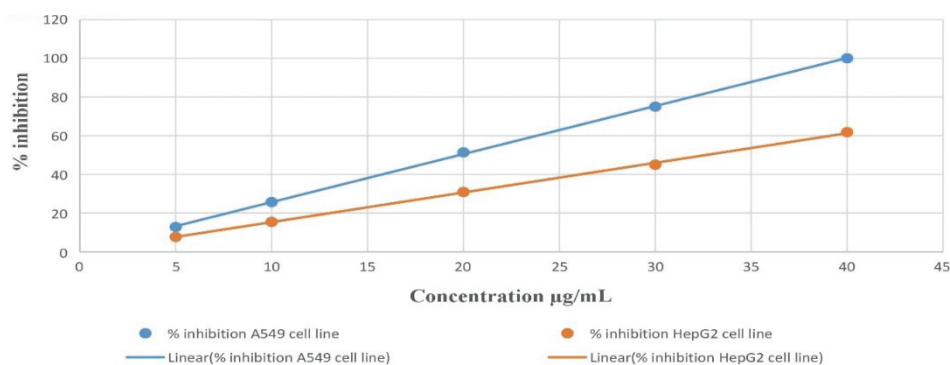
Fig. 6. Inhibition percentage of cell viability of crude extracts of the aerial parts of *A. valentinus* against the A549 cell line and the HepG2 cell line.

The use of *Anacyclus* species in folk medicine in North Africa is widely attributed to their recognized therapeutic properties, which are attributed to the presence of different compounds,[28–30] including terpenoids, flavonoids and alkaloids.[31]

The results obtained in this study are agreed with the composition of aerial parts of other species,[32,33] of gender *Anacyclus*, confirmed that the methanolic

extract from the aerial parts of *A. maroccanus* and *A. radiatus* contained chloro-
genic acid, that joint to rutin were the major identified compounds in these species.
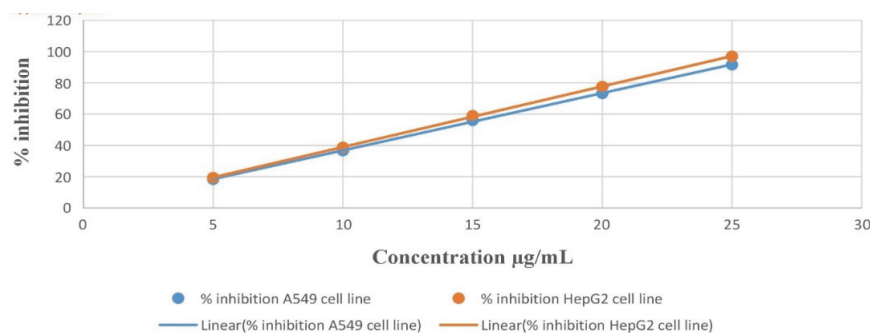
Fig. 7. Inhibition percentage of cell viability of chlorogenic compound against the A549 cell
line and the HepG2 cell line.

Nevertheless, this is the first time that have been identified the following
compounds: vitexin, isovitexin, and derivatives β-glucosides in *A. Valentinus* and
suggest that the identified compounds may play a role in the bioactivities of the
extracts, which needs further research.

Some flavones like vitexin and isovitexin are active components of many
traditional Chinese medicines and were found in various medicinal plants. Vit-
exin (8-*C*-glucosylapigenin) has recently received increased attention due to its
wide range of pharmacological effects, including but not limited to anti-oxidant,
cytotoxic, anti-inflammatory, antispasmodic and neuroprotective effects. Isovitexin
(apigenin-6-*C*-glucoside), an isomer of vitexin, generally purified together with
vitexin,[34] also exhibits diverse biological activities.[35,36] Flavonoids have various
bioactive effects, including anti-inflammatory, cardioprotective, anti-diabetic,
anti-viral and anti-cancer. For that, the knowledge of these compounds will help
in formulating pharmaceutical products.

Our results showed that the plant extract of *A. valentinus* could significantly
inhibit cancer cells. It could therefore be a preventive agent against the
development of cancer cells. Several extracts and chlorogenic compound were
exhibited antiproliferative activity against the two of the cell lines. Chlorogenic
acid was isolated from *Anacyclus* species for the first time and showed the
highest cytotoxic activities on the A549 and HepG2 breast cancer cell lines.

In fact, several studies[37–39] showed that chlorogenic acid, an important bio-
logically active dietary polyphenol, can be produced by certain plant species.
Reduction in the risk of a variety of diseases.

CONCLUSION

This is the first phytochemical and cytotoxic investigation of an endemic species of *A. valentinus*. The identification of phenolic compounds in the air extract of *A. valentinus* was evaluated.

In the present study, phytochemical analysis of *A. valentinus*, revealed the presence of other phenolic acid and flavonoid compounds. The compounds found in this study of the plant *A. valentinus* has shown many biological activities. Chlorogenic acid and methanolic extracts of *A. valentinus* showed significant anticancer activity against cancer cell lines. Herbal-based products exist for hundreds of years and have been identified as a potent approach for the treatment of various human diseases, such as cancer.[40]

In future studies, the level of other chemical components of *A. valentinus* and the major extracts responsible for anticancer activity will be determined, and the molecular mechanisms of cell death will be analysed in more detail.

ИЗВОД

ХЛОРОГЕНА КИСЕЛИНА СА ЦИТОТОКСИЧНОМ АКТИВНОШЋУ И ДРУГИ САСТОЈЦИ
Anacyclus valentinus ИЗ АЛЖИРА

БАКНТА РАМЛИ[1], МОХАМЕД РАБИЕ МОКРЕД[1], АБДЕЛКАДЕР ХАМИАНИ[1], САЛИМА БЕЛЛАХОУЕЛ БЕНЗИНЕ[1],
ЧОУКРY КАМЕЛ БЕНДЕДДОУЧЕ[1], МАРИА ТЕРЕСА ЛАО[2], МАРИЕ-ЛАУРЕ ФАУЦОННИЕР[3]
и НАДИА КАМБОУЧЕ БОУЗИДИ[1]

[1]*Organic Synthesis Laboratory, Department of Chemistry, Faculty of Exact and Applied Sciences, Oran 1 Ahmed Ben Bella University, Oran, Algeria,* [2]*Agronomy Department, Research Center for Mediterranean Intensive Agrosystems and Agri-Food Bio-technology CIAMBITAL, Agrifood Campus of International Excellence ceiA3, University of Almeria, Almeria, Spain u* [3]*Laboratory of Chemistry of Natural Molecules, Gembloux Agro-Bio Tech. University of Liège, Passage des Déportés 2, Gembloux, Belgium*

Anacyclus valentinus је биљка Сахаре која припада породици Asteraceae. У овој студији су идентификована једињења изолована из сировог екстракта *A. valentinus* и одређена је њихова структура. Испитан је њихов цититоксични ефекат на две хумане канцерске ћелијске линије. Екстракт надземних делова *A. valentinus* је фракционисан методом екстракције на чврстој фази (SPE). Добијене фракције су анализиране NMR спектроскопијом и методом HPLC-DAD–MS. Ово је прва студија која анализира цитотоксичност *A. valentinus*. Цитотоксичност екстраката је тестирана на хуманим канцерским ћелијским линијама A549 (аденокарцином плућа) и HepG2 (хепатоцелуларни карцином) применом MTT теста. Идентификовано је више једињења, укључујући и два нова: хлорогена киселина и β-гликозидни дериват. Такође, детектовано је присуство C-гликозида (2 изомера апигенина). Вредност IC_{50} сировог екстракта надземних делова *A. valentinus* спрам A549 ћелијске линије је била 19,79 µg/mL, а спрам HepG2 32,63 µg/mL. Хлорогена киселина је испољила највећу цитотоксичност спрам A549 и HepG2 ћелијских линија, са IC_{50} вредностима 13,59, односно 12,84 µg/mL.

(Примљено 13. априла, ревидирано 25. маја, прихваћено 25. августа 2024)

REFERENCES

1. S. H. Nile, S. W. Park, *Nutrition* **30** (2014) 134 (https://doi.org/10.1016/j.nut.2013.04.007)
2. A. Shomali, S. Das, N. Arif, M. Sarraf, N. Zahra, V. Yadav, S. Aliniaeifard, D. K. Chauhan, M. Hasanuzzaman, *Plants* **11** (2022) 3158 (https://doi.org/10.3390/plants11223158)
3. C. Selles, N. Djabou, F. Beddou, A. Muselli, B. Tabti, J. Costa, B. Hammouti, *Nat. Prod. Res.* **27** (2013) 2231 (https://doi.org/10.1080/14786419.2013.811409)
4. A. Bruno Agudo, F. Xavier Picó, R. G. Mateo, A. Marcer, R. Torices, I. Álvarez, *Am. J. Bot.* **110** (2023) e16121 (https://doi.org/10.1002/ajb2.16121)
5. A. Tahraoui, J. El-Hilaly, Z. H. Israili, B. Lyoussi, *J. Ethnopharmacol.* **110** (2007) 105 (https://doi.org/10.1016/j.jep.2006.09.011)
6. S. M. Mahlo, H. R. Chauke, L. McGaw, J. Eloff, *Afr. J. Tradit. Complement. Altern. Med.* **13** (2016) 216 (https://doi.org/10.21010/ajtcam.v13i4.28)
7. N. Ainseba, A. Soulimane, I. R. Mami, M. E. A. Dib, A. Muselli, *Comb. Chem. High Throughput Screen.* **26** (2023) (https://doi.org/10.2174/1386207326666230418093319)
8. A. Houicher, M. Hamdi, H. Hechachna, F. Özogul, *Food Biosci.* **25** (2018) 28 (https://doi.org/10.1016/j.fbio.2018.07.005)
9. S. Desai, P. Tatke, T. Mane, S. Gabhe, *Food Chem.* **345** (2021) 128717 (https://doi.org/10.1016/j.foodchem.2020.128717)
10. K. S. Larbi, B. Meddah, H. Belkhodja, A. Belmimoun, K. Slimani, P. Sonnet, *Int. J. Environ. Agric. Biotechnol.* **2** (2017) 3025 (https://doi.org/10.22161/ijeab/2.6.31)
11. A. Dif, B. Mokhtaria Yasmina, A. Ammam, M. Slimani, *J. Microbiol. Biotechnol. Food Sci.* (2022) e5290 (https://doi.org/10.55251/jmbfs.5290)
12. B. Kalaycı, N. Şimşek Özek, F. Aysin, H. Özbek, C. Kazaz, M. Önal, Z. Güvenalp, *Saudi Pharm. J.* **31** (2023) 101682 (https://doi.org/10.1016/j.jsps.2023.06.015)
13. T. Huang, W.-H. Gong, X.-C. Li, C.-P. Zou, G.-J. Jiang, X.-H. Li, D.-P. Feng, *Asian Pac. J. Cancer Prev.* **13** (2012) 81 (https://doi.org/10.7314/APJCP.2012.13.1.081)
14. G. A. King, D. C. Woollard, D. E. Irving, *Physiol. Plant.* **80** (1990) 393 (https://doi.org/10.1111/j.1399-3054.1990.tb00058.x)
15. M. Pandi, R. S. Kumaran, Y.-K. Choi, H. J. Kim, J. Muthumary, *Afr. J. Biotechnol.* **10** (2011) 1428 (https://www.ajol.info/index.php/ajb/article/view/92953/82366)
16. H. J. Park, M.-J. Kim, E. Ha, J.-H. Chung, *Phytomedicine* **15** (2008) 147 (https://doi.org/10.1016/j.phymed.2007.07.061)
17. M. K. Temel, *Turk. J. Oncol.* **30** (2015) 96 (https://doi.org/10.5505/tjoncol.2015.1151)
18. Y. Wang, J. Wang, H. Wang, W. Ye, *Chem. Biol. Drug Des.* **88** (2016) 556 (https://doi.org/10.1111/cbdd.12782)
19. A. Mohammadi, B. Mansoori, M. Aghapour, S. Shirjang, S. Nami, B. Baradaran, *Biomed. Pharmacother.* **83** (2016) 835 (https://doi.org/10.1016/j.biopha.2016.07.056)
20. B. Mansoori, A. Mohammadi, S. Hashemzadeh, S. Shirjang, A. Baradaran, M. Asadi, M. A. Doustvandi, B. Baradaran, *Biomed. Pharmacother.* **93** (2017) 95 (https://doi.org/10.1016/j.biopha.2017.06.021)
21. E. Tuzlaci, *MARMARA Pharm. J.* **14** (2010) 47 (https://dergipark.org.tr/en/download/article-file/165971)
22. M. A. Bello, I. Álvarez, R. Torices, J. Fuertes-Aguilar, *Ann. Bot.* **112** (2013) 1597 (https://doi.org/10.1093/aob/mcs301)

23. S. Sissi, S. Di Giacomo, C. Ferrante, P. Angelini, A. Macone, A. M. Giusti, C. Toniolo, A. Vitalone, A. Abdellah, M. Larhsini, L. Menghini, M. Markouk, G. Mazzanti, A. Di Sotto, *Molecules* **27** (2022) 692 (https://doi.org/10.3390/molecules27030692)

24. M. Faisal, A. I. Hossain, S. Rahman, R. Jahan, M. Rahmatullah, *BMC Complement. Altern. Med.* **14** (2014) 335 (https://doi.org/10.1186/1472-6882–14-335)

25. L. M. Fernandes, Z. Da Rosa Guterres, I. V. Almeida, V. E. P. Vicentini, *J. Med. Food* **20** (2017) 601 (https://doi.org/10.1089/jmf.2016.0149)

26. D. Bagdas, H. Y. Ozboluk, N. Cinkilic, M. S. Gurun, *J. Med. Food* **17** (2014) 730 (https://doi.org/10.1089/jmf.2013.2966)

27. Y. Jiang, K. Kusama, K. Satoh, F. Takayama, S. Watanabe, H. Sakagami, *Phytomedicine* **7** (2000) 483 (https://doi.org/10.1016/S0944-7113(00)80034-3)

28. A. Venditti, A. Bianco, C. Frezza, F. Conti, L. M. Bini, C. Giuliani, M. Bramucci, L. Quassinti, S. Damiano, G. Lupidi, D. Beghelli, S. Caterbi, D. Petrelli, L. A. Vitali, F. Papa, G. Caprioli, F. Maggi, *Ind. Crops Prod.* **77** (2015) 353 (https://doi.org/10.1016/j.indcrop.2015.09.002)

29. N. Pantelic, B. Zmejkovski, T. Stanojkovic, V. Jeftic, G. Radic, S. Trifunovic, G. Kaludjerovic, T. Sabo, *J. Serbian Chem. Soc.* **79** (2014) 649 (https://doi.org/10.2298/JSC130512022P)

30. N. Jankovic, Z. Bugarcic, S. Markovic, *J. Serbian Chem. Soc.* **80** (2015) 595 (https://doi.org/10.2298/JSC141028011J)

31. D. Tine, A. D. Fall, S. I. M. Dieng, A. Sarr, E. Bassene, *Int. J. Biol. Chem. Sci.* **13** (2019) 1817 (https://doi.org/10.4314/ijbcs.v13i3.48)

32. D. Bisht, R. Padalia, L. Singh, V. Pande, P. Lal, C. Mathela, *J. Serb. Chem. Soc.* **75** (2010) 739 (https://doi.org/10.2298/JSC091106052B)

33. S. Glisic, S. Milojevic, S. Dimitrijevic, A. Orlovic, D. Skala, *J. Serb. Chem. Soc.* **72** (2007) 311 (https://doi.org/10.2298/JSC0704311G)

34. L. Boulekbache-Makhlouf, E. Meudec, M. Chibane, J.-P. Mazauric, S. Slimani, M. Henry, V. Cheynier, K. Madani, *J. Agric. Food Chem.* **58** (2010) 12615 (https://doi.org/10.1021/jf1029509)

35. D. Cardoso, A. Narcy, S. Durosoy, C. Bordes, Y. Chevalier, *Powder Technol.* **378** (2021) 746 (https://doi.org/10.1016/j.powtec.2020.10.049)

36. H. Kataoka, *TrAC Trends Anal. Chem.* **22** (2003) 232 (https://doi.org/10.1016/S0165-9936(03)00402-3)

37. P. Lopez-Roldan, M. J. Lopez De Alda, D. Barcelo, *Anal. Bioanal. Chem.* **378** (2004) 599 (https://doi.org/10.1007/s00216-003-2187-4)

38. J. Bhattacharyya, D. Read, S. Amos, S. Dooley, K. Killham, G. I. Paton, *Environ. Pollut.* **134** (2005) 485 (https://doi.org/10.1016/j.envpol.2004.09.002)

39. T. Mosmann, *J. Immunol. Methods* **65** (1983) 55 (https://doi.org/10.1016/0022–1759(83)90303-4)

40. S. Nobili, D. Lippi, E. Witort, M. Donnini, L. Bausi, E. Mini, S. Capaccioli, *Pharmacol. Res.* **59** (2009) 365 (https://doi.org/10.1016/j.phrs.2009.01.017).

The effects of silver nanoparticles synthesized with an aqueous extract of *Agrimonia eupatoria* L. on winter wheat and barley varieties

DJORDJE D. MINIĆ[1]*, KATARINA G. MARKOVIĆ[2], ANA S. KESIĆ[2], MIRJANA Z. GRUJOVIĆ[2], STEFAN M. MARKOVIĆ[1], ALEKSANDRA M. TORBICA[3] and NEVENA H. DJUKIĆ[1]

[1]*University of Kragujevac, Faculty of Science, Department of Biology and Ecology, Radoja Domanovica 12, Kragujevac, Serbia,* [2]*University of Kragujevac, Institute for Information Technologies, Department of Science, Jovana Cvijića bb, Kragujevac, Serbia and* [3]*University of Novi Sad, Institute of Food Technology, Bulevar cara Lazara 1, Novi Sad, Serbia*

Abstract: Silver nanoparticles represent a potential solution for mitigating the negative effects of temperature stress on cereals. This study investigates the impact of silver nanoparticles on winter varieties of wheat and barley during the tillering phase, focusing on proline concentration, antioxidant activity and extract yield under winter field conditions. Silver nanoparticles (AgNPs) were synthesized using a green method with an aqueous extract of the plant *Agrimonia eupatoria* L. (fam. Rosaceae). Two winter cereal varieties, Simonida (*Triticum aestivum* L.) and Nonius (*Hordeum vulgare* L.), were foliar treated with 5 and 10 mg/mL AgNPs–H_2O. The experiment lasted for 10 days, during which the minimum recorded temperature was –7 °C under field conditions. The proline concentration was increased in both varieties treated with nanoparticles compared to the controls. Antioxidant activity was assessed using the DPPH method for both treated and untreated samples, with ascorbic acid used as a positive control. Antioxidant activity has increased in all treated samples compared to the untreated samples. Only specific concentrations of AgNPs––H_2O increased the extract yield. Based on these results, our study emphasizes the potential of AgNPs–H_2O to improve the tolerance of winter cereals to low temperatures.

Keywords: green synthesis; cereals; proline; antioxidant activity; low temperatures.

INTRODUCTION

Temperature changes, whether in the form of increases or decreases, affect the rate of plant development, with temperature stress disrupting cellular

---

175

metabolism and functionality. Such stress induces morphological, physiological and biochemical changes, depending on the plant species and the duration of stress exposure.[1] Low temperatures (< 0 °C) represent temperature stress, while the acclimatization of winter cereal varieties begins at temperatures below 10 °C. Low temperatures, as stress factors, cause yield loss through a reduction in the number of productive tillers, spikes and grains, resulting in shorter stems, smaller leaf area and decreased photosynthesis. Tillering in cereals is a growth and development phenophase during which secondary shoots are formed at the tillering node. The rate and intensity of tillering largely depend on climatic conditions. The optimal temperature for the tillering phase is 15–17 °C. When temperatures are lower, tillering slows down, and it ceases below 6 °C. During the tillering phase, winter cereal varieties can be sensitive to low temperatures, depending on their intensity and duration. Under stressful conditions, one of the most detrimental effects on plants is oxidative stress, which leads to the formation of reactive oxygen species, causing protein and nucleic acid damage, lipid oxidation, cell membrane damage and ultimately the inhibition of plant growth and development, which may result in the plants' inability to survive.[2–4]

Silver nanoparticles (AgNPs) are a type of metal nanoparticles with unique biological, chemical and physical characteristics, such as: catalytic activity, chemical stability, high electrical conductivity, specific optical and thermal properties.[5] The application of silver nanoparticles in agriculture holds multiple significances, including their use as nanofertilizers,[6] nanopesticides,[7] nanobiosensors and nanometeorological instruments,[8] for improving soil properties,[9] as growth stimulators and as agents for fruit ripening.[10] Silver nanoparticles enhance yield, antioxidant activity and proline content in cereals under cold stress conditions.[11,12]

The synthesis of AgNPs, as well as other nanomaterials, can be physical, chemical or biological. Biological synthesis is also referred to as green synthesis.[13] The green synthesis of silver nanoparticles offers ecological advantages over chemical and physical methods. These methods are simple, environmentally friendly and suitable for commercial applications, as they do not require high energy consumption, high temperatures, pressures or toxic chemicals.[14] The synthesis consists of three steps: extraction, the use of reducing agents and the application of nontoxic materials. Biological methods can yield nanoparticles of specific sizes and shapes, which is one of the most important requirements in synthesis. Green synthesis of silver nanoparticles utilizes molecules derived from biological systems such as plants, microorganisms, fungi and algae.[15] Molecules obtained from extraction from biological systems, such as phenols, terpenoids, amino acids, vitamins, polysaccharides, proteins, enzymes, tannins, alkaloids and alcohol compounds, are important as reducing and stabilizing agents.[16] Silver

nanoparticles obtained through green synthesis, in contrast to chemical synthesis, exhibit long-lasting antibacterial effects and lower phytotoxicity.[17]

In our study, an aqueous extract of the plant *Agrimonia eupatoria* L. (fam. Rosaceae) was used to synthesize nanoparticles. In addition to its antioxidant and antibacterial properties, this plant possesses anti-inflammatory, neuroprotective, antidiabetic, hepatoprotective and anticancer properties.[18] Due to its high content of bioactive compounds*, A. eupatoria* has exceptional reducing ability, which is a crucial step in the synthesis of metallic nanoparticles. Furthermore, Marković *et al.*[19] identified optimal conditions for the synthesis of silver nanoparticles using this plant in their study, which further supports its selection.

Various strategies have been employed to overcome the negative effects of stress: selection of tolerant genotypes, application of different plant growth regulators and use of organic fertilizers. Species and varieties that can tolerate stress, combined with nanotechnology in agriculture, could be an effective strategy for achieving sustainable production and increasing yields under stress conditions.[20,21]

The aim of this research is to investigate the effect of silver nanoparticles on winter varieties of wheat and barley during the tillering phase, focusing on increasing resistance to low temperatures by analysing proline content, antioxidant activity and extract yield.

EXPERIMENTAL

Chemicals

Silver nitrate (AgNO$_3$, Sigma Aldrich). 1,1-Diphenyl-2-picrylhydrazyl (DPPH, Tokyo Chemical Industry, Tokyo). L-Ascorbic acid (C$_6$H$_7$O$_6$Na, Carl Roth GmbH, Germany). Methanol (CH$_3$OH, Zorka, Serbia). Ninhydrin and orthophosphoric acid (C$_9$H$_6$O$_4$ and H$_3$PO$_4$, Centrohem, Serbia). Glacial acetic acid, toluene and sulfosalicylic acid (CH$_3$COOH, C$_7$H$_8$ and C$_7$H$_6$O$_6$S, Hemos, Serbia). The solutions and chemicals were of analytical grade.

Preparation of plant aqueous extract for the synthesis of silver nanoparticles

The aqueous extract of the plant *A. eupatoria* was prepared using Muruzović *et al*[18] method. Dried and powdered plant material weighing 60 g was immersed in 800 mL of distilled water and left at room temperature for 24 h. The plant material was soaked with the same amount of distilled water and filtered every 24 h, three times. The obtained filtrate was collected and then dried using a rotary evaporator (DLAB, RE 100 S) at 40 °C. The dried extracts were subsequently stored in a refrigerator at 4 °C.

Green synthesis of silver nanoparticles

The synthesis of silver nanoparticles was carried out according to the Marković *et al.*[19] method AgNO$_3$ was used as the silver source to produce AgNPs, while the aqueous extract of *A. eupatoria* served for the reduction and stabilization of silver ions (the color change from light yellow to dark brown confirmed the synthesis). AgNO$_3$ was dissolved at a concentration of 5 mM, and the reaction was performed at 25 °C, pH 4, using 1 % plant extract and stirred for 3 h on a magnetic stirrer (magnetic stirrer MSH 300). After synthesis, the suspension was centrifuged at 4500 rpm for 20 min (Centric 150). After centrifugation, the supernatant was

removed and the precipitated nanoparticles were dried at 40 °C and stored at 4 °C. The synthesis of silver nanoparticles was monitored spectrophotometrically at wavelengths ranging from 200 to 800 nm. The characterization of AgNPs–H$_2$O, including transmission electron microscopy (TEM), UV–Vis spectrophotometry and FTIR spectroscopy was described previously by Marković *et al.*[19]

Growing conditions for cereals, treatment and sampling

Two varieties of winter cereals were analyzed: wheat (*Triticum aestivum* L.), variety Simonida and barley (*Hordeum vulgare* L.) variety Nonius. These varieties are known for their resistance to low temperatures and considering the variability of these factors, it is important to investigate their additional resistance through the application of silver nanoparticles. The experiment was conducted over a period of 10 days in an experimental field of the Agricultural Advisory Service in Kragujevac (44º10′00″N, 20º58′00″E) during the 2023/2024 growing season. Meteorological data on minimum and maximum temperatures were collected through daily measurements. Each variety was sown on an experimental plot of 9 m^2, with a sowing density of 500 seeds per m^2. The experiment was conducted in three replications. One replication was 3 m^2, with each square meter representing different growth conditions for the plants. Within each variety, one square was a control, the second was treated with 5 mg/mL and the third square was treated with 10 mg/mL. The treatment was applied foliarly at concentrations of 5 and 10 mg/mL AgNPs–H$_2$O. After ten days of the treatment, the aboveground parts of the cereals were collected and transported to the laboratory in liquid nitrogen. In the laboratory, the plant material was macerated using the Muruzović *et al*. method, employing a methanolic solvent. The obtained filtrate was collected and dried in a rotary evaporator at 40 °C (DLAB, RE 100 S). The extracts were then stored in a refrigerator at 4 °C. This procedure was used to prepare extracts that were analyzed for proline content, antioxidant activity and extract yield.

Preparation of extracts for determining the extract yield from wheat and barley samples

The extract yield was calculated for all samples collected. Methanol was used in the maceration process to determine the extract yield. For each sample, 5 g of dried and ground aboveground plant material stems and leaves (LSA) was used.

Determination of proline

The proline content was determined spectrophotometrically using Bates *et al*[22] method. The plant extract was homogenized in a porcelain mortar with a 3 % solution of sulfosalicylic acid, after which the homogenate was filtered. Ninhydrin reagent and glacial acetic acid were added to the filtrate. The mixture was then incubated at 100 °C for 1 h. The reaction was interrupted by transferring the test tubes to ice and then toluene was added while stirring. After separating the toluene phase from the aqueous layer, the toluene phase containing proline was taken for absorbance measurement spectrophotometrically at a wavelength of 520 nm (UV-5100B spectrophotometer). Pure toluene was used as a blank. The proline concentration was determined from a standard curve prepared with known concentrations of proline, using the same method as for the samples. The proline concentration was expressed in μmol/g of extract. Each sample was measured in three replicates.

Determination of antioxidant activity

The determination of antioxidant activity was conducted using the DPPH method according to the description by Kumarasamy *et al*.[23] The dry extract was dissolved in methanol (1000 μg/mL), after which a series of double dilutions was prepared. To each diluted sample

of 2 mL, 2 mL of 40 mM DPPH solution was added and allowed to stand in the dark for 30 min at room temperature. After that, the absorbance was measured at 517 nm using a UV--5100B spectrophotometer. A control with methanol, instead of the sample, was prepared in parallel. Ascorbic acid was used as the standard. All samples and controls were tested in three replicates. Based on the obtained results, the percentage inhibition of DPPH radicals and the IC_{50} value were determined. The inhibition assessment was calculated using the following equation:

$$\text{Inhibition (\%)} = 100((A_{\text{control}} - A_{\text{sample}})/A_{\text{control}}) \quad\quad (1)$$

where A_{control} is the absorbance of the control sample and A_{sample} the absorbance of the extract. The IC_{50} value is the effective concentration at which 50 % of the DPPH radicals are neutralized. This value was obtained from the graph of neutralization activity (%) versus sample concentration, as described in detail in the work by Comic et al.[24]

Statistical analysis

Statistical analysis of the data was performed using Excel software (build 16.0.17328.20124, version 2402) and SPSS software (IBM SPSS Statistics, version 26). The obtained mean values of proline concentration and mean values of antioxidant activity expressed as IC_{50} for DPPH were analyzed using two-way analysis of variance (ANOVA) with a significance threshold of $p \leq 0.05$. This test evaluate whether there are statistically significant differences between the analyzed groups.

RESULTS AND DISCUSSION

Based on the characterization of the nanoparticles at the Institute of Nuclear Sciences Vinča, the nanoparticles exhibit isometric morphology and a uniform size distribution (average diameter of 35±1 nm), as confirmed by transmission electron microscopy (TEM) and high-resolution TEM (HRTEM) analyses. The use of scanning transmission electron microscopy (STEM) with high-angle annular dark-field (HAADF) imaging and energy-dispersive spectroscopy (EDS) confirms the crystalline nature of AgNPs. Fourier transform infrared spectroscopy (FTIR) analysis identifies identical functional groups in the plant extracts and corresponding AgNPs, indicating the role of phytochemicals in the reduction of silver ions. Spectrophotometric monitoring of the synthesis process, influenced by various parameters, provides insights into the kinetics and optimal conditions for the formation of AgNP–H_2O Marković et al.[19]

During the ten-day experiment, daily temperatures ranged from –7 to 12 °C, Fig 1. Temperature, as a negative abiotic factor affecting cereals, has primarily been studied in the context of high temperatures and heat stress. There is a substantial body of research addressing the various effects of silver nanoparticles under heat stress conditions.[25,26] However, it is interesting to note that there is limited research examining the impact of silver nanoparticles on cereals in the early developmental stages exposed to low temperatures.

The highest proline concentration was recorded in the barley samples treated with a concentration of 5 mg/mL AgNPs–H_2O (1.213 µmol/g), followed by the wheat samples treated with a concentration of 5 mg/mL AgNPs–H_2O (1.17

μmol/g). The lowest concentrations were recorded in the control samples of wheat (1.074 μmol/g) and barley (1.031 μmol/g), as shown in Fig. 2. The wheat and barley samples treated with the concentration of 5 mg/mL AgNPs–H_2O had higher proline concentrations than those treated with the concentration of 10 mg/mL AgNPs–H_2O. Control samples of wheat and barley exhibited the lowest proline concentrations compared to both treatments with 5 and 10 mg/mL AgNPs–H_2O. Overall, the proline concentration was higher in the treated samples compared to the control samples, indicating that treatment with AgNPs––H_2O positively affects proline accumulation in wheat and barley during exposure to low temperatures, Fig. 2.
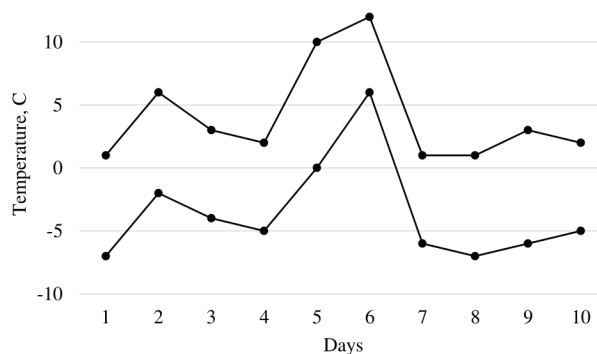
Fig. 1. Temperature fluctuations during the ten-day duration of the experiment.
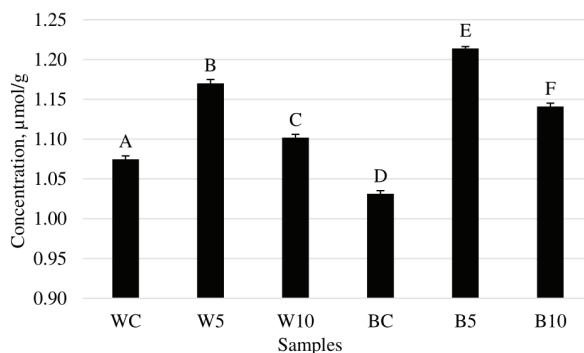
Fig. 2. The average proline content in wheat and barley samples, expressed in μmol/g of extract with standard error. The tested samples are labeled as follows: control – WC, treatment with 5 mg/mL – W5 and with 10 mg/mL – W10. Barley samples are labeled as follows: control – BC, treatment with 5 mg/mL – B5 and with 10 mg/mL – B10.

The obtained average values of proline concentration were subjected to a two-way analysis of variance (ANOVA test) with a significance threshold of $p \leq 0.05$, which showed statistically significant differences among the groups. The student Newman–Keuls test for multiple comparisons confirmed significant

differences between all groups. The mean values of the samples are labeled with different letters. Based on these analyses, it was concluded that there are significant statistical differences in proline concentration among the examined groups, Fig. 2.

Our results on proline accumulation are consistent with the previous studies.[30,31] These studies have shown that gold nanoparticles stimulate proline accumulation in plants exposed to low temperatures. Similarly, in our study, silver nanoparticles also increased proline concentration during exposure to low temperatures, suggesting their potential as cryoprotectants in plants under stress conditions.

According to Li *et al.*[3] repeated exposure to low temperatures over a certain period can also affect cereal productivity. While lower concentrations of nanoparticles may stimulate antioxidant mechanisms in plants, higher concentrations can lead to oxidative stress that the plants cannot overcome.[27] The highest antioxidant activity was recorded in the wheat samples treated with a concentration of 10 mg/mL AgNPs-H$_2$O (IC_{50} = 80.73 µg/mL) and in the wheat samples treated with a concentration of 5 mg/mL AgNPs-H$_2$O (IC_{50} = 118.51 µg/mL). Meanwhile, the barley samples treated with 5 mg/mL AgNPs–H$_2$O had the highest level of antioxidant activity compared to all other barley samples. However, compared to the positive control (ascorbic acid IC_{50} = 54.01 µg/mL), all tested samples, both treated and untreated, showed limited antioxidant activity. The antioxidant activity of AgNPs–H$_2$O was low, Fig. 3.
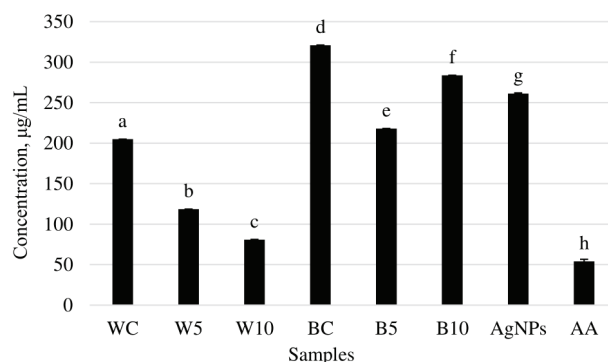
Fig. 3. The antioxidant activity, expressed as average IC_{50} values for DPPH, measured in wheat and barley samples, silver nanoparticles and ascorbic acid with standard error. The tested samples are labeled as follows: control – WC, treatment with 5 mg/mL – W5 and with 10 mg/mL – W10. Barley samples are labeled as follows: control – BC, treatment with 5 mg/mL – B5 and with 10 mg/mL – B10. AA and AgNPs refer to ascorbic acid and silver nanoparticles, respectively.

The obtained antioxidant activity values, expressed as average IC_{50} values for DPPH, were also subjected to an ANOVA test with a significance threshold

of $p \leq 0.05$, which showed statistically significant differences among the groups. Subsequently, the student Newman–Keuls test for multiple comparisons was used, confirming that all groups differ statistically significantly from each other. The mean values of the samples are labeled with different letters. Based on these tests, it was concluded that there are statistically significant differences in antioxidant activity among the examined groups.

Similar to our study, Islam *et al.*[27] used silver nanoparticles and examined their effect on antioxidant activity in wheat and barley grass exposed to temperatures of 5–10 °C. The obtained values showed that wheat grass had higher antioxidant activity than barley grass. Gorczyca *et al.*[28] investigated the antioxidant activity in the roots and leaves of wheat, with and without the presence of nanoparticles. Antioxidant activity was assessed using the enzymes catalase and superoxide dismutase, revealing that the values in treated plants did not differ from the control group. In the study by Budhani *et al.*[29] five different commercial silver nanoparticles negatively affected germination, root growth and shoot length in wheat. Venzhik *et al.*[30] demonstrated that gold nanoparticles at a concentration of 20 μg/mL had the most favorable effect on wheat seedling survival at –3 °C, increasing leaf length, chlorophyll content and carotenoid levels without MDA accumulation. Their subsequent research confirmed that gold nanoparticles can enhance wheat seedling tolerance to low temperatures, with higher survival rates at –3 °C compared to the control, although damage increased at –5 and –7 °C.[31]

Extraction of the aerial parts of plants, stems and leaves (LSA) was performed for 3 wheat samples and 3 barley samples to determine the extract yield for each sample. After complete solvent removal, the extract yield was obtained in g and %, as shown in Table I. The extract yield varied depending on the cereal species and treatment. The wheat samples showed an extract yield of 1.39 g (27.8 mass %) for samples treated with a concentration of 5 mg/mL AgNPs-H_2O (W5), while the samples treated with a concentration of 10 mg/mL AgNPs-H_2O (W10) had a slightly higher yield of 1.62 g (32.4 mass %). The control wheat sample (WC) had a yield of 1.42 g (28.4 mass %). For the barley samples, the control sample (BC) recorded the highest extract yield of 1.67 g (33.4 mass %). The sample treated with 5 mg/mL AgNPs-H_2O (B5) had a yield of 1.65 g (33 mass %), while the sample treated with 10 mg/mL AgNPs-H_2O (B10) showed a slightly lower yield of 1.59 g (31.8 mass %), as shown in Table I.

Numerous studies highlight the importance of silver nanoparticles with effects depending on the genotype of the studied organism, particle size, concentration, nanoparticle coating agents, application method, degree of dispersion and phytochemical properties.[32–35] In our research, silver nanoparticles with an average diameter of 35±1 nm were used, which contributed to increased antioxidant activity and proline content in both wheat and barley varieties compared

to the control groups. Accordingly, the application of silver nanoparticles in agriculture could be an effective approach to enhance resilience and mitigate stress caused by low temperatures during the tillering stage.

TABLE I. Extract yield for wheat and barley samples

Sample	Yield, g	Yield, mass %
WC	1.42	28.4
W5	1.39	27.8
W10	1.62	32.4
BC	1.67	33.4
B5	1.65	33
B10	1.59	31.8

CONCLUSION

Foliar application of silver nanoparticles at concentrations of 5 and 10 mg/mL affected antioxidant activity and proline concentration in both winter cereal varieties: Simonida (*T. aestivum* L.) and Nonius (*H. vulgare* L.) at the tillering stage during low temperatures. Treated plants exhibited better antioxidant activity compared to untreated plants. The highest antioxidant activity was recorded in the wheat samples treated with 10 mg/mL AgNPs–H_2O and the barley samples with 5 mg/mL AgNPs-–H_2O, suggesting that lower nanoparticle concentrations more effectively stimulate antioxidant mechanisms in barley. Overall, the wheat samples demonstrated better antioxidant activity than the barley samples. The highest proline concentrations were recorded in the plants treated with 5 mg/mL, both in wheat and barley, while the plants treated with 10 mg/mL had lower proline concentrations. These results confirm that a lower concentration of silver nanoparticles more effectively increases proline concentration. The yield of the extracts was highest in the wheat treated with 10 mg/mL and in the control barley sample. These results suggest that silver nanoparticles may potentially mitigate the negative effects of low temperatures on cereals and further enhance their resilience.

ИЗВОД

ЕФЕКТИ СРЕБРНИХ НАНОЧЕСТИЦА СИНТЕТИСАНИХ ВОДЕНИМ ЕКСТРАКТОМ
Agrimonia eupatoria L. НА ОЗИМЕ СОРТЕ ПШЕНИЦЕ И ЈЕЧМА

ЂОРЂЕ Д. МИНИЋ¹*, КАТАРИНА Г. МАРКОВИЋ², АНА С. КЕСИЋ², МИРЈАНА З. ГРУЈОВИЋ², СТЕФАН М. МАРКОВИЋ¹, АЛЕКСАНДРА М. ТОРБИЦА³ и НЕВЕНА Х. ЂУКИЋ¹

¹*Универзитет у Крагујевцу, Природно–математички факултет, Катедра за биологију и екологију, Радоја Домановића 12, Крагујевац, ²Универзитет у Крагујевцу, Институт за информационе технологије, Одељење за науку, Јована Цвијића бб, Крагујевац и ³Универзитет у Новом Саду, Научни институт за прехрамбене технологије, Булевар цара Лазара 1, Нови Сад*

Сребрне наночестице представљају потенцијално решење за ублажавање негативних ефеката температурног стреса на житарице. Ова студија испитује утицај сребрних нано-честица на озиме сорте пшенице и јечма током фазе бокорења, фокусирајући се на кон-центрацију пролина, антиоксидативну активност и принос екстракта у зимским пољским условима. Сребрне наночестице (AgNPs) синтетисане су коришћењем зелене методе са воденим екстрактом биљке *Agrimonia eupatoria* L. (fam. Rosaceae). Две сорте озимих житарица, Simonida (*Triticum aestivum* L.) и Nonius (*Hordeum vulgare* L.), третиране су фолијарно са 5 и 10 mg/mL AgNPs–H_2O. Експеримент је трајао 10 дана, током ког је мини-мална забележена температура била −7 °C, у пољским условима. Концентрација пролина била је повећана код сорти третираних наночестицама у поређењу с контролама. Анти-оксидативна активност, одређена је DPPH методом за третиране и нетретиране узорке, уз аскорбинску киселину као позитивну контролу. Антиоксидативна активност била је пове-ћана код свих третираних узорака у односу на нетретиране узорке. Принос екстраката су незнатно повећале само одређене концентрације AgNPs–H_2O. Ово наглашава потенцијал AgNPs–H_2O за побољшање толеранције озимих житарица на ниске температуре.

REFERENCES

1. N. Djukic, D. Knezevic, D. Pantelic, D. Zivancev, A. Torbica, S. Markovic, *J. Plant. Physiol.* **240** (2019) 153015 (https://doi.org/10.1016/j.jplph.2019.153015)
2. X. Li, J. Cai, F. Liu, T. Dai, W. Cao, D. Jiang, *Plant Physiol. Biochem.* **82** (2014) 34 (https://doi.org/10.1016/j.plaphy.2014.05.005)
3. X. Li, H. Pu, F. Liu, Q. Zhou, J. Cai, T. Dai, W. Cao, D. Jiang, *Agron. J.* **107** (2015) 1002 (https://doi.org/10.2134/agronj14.0460)
4. R. Awasthi, K. Bhandari, H. Nayyar, *Front. Environ. Sci.* **3** (2015) (https://doi.org/10.3389/fenvs.2015.00011)
5. A. W. Shaikh, S. Chakraborty, U. R. Islam, *Desalin. Water. Treat.* **130** (2018) 232 (https://doi.org/10.5004/dwt.2018.23004)
6. F. Fatima, A. Hashim, S. Anees, *Environ. Sci. Pollut. Res.* **28** (2021) 1292 (https://doi.org/10.1007/s11356-020-11218-9)
7. K. D. Kapinder, K. A. Verma, *Mater. Today Proc.* **45** (2021) 3819 (https://doi.org/10.1016/j.matpr.2021.03.211)
8. I. Manna, M. A. Bandyopadhyay, *Plant Gene* **17** (2019) 100167 (https://doi.org/10.1016/j.plgene.2018.100167)
9. S. Khan, M. Zahoor, R. Sher-Khan, M. Ikram, U. N. Islam, *Heliyon* **9** (2023) e16928 (https://doi.org/10.1016/j.heliyon.2023.e16928)

10. A. M. Alghuthaymi, H. Almoammar, M. Rai, E. Said-Galiev, A. K. Abd-Elsalam, *Biotechnol. Biotechnol. Equip.* **29** (2015) 221 (https://doi.org/10.1080/13102818.2015.1008194)
11. Z. Almutairi, A. Alharbi, *J. Adv. Agricult.* **4** (2015) 280 (https://doi.org/10.24297/jaa.v4i1.4295)
12. J. Karimi, S. Mohsenzadeh, *Iran J. Sci. Technol. Trans. Sci.* **41** (2017) 111 (https://doi.org/10.1007/s40995-017-0200-6)
13. S. H. Lee, H. B. Jun, *Int. J. Mol. Sci.* **20** (2019) 865 (https://doi.org/10.3390/ijms20040865)
14. P. Banerjee, M. Satapathy, A. Mukhopahayay, P. Das, *Bioresour. Bioprocess.* **1** (2014) (https://doi.org/10.1186/s40643-014-0003-y)
15. T. Mustapha, N. Misni, R. N. Ithnin, M. A. Daskum, Z. A. Unyah, *Int. J Env. Res. Pub. Health* **19** (2022) 674 (https://doi.org/10.3390/ijerph19020674)
16. S. Sudheer, G. R. Bai, K. Muthoosamy, R. Tuvikene, K. V. Gupta, S. Manickam, *Environ. Res.* **204** (2022) 111963 (https://doi.org/10.1016/j.envres.2021.111963)
17. H. Zhang, S. Chen, X. Jia, Y. Huang, R. Ji, L. Zhao, *Sci. Total Environ.* **752** (2021) 142264 (https://doi.org/10.1016/j.scitotenv.2020.142264)
18. M. Z. MuruzoviC, K. G. Mladenović, O. D. Stefanović, S. M. Vasic, L. R. Čomić, *JFDA* **24** (2016) 539 (https://doi.org/10.1016/j.jfda.2016.02.007)
19. K. Markovic, A. Kesic, M. Novakovic, M. Grujovic, D. Simijonovic, E. H. Avdovic, S. Matic, M. Paunovic, M. Milutinovic, D. Nikodijevic, O. Stefanovic, Z. Markovic, *RSC Adv.* **14** (2024) 4591 (https://doi.org/10.1039/D3RA07819A)
20. Y. Arif, P. Singh, H. Siddiqui, A. Bajguz, S. Hayat, *Plant Physiol. Biochem.* **156** (2020) 64 (https://doi.org/10.1016/j.plaphy.2020.08.042)
21. S. Kumari, R. R. Khanna, F. Nazir, M. Albaqami, H. Chhillar, I. Wahid, R. I. Khan, *Int. J. Mol. Sci.* **23** (2022) 4452 (https://doi.org/10.3390/ijms23084452)
22. S. l. Bates, P. R. Waldren, D. I. Teare, *Plant and Soil* **39** (1973) 205 (https://doi.org/10.1007/BF00018060)
23. Y. Kumarasamy, M. Byres, J. P. Cox, M. Jaspars, L. Nahar, D. S. Sarker, *Phytother. Res.* **21** (2007) 615 (https://doi.org/10.1002/ptr.2129)
24. L. R. Comic, B. Z. Licina, I. D. Radojevic, O. D. Stefanovic, S. M. Vasic, *EXCLI J.* **11** (2012) 208 (http://dx.doi.org/10.17877/DE290R-5758)
25. M. J. Al-Khayri, R. Rashmi, R. U. Surya, N.W. Sudheer, A. Banadka, P. Nagella, I. M. Aldaej, S. A. Rezk, F. W. Shehata, I. M. Almaghasla, *Plants* **12** (2023) 292 (https://doi.org/10.3390/plants12020292)
26. G. Shukla, A. Singh, N. Chaudhary, S. Singh, N. Basnal, S. S. Gaurav, *Nanotechnology* **35** (2024) 205101 (https://doi.org/10.1088/1361-6528/ad27af)
27. Z. M. Islam, J. B. Park, T. Y. Lee, *Foods* **10** (2021) 2742 (https://doi.org/10.3390/foods10112742)
28. A. Gorczyca, E. Pociecha, M. Kasprowicz, M. Niemiec, M. *Eur. J. Plant. Pathol.* **142** (2015) 251 (https://doi.org/10.1007/s10658-015-0608-9)
29. S. Budhani, P. N. Egboluche, Z. Arslan, H. Yu, H. Deng, *J. Environ. Sci. Health, C* **37** (2019) 330 (https://doi.org/10.1080/10590501.2019.1676600)
30. Y. Venzhik, A. Deryabin, V. Popov, L. Dykman, I. Moshkov, *Acta Physiol. Plant.* **11** (2022) 113 (https://doi.org/10.1007/s11738-022-03456-w)
31. Y. Venzhik, A. Deryabin, V. Popov, L. Dykman, I. Moshkov, *Plant Physiol. Biochem.* **190** (2022) 145 (https://doi.org/10.1016/j.plaphy.2022.09.006)

32.   B. Mughal, J. Z. Zaidi, X. Zhang, U. S. Hassan, *Appl. Sci.* **11** (2021) 2598 (https://doi.org/10.3390/app11062598)
33.   F. M. Khalid, R. Iqbal-Khan, Z.M. Jawaid, W. Shafqat, S. Hussain, T. Ahmed, M. Rizwan, S. Ercisli, L. O. Pop, R. Alina-Marc, *Nanomaterials* **12** (2022) 3915 (https://doi.org/10.3390/nano12213915)
34.   T. M. El-Saadony, M. A. Saad, M. S. Soliman, M. H. Salem, M. S. Desoky, O. A. Babalghith, M. A. El-Tahan, O. M. Ibrahim, M. A. Ebrahim, A. T. Abd-El-Mageed, S. A. Elrys, A. A. Elbadawi, K. A. El-Tarabily, F. S. AbuQamar, *Front. Plant Sci.* **13** (2022) 946717 (https://doi.org/10.3389/fpls.2022.946717)
35.   R. Prażak A. Święciło, A. Krzepiłko S. Michałek, M. Arczewska, *Agriculture* **10** (2020) 312 (https://doi.org/10.3390/agriculture10080312).

Selected phytochemicals as potent acetylcholinesterase inhibitors: An *in silico* prediction

RAM LAL SWAGAT SHRESTHA[1-3], PRABHAT NEUPANE[1], SUJAN DHITAL[1], NIRMAL PARAJULI[1], BINITA MAHARJAN[1,2], TIMILA SHRESTHA[1,2], SAMJHANA BHARATI[1,2], BISHNU PRASAD MARASINI[3,4] and JHASHANATH ADHIKARI SUBIN[5]∗

[1]Department of Chemistry, Amrit Campus, Tribhuvan University, Lainchour, Kathmandu 44600, Nepal, [2]Kathmandu Valley College, Syuchatar Bridge, Kalanki, Kathmandu 44600, Nepal, [3]Institute of Natural Resources Innovation, Kalimati, Kathmandu 44600, Nepal, [4]Nepal Health Research Council, Ramshah Path, Kathmandu 44600, Nepal and [5]Bioinformatics and Cheminformatics Division, Scientific Research and Training Nepal P. Ltd., Bhaktapur 44800, Nepal

Abstract: In recent times, there has been a notable increase in the widespread presence of Alzheimer's disease. The disease could be controlled by the inhibition of acetylcholinesterase, an enzyme associated with the degradation of acetylcholine. Plants have been used to treat neurogenerative diseases and their phytochemicals could act as acetylcholinesterase inhibitors, impeding the protein's catalytic activity. This study includes a computational assessment of phytocompounds as potent inhibitors of the enzyme. The molecular docking calculations revealed binding affinities of −50.651, –49.446 , –48.400, –47.977, –47.839 and –47.417 kJ/mol for allanxanthone B, stigmasterol, 5'-*O*-methyl dioncophylline D, ismailin, wistin and dioncophylline C2, respectively, indicating firm binding of these molecules with the receptor. Donepezil (a native and FDA-approved drug) exhibited a binding affinity of –46.789 kJ/mol, which was significantly lower than that of the proposed phytochemicals. The successful candidates demonstrated good stability of the complex with the protein, showing smooth *RMSD* of ligands below 6 Å from the 200 ns molecular dynamics simulation. The thermodynamic stability from the MMPBSA method indicated the sustained spontaneity and feasibility of the adducts. Thus, the proposed candidates could be used as remedies for Alzheimer's disease after the experimental verification for their safety and efficacy.

Keywords: binding affinity; catalytic gorge; geometrical stability; free energy changes; molecular dynamics simulation.

187

INTRODUCTION

Alzheimer's disease (AD) is a neurological disorder resulting in a gradual and irreversible deterioration of the cognitive function.[1] It is rapidly emerging as one of the most lethal, costly and burdensome illnesses of the current era.[2] Alzheimer's disease stands as the primary contributor to dementia, a condition that ranks as the seventh most common cause of mortality.[3] Current estimates suggest that around 55 million individuals globally are suffering from it.[3]

The disease could be treated through the inhibition of acetylcholinesterase (AChE), a crucial enzyme involved in the degradation of acetylcholine by increasing the efficiency of the signal given by the brain.[4] It is a neurotransmitter and neuromodulator that binds to receptors of cells that help to contract muscle, dilate blood vessels, reduce heart rate, *etc*.[5] In the treatment of AD, the use of AChE inhibitors is intended to prevent the breakdown of acetylcholine and thus promote improvement in cholinergic neurotransmission.[4] Donepezil, rivastigmine, tacrine and galantamine are some of the promising inhibitors of the enzyme from the clinical trials.[6] The active site gorge of AChE comprises both the peripheral anionic site (PAS) and the catalytic active site (CAS, Fig. 1), which serves as the binding site for competitive inhibitors.[7] The CAS consist of SER203, GLU334 and HIS447 whereas PAS includes TYR72, ASP74, TYR124, TRP286 and TYR341 situated around the gorge of the active site. PAS has a significant role as it binds temporarily with the substrate and could block the substrate from the catalytic site.[8]
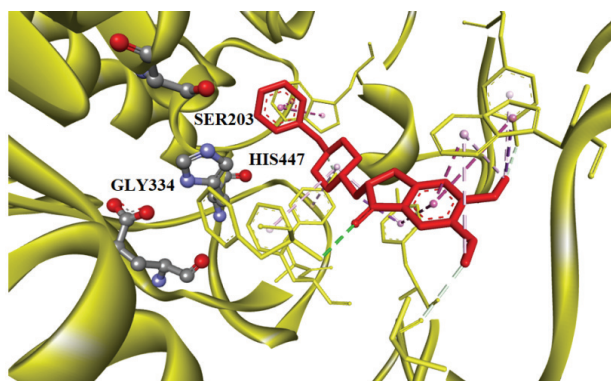
Fig. 1. Native ligand docked (red) in between the peripheral anionic site (PAS) and catalytic active site (CAS) of the protein (PBD ID: 7E3H) showing no interaction with a catalytic triad (SER203, GLY334 and HIS447).

Medicinal plants have been used in ancient Ayurvedic and folk medicines for the treatment of Alzheimer's disease.[9] Phytochemicals have been extensively explored as AChE inhibitors due to various adverse effects associated with current medications.[10] Several literatures have reported plant sources as potent inhi-

bitors of the enzyme as a means for the treatment of Alzheimer's disease.[11] Different computational approaches have been employed in the drug discovery process to facilitate experiments for cost-efficiency and enhanced effectiveness during preliminary screening.[12] Many studies have proposed phytochemicals of different medicinal plants as AChE inhibitors using computational approaches.[13] Computational drug discovery could be employed to accelerate the tedious high throughput experimental screening process by minimizing the likelihood of subsequent failures and recall during clinical trials.[14] This study incorporates *in silico* tools and techniques such as molecular docking, molecular dynamics simulation, binding free energy estimation and ADMET prediction for the exploration of potent AChE inhibitors from plant-based sources.

EXPERIMENTAL

Preparation of ligand and protein structures

A database of 77 bioactive ligands was made from the selected phytochemicals derived from African plants.[15] The 3D structure of the ligands was downloaded in sdf format from the PubChem database[16] and their molecular structures and bond order were checked using the Avogadro software.[17] The protein 3D crystalline structure with PDB ID: 7E3H[18] (X-ray resolution = 2.45 Å, expression system = *Homo sapiens*) was downloaded from the RCSB protein data bank server.[19] The protein was cleaned by removing water molecules, co-crystallized native ligand and chain B using the PyMOL program.[20] The receptor was further subjected to evaluation of geometrical structure through the ERRAT, PROCHECK and VERIFY modules of the SAVES v6.0 server.[21]

Molecular docking calculations

The DockThor server was employed for the flexible docking calculations.[22] Choice of the docking method was based on its ability to undergo multiple docking calculations within a short period of time using a freely available web server, as well as its ability to reproduce the same results.[22] The inclusion of solvated environment and protein flexibility tends to provide the best possible model to the natural system. The details of the docking parameters were adopted from recently published literature.[23] The selected parameters include the box coordinates of (–43, 36, –32), the box size of (16, 16, 16), the population size of 750, the discretization of 0.17, 24 runs and 1,000,000 evaluations. The interactions between the ligand and the amino acid residues were visualized using Biovia Discovery Studio.[24] The docking protocol was validated by achieving a root mean square deviation (*RMSD*) of less than 2 Å for the heavy atoms of the ligand, as obtained through superimposing the native ligand and the re-docked ligand (Fig. 2).

Molecular dynamics simulation (MDS) and binding free energy estimation

GROMACS program[25] was used for the simulation studies and a combination of Charmm27 force field[26] and TIP3P solvation model[27] were utilized. Other parameters were adopted from recent literature.[28] The equilibration process involved running two simulations: one under NPT conditions and another under NVT conditions, each lasting 500 ps and totalling 2 ns. These simulations were conducted at a standard body temperature of 310K. Following equilibration, a production run of 200 ns was carried out using a time step of 2 fs. Various molecular dynamics (MD) parameters were extracted from GROMACS software's built-in modules. The binding free energy post-MD simulation was determined by analysing the equilib-

rated 20 ns of the MD trajectory, employing the molecular mechanics Poisson Boltzmann solvation model.[29]
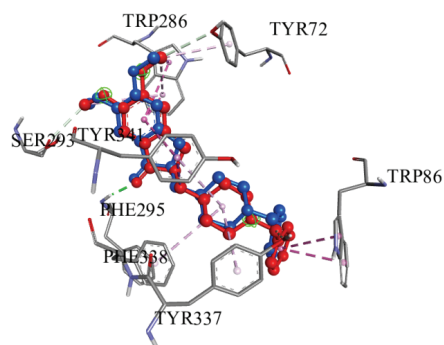
Fig. 2. Superimposition of native (red) and redocked ligand (blue) along with their interactions with amino acid residues at the catalytic pocket of protein.

The changes in binding free energy of the protein–ligand complex are given as:[28]

$$\Delta G_{BFE} = \Delta G_{complex} - \Delta G_{protein} - \Delta G_{ligand} \qquad (1)$$

ADMET Prediction

The safety and drug-likeness such as toxicity, excretion, distribution, metabolism and absorption properties of the hit candidates were determined through the pkCSM server.[30]

RESULTS AND DISCUSSION

For the disruption of normal functioning of a protein through competitive inhibition, the ligand should strongly bind to the active site of the receptor protein.[31,32] The crystalline protein (PDB ID: 7E3H) contains the FDA-approved drug, donepezil[33] as a native ligand docked in between the CAS and PAS.[18] The docked ligand with stronger binding in terms of binding affinity than the native could stop the catalytic activity of the enzyme by blocking the binding to the catalytic triad.

Protein structure evaluation

The quality of protein geometry in terms of the ERRAT module was 94.21 indicating the high overall quality of the protein structure. Around 91.65 % of the amino acid residues passed the VERIFY module suggesting the good 3D structure of the protein appropriate for computational assessment. Ramachandran plots depicted that no amino acid residues were on the disallowed region out of 528 with 90 % on the most favoured region as shown in the supplementary information (Fig. S-1 of the Supplementary material to this paper).

Binding affinity from molecular docking calculation

From the molecular docking calculation, 12 compounds exhibited greater binding affinity than that of native with –46.789 kJ/mol and are shown in Tables I and S-I (Supplementary material). The best binding affinity of –50.651 kJ/mol

was observed with allanxanthrone B having a significant difference of 3.861 kJ/mol than that of donepezil. The binding affinities of –49.446, –48.400 and –48.216 kJ/mol were observed with stigmasterol, 5'-*O*-methyldioncophylline D and durallone, respectively. Other compounds like simplexin, ismailin, witsin, dioncophylline C2, asphodelin, sungucine, rotenone and azadirone also showed better binding than that of the native exceeding binding affinity of 46 kJ/mol. In addition, majority of the docked compounds showed better binding affinities than that of reference drugs, galantamine (–39.840 kJ/mol) and rivastigmine (–37.166 kJ/mol).

The stronger binding of several ligands compared to the native ligand at the orthosteric pocket of the AChE suggests their potential for superior protein inhibition.

TABLE I. Binding affinity of top candidates with protein AChE

S.N.	Ligand	PubChem CID	Binding affinity, kJ/mol
1	Allanxanthone B	11328706	–50.651
2	Stigmasterol	5280794	–49.446
3	5′-O-methyldioncophylline D	132542154	–48.400
4	Durallone	1023565	–48.216
5	Simplexin	119045	–47.990
6	Ismailin	135454728	–47.977
7	Wistin	10095770	–47.839
8	Dioncophylline C2	132500912	–47.417
9	Asphodelin	182665	–47.325
10	Sungucine	189778	–47.237
11	Rotenone	6758	–46.944
12	Azadirone	10906239	–46.814
13	Native	1150567	–46.789
14	Galantamine	9651	–39.840
15	Rivastigmine	77991	–37.166

Protein–ligand interactions

From the 2D interaction between ligand and the amino acid residues of top candidates, several interactions such as π–π stacked, alkyl, π–alkyl, π–cation, hydrogen bonds, carbon–hydrogen bonds and van der Waals were observed (Table S-II of the Supplementary material). The interactions with amino acid residues such as TRY72, TRP286, PHE295, TYR337 and TYR341 as well as one of the catalytic triad, HIS477 were observed between the docked ligand and amino acid residues of AchE (Figs. 3 and S2). The majority of interactions of the docked ligands were similar to the ones observed with the native as shown in Figs. 2 and 3 indicating that the ligands were docked at the same location as the native. Despite several electronegative centres in the majority of ligands, only a few hydrophilic interactions were detected, specifically forming hydrogen bonds

with amino acid residues ASP74, PHE295 and HIS447. In addition, one of the ligands, ismailin, showed the π–cation interaction with amino acid residue ASP74 and π–lone pair interaction with TYR124. Several van der Waals interactions with the amino acid residues of PAS and catalytic triad were observed. However, there was no observed interaction with the catalytic triad residue, GLY334, as it was positioned further away from the docked site. Similar interactions were observed in recent literature with molecular docking of AChE.[34]
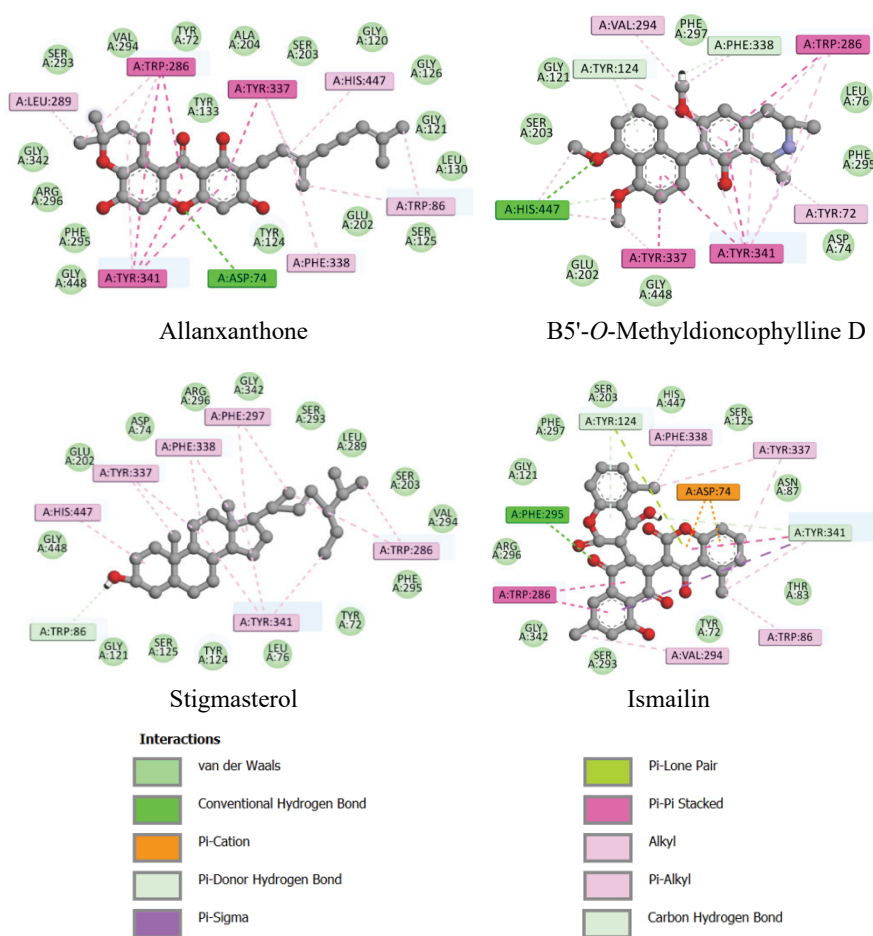
Fig. 3. 2D interaction between amino acid residues of protein (PDB ID: 7E3H) and docked ligands.

It could be deduced that the ligands were docked between the peripheral anionic site (PAS) and catalytic active site (CAS), similar to that of the native

ligand, donepezil.[7] Thus, the docked ligand could block competitive ligands reaching the catalytic triad halting the catalytic function of the receptor.

*Root mean square deviation (*RMSD*)*

RMSD of protein backbone and ligands, both with respect to the protein backbone, helps to determine the geometrical stability of the ligand with the receptor protein.[23] The deviation of ligands within the orthosteric pocket could be monitored from the *RMSD* plots shown in Fig. 4A. The plots depicted no significant deviation of the ligand from the docked pose with few trivial spikes in the *RMSD* trajectory. Dioncophylline C2, wistin, ismailin, stigmasterol, allanxanthrone B and 5'-*O*-methyldioncophylline D exhibited good stability with the enzyme having heavy atom *RMSD* of ligand below 6 Å. Dioncophylline demonstrated the best stability with a smooth trajectory and *RMSD* at around 3 Å. Stigmasterol, ismailin and wistin also exhibited good geometrical stability, with *RMSD* below 4 Å, albeit with occasional spikes in the trajectory. Despite the rise of *RMSD* of allanxanthrone B at the beginning, the system attained equilibrium after *ca.* 100 ns and smooth *RMSD* was observed up to 200 ns. In the case of 5'--*O*-methyldioncophylline D, a comparative smooth trajectory with *RMSD* of ligand at approximately 5 Å was observed. Slightly unstable nature of curve with multiple bumps and higher *RMSD* was observed in case of durallone and simplexin as depicted in Fig. S-3 of the Supplementary material. The protein backbone *RMSD* remained steady and smooth at around 2 Å (Fig. 4B) without noticeable bumps or spikes inferring the stability of protein structure upon ligand binding.

From the *RMSD* trajectory, it could be deduced that the ligand attained geometrical stability within the orthosteric pocket of AChE without significant deviation in terms of the *RMSD* of the ligand.

Fig. 4. *RMSD* of ligands (A) and protein (B) of dioncophylline C2 (magenta), wistin (orange), ismailin (red), stigmasterol (blue), allanxanthrone B (dark) and 5'-*O*-methyldioncophylline D (green) complexes.

The relative rotational and translation motion of the ligands could be monitored from the snapshots retrieved at different times from the molecular dynamics simulation.[23,28] From the snapshots (Fig. S-4 of the Supplementary material) it was evident that the ligand remained in its docked location between the PAS and CAS with minute alteration of position and orientation. Despite lower translational motion, a significant rotational motion could be observed for the majority of ligands which were reflected by a few spikes and bumps in the *RMSD* profiles. The shift of position of witsin could have contributed to sudden spikes in the *RMSD* curve. The *RMSD* curve of the ligand of allanxanthrone B complex and the relative position of the ligand at the docked site were correlated as the ligand underwent significant rotation and was localized after the attainment of equilibrium as depicted in Fig. 4. In spite of a noticeable rotational shift, the docked ligands remained localized within the orthosteric pocket and thus could result in inhibition of the AChE enzyme.

The radial-distribution curve depicts the presence of a single sharp peak for dioncophylline C2, wistin and stigmasterol inferring the localization of ligands without any change in center of mass[35] as shown in Fig. 5. However, ismailin, allanxanthrone B and 5'-*O*-methyldioncophylline D demonstrated two peaks, one large peak and another small ridge signifying that the ligand's centre of mass shifted between the two, with a predominant presence at one particular site.
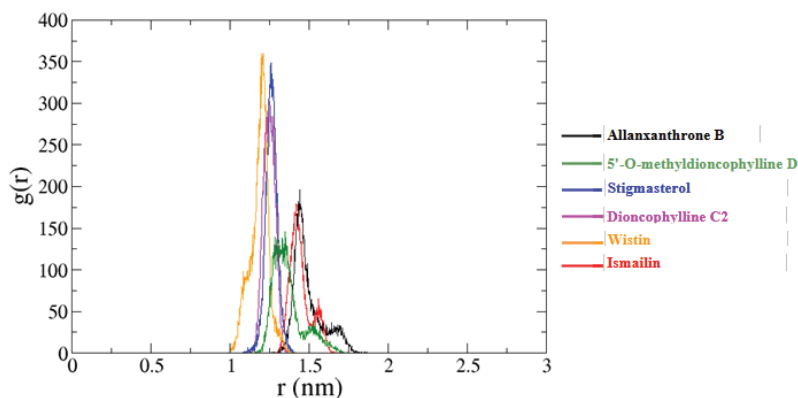
Fig. 5. Radial pair distribution function ($g(r)$) of the ligands' centre of mass with reference to that of the protein in dioncophylline C2 (magenta), wistin (orange), ismailin (red), stigmasterol (blue), allanxanthrone B (dark) and 5'-*O*-methyldioncophylline D (green) complexes.

*Other geometrical evaluators (*RMSF*, R$_g$,* SASA *and H-bond)*

The root mean square fluctuation (*RMSF*) plot of the protein backbone (α-carbon) is depicted in Fig. 6. *RMSF* plot helps to evaluate the stability of the protein structure as an unstable loop structure shows greater fluctuation as com-

pared to stable sheet and helix structures.[36] The fluctuation of amino acid residues was less than 2 Å with an exception at *ca.*76 and 430 amino acid residue numbers. The amino acid residues of PAS and the catalytic triad were not in the proximity of the spiked region, demonstrating a fluctuation less than approximately 1.5 Å. Among the catalytic triad, GLU334 showed slightly higher fluctuation than SER203 and HIS447. This might be attributed to the binding of the docked ligand with SER203 and HIS447 only. The amino acids interacting with the docked ligands such as TRP72, ASP74, TRY124, TRP286 and TYR341 demonstrated lesser fluctuations as compared to other amino acid residues which might be due to induced stability from stronger binding with the docked ligands.
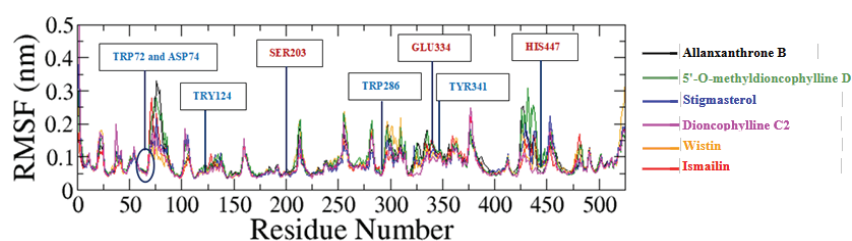
Fig. 6. *RMSF* plot of protein backbone of dioncophylline C2 (magenta), wistin (orange), ismailin (red), stigmasterol (blue), allanxanthrone B (black) and 5'-O-methyldioncophylline D (green) complexes.

The solvent-accessible surface area (*SASA*) of all the complexes were nearly the same at approximately 215 ± 10 nm^2 inferring the stability of protein structure upon the interaction with the ligands[37] as depicted in Fig. 7. The *SASA* trajectory remained smooth without any significant bumps and spikes indicating that the hydrophobic region of the receptor was not exposed upon ligand binding. A similar smooth trajectory was seen in the case of the radius of gyration (R_g) of complexes at *ca.* 23 ± 0.25 Å, signifying no change in protein conformation in terms of expansion and contraction.[38] The steady and smooth trajectory of R_g and *SASA* retrieved from the MDS trajectory emphasized the geometrical stability of the protein structure upon ligand binding.
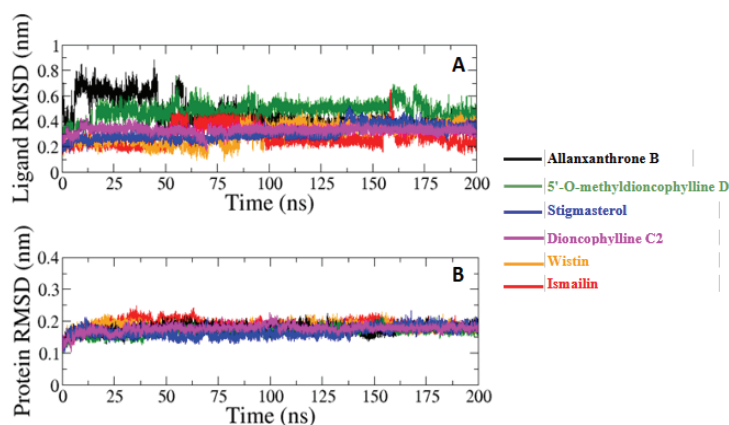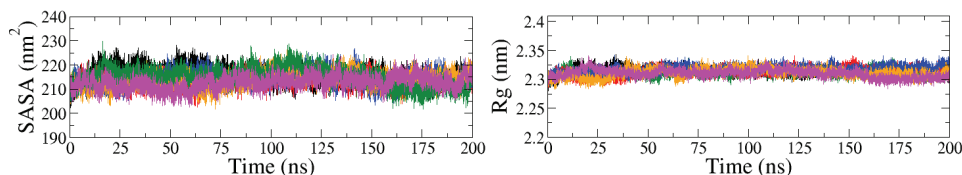

Fig. 7. *SASA* (left) and R_g (right) of protein of dioncophylline C2 (magenta), wistin (orange), ismailin (red), stigmasterol (blue), allanxanthrone B (dark) and 5'-*O*-methyldioncophylline D (green) complexes.

The hydrogen bonds formed between the amino acid residues throughout the 200 ns production run was monitored since hydrogen bond governs several biological processes such as metabolism, adsorption, drug affinity and specificity.[39] From the MD simulation, a noticeable variation in the number of hydrogen bond formation of each complex could be observed as shown in Fig. 8. Allanxanthrone B, stigmasterol, 5'-*O*-methyldioncophylline D and dioncophylline C2 demonstrated almost similar number of hydrogen bond formation around 2 to 4. A significant contrast could be observed in case of wistin and ismailin. Wistin demonstrated a maximum number of hydrogen bond formations with 7 to 8, whereas, the lowest hydrogen bond count was seen in isamailin complex.
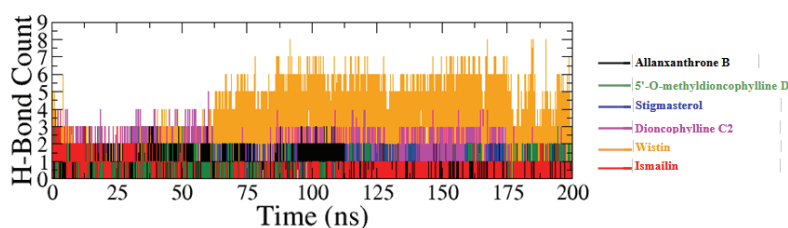
Fig. 8. Number of hydrogen bonds formed between the amino acid residues and dioncophylline C2 (magenta), wistin (orange), ismailin (red), stigmasterol (blue), allanxanthrone B (dark) and 5'-*O*-methyldioncophylline D (green).

Binding free energy change estimation (ΔG$_{BFE}$)

The change in binding free energy of the adducts from the MMPBSA method was used to assess the spontaneity and feasibility of the reaction as shown in Table II. A higher negative binding free energy (ΔG_{BFE}) indicates higher spontaneity and feasibility of the reaction.[40] The best binding free energy change was observed with stigmasterol with –131.33±18.24 kJ/mol. Binding free energy change of –108.36±18.66, –94.60±19.49, –93.59±29.32, –89.99±18.49 and –77.61±17.07 kJ/mol was observed with dioncophylline C2, allanxanthone B, wistin, 5′-*O*-methyldioncophylline D and ismailin, respectively. Except for the highest and the lowest scorers, all other complexes showed nearly identical changes in binding free energy. Among the several components, the change in energy due to van der Waals force of interaction was significant compared to

TABLE II. Change in binding free energy (kJ/mol) of hit candidates

Complex	ΔG_{BFE}
Allanxanthone B	–94.64±19.49
Stigmasterol	–131.33±18.24
5′-*O*-Methyldioncophylline D	–89.99±18.49
Ismailin	–77.61±17.07
Wistin	–93.59±29.32
Dioncophylline C2	–108.36±18.66

others. This outcome could be due to the cumulative contribution of several van der Waals interactions as shown in 2D protein–ligand interactions (Fig. 3 and Table S-III of the Supplementary material). All the complexes exhibited negative ΔG_{BFE} indicating thermodynamically stable complexes with sustained spontaneity.

Drug-likeness and safety

The comparative prediction of ADMET properties of the successful candidates, native and reference drug compounds is shown in Tables S-IV and S-V of the Supplementary material. From the comparative analysis, it was found that wistin and stigmasterol showed moderate to good drug-likeness properties with almost no toxicity. These results were better than that of other successful candidates and comparable with the native and the two reference drugs. However, *in vivo* and *in vitro* experiments should still be performed to ascertain these predictions.

CONCLUSION

The *in silico* approach revealed the phytochemicals such as dioncophylline C2, wistin, ismailin, stigmasterol, allanxanthrone B and 5'-*O*-methyldioncophylline D as potent inhibitors of the acetylcholinesterase enzyme. The compounds showed good geometrical and thermodynamical stability with the protein and could inhibit the enzyme by preventing its catalytic functions. However, several *in vitro* and *in vivo* experiments need to be done to evaluate their safety and effectiveness. Therefore, plant-based compounds could be applied in the treatment of neurodegenerative diseases like Alzheimer's.

SUPPLEMENTARY MATERIAL

Additional data and information are available electronically at the pages of journal website: https://www.shd-pub.org.rs/index.php/JSCS/article/view/12876, or from the corresponding author on request.

И З В О Д

ОДАБРАНЕ ФИТОХЕМИКАЛИЈЕ КАО МОЋНИ ИНХИБИТОРИ АЦЕТИЛХОЛИНЕСТЕРАЗА: *IN SILICO* ПРЕДВИЂАЊЕ

RAM LAL SWAGAT SHRESTHA[1-3], PRABHAT NEUPANE[1], SUJAN DHITAL[1], NIRMAL PARAJULI[1], BINITA MAHARJAN[1,2], TIMILA SHRESTHA[1,2], SAMJHANA BHARATI[1,2], BISHNU PRASAD MARASINI[3,4] и JHASHANATH ADHIKARI SUBIN[5]

[1]Department of Chemistry, Amrit Campus, Tribhuvan University, Lainchour, Kathmandu 44600, Nepal, [2]Kathmandu Valley College, Syuchatar Bridge, Kalanki, Kathmandu 44600, Nepal, [3]Institute of Natural Resources Innovation, Kalimati, Kathmandu 44600, Nepal, [4]Nepal Health Research Council, Ramshah Path, Kathmandu 44600, Nepal и [5]Bioinformatics and Cheminformatics Division, Scientific Research and Training Nepal P. Ltd., Bhaktapur 44800, Nepal

У скорије време је дошло до приметног распрострањивања Алцхајмерове болести. Болест се може контролисати инхибицијом ацетилхолинестеразе, ензима повезаног са деградацијом ацетилхолина. Биљке које су коришћене за лечење неурогенеративних

болести и њихове фитохемикалије могу деловати као инхибитори ацетилхолинестеразе, спречавајући каталитичку активност протеина. Ова студија садржи рачунарску процену фитоједињења као моћних инхибитора ензима. Израчунавања молекулског докинга показују афинитете везивања од −50,651, −49,446, −48,400, −47,977, −47,839 и −47,417 kJ/mol за алаксантон B, стигмастерол, 5'-О-метил дионкофилин D, исмаилин, вистин, односно дионкофилин C2, што указује на чврсто везивање ових молекула за рецептор. Донезепил (нативни и од FDA одобрен лек) испољава везивни афинитет од −46,789 kJ/mol, који је знатно нижи него код предложених фитохемикалија. Успешни кандидати су показали добру стабилност комплекса са протеином, показујући глатку *RMSD* лиганада испод 6 Å из симулације молекулске динамике током 200 ns. Термодинамичка стабилност по MM-PBSA методи указује на сталну спонтаност и остварљивост адуката. Тако се предложени успешни кандидати могу користити као лекови за Алцхајмерову болест након експерименталне провере њихове безбедности и ефикасности.

REFERENCES

1. B. Ibach, E. Haen, H. E. Klein, *Curr. Pharm. Des.* **10** (2004) 231 (https://doi.org/10.2174/1381612043386509)
2. P. Scheltens, B. D. Strooper, M. Kivipelto, H. Holstege, G. Chételat, C. E. Teunissen, J. Cummings, W. M. van der Flier, *Lancet* **397** (2021) 1577 (https://doi.org/10.1016/S0140-6736(20)32205–4)
3. World Health Organization (WHO), https://www.who.int/news-room/fact-sheets/detail/dementia (3 March 2024)
4. V. N. Talesa, *Mech. Ageing Dev.* **122** (2001) 1961 (https://doi.org/10.1016/S0047-6374(01)00309-8)
5. M. R. Picciotto, M. J. Higley, Y. S. Mineur, *Neuron* **76** (2012) 116 (https://doi.org/10.1016/j.neuron.2012.08.036)
6. M. Racchi, M. Mazzucchelli, E. Porrello, C. Lanni, S. Govoni, *Pharmacol. Res.* **50** (2004) 441 (https://doi.org/10.1016/j.phrs.2003.12.027)
7. D. A. Belinskaia, P. A. Voronina, D. V. Krivorotov, R. O. Jenkins, N. V. Goncharov, *Pharmaceutics* **15** (2023) 2159 (https://doi.org/10.3390/pharmaceutics15082159)
8. G. Johnson, S. W. Moore, *Curr. Pharm. Des* **12** (2006) 217 (https://doi.org/10.2174/138161206775193127)
9. T. Dubey, S. Chinnathambi, *Arch. Biochem. Biophys.* **676** (2019) 108153 (https://doi.org/10.1016/j.abb.2019.108153)
10. H. Khan, Marya, S. Amin, M. A. Kamal, S. Patel, *Biomed. Pharmacother.* **101** (2018) 860 (https://doi.org/10.1016/j.biopha.2018.03.007)
11. N. A. Masondo, G. I. Stafford, A. O. Aremu, N. P. Makunga, *South African J. Bot.* **120** (2019) 39 (https://doi.org/10.1016/j.sajb.2018.09.011)
12. C. L. Hung, C. C. Chen, *Drug Dev. Res.* **75** (2014) 412 (https://doi.org/10.1002/ddr.21222)
13. B. Sarkar, S. Alam, T. K. Rajib, S. S. Islam, Y. Araf, M. A. Ullah, *Egypt. J. Med. Hum. Genet.* **22** (2021) 10 (https://doi.org/10.1186/s43042-020-00127-8)
14. S. S. Ou-Yang, J. Y. Lu, X. Q. Kong, Z. J. Liang, C. Luo, H. Jiang, *Acta Pharmacol. Sin.* **33** (2012) 1131 (https://doi.org/10.1038/aps.2012.109)
15. B. D. Bekono, F. Ntie-Kang, P. A. Onguéné, L. L. Lifongo, W. Sippl, K. Fester, L. C. O. Owono, *Malar. J.* **19** (2020) 183 (https://doi.org/10.1186/s12936-020-03231-7)

16. S. Kim, J. Chen, T. Cheng, A. Gindulyte, J. He, S. He, Q. Li, B. A. Shoemaker, P. A. Thiessen, B. Yu, L. Zaslavsky, J. Zhang, E. E. Bolton, *Nucleic Acids Res.* **51** (2023) D1373 (https://doi.org/10.1093/nar/gkac956)
17. M. D. Hanwell, D. E. Curtis, D. C. Lonie, T. Vandermeerschd, E. Zurek, G. R. Hutchison, *J. Cheminform.* **4** (2012) 17 (https://doi.org/10.1186/1758-2946–4-17)
18. K. V. Dileep, K. Ihara, C. Mishima-Tsumagari, M. Kukimoto-Niino, M. Yonemochi, K. Hanada, M. Shirouzu, K. Y. J. Zhang, *Int. J. Biol. Macromol.* **210** (2022) 172 (https://doi.org/10.1016/j.ijbiomac.2022.05.009)
19. H. M. Berman, J. Westbrook, Z. Feng, G. Gilliland, T. N. Bhat, H. Weissig, I. N. Shindyalov, P. E. Bourne, *Nucleic Acids Res.* **28** (2000) 235 (https://doi.org/10.1093/nar/28.1.235)
20. S. Yuan, H. C. S. Chan, Z. Hu, *WIREs Comp. Mol. Sci.* **7** (2017) e1298 (https://doi.org/10.1002/wcms.1298)
21. C. Colovos, T. O. Yeates, *Protein Sci.* **2** (1993) 1511 (https://doi.org/10.1002/pro.5560020916)
22. K. B. Santos, I. A. Guedes, A. L. M. Karl, L. E. Dardenne, *J. Chem. Inf. Model.* **60** (2020) 667 (https://doi.org/10.1021/acs.jcim.9b00905)
23. R. L. S. Shrestha, B. Maharjan, T. Shrestha, B. P. Marasini, J. Adhikari Subin, *Results Chem.* **7** (2024) 101363 (https://doi.org/10.1016/j.rechem.2024.101363)
24. U. Baroroh, M. Biotek, Z. S. Muscifa, W. Destiarani, F. G. Rohmatullah, M. Yusuf, *Indones. J. Comput. Biol.* **2** (2023) 22 (https://doi.org/10.24198/ijcb.v2i1.46322)
25. M. J. Abraham, T. Murtola, R. Schulz, S. Páll, J. C. Smith, B. Hess, E. Lindah, *SoftwareX* **1** (2015) 19 (https://doi.org/10.1016/j.softx.2015.06.001)
26. V. Zoete, M. A. Cuendet, A. Grosdidier, O. Michielin, *J. Comput. Chem.* **32** (2011) 2359 (https://doi.org/10.1002/jcc.21816)
27. W. L. Jorgensen, J. Chandrasekhar, J. D. Madura, R. W. Impey, M. L. Klein, *J. Chem. Phys.* **79** (1983) 926 (https://doi.org/10.1063/1.445869)
28. P. Neupane, J. Adhikari Subin, R. Adhikari, *J. Biomol. Struct. Dyn.* (2024) 1 (https://doi.org/10.1080/07391102.2024.2314262)
29. M. S. Valdés-Tresanco, M. E. Valdés-Tresanco, P. A. Valiente, E. Moreno, *J. Chem. Theory Comput.* **17** (2021) 6281 (https://doi.org/10.1021/acs.jctc.1c00645)
30. D. E. Pires, T. L. Blundell, D. B. Ascher, *J. Med. Chem.* **58** (2015) 4066 (https://doi.org/10.1021/acs.jmedchem.5b00104)
31. R. L. S. Shrestha, R. Panta, B. Maharjan, T. Shrestha, S. Bharati, S. Dhital, P. Neupane, N. Parajuli, B. P. Marasini, J. Adhikari Subin, *Mor. J. Chem* **12** (2024) 776 (https://doi.org/10.48317/IMIST.PRSM/morjchem-v12i2.46845)
32. P. Neupane, S. Dhital, N. Parajuli, T. Shrestha, S. Bharati, B. Maharjan, J. Adhikari Subin, R. L. S. Shrestha, *J. Nepal Phys. Soc.* **9** (2023) 95 (https://doi.org/10.3126/jnphyssoc.v9i2.62410)
33. E. Y. Shintani, K. M. Uchida, *Am. J. Health-Syst. Pharm.* **54** (1997) 2805 (https://doi.org/10.1093/ajhp/54.24.2805)
34. Q. M. S. Jamal, M. I. Khan, A. H. Alharbi, V. Ahmad, B. S. Yadav, *Nutrients* **15** (2023) 1579 (https://doi.org/10.3390/nu15071579)
35. T. R. Lamichhane, M. P. Ghimire, *Heliyon* **7** (2021) E08220 (https://doi.org/10.1016/j.heliyon.2021.e08220)
36. B. K. Raut, S. R. Upadhyaya, J. Bashyal, N. Parajuli, *ACS Omega* **8** (2023) 43617 (https://doi.org/10.1021/acsomega.3c05082)

37. E. Durham, B. Dorr, N. Woetzel, R. Staritzbichler, J. Meiler, *J. Mol. Model.* **15** (2009) 1093 (https://doi.org/10.1007/s00894-009-0454-9)
38. M. Y. Lobanov, N. S. Bogatyreva, O. V. Galzitskaya, *Mol. Biol.* **42** (2008) 623 (https://doi.org/10.1134/S0026893308040195)
39. A. Shrestha, S. R. Upadhyaya, B. K. Raut, S. Bhattarai, K. R. Sharma, N. Parajuli, J. K. Sohng, & B. P. Regmi, *Processes* **12** (2024) 230 (https://doi.org/10.3390/pr12010230)
40. Z. Cournia, B. Allen, W. Sherman, *J. Chem. Inf. Model.* **57** (2017) 2911 (https://doi.org/10.1021/acs.jcim.7b00564).

Selected phytochemicals as potent acetylcholinesterase inhibitors: An *in silico* prediction

RAM LAL SWAGAT SHRESTHA[1-3], PRABHAT NEUPANE[1], SUJAN DHITAL[1], NIRMAL PARAJULI[1], BINITA MAHARJAN[1,2], TIMILA SHRESTHA[1,2], SAMJHANA BHARATI[1,2], BISHNU PRASAD MARASINI[3,4] and JHASHANATH ADHIKARI SUBIN[5]∗

[1]*Department of Chemistry, Amrit Campus, Tribhuvan University, Lainchour, Kathmandu 44600, Nepal,* [2]*Kathmandu Valley College, Syuchatar Bridge, Kalanki, Kathmandu 44600, Nepal,* [3]*Institute of Natural Resources Innovation, Kalimati, Kathmandu 44600, Nepal,* [4]*Nepal Health Research Council, Ramshah Path, Kathmandu 44600, Nepal and* [5]*Bioinformatics and Cheminformatics Division, Scientific Research and Training Nepal P. Ltd., Bhaktapur 44800, Nepal*

Fig. S-5. Ramachandran plot with statistics (SAVES v6.0 server. Procheck program).
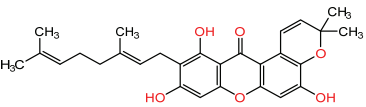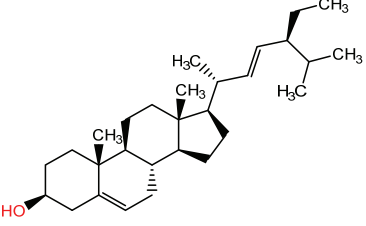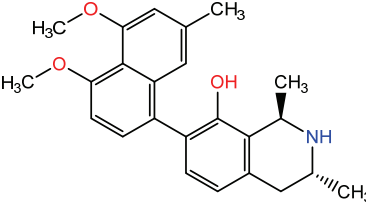
∗ Corresponding author. E-mail: subinadhikari2018@gmail.com

SHRESTHA *et al.*
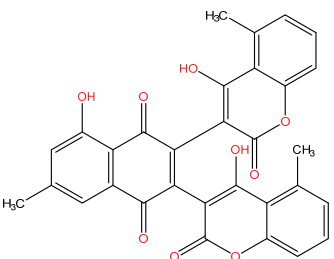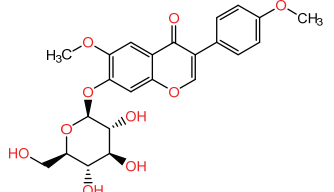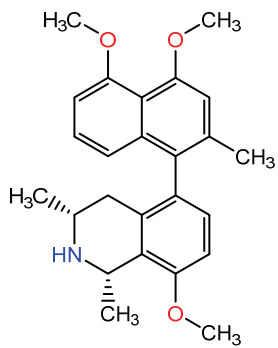
TABLE S-I: Binding affinity (kJ/mol) of the docked ligands with protein (PDB ID: 7E3H)

S. N	Ligands	PubChem CID	Binding affinity (kJ/mol)
1	Allanxanthone B	11328706	–50.651
2	Stigmasterol	5280794	–49.446
3	5′-O-methyldioncophylline D	132542154	–48.400
4	Durallone	1023565	–48.216
5	Simplexin	119045	–47.990
6	Ismailin	135454728	–47.977
7	Wistin	10095770	–47.839
8	Dioncophylline C2	132500912	–47.417
9	Asphodelin	182665	–47.325
10	Sungucine	189778	–47.237
11	Rotenone	6758	–46.944
12	Azadirone	10906239	–46.814
13	Native	1150567	–46.789
14	Niloticin	14021529	–46.651
15	Strychnogucine C	5321534	–46.505
16	7,2′-dimethoxy–4′,5′-methylenedioxyisofavone	343083	–46.496
17	Mellerin B	102317133	–46.061
18	Dioncophylline F	132500908	–46.032
19	Hispidol B	13967183	–45.923
20	Isoacteoside	6476333	–45.835
21	Piscidinol A	12004524	–45.814
22	Isoknipholone	11729754	–45.781
23	Seco-tiaminic acid A	122178985	–45.697
24	Stachannin	44258461	–45.501
25	Jamaicin	12304682	–45.203
26	Microdontin A	101629131	–45.053
27	Maximaisoflavone B	44257236	–44.986
28	Salaterpene A	102583505	–44.969
29	Retusin	5352005	–44.915
30	Busseihydroquinone C	60201022	–44.911
31	Microdontin B	101629132	–44.777
32	Tetrahydropalmatine	5417	–44.764
33	Quercetin-3-O-β-dglucopyranoside	5280804	–44.689
34	Deguelin	107935	–44.685
35	Volkensiflavone	5480834	–44.584
36	Montrifoline	157014	–44.555
37	5-Demethyltangeretin	96539	–44.517
38	Pectolinarigenin-7-glucoside	44258439	–44.488
39	Tephrodin	44257635	–44.475
40	Calopogoniumisoflavone A	354119	–44.404
41	Kaempferol 3-O-beta-D-glucoside	5282102	–44.379
42	Mzikonone	14109464	–44.367
43	Ekeberin A	101843374	–44.061
44	Busseihydroquinone D	60201023	–43.994

45	Dianellin	422284	–43.798
46	Ursolic acid	64945	–43.722
47	Lupeol	259846	–43.706
48	Macluraxanthone	5281646	–43.672
49	Maximaisoflavone J	177731	–43.643
50	Betulin	72326	–43.559
51	Aloin A	12305761	–43.538
52	Acteoside	5281800	–43.526
53	11-EPi–toonacilin	73348892	–43.496
54	Azadironolide	10814144	–43.400
55	Aloin B	14989	–42.743
56	Rhamnazin	5320945	–42.639
57	3-EPi–oleanolic acid	11869658	–42.513
58	Quercetin-3,4′-dimethyl ether	5380905	–42.404
59	Lysicamine	122691	–42.103
60	Proceranolide	23258999	–41.350
61	Maximaisoflavone H	13873188	–41.346
62	Salaterpene B	102583506	–41.342
63	Skimmiamine	6760	–40.258
64	3-Epioleanolic acid	11869658	-39.714
65	Busseihydroquinone B	70688905	-39.655
66	Montanin	442060	-39.463
67	Darienine	130672	-39.199
68	Heliparvifoline	5281846	-38.630
69	Maculine	68232	-38.225
70	Bisnordihydrotoxiferine	6440874	-37.049
71	Bergenin	66065	-36.342
72	Gadenine	436042	-32.605
73	Cyclombandakamine A2	132608472	-13.275
74	Cyclombandakamine A1	132608471	-11.844

TABLE S-II: Chemical structures of top candidates, their binding affinities and type of interactions with amino acid residues of AChE

Lig.	Structure	Types of interactions	Active site residues (Distance Å)
Allanxanthone B		Hydrogen Bond	ASP74 (2.55)
		Pi–Pi Stacked	TRP286 (5.95, 6.19), TYR337 (5.38), TYR341 (3.46, 3.99, 4.48)
		Alkyl	LEU289 (5.33)
		Pi–Alkyl	TRP86 (4.11, 4.33), TRP286 (4.44, 4.66), TYR337 (4.49), PHE338 (5.02), TYR341 (5.39), **HIS447 (4.74)**
		van der Waals	TYR72, GLY121, GLY120, TYR124, SER125, GLY126, LEU130, TYR133, GLU202, **SER203**, ALA204, SER293, VAL294, PHE295, ARG296, GLY342, GLY448
Stigmasterol		Pi–Donor Hydrogen Bond	TRP86 (2.67)
		Pi–Alkyl	TRP286 (3.75, 4.55), PHE297 (4.88, 5.25), TYR337 (3.43, 5.26), PHE338 (4.69, 4.71), TYR341 (4.56, 4.67, 4.84), **HIS447 (4.82)**
		van der Waals	TYR72, ASP74, LEU76, GLY121, TYR124, SER125, GLU202, **SER203**, LEU289, SER293, VAL294, PHE295, ARG296, GLY342, GLY448
5′-O-methyl dioncophylline D		Hydrogen Bond	**HIS447 (3.08)**
		Carbon-hydrogen bond	PHE338 (2.89), **HIS447 (3.14, 3.41)**
		Pi–Donor Hydrogen Bond	TYR124 (2.78)
		Pi–Pi Stacked	TRP286 (5.33), TYR337 (5.04), TYR341 (3.88, 4.92)
		Alkyl	VAL294 (3.81)
		Pi–Alkyl	TYR72 (4.35), TYR124 (4.74), TRP286 (4.25, 6.16), TYR337 (3.64), PHE338 (4.26), TYR341 (4.52, 4.72, 4.80, 5.38), **HIS447 (4.79, 5.29)**
		van der Waals	ASP74, LEU76, GLY121, GLU202, **SER203**, PHE295, PHE297, GLY448

Ismailin		Hydrogen Bond	PHE295 (2.66)
		Pi–Cation	ASP74 (2.75, 3.18)
		Pi–Donor Hydrogen Bond	TYR124 (2.20), TYR341 (2.68)
		Pi–Pi Stacked	TRP286 (4.62, 5.06), TYR341 (5.49)
		Pi–Sigma	TYR341 (3.65)
		Pi–Lone Pair	TYR124 (2.36)
		Alkyl	VAL294 (5.15)
		Pi–Alkyl	TRP86 (4.69), TYR337 (3.61, 5.06), PHE338 (3.80), TYR341 (5.37)
		van der Waals	TYR72, THR83, ASN87, GLY121, SER125, **SER203**, SER293, ARG296, PHE297, GLY342, **HIS447**
Wistin		Hydrogen Bond	ASP74 (2.55), SER293 (2.59)
		Carbon-hydrogen bond	SER125 (2.70), SER293 (2.94)
		Pi–Pi Stacked	TYR337 (5.56), TYR341 (3.92, 4.24)
		Alkyl	LEU289 (5.49)
		Pi–Alkyl	TRP86 (4.47), TRP286 (5.48)
		van der Waals	TYR72, THR83, ASN87, GLY121, TYR124, GLY126, LEU130, TYR133, GLU202, **SER203**, VAL294, PHE295, ARG296, PHE297, PHE338, **HIS447**, GLY448
Dioncophylline C2		Carbon Hydrogen Bond	TYR341 (2.90, 3.05)
		Pi–Sigma	TRP86 (2.32)
		Pi–Pi Stacked	TRP86 (5.61), TYR124 (5.15), TRP286 (4.94), TYR337 (4.78), TYR341 (3.29, 4.26)
		Alkyl	VAL294 (4.07)
		Pi–Alkyl	TRP86 (3.33), TRP286 (4.42), PHE295 (4.75), PHE297 (3.90), TYR337 (5.09), PHE338 (3.26, 4.88), TYR341 (4.27, 5.23)
		van der Waals	TYR72, ASP74, THR83, GLY121, SER125, **SER203**, SER293, ARG296, **HIS447**, GLY448, TYR449
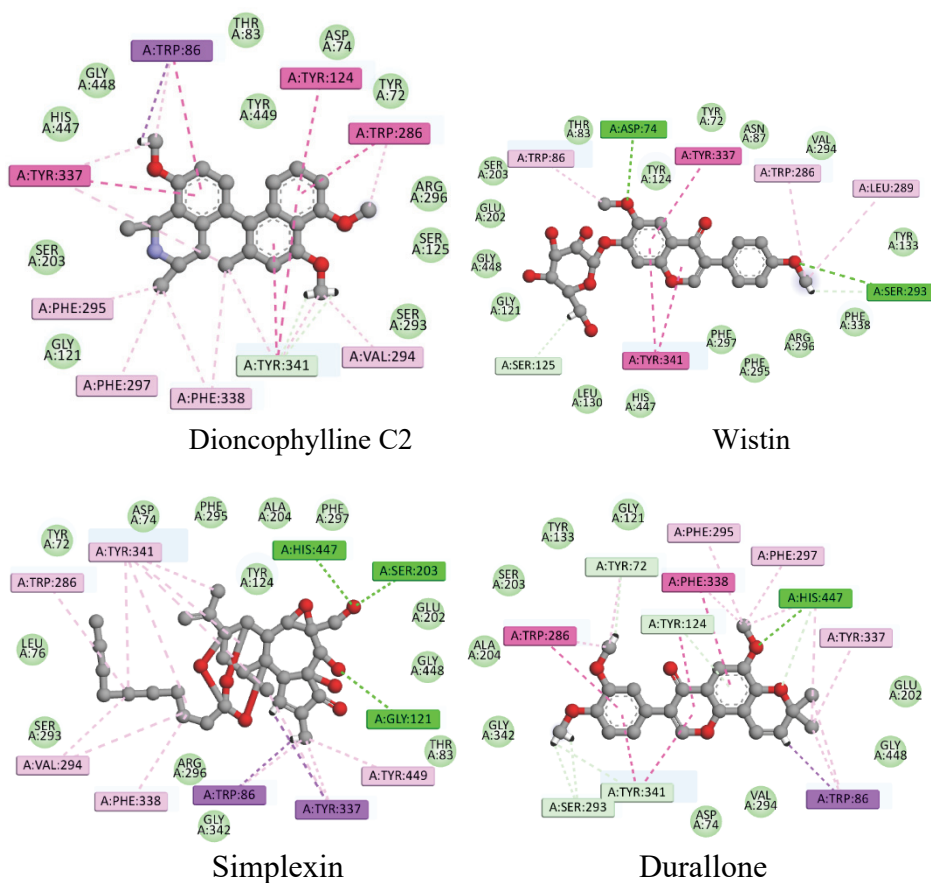
Fig. S-6. 2D interaction of dioncophylline C2, wistin, simplexin and durallone with amino acid residues of the receptor
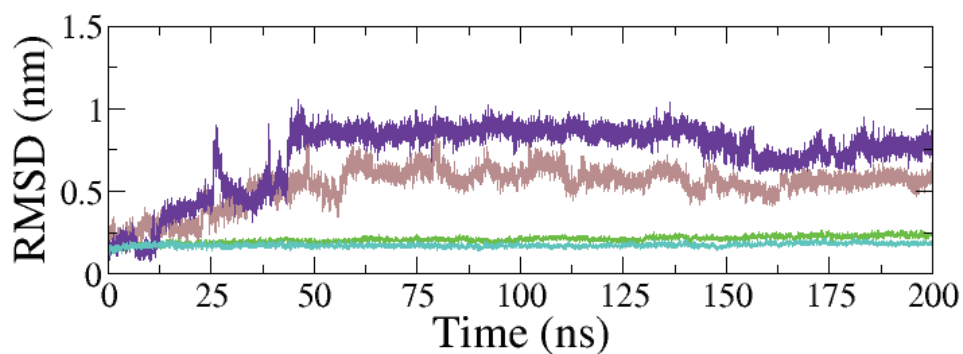
Fig. S-7. RMSD curves of simplexin (brown) and durallone (violet) with RMSD curve of protein backbone of simplexin (green) and durallone complex (turquoise)

Spatial analysis of ligand and protein
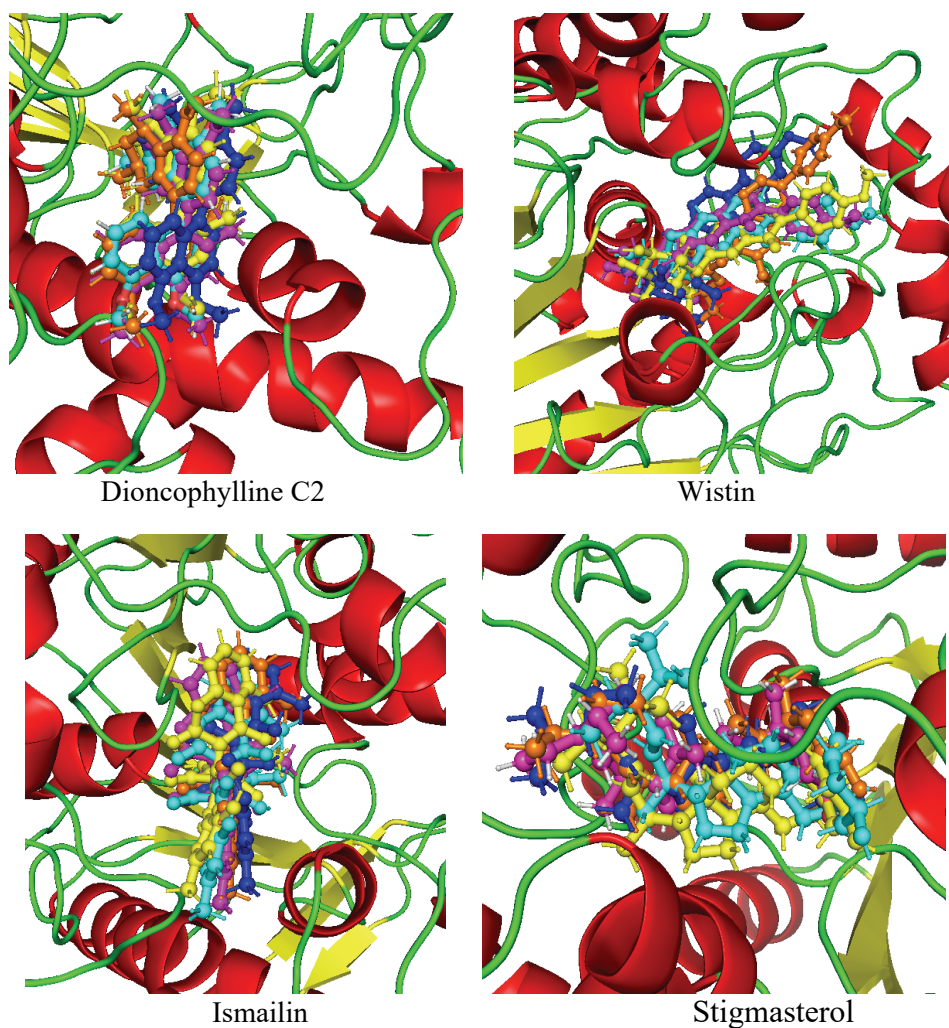
Fig. S-4. Snapshots of protein-ligand interactions in three complexes captured at various time points (1 ns in blue, 50 ns in orange, 100 ns in magenta, 150 ns in cyan and 200 ns in yellow) during MDS

SHRESTHA *et al.*

Allanxanthrone B   5'-O-methyldioncophylline D
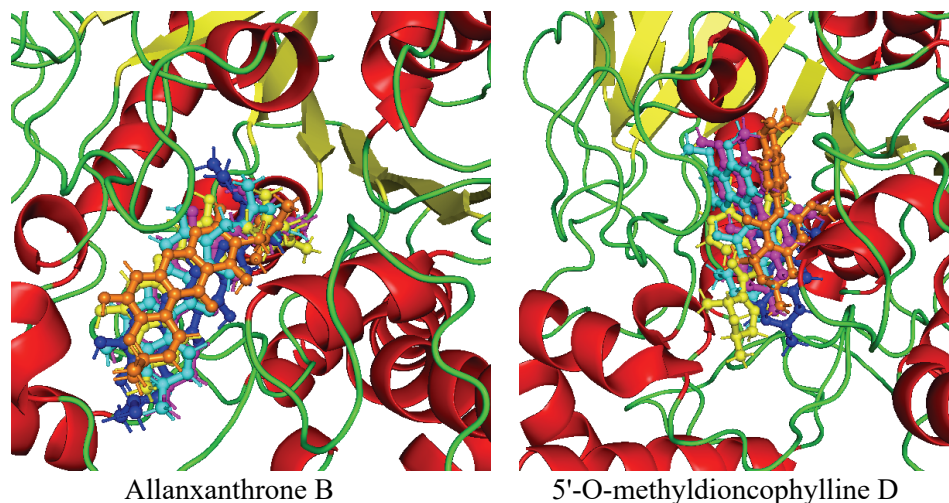
Fig. S-4. Snapshots of protein-ligand interactions in three complexes captured at various time points (1 ns in blue, 50 ns in orange, 100 ns in magenta, 150 ns in cyan and 200 ns in yellow) during MDS

TABLE-SIII: Binding free energy changes (ΔG_{BFE}) along with its components in complexes

Complexes	$\Delta E_{VDWAALS}$	ΔE_{EL}	ΔE_{PB}	ΔE_{NPOLAR}	ΔG_{GAS}	ΔG_{SOLV}	ΔG_{BFE}
Allanxanthone B	-237.90 ± 11.29	−49.70 ± 20.25	216.52 ± 23.05	-23.55 ± 0.75	-287.60 ± 23.97	192.96 ± 22.71	-94.64 ± 19.49
Stigmasterol	-205.89 ± 11.50	-39.83 ± 13.13	136.23 ± 16.98	-21.79 ± 0.54	-245.72 ± 18.45	114.39 ± 16.94	-131.33 ± 18.24
5′-O-methyldioncophylline D	-182.79 ± 11.71	-21.12 ± 13.17	133.80 ± 21.25	-19.83 ± 0.71	-203.92 ± 16.31	113.93 ± 21.04	-89.99 ± 18.49
Ismailin	-225.93 ± 10.33	-71.63 ± 16.73	242.42 ± 22.04	-22.46 ± 0.62	-297.56 ± 20.12	219.95 ± 21.92	-77.61 ± 17.07
Wistin	-196.77 ± 11.58	-120.75 ± 42.04	246.06 ± 28.36	-22.13 ± 0.50	-317.52 ± 43.17	223.96 ± 28.24	-93.59 ± 29.32
Dioncophylline C2	-210.58 ± 12.46	-99.66 ± 13.80	222.71 ± 22.00	-20.83 ± 0.54	-310.20 ± 20.04	201.83 ± 22.75	-108.36 ± 18.66

TABLE-S-IV: ADMET properties of six hit candidates

ADMET parameters	Compounds					
	Allanxanthone B	Stigmasterol	5′-O-methyldioncophylline D	Ismailin	Wistin	Dioncophylline C2
Caco2 permeability	Low	High	High	Low	Low	Low
Intestinal absorption	High	High	High	High	High	High
Skin Permeability	High	High	High	High	High	High
BBB permeability	-1.1	0.771	-0.314	-1.126	-1.478	-0.132
CNS permeability	-1.767	-1.652	-1.563	-3.154	-3.784	-1.341
CYP2D6 substrate	No	No	Yes	No	No	No
CYP3A4 substrate	Yes	Yes	Yes	Yes	No	Yes
CYP1A2 inhibitor	No	No	Yes	No	No	Yes
CYP2C19 inhibitor	Yes	No	No	Yes	No	Yes
CYP2C9 inhibitor	Yes	No	No	Yes	No	No
CYP2D6 inhibitor	No	No	Yes	No	No	Yes
CYP3A4 inhibitor	Yes	No	Yes	No	No	Yes
Total clearance	-0.213	0.618	0.8	0.21	0.162	0.743
AMES toxicity	No	No	Yes	No	No	Yes
hERG I inhibitor	No	No	No	NO	No	Yes
hERG II inhibitor	Yes	Yes	Yes	Yes	No	Yes
Hepatotoxicity	Yes	No	Yes	Yes	No	Yes
Skin sensitisation	No	No	No	No	No	No

TABLE-S-V: ADMET properties of native and reference drugs

ADMET parameters	Compounds		
	Donepezil (native)	Rivastigmine	Galantamine
Caco2 permeability	High	High	High
Intestinal absorption	High	High	High
Skin Permeability	High	High	High
BBB permeability	0.157	0.508	-0.081
CNS permeability	-1.464	-2.255	-2.511
CYP2D6 substrate	Yes	No	No
CYP3A4 substrate	Yes	No	Yes
CYP1A2 inhibitor	No	No	No
CYP2C19 inhibitor	No	No	No
CYP2C9 inhibitor	No	No	No
CYP2D6 inhibitor	Yes	Yes	No
CYP3A4 inhibitor	Yes	No	No
Total clearance	0.987	0.557	0.991
AMES toxicity	No	No	No
hERG I inhibitor	No	No	No
hERG II inhibitor	Yes	No	Yes
Hepatotoxicity	Yes	No	Yes
Skin sensitisation	No	No	No

Chemical composition and bioactivities of *Phellinus pini* extracts and quality evaluation of healthy drinks prepared from the mushroom

NGUYEN THI NGAN[1]* and TRANG H. D. NGUYEN[2]

[1]Institute of Biotechnology and Food Technology, Industrial University of Ho Chi Minh City, Ho Chi Minh City, Vietnam and [2]Food Science Program, Department of Kinesiology, Missouri Southern State University, Joplin, MO 64801, USA

Abstract: *Phellinus pini*, a mushroom species found in East Asian countries, is commonly consumed as a medicinal beverage known for its stomach-warming effects and purported ability to alleviate pain and tumours. In this study, *P. pini* was extracted using different methods (hot water, sonication, microwave, and soaking). The extracts were analysed for phenolic and polysaccharide contents. Additionally, the extracts were evaluated for their antioxidant potential and ability to inhibit albumin denaturation. The results demonstrated that the extract obtained with hot water extraction contained the greatest amount of phenolics (105.98±0.53 mg GAE/mL). The hot water and microwave extraction methods showed more effective in extracting polysaccharide from the mushroom. Moreover, the extract from the ultrasound extraction method presented the strongest antioxidant activity by scavenging DPPH and ABTS radicals by 41.26 and 97.84 %, respectively while the hot water extract exhibited the most potent ability to inhibit albumin denaturation by 96.40 %. Among the four healthy drinks formulated, the formulation with the greatest proportion of *P. pini* extract contained the highest total phenolic content, antioxidant activity, and the most favorable sensory overall liking. The described findings deepen our understanding of the chemical composition and potential health-promoting properties of *P. pini*, as well as revealing new potential applications for the mushroom in the food and nutraceutical industries.

Keywords: mushroom; phenolics; antioxidant activity; healthy drinks; *Phellinus pini*.

INTRODUCTION

Phellinus, a genus of mushrooms from the family Hymenochaetaceae, is primarily found in tropical regions of the America, Africa and Asia, especially in

201

Uzbekistan, China, Vietnam, Japan and South Korea.[1,2] In Vietnam, this genus is composed of 26 species that can be found in humid mountainous forests from the north to the south.[3] *Phellinus* mushrooms are highly valued for their medicinal properties and are widely used in traditional medicine. They are known to promote and improve health, as well as to prevent or treat various conditions, such as oral ulcers, certain gastrointestinal disorders, and blood-related diseases, as reported in studies.[4,5] Previous studies have revealed that *Phellinus* mushrooms contain phytochemical constituents such as polyphenols, terpenoids and polysaccharides, all of which exhibit antioxidant, anticancer, antiviral, immunomodulatory properties and other biological effects.[6]

Phellinus pini is one of the commonly found species in Vietnam, particularly in the central and central highlands regions. It is also prevalent in various regions worldwide, such as the Americas, Africa and East Asia, with significant prevalence and extensive use in countries like China, South Korea and Japan.[6] People in Asian countries commonly use *P. pini* as a beverage with medicinal effects, including warming the stomach and treating pain and tumours. Similar to other species in the genus *Phellinus*, *P. pini* contains numerous biologically active compounds, including lignan, (+)-pinoresinol, sterol, stirypirol, ergosterol peroxide, ceramide and polysaccharides.[7] Among these compounds, polysaccharides extracted from this mushroom possess multiple health-promoting activities that have been demonstrated through numerous studies, such as antioxidant, antiviral, anticancer, and immune-enhancing properties.[8,9] Moreover, extracts from *P. pini* have shown inhibitory effects on enzymes like α-glucosidase and α-amylase, suggesting potential benefits in managing blood sugar levels.[10] Several solvents were employed for crude extraction of bioactive compounds from *Phellinus* species. Various extraction techniques, such as decoction, soaking, ultrasound, and microwave-assisted methods, are commonly utilized for isolating natural products from *Phellinus* species. Zhang *et al.* demonstrated that ultrasonic treatment enhanced the antioxidant activities of polysaccharides extracted from *Phellinus linteus* mycelia.[11] Recently, decoction technique was used to extract bioactive components from dried powder of fruiting bodies of various *Ganoderma* species to prepare tea.[12] Despite numerous studies investigating the bioactivities of *Phellinus* extracts from different species, limited data are available regarding the applications of *P. pini* extracts in developing healthy beverage formulations. Therefore, this study aimed to determine the chemical composition, bioactivities, and sensory acceptability of *P. pini* extracts incorporated into beverage formulations. The objectives of this study were:

1) Compare phenolic and polysaccharide contents, antioxidant activity and albumin denaturation inhibitory effect of *P. pini* extracts obtained through various extraction methods and

2) Assess the quality of healthy beverages formulated from the selected *P. pini* extract.

The findings of this study will contribute to our understanding of the chemical composition and bioactivities of *P. pini*, while also unveiling new potential applications of the mushroom within the food and nutraceutical industries.

EXPERIMENTAL

Sample collection

Phellinus pini was collected at the Pu Mat National Park in Nghe An province, Vietnam. The sample was thoroughly cleaned with water, air dried, sliced, and ground to 1 mm size. The powder was carefully stored in a polyethylene bag at a refrigerator (4 °C) for further analysis.

Chemicals

Phenolic acid standards were purchased from Sigma–Aldrich. Ethanol and water (HPLC grade) were obtained from Fisher Scientific (Pittsburg, PA, USA). 2,2′-Azino-bis(3-ethylbenzothiazoline-6-sulfonic acid) (ABTS) and 2,2-diphenyl-1-picrylhydrazyl (DPPH) and were purchased from Sigma–Aldrich and Sisco Research Laboratories (Maharashtra, India), respectively. Food ingredients, including honey, dried jujube, and liquorice, were purchased at a local grocery store.

Extraction

Briefly, 5 g of the sample were mixed with 500 mL of deionized water, and the extraction was carried out using different extraction methods, including hot water (closed lid), sonication (closed lid, Sonica 3200 EP S3, 360 W, 39 kHz), microwave (closed lid, Sanyo EM-S2052W, 700 W, 2.45 MHz) and soaking. The parameters of each extraction method were shown in Table I. After the extraction step, the mixture was then filtered by a Whatman filter paper (110 mm in diameter, GE Healthcare, Chicago, IL, USA). The filtrate obtained were analysed for phenolic contents, total polysaccharide content, and bioactivities.

TABLE I. Parameters of the various extraction methods of *Phellinus pini*

Extraction method	Hot water	Sonication	Microwave	Soaking
Time, min	5	15	2	60
Temperature, °C	95–100	50	30	30

Determination of phenolics

Total phenolic content (*TPC*) of extracts was determined by the Folin–Ciocalteu approach.[13] A volume of an extract (0.5 mL) was pipetted into a test-tube containing 2.5 mL of 10 % Folin–Ciocalteu solution, followed by shaking and 5 min incubation in darkness. 2 mL of 7.5 % Na_2CO_3 were added, and the mixture was then incubated in darkness for 60 min. The absorbance was measured by a UV–Vis spectrophotometer (Thermo Genesys 20 UV–Vis) at 765 nm. Gallic acid was used as a reference standard.

To identify and quantify individual phenolic acids and flavonoids, the extracts were injected into a high performance liquid chromatography system equipped with a UV detector (Prominent, Shimazu, Japan), following the method of Nguyen *et al.* (2023).[14] The separation was performed using a VertiSep GES C18 reverse-phase column (250 mm×4.6 mm×5 μm). The mobile phases were methanol (A) and 2 % formic acid (B) with the elution gradient as

follows: from 0–3 min, 25 % A; 3–10 min 25–40 % A; 10–20 min 40–60 % A; 20–30 min 60–80 % A; 30–40 min 80 % A; from 40–48 min 80–25 %. The flow rate was set at 1.0 mL/min. The detection wavelengths were 295 and 340 nm. The column was operated at room temperature (30 °C). Sample injection by system was automatically set with a sample volume of 10 µL. Quantification of phenolics was based on calibration curves of the external standards at the same condition.

*Determination of total polysaccharide content (*TPSC*)*

Total polysaccharide content of each extract was determined by Nielsen's method with minor modifications.[15] Five grams of the ground mushroom were combined with water at a ratio of 1:10 (g/mL). The extraction methods were the same as those described in the earlier section. The extracts were collected after removing the sample solids. 80 % ethanol in water was added in the extracts at a volume ratio of 1:4, and the mixture was kept under low temperature (4 °C) for 12 h, followed by centrifugation (5000 rpm, 10 min). The resulting residue (*i.e.*, polysaccharide) was dried and dissolved in 5 mL of sodium hydroxide. Water was added to the solution to make a volume of 10 mL. 1 mL of this mixture was combined with 1 mL of 5 % phenol and 5 mL of concentrated sulfuric acid, followed by storage at room temperature for 10 min. Absorbance was spectrophotometrically measured at 490 nm. Glucose served as a reference standard.

Antioxidant activity

Antioxidant activity evaluated by DPPH and ABTS methods was described by Tuan *et al.* (2023).[16] One mL of an extract obtained in Section 2.2 was pipetted into a tube containing 5 mL of 0.1 mM DPPH solution, the mixture was thoroughly shaken and kept in darkness for 30 min, and absorbance was determined at 517 nm. Regarding ABTS assay, 38.4 mg of ABTS were mixed in methanol, 6.6 mg potassium persulfate were added, followed by vigorous shaking and storage in darkness for 16 h. The ABTS solution was adjusted in methanol to absorbance at 0.7±0.02 at the wavelength of 734 nm. 100 µL of an extract combined with 3 mL of the ABTS solution were shaken and kept in darkness for 6 min. Afterwards, absorbance of the mixture was measured using a UV–Vis spectrophotometer.

Inhibition of albumin denaturation

The inhibitory activity of the extracts was evaluated and compared with that of diclofenac, a nonsteroidal anti-inflammatory drug.[17] Each *P. pini* extract obtained from the various extraction methods or diclofenac sodium solution (100 µL) was combined with 100 µL of bovine serum albumin solution (0.16 %) and 200 µL of sodium acetate buffer (25 mM, pH 5.5). The mixture was subjected to incubation at 37 °C for 45 min, followed by a heating step to 67 °C for 3 min. After cooling down to room temperature, the absorbance of the mixture was measured at 660 nm.

Healthy drink formulation and quality evaluation

The *P. pini* extract with the highest TPC was selected to be applied to drink formulation. First, the extract was diluted with deionized water at the extract/water volume ratios of 1:3, 1:2, 1:1 and 2:1, resulting in four drink formulae (S13, S12, S11 and S21), respectively. Afterwards, each of the mixtures (1000 mL) was combined with honey, jujube juice and liquorice juice as shown in the diagram. The resulting mixtures were evaluated for TPC, antioxidant activity, soluble solids, pH, colour and sensory overall linking.

Liquorice and jujube juices were prepared by mixing 5 g of dried liquorice and 12 g of dried jujube in 200 and 600 mL of water, respectively. The mixtures were then boiled for 5 min, followed by cooling for 30 min before use.

The colour (CIE $L*$, $a*$, $b*$) of the drink was measured using a colorimeter (Konica Minolta, CR-400 Ramsey). The pH measurement was conducted using a benchtop pH meter (Hanna Instruments, German) and Brix value was recorded by a portable refractometer (Cole––Palmer). Overall sensory acceptance was run on the four drink formulations (S13, S12, S11, S21) prepared as described in Fig. 1. The drinks were served at room temperature and in red light. Overall liking of each sample was recorded from 50 panellists, using a nine-point hedonic scale (1 – extremely dislike, 5 – neither like nor dislike, 9 – extremely like). All samples were coded with 3 digit numbers and served in a random order.
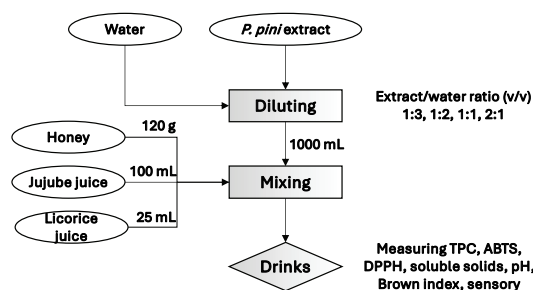
Fig. 1. The diagram of healthy drink formulation.

Statistical analysis

The measurements were performed three times, and the findings were presented as mean value ± standard deviation. Data were analysed using one-way ANOVA alongside Tukey's HSD test at a significance level of 0.05. Statistical analysis was carried out using XLSTAT, version 2016 (Addinsoft, Paris, France).

RESULTS AND DISCUSSION

Total phenolic content

Phenolic compounds are prevalent in mushrooms and play a crucial role in their antioxidant properties.[18–20] The hydroxyl groups of phenolics, confirmed in extracts from various mushroom species such as *Ganoderma s*pp. and *Hydnum repandum*, enhance the efficiency of scavenging free radicals and reducing ferrous ions. The results presented in Table II indicated that the examined *P. pini* extracts are abundant in phenolic compounds (25.00 to 105.98 mg GAE/mL). The highest *TPC* was detected in the hot water extract (105.98±0.53 mg GAE//mL) while the ultrasonic extract has the lowest TPC (25.00±0.10 mg GAE/mL). Hot water extraction was shown to be among the most effective methods in recovering phenolics. For example, one study on shiitake mushroom showed that extracts obtained with hot water had significantly higher *TPC* than with conventional organic solvents and equivalent to that of microwave extraction.[21] In another study, hot water extraction produced the lemon-byproduct extracts rich-

est in phenolics compared to ultrasound and organic solvent extractions.[22] The higher *TPC* in hot water extracts could be due to the combined effects of breaking bonds, increasing solubility, disrupting cell walls, enhancing diffusion and hydrolysing complexes, all of which help release and dissolve more phenolic compounds from the mushroom material. In comparison with some medicinal mushrooms, such as turkey tail (*Trametes versicolor*) and other *Phellinus* species,[23,24] total phenolic content in the *P. pini* extracts were higher.

TABLE II. The total phenolic and total polysaccharide content of *P. pini* extracts; GAE: gallic acid equivalents; GE: glucose equivalents. Different letters (a, b, c) indicate significant differences in concentrations of phenolics among the extracts

Parameter	Hot water extract	Microwave extract	Ultrasonic extract	Soaking extract
TPC (in mg GAE/mL)	105.98[a]±0.53	28.33[b]±0.10	25.35[b]±1.50	25.00[b]±0.10
TPSC (in mg GE/g)	5.60[a]±0.03	5.67[a]±0.03	1.69[c]±0.02	1.93[b]±0.02

Phenolic compound contents

Ten phenolic compounds, including gallic acid, chlorogenic acid, caffeic acid, *p*-coumaric acid, ferulic acid, DHBA (dihydroxybenzoic acid), salicylic acid, cinnamic acid, rutin and quercetin in the four *P. pini* extracts were analysed by HPLC-DAD, and the results were presented in Table III. In total, seven phenolics were identified and quantified in the extracts. Among these, four compounds, namely gallic acid, chlorogenic acid, caffeic acid and ferulic acid, were present in all the extracts. Quercetin, salicylic acid, and cinnamic acid were not detected in any of the extracts. The hot water extract with the highest TPC was shown to contain all the seven phenolic compounds. The microwave extract consisted of six compounds while the soaking and ultrasound extracts were found with four compounds. Gallic acid was the most dominant compound in all the extracts, with the concentrations ranging from 19.38 to 40.55 μg/mL. The hot water extract contained twice as much of this compound as the others. Gallic acid was previously reported to be much more abundant in an aqueous extract of *Ganoderma lucidum* compared to extracts prepared from organic solvents.[25] The hot water extract also contained the highest amount of chlorogenic acid (7.39±1.00 μg/mL), followed by the microwave extract (0.76±0.22 μg/mL) and the soaking extract (0.71±0.08 μg/mL). The ultrasonic extract had the lowest chlorogenic acid content (0.48±0.08 μg/mL). The other phenolic acids that had the greatest levels in the hot water extract than in the others were caffeic acid and HBA. Previously, hydroxybenzoic acids were reported to be abundant in extracts of *Flammulina velutipes, Trametes versicolor* and *Ganodema* spp.[18,26] Rutin was the only flavonoid that was found to be present in the extract, which is the hot water extract. Unlike the aforementioned compounds, ferulic acid and *p*-coum-

aric acid were detected at the highest levels in the microwave extract (1.80±1.65 and 2.56±0.31, respectively).

TABLE III. Phenolic compound contents (µg/mL) of *P. pini* extracts obtained with different extraction methods; different letters (a, b, c) indicate significant differences in concentrations of phenolics among the extracts; n.d.: not detectable

Compound	Soaking extract	Microwave extract	Ultrasonic extract	Hot water extract
Gallic acid	19.89[b]±0.00	20.33[b]±0.58	19.38[b]±0.23	40.55[a]±0.40
Chlorogenic acid	0.71[b]±0.08	0.76[b]±0.22	0.48[c]±0.08	7.39[a]±1.00
Caffeic acid	0.44[c]±0.18	0.43[c]±0.03	0.85[b]±0.04	2.09[a]±0.92
p-Coumaric acid	n.d.	2.56[a]±0.31	n.d.	0.85[b]±0.21
Ferulic acid	0.44[c]±0.28	1.80[a]±1.65	1.25[b]±0.13	1.52[a]±0.15
Salicylic acid	n.d.	n.d.	n.d.	n.d.
Cinnamic acid	n.d.	n.d.	n.d.	n.d.
Dihydroxybenzoic acid	n.d.	1.76[b]±0.32	n.d.	15.18[a]±2.97
Rutin	n.d.	n.d.	n.d.	3.11±0.50
Quercetin	n.d.	n.d.	n.d.	n.d.

The results demonstrated the superiority of hot water and microwave extractions over soaking and ultrasonic methods for extracting phenolics from *P. pini*. The effectiveness of hot water and microwave extractions can be attributed to several factors, including thermal effects, increased solubility, inactivation of enzymes and microwave effects. The high temperature involved in the methods can break down the plant cell walls and disrupt the hydrogen bonds and hydrophobic interactions that bind phenolic molecules to plant matrices,[1] facilitating their extraction. The high temperature also increases the solubility and diffusion rates of phenolics in the extraction solvent, leading to more efficient extraction.[27] The inactivation of enzymes like polyphenol oxidases can occur under high temperature, preventing degradation of phenolics during extraction. Microwave irradiation can cause molecular motion and dipole rotation, leading to the disruption of hydrogen bonds and increased mass transfer of phenolic compounds from the sample to the solvent.[28]

Total polysaccharide content

Total polysaccharide contents of the four different extracts from *P. pini* were examined and shown in Table II. The *TPSC* ranged between 1.69 and 5.67 mg GE/g. Due to the high temperature, the microwave extract (5.67 mg GE/g) and hot water extract (5.60 mg GE/g) samples had the highest *TPSC*. The two samples with the lowest concentrations were soaking and ultrasonic extracts (1.93 and 1.69 mg GE/g, respectively). Mushroom polysaccharides primarily belong to the category of *β*-glucans, similar to the digestive enzymes secreted by the pancreas that aid in the digestion process.[29] In addition to their significance

as prebiotics, mushroom polysaccharides have been shown to possess a wide range of other bioactivities, including antitumor, antimicrobial, antioxidant, antiviral and immunomodulatory activities.[30, 31]

Antioxidant activity

As presented in Table IV, the ultrasonic extract may show the strongest DPPH and ABTS scavenging activities (41.26 and 97.84 %, respectively). In contrast, the hot water extract could have the weakest ability to remove the radicals. The microwave and soaking extraction methods resulted in the extracts with comparable scavenging activities. The findings are in agreement with the previous studies reporting that ultrasound-assisted extraction can enhance antioxidant potential and other bioactivities of *Phellinus* medicinal mushroom extracts, such as *Phellinus igniarius* and *P. linteus*.[11,32] The ultrasound-assisted extraction can break down the tough and woody structure of *Phellinus* mushrooms into smaller particles, increasing the surface area available for solvent penetration. This finer particle size exposes more fungal cells to the solvent, promoting the release of antioxidants and other bioactive compounds.

TABLE IV. Antioxidant activity of the *Phellinus pini* extracts; different letters (a, b, c) indicate significant differences in concentrations of phenolics among the extracts

Parameter	Hot water extract	Microwave extract	Soaking extract	Ultrasonic extract
DPPH activity, %	26.21[b]±2.37	36.21[a]±1.26	37.01[a]±1.61	41.26[a]±2.07
ABTS activity, %	96.09[d]±0.07	97.57[b]±0.07	97.19[c]±0.07	97.84[a]±0.00

Albumin denaturation inhibitory activity

Fig. 2 shows that the extract obtained with hot water may possess the most potent inhibitory activity against albumin denaturation, followed by the extract from the microwave extraction method, with the percentages of inhibition as high as 96.40 and 89.10 %, respectively. The extracts from the ultrasound and soaking methods showed lower effects to inhibit albumin denaturation. The results also demonstrated that all the extracts could have higher capacities to protect albumin from denaturation than the 50 and 100 µg/mL diclofenac solutions. In the present study, the ability of *P. pini* to inhibit albumin denaturation was used to understand the potential anti-inflammatory properties of the mushroom species. Research has shown that *Phellinus* species may possess strong anti-inflammatory activity.[33] This could be due to the presence of chemical constituents in their composition. For example, polysaccharides of *P. linteus* reportedly reduce the release of pro-inflammatory cytokines (TNF-α, IL-1β, IL-2, IL-6 and IL-12) in lipopolysaccharide-induced inflammatory cell model.[34] Another study revealed that inotilone isolated from *P. linteus* inhibited LPS-induced MMP-9 expression

by inactivation of NF-κB *via* ERK, p38 and JNK signaling pathways in RAW 264.7 cells.[35]
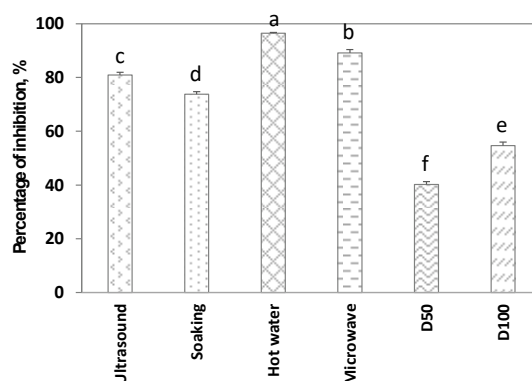
Fig. 2. Inhibitory effect (%) of the extracts and diclofenac solutions on albumin denaturation. D50 and D100 denote the solution of diclofenac at 50 and 100 μg/mL, respectively. Different letters (a, b, c, d, e, f) indicate significant differences in concentrations of phenolics among the extracts.

Healthy drink formulation

Total phenolic content and antioxidant activity. In the present study, the cook extract with the highest TPC was used for healthy drink formulation. In traditional folk medicine, mushroom decoctions frequently entail immersing crushed or small pieces of the fruiting body in hot water to extract soluble components. The resulting decoction is then ingested. Additionally, mushrooms are typically not consumed raw but undergo various food processing methods to enhance digestion and assimilation. Consequently, preparing hot water extracts replicates cooking conditions, imitating the typical culinary practice for consuming edible mushrooms. Table V shows the total phenolic content and the antioxidant activity measured by the ABTS and DPPH radical scavenging assays for four healthy drink formulae (S13, S12, S11, S21) containing *P. pini* extract. Among these, S21 was the phenolic-richest drink (126.53±0.59 mg GAE/mL), followed by S13 (112. 5 ng GAE/mL) and S12 (118.4±0.26 mg GAE/mL). An increase in TPC indicated that as the level of the extract proportion increased, the antioxidant activity (through ABTS and DPPH values) increased in most cases. Notably S11, formulated with half the proportion of the *P. pini* extract, demonstrated the lowest phenolic content (86.49±0.06 mg/mL GAE) and thus possessed the lowest DPPH value (66.14 %). As described earlier, honey, jujube juice, and liquorice were used in the formulation, it is important to note that the various ingredients might interact with each other and other components in the extract, resulting in changes in TPC of the formulated drinks. Previously, a research

showed that both honey and fruit juice rich in phenolics and vitamin C, when used as ingredients, can impact the final phenolic content of beverages.[36]

TABLE V. Total phenolic content, ABTS and DPPH radical scavenging activities, physico-chemical properties and sensory acceptance of the four healthy drink formulae from the *P. pini* extract

Parameter	S13	S12	S11	S21
TPC (in mg GAE/mL)	112.50[c]±0.00	118.4[b]±0.26	86.49[d]±0.06	126.53[a]±0.59
ABTS activity, %	93.76[d]±0.06	99.11[c]±0.06	99.61[a]±0.06	99.54[a]±0.06
DPPH activity, %	65.64[c]±0.62	73.01[b]±0.39	66.14[c]±0.16	82.52[a]±0.31
Soluble solids, °Brix)	7.60±0.14	8.00±0.57	7.70±0.00	7.80±0.28
Brown index	82.47[c]±0.03	84.36[b]±0.30	86.73[e]±0.38	88.02[a]±0.31
pH	6.11±0.01	6.21±0.16	6.13±0.03	6.16±0.06
Overall liking	5.62[a]±1.62	5.40[a]±1.77	5.52[a]±1.85	5.62[a]±1.83

The results also revealed that all the formulated drinks had higher ABTS percentage of inhibition, falling within 93.76–99.61 %. S11 and S21 exhibited the strongest activity while S13 showed the lowest activity to remove ABTS radicals. S21 also had the most potent capacity to inhibit the formation of DPPH radicals (82.52±0.31 %). Similarly, S13 exerted the weakest DPPH scavenging activity (65.64±0.62 %). Studies have consistently demonstrated a positive correlation between TPC and antioxidant potential in various foods, beverages and plant extracts.[17,37] Phenolic compounds, including flavonoids, phenolic acids and other polyphenols, are well-known antioxidants that can scavenge free radicals and inhibit oxidative stress. These can partly explain the high *TPC* of S21 accompanying its free radical scavenging activities. In comparison with the mushroom extract obtained with the hot water extraction as described earlier, the formulated drinks all had a higher potential to scavenge DPPH radicals. This means that adding honey, jujube juice, and liquorice led to an increase in *TPC* of the final drinks. The mechanism underlying this phenomenon has been poorly elucidated, primarily due to the intricate composition of the mixtures, especially plant extracts. Possible explanations could be the formation of stable dimers, oligomers, adducts, and/or even new phenolics with elevated antioxidant activity, compared to the parent components during the formulation of the drinks.

Soluble solids. The observed soluble solids content ranging from 7.60 to 8.00 °Brix can be attributed to the combined contributions of the sugars present in the extract, honey, jujube juice, and liquorice juice used in the formulations. The slight variations could be due to differences in the proportions of the extract across the formulations.

Color measurement

The brown index, a measure of browning or colour intensity, varied significantly among the formulations. S21 had the highest brown index (88.02±0.31),

indicating a darker colour, followed by S11 (86.73±0.38), S12 (84.36±0.30) and S13 (82.47±0.03). The significant differences in the brown index values can be explained by the varying proportions of the *P. pini* extract in the drink. Although jujube juice and liquorice juice used in the formulations are known to contain natural pigments and can contribute to the brown coloration of the drinks, their ratios are constant across the formulations. Therefore, their contribution to brown colour intensity should be the same.

pH. The pH values of the formulations ranged from 6.11 (S13) to 6.21 (S31), indicating slightly acidic conditions. The pH values were relatively similar across the formulations, suggesting comparable acidity levels.

Sensory evaluation. The sensory overall liking revealed insignificant differences among the formulations. These results highlighted that the contribution of different proportions to the overall liking of the sample were not significant. Generally, data have shown a moderate sensory acceptability in overall liking. The data suggest that up to two thirds of the extract may be substituted by water in drink formulation with acceptable sensory properties. A study by Thumrongchote found that adding honey and lemon juice to a drink extract of *Schizophyllum commune Fr.*, an edible macro-fungus, helped increasing aroma, taste, and overall acceptability.[38] Similarly, the ratio of apple juice and honey significantly influenced colour, pH and sensory attributes of apple-honey beverages.[39] A study by Azami *et al.* also reported that the addition of liquorice extract in beverages affected their overall acceptability.[40]

CONCLUSION

This study represents the first investigation into the comparative effects of various extraction techniques on the phenolic and polysaccharide content, as well as the bioactivities of *Phellinus pini*. Additionally, it assesses the quality of healthy beverages formulated from the mushroom extract. The results indicated that the hot water extract exhibited the highest levels of phenolics, polysaccharides and albumin denaturation inhibitory activity. Conversely, the ultrasound extract displayed the most potent antioxidant activity, as determined by DPPH and ABTS assays. Notably, the beverage formulated with the greatest proportion of *P. pini* extract showcased the highest total phenolic content, antioxidant activity, and garnered moderate overall liking. The future investigations should focus on formulating beverages with Phellinus mushroom extract combined with other nutritious ingredients to enhance their health-promoting properties. Studies should also aim to optimize the taste, texture and shelf-life of the formulations to ensure consumer acceptance and marketability.

И З В О Д

ХЕМИЈСКИ САСТАВ И БИОАКТИВНОСТ ЕКСТРАКТА *Phellinus pini* И ЕВАЛУАЦИЈА
КВАЛИТЕТА ЗДРАВИХ НАПИТАКА ПРИПРЕМЉЕНИХ ОД ПЕЧУРАКА

NGUYEN THI NGAN[1] и TRANG H.D. NGUYEN[2]

*[1]Institute of Biotechnology and Food Technology, Industrial University of Ho Chi Minh City, Ho Chi Minh
City, Vietnam и [2]Food Science Program, Department of Kinesiology, Missouri Southern State University,
Joplin, MO 64801, USA*

    Phellinus pini, врста печурака која се налази у земљама источне Азије, обично се кон-
зумира као медицински напитак познат по својим ефектима загревања стомака и наводној
способности да ублажи бол и туморе. У овој студији, *P. pini* је екстрахован различитим
методама (топла вода, сонификација, микроталасна дигестија и квашење). У екстрактима
је одређиван садржај фенола и полисахарида. Додатно, екстракти су испитивани због
њиховог антиоксидативног потенцијала и способности да инхибирају денатурацију албу-
мина. Резултати су показали да екстракт добијен екстракцијом топлом водом садржи нај-
већу количину фенола (105,98±0,53 mg GAE/mL). Екстракција топлом водом и микрота-
ласна дигестија су се показале ефикаснијим поступцима у екстраховању полисахарида из
печурака. Штавише, екстракт добијен ултразвучном екстракцијом је показао највишу
антиоксидативну активност уклањањем DPPH и ABTC радикала за 41,26 и 97,84 %, редом,
док је екстракт добијен екстракцијом топлом водом показао најснажнију способност да
инхибира денатурацију албумина 96,40 %. Међу четири формулисана здрава напитка,
формулација са највећим уделом екстракта *P. pini* садржи највећи укупни садржај фенола,
највећу антиоксидативну активност и најповољнију сензорну укупну допадљивост. Доби-
јени резултати продубљују наше разумевање хемијског састава и потенцијалних здрав-
ствених својстава *P. pini,* као и откривање нових потенцијалних примена гљиве у прехрам-
беној индустрији.

REFERENCES

1. Y.-C. Dai, L.-W. Zhou, B.-K. Cui, Y.-Q. Chen, C. Decock, *Appl. Microbiol. Biotechnol.*
   87 (2010) 1587 (https://doi.org/10.1007/s00253-010-2711-3)
2. Y. Gafforov, O. Mykchaylova, M. Ghobad-Nejhad, M. Tomšovský, M. Yarasheva, H.
   Hüseyin Doğan, S. Rapior, L. Zhou, in *Ethnobiology*, Springer Nature, Basel, 2023
   (https://doi.org/10.1007/978-3-031-23031-8)
3. T. K. Trinh, *Preliminary list macrofungi of Vietnam*, Ha Noi Academy of Agriculture
   Publisher, Ha Noi, 1996
4. T. Zhu, S.-H. Kim, C.-Y. Chen, *Curr. Med. Chem.* **15** (2008) 1330
   (https://doi.org/10.2174/092986708784534929)
5. T.-Y. Song, H.-C. Lin, N.-C. Yang, M.-L. Hu, *J. Ethnopharmacol.* **115** (2008) 50
   (https://doi.org/10.1016/j.jep.2007.09.001)
6. P. Roupas, J. Keogh, M. Noakes, C. Margetts, P. Taylor, *J. Funct. Foods* **4** (2012) 687
   (https://doi.org/10.1016/j.jff.2012.05.003)
7. A. Lourenço, A. M. Lobo, B. Rodríguez, M.-L. Jimeno, *Phytochemistry* **43** (1996) 617
   (https://doi.org/10.1016/0031-9422(96)00335-4)
8. S. M. Lee, S. M. Kim, Y. H. Lee, W. J. Kim, J. K. Park, Y. I. Park, W. J. Jang, H.-D.
   Shin, A. Synytsya, *Macromol. Res.* **18** (2010) 602 (https://doi.org/10.1007/s13233-010-
   0615-9)

9. P. Jiang, L. Yuan, G. Huang, X. Wang, X. Li, L. Jiao, L. Zhang, *Int. J. Biol. Macromol.* **93** (2016) 566 (https://doi.org/10.1016/j.ijbiomac.2016.09.020)
10. K. H. Im, J. Choi, S.-A. Baek, T. S. Lee, *Mycobiology* **46** (2018) 159-167 (https://doi.org/10.1080/12298093.2018.1461316)
11. H. Zhang, H. Ma, W. Liu, J. Pei, Z. Wang, H. Zhou, J. Yan, *Carbohydr. Polym.* **113** (2014) 380 (https://doi.org/10.1016/j.carbpol.2014.07.027)
12. S. Ghosh, S. Das, R. Saha, K. Acharya, *Int. J. Med. Mushrooms* **25** (2023) 53 (https://doi.org/10.1615/IntJMedMushrooms.2023050232)
13. J.-S. Kim, *Prev. Nutr. Food Sci.* **21** (2016) 263 (https://doi.org/10.3746/pnf.2016.21.3.263)
14. T. H. D. Nguyen, D. C. Vu, P. Q. P. Hanh, X. T. Vo, V. C. Nguyen, T. N. Nguyen, L. L. P. Nguyen, L. Baranyai, *J. Agric. Food Res.* **14** (2023) 100879 (https://doi.org/10.1016/j.jafr.2023.100879)
15. S. S. Nielsen, in *Food analysis laboratory manual*, S.S. Nielsen, Ed., Kluwer Academic/Plenum Publishers, New York, 2017, p. 137 (https://doi.org/10.1007/978-3-319-44127-6)
16. P. M. Tuan, N. T. Ngan, N. X. Ha, H. V. Trung, *Trop. J. Nat. Prod. Res.* **7** (2023) 5606 (https://doi.org/10.26538/tjnpr/v7i12.34)
17. T. H. D. Nguyen, D. C. Vu, N. T. Ngan, H. Tran-Trung, V. S. Dang, *Anal. Lett.* **57** (2023) 1666 (https://doi.org/10.1080/00032719.2023.2264422)
18. M. Rašeta, M. Popović, I. Beara, F. Šibul, G. Zengin, S. Krstić, M. Karaman, *Chem. Biodivers.* **18** *(2021)* e2000828 (https://doi.org/10.1002/cbdv.202000828)
19. M. Rašeta, M. Karaman, M. Jakšić, F. Šibul, M. Kebert, A. Novaković, M. Popović, *Int. J.Food Sci Technol.* **51** (2016) 2583 (https://doi.org/10.1111/ijfs.13243)
20. M. Rašeta, J. Mišković, S. Berežni, S. Kostić, M. Kebert, M. Matavulj, M. Karaman, *Nat. Prod. Res.* (2024) (https://doi.org/10.1080/14786419.2024.2341300)
21. W. Xiaokang, J. G. Lyng, N. P. Brunton, L. Cody, J.-C. Jacquier, S. M. Harrison, K. Papoutsis, *Biotechnol. Rep.* **27** (2020) e00504 (https://doi.org/10.1016/j.btre.2020.e00504)
22. K. Papoutsis, P. Pristijono, J. B. Golding, C. E. Stathopoulos, M. C. Bowyer, C. J. Scarlett, Q. V. Vuong, *Eur. Food Res. Technol.* **244** (2018) 1353 (https://doi.org/10.1007/s00217-018-3049-9)
23. S. Bulam, M. Karadeniz, T. K. Bakır, S. Ünal, *Acta Sci. Pol. Hortorum Cultus* **21** (2022) 39 (https://doi.org/10.24326/asphc.2022.5.4)
24. P. Seephonkai, S. Samchai, A. Thongsom, S. Sunaart, B. Kiemsanmuang, K. Chakuton, *Chin. J. Nat. Med.* **9** (2011) 441 (https://doi.org/10.3724/SP.J.1009.2011.00441)
25. D. Vu, *Egypt. J. Chem.* **66** (2023) 581 (https://doi.org/10.21608/ejchem.2023.172356.7142)
26. N. Krsmanović, M. Rašeta, J. Mišković, K. Bekvalac, M. Bogavac, M. Karaman, O. S. Isikhuemhen, *Antioxidants* **12** (2023) 302 (https://doi.org/10.3390/antiox12020302)
27. L. Wang, C. L. Weller, *Trends Food Sci. Technol.* **17** (2006) 300 (https://doi.org/10.1016/j.tifs.2005.12.004)
28. W. Routray, V. Orsat, *Food Bioprocess Technol.* **5** (2012) 409 (https://doi.org/10.1007/s11947-011-0573-z)
29. S. Wasser, *Appl. Microbiol. Biotechnol.* **60** (2002) 258 (https://doi.org/10.1007/s00253-002-1076-7)
30. H. Thatoi, S. K. Singdevsachan, *Afr. J. Biotechnol.* **13** (2014) 523 (https://doi.org/10.5897/AJB2013.13446)

31. U. Lindequist, T. H. J. Niedermeyer, W.-D. Jülich, *Evid. Based Complementary Altern. Med.* **2** (2005) 285 (https://doi.org/10.1093/ecam/neh107)
32. N. Gao, W. Zhang, D. Hu, G. Lin, J. Wang, F. Xue, Q. Wang, H. Zhao, X. Dou, L. Zhang, *Molecules* **28** (2023) 5102 (https://doi.org/10.3390/molecules28135102)
33. P. He, Y. Zhang, N. Li, *Food Funct.* **12** (2021) 1856 (https://doi.org/10.1039/D0FO02342F)
34. Z. Xie, Y. Wang, J. Huang, N. Qian, G. Shen, L. Chen, *Int. J.Biol. Macromol.* **129** (2019) 61 (https://doi.org/10.1016/j.ijbiomac.2019.02.023)
35. G.-J. Huang, S.-S. Huang, J.-S. Deng, *PloS ONE* **7** (2012) e35922 (https://doi.org/10.1371/journal.pone.0035922)
36. C. Doguer, S. Yıkmış, O. Levent, M. Turkol, *J. Food Process. Preserv.* **45** (2021) e15436 (https://doi.org/10.1111/jfpp.15436)
37. K. D. Nguyen, C. M. Nguyen, D. A. Le, H. T. Huynh, M. T. Tran, A. T. N. Truong, T. H. D. Nguyen, D. C. Vu, L.-T. T. Nguyen, *J. Agric. Food Res.* **15** (2024) 101045 (https://doi.org/10.1016/j.jafr.2024.101045)
38. N. Mongkontanawat, D. Thumrongchote, *Food Res*. **5** (2021) 410 (https://doi.org/10.26656/fr.2017.5(4).259)
39. I. B. Leite, C. D. Magalhães, M. Monteiro, E. Fialho, *Foods* **10** (2021) 1525 (https://doi.org/10.3390/foods10071525)
40. T. Azami, M. Niakousari, S. M. B. Hashemi, L. Torri, *LWT* **91** (2018) 375 (https://doi.org/10.1016/j.lwt.2018.01.064).

Malachite green removal by *Eryngium caeruleum* ash

SHAGHAYEGH AZIZI and HASSAN ZAVVAR MOUSAVI*

Department of Analytical Chemistry, Faculty of Chemistry, University of Guilan, P. O. Box 41335-1914, Rasht, Iran

Abstract: In this study, malachite green (MG) has been successfully removed from an aqueous solution with the use of *Eryngium caeruleum* ash as an adsorbent. The influence of effective factors on the dye removal process, like contact time, the initial concentration of dye, amount of adsorbent, temperature and pH, has been studied. The results revealed that the optimal malachite green adsorption occurred at pH 7, 120 min of contact time, 0.01 g of adsorbent and 100 mg L^{-1} of initial dye concentration. Furthermore, the adsorption results follow the Langmuir isotherm with a correlation coefficient $R^2 = 0.98$ ($q_{max} = 476.19$ mg g^{-1}) and pseudo–second order kinetic ($R^2 = 0.97$). Endothermic and spontaneous adsorption were implied by the positive $\Delta H°$, $\Delta S°$ and negative $\Delta G°$. Therefore, in order to remove MG from aqueous solutions, *E. caeruleum* ash can be exploited as a low-cost and environmentally friendly adsorbent.

Keywords: adsorption; low-cost adsorbent; isotherm; kinetics; thermosdynamics.

INTRODUCTION

Dyes are applied in many manufacturing sectors, which include food processing, pharmaceuticals, textiles, plastic, rubber and paper.[1] Furthermore, dyes are organic compounds and have high solubility in water, especially those classified as reactive, direct, acidic and basic, which makes it a problem to remove them with conventional methods. The existence of dyes in textile wastewater, in addition to harming the environment and water bodies, prevents the light penetration into the water, which ultimately causes the photosynthetic rate to decline and the level of dissolved oxygen to drop, endangering the lives of the aquatic creatures.[2,3] The malachite green dye is extensively used for several purposes in agriculture, health, food, textiles and other industries.

215

Due to its carcinogenicity, this dye is dangerous and poisonous for blue species, such as fish and mammals. The concentrations of malachite green increase with time and exposure to temperature and it also can cause many diseases, including cancer, respiratory poisoning, Chromosome breaks, gene mutations, *etc*. Therefore, it is necessary to remove and separate this colour before discharging dye wastewater into the water.[4] Furthermore, various pollutants are included in dye wastewater, such as salts, adhesives, acids and additives, which are toxic, carcinogenic, teratogenic and xenobiotic.[5,6] These features are responsible for the creation of allergic conjunctivitis, skin irritation, eye burns and occupational asthma in the human body.[7,8] Dyes are a significant sort of harmful substances that are easily recognized by the human eye. However, it is important to prevent the discharge of dyes into water sources. Various treatment technologies are employed in order to reach this goal. The adsorption process is also considered an effective and economical method due to its simplicity and accessibility.[9,10] Currently, the search to find the most effective technique, among many for dye removal, is active. The adsorption methods are frequently employed to remove specific types of contaminants from water, particularly those that are difficult to biodegrade. The surface adsorption cheap and easily accessible adsorbents have attracted the attention of many researchers and now they are looking for economical and effective methods, using synthetic and natural materials as adsorbents.[11] In this study, we used *Eryngium caeruleum* ash for removing the malachite green dye (MG) from aqueous solutions through the surface adsorption method.

EXPERIMENTAL

Materials

Each of the chemical substances has been procured from Merck. HCl (36 %) and sodium hydroxide granules of 99.9 % purity were used (M) for pH adjustment, whereas sodium chloride was used to measure the ionic strength. Malachite green (MG) dye was dissolved in distilled water as well.

Preparation of the MG dye solution

The adsorbate for this study was MG, a common cationic dye. MG, known by the chemical formula $C_{23}H_{26}N_2Cl$, is one of the dye derivatives of aniline with a solid green appearance. MG dye has been weighed and dissolved in distilled water to achieve a concentration of 600 ppm. The pH had been modified to 2–12 through the addition of 0.1 M HCl and NaOH solutions.

Preparation of the adsorbent

Initially, the *Eryngium caeruleum* was collected from mountainous regions and washed utilizing distilled water to eliminate all contaminants. Subsequently, the plant had been dried and subjected to gentle heat for crushing. Then that was placed in the oven to turn into ash after 6 h at 350 °C. The acquired ash was slightly ground and finally made into a fine powder and can be utilized as an adsorbent.

Adsorption studies

In this case, the batch adsorption studies have been carried out for studying the removal of MG dye by utilizing *E. caeruleum* ash as the adsorbent. All the parameters were considered fixed, and only the parameter that should be optimized was changed. 25 mL of MG dye solution was prepared and the effects of parameters such as adsorbent dosage (0.01–0.07 g), solution pH (2–12), initial dye concentration (100–500 mg L^{-1}), contact time (15–135 min) and the temperature (0–40 °C) were studied. The pH solutions were modified with the addition of 0.1 M HCl and NaOH solutions. The following formula has been used to compute the percentage removal and MG dye solution adsorption capacity:[12]

$$q_e = (C_0 - C_e)\frac{V}{W} \tag{1}$$

$$\text{Removal percentage} = 100\frac{C_0 - C_e}{C_0} \tag{2}$$

in which C_0 and C_e (mg L^{-1}) are the liquid-phase of the dye concentrations at the initiation and equilibrium, accordingly. W / g is the mass of dry sorbent used and V / L is solution volume.

Adsorption isotherms

To investigate and enhance the adsorption system design and understand the adsorption equilibrium, it is essential to study the adsorption isotherm. The adsorption isotherm at equilibrium describes the distribution of adsorbed molecules in solid and liquid phases. The adsorption isothermal models can be used for evaluating adsorption phenomena and predicting maximum adsorption capacity. Also, Freundlich, Langmuir and Temkin are the most applied:

$$R_L = \frac{1}{1 + k_L C_e} \tag{3}$$

Adsorption kinetics and mechanisms

For the determination of adsorption system and kinetics, different kinetic and adsorption models like pseudo-first and second-order models, internal particle diffusion, and Elovich kinetic models have been studied. Also, different correlation coefficient (R^2) values were calculated for various kinetic and isothermal models.

RESULTS AND DISCUSSION

SEM adsorbent characterization

Scanning electron microscope (SEM) images were used for the information on the morphology of the adsorbent. According to the images (Fig. 1), the *Eryngium caeruleum* ash has porous surfaces and a porous structure which makes them the suitable sites for the MG dye adsorption.

FT-IR adsorbent study

The FT-IR analysis was interpreted in order to investigate the functional groups included in the adsorbent. Fig. 2 reveals the FT-IR spectrum for the *E. caeruleum* ash. According to this analysis, the adsorption peaks within the spectral range of 1464 to 2962 cm^{-1} correspond to various functional groups, namely,

–CH$_2$– bending, N–H stretching amine, C–O carboxylic acid stretching, Si–O–Si stretching, O–H carboxylic acid, C–O–O peroxide stretching, C–S stretching, S–S stretching and C–H methyl stretching groups.[14–16]
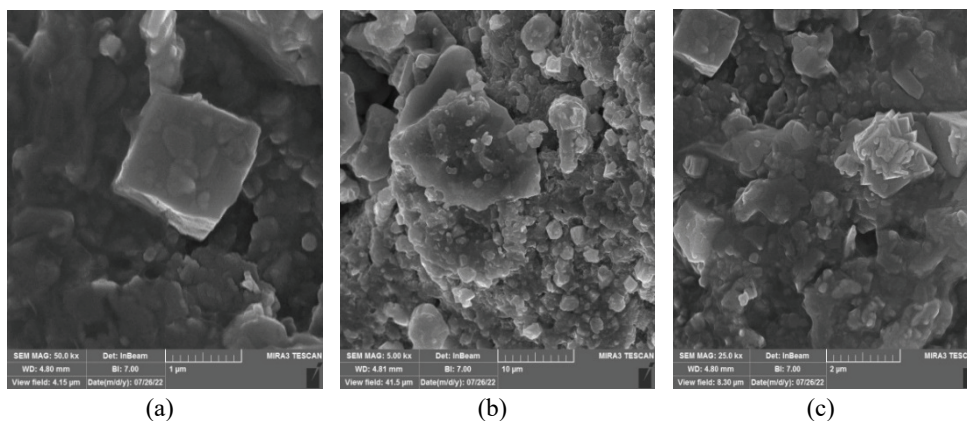
Fig. 1. *Eryngium caeruleum* ash adsorbent SEM images: a) 1, b) 10 and c) 2 µm mgnification.
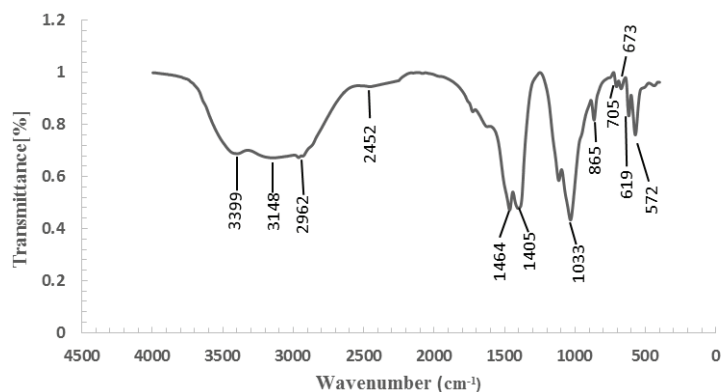
Fig. 2. The FT-IR spectrum for the *Eryngium caeruleum* ash.

Effect of solution pH

Several studies have shown that the initial solution pH can influence surface charge, the solubility of the adsorbate and the ionization degree in the adsorption method, so the initial solution pH is one of the main environmental factors. Diluted solutions of 0.1 M HCl and NaOH were added to 25 mL of MG dye solutions, which had a concentration of 100 mg L^{-1}, to optimize pH from 2–12. Then, 0.01 g of the adsorbent has been added to the flasks and agitated for 60 min on a shaker (at a constant 160 rpm shaking rate) at ambient temperature. The concentrations of the dye at equilibrium had been measured by a UV/Vis spectrophotometer (Perkin-Elmer, Junior model 35, U.S.) at 618 nm. The maximum MG dye

removal percentage (66.90 %) had been achieved at a pH of 7.0. Also, the zero point charge (pHzpc) value for *E. caeruleum* ash was found to be 6.0 (Fig. 3b). This result confirms that at a pH > pHzpc, the negative charge density on the MG dye surface increases, leading to MG elimination.[17] In fact, the adsorption capacity of MG dye is minimal in acidic solutions. This phenomenon could be attributed to the positive charge of the adsorbents, which leads to the repulsion of the cationic dye MG as they share the same charge.[18] According to Fig. 3a, at pH above 7, because of the existence of hydrogen bonds, the repulsive force between H^+ and cationic dye molecules causes a decrease in adsorption at first and then reaches a constant value.[19]

(a)   (b)
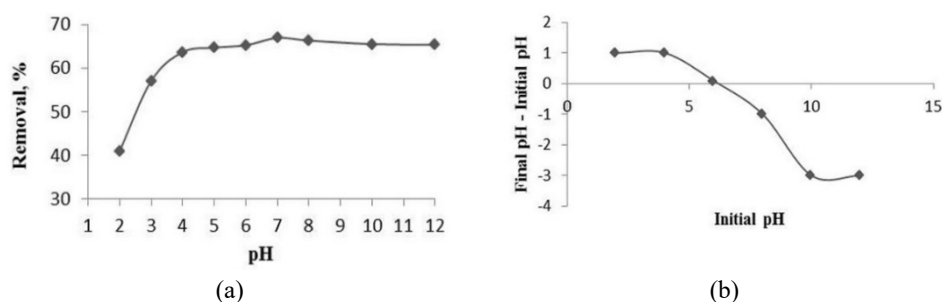
Fig. 3. a) Effect of initial pH on MG adsorption; b) point of zero charge.

Effect of adsorbent dosage

The influence of changing the adsorbent dosage (0.005–0.07 g) on MG removal % is shown in Fig. 4. One key factor that significantly impacts the adsorption process and requires the examination in adsorption studies is the influence of the dosage of the adsorbent. In order to investigate this factor, MG dye solutions at 100 mg L^{-1} concentration were prepared in a volume of 25 mL under optimum pH 7 and then different doses of adsorbent in the range of 0.005 to 0.07 g were added to the dye solutions and they were stirred for 120 min at ambient temperature on a shaker (at a constant 160 rpm shaking rate). According to Fig. 4, the highest percentage of MG dye removal can be seen in the dosage of 0.01 g of adsorbent (74.12 %) since, in the graph after this point, the slope of the curve has reached an almost constant value. Therefore, the optimum dosage of adsorb-
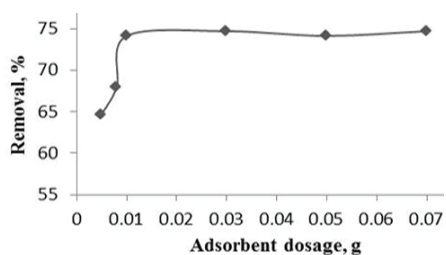
Fig. 4. Effect of adsorbent dosage on MG adsorption.

ent was considered to be 0.01 g because a higher adsorbent dosage can increase surface area.[20]

Effect of contact time

The optimal contact time should give enough time for the dye to adsorb the sites of the adsorbent surface so that the adsorption sites can adsorb the cationic dye molecules. To investigate this effect, 25 mL solutions of MG dye were prepared at a 100 mg L^{-1} concentration (pH 7). Also, 0.01 g of adsorbent has been added to the flasks and they have been stirred in the contact time range of 15 to 135 min at ambient temperature on a shaker (at a constant 160 rpm shaking rate). Fig. 5 displays the influence of contact time on the MG adsorption. Initially, the curve slope is steeper, considering the accessibility of the unoccupied adsorbent sites. However, the line's slope smooths after 120 min and the MG dye removal percentage remains constant. In other words, as time increases, the percentage of MG removal increases and after a while, it starts to rise with less intensity and then it reaches a constant value. After 120 min, the unoccupied sites on the adsorbent surface are saturated with the pollutant and the adsorption system reaches equilibrium. As a result, the optimal contact time was 120 min with 74.12 % MG dye removal.
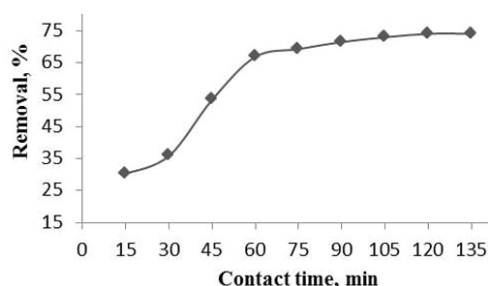
Fig. 5. Effect of contact time on MG adsorption.

Effect of initial concentration

Fig. 6 shows that variations in the initial dye concentration can influence the percentage removal of the MG. To investigate this effect, 25 mL solutions of MG dye were prepared at various concentrations (100–500 mg L^{-1} at pH 7). Then, 0.01 g of adsorbent has been added to the solutions and they have been stirred for 120 min at ambient temperature on a shaker (at a constant 160 rpm shaking rate). According to Fig. 6, at low concentrations, fewer pollutants were present in the solution and more sites on the adsorbent surface were ready to accept dye molecules. However, after the increase in dye concentration, a large number of adsorbed molecules competed to occupy the empty sites on the adsorbent and consequently, the percentage of dye removal decreased.[21] Therefore, the concen-

tration of 100 ppm (74.17 removal %) was considered as the optimal concentration.
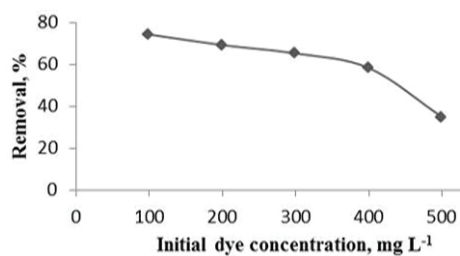
Fig. 6. Effect of initial dye concentration on MG adsorption.

Effect of temperature

The temperature is an essential parameter in determining the adsorbent capacity for physical and chemical adsorption.[22] In fact, temperature can provide useful information about thermodynamic parameters. In order to test the temperature factor, 100 mg L^{-1} of the MG solutions were prepared under conditions of pH 7 in a volume of 25 mL. Also, 0.01 g of adsorbent was added to flasks and the solutions were stirred for 120 min. According to Fig. 7, the studied temperature range was 0 up to 40 °C. The results show that as the temperature increases, the viscosity of the MG dye solution decreases, which can lead to a higher diffusion rate of MG dye molecules in the outer boundary layers and facilitate their penetration into the inner pores of the absorbent. Therefore, the optimal adsorption temperature is 40 °C. (313 K, removal 99.87 %).
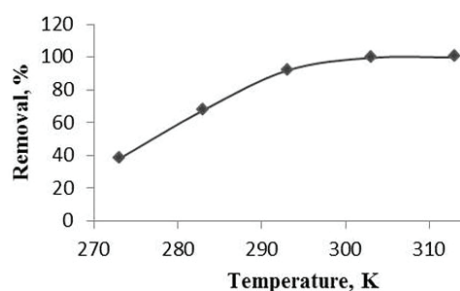
Fig. 7. Effect of temperature on MG adsorption.

Effect of ionic strength

In addition to dyes, textile wastewater contains various types of ions and these ions can be effective in removing dyes through surface adsorption. In order to study this parameter, 25 mL of MG dye solutions at pH 7 (concentration of 100 mg L^{-1}) were prepared, then 0.01 g of adsorbent was added to solutions. Then 2 mL of NaCl with concentrations of 0.1, 0.3, 0.6 and 1 M was added to each of these prepared solutions and they were agitated for 120 min at ambient temperature on a shaker (at a constant 160 rpm shaking rate). According to Fig.

8, as the sodium chloride concentration increases, the percentage of MG dye removed decreases and this is due to the competition between sodium ions and contaminant molecules to occupy all accessible sites.[23]
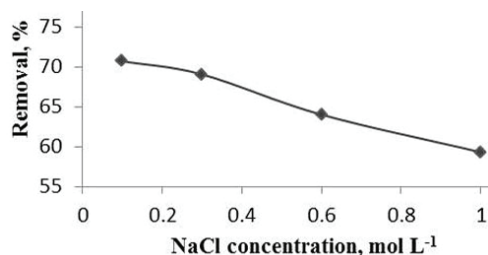
Fig. 8. Effect of ionic strength on MG dye adsorption.

Adsorption isotherms studies

The efficiency of adsorbents used for the adsorption can be investigated using adsorption isotherms such as Freundlich, Langmuir and Temkin and it is also possible to determine the nature of the interaction between the adsorbent and the adsorbate material.[24]

Langmuir adsorption isotherm

The maximum adsorbent capacity was calculated using the Langmuir isotherm model and is shown as follows: [25]

$$\frac{C_e}{q_e} = \frac{1}{K_L q_{max}} + \frac{C_{eq}}{q_{max}} \tag{4}$$

where q_e is the amount of adsorbate at equilibrium, q_{max} / mg g^{-1} is the maximum capacity of adsorbent, K_L / L mg^{-1} is the Langmuir isotherm constant that refers to the adsorption rate and C_e / mg L^{-1} is the equilibrium adsorbate concentration. Through the charting of C_e/q_e *versus* C_e, q_{max} and K_L values were obtained. The fundamental characteristics of a Langmuir isotherm could be defined through a dimensionless parameter recognized as the separation factor R_L, which value was found to be 0.14. The $R_L < 1$ means that the adsorption of MG is favourable in this investigated study. The Langmuir adsorption isotherm diagram can also be seen in Fig. 9. Table I shows that the adsorption process follows the Langmuir isotherm ($R^2 = 0.98$) with a q_{max} of 476.19 mg g^{-1}.

Freundlich adsorption isotherm

In the Freundlich isotherm model, adsorption can occur on the heterogeneous surface of the adsorbent with a non-uniform distribution of heat. The following formula refers to the linear form of this model:[26]

$$\ln q_e = \ln K_F + \frac{1}{n} \ln C_e \tag{5}$$
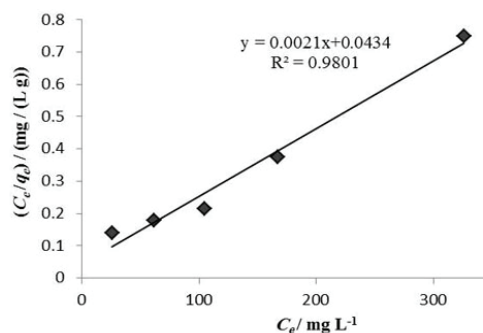
Fig. 9. Langmuir *Eryngium caeruleum* ash plot for adsorption of MG.

TABLE I. Equilibrium isotherm modeling of MG adsorption onto *Eryngium caeruleum* ash

Isotherm	*Eryngium caeruleum* ash
Langmuir	
q_{max} / mg g^{-1}	476.19
K_L	0.04
R_L	0.14
R^2	0.98
Freundlich	
N	2.64
K_F / L mg^{-1}	67.26
R^2	0.67
Temkin	
B / J mol^{-1}	122.39
K_T / L mg^{-1}	0.28
R^2	0.61

where q_e is the adsorbed amount of dye at equilibrium, K_F and $1/n$ are the Frendulich constants and C_e is the equilibrium concentration. The values of $1/n$ express the non-linearity of the relationship between the solution concentration and the adsorption. When the value of n is less than one and n is greater than one, chemical adsorption and physical adsorption are implied, respectively. And also, if $n = 1$, adsorption is linear. Fig. 10 shows ln q_e *versus* ln C_e plotted for MG adsorption on the adsorbent. The values of n and K_F are computed using the
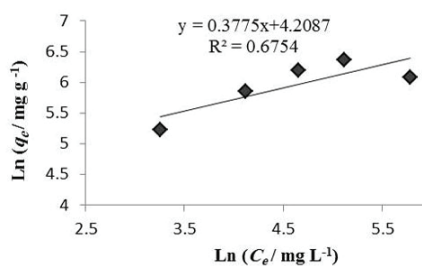
Fig. 10. Freundlich *Eryngium caeruleum* ash plot for adsorption of MG.

slope and the intercept separately, which were (2.64) and (67.26 mg g^{-1}) and also $R^2 = 0.67$ was obtained, which did not seem appropriate. As a result, since the value of $n > 1$ the adsorption has been carried out as a chemical process.

Temkin adsorption isotherm

Variations in adsorption energy and the adsorbent surface were evaluated utilizing the Temkin adsorption isotherm. The R^2 value has been used as a criterion for effectiveness and efficiency. The Temkin isothermal model is shown using the following linear formula:[27]

$$q_e = \frac{RT}{b} \ln K_T + \frac{RT}{b} \ln C_e \tag{6}$$

where R, 8.314 J mol^{-1} K^{-1}, is the universal constant of the gas and T / K represents temperature (absolute).[24] The Temkin isotherm model of MG dye adsorption onto *E. caeruleum* ash is shown in Fig. 11 by charting q_e *versus* $\ln C_e$ at a constant temperature. According to Table I, R^2 for the Temkin isotherm model is 0.61. The results show that the Langmuir isotherm is more accurate than other isotherms in describing the adsorption of MG dye on the adsorbent.
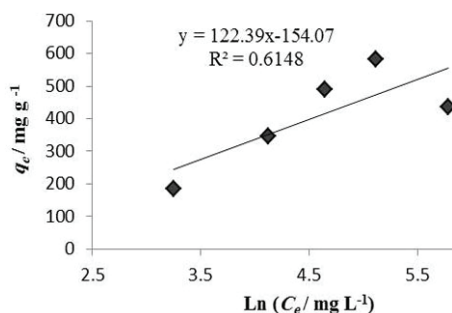
Fig. 11. Temkin *Eryngium caeruleum* ash plot for adsorption of MG.

Adsorption kinetic study

To provide information about the factors that impact reaction speed, it is necessary to carry out kinetic evaluations. In this study, various kinetic models have been used for the analysis of the data to investigate the mechanisms of MG dye adsorption on the adsorbent, including Elovich, intra-particle, pseudo-first order and pseudo-second order.

Pseudo-first-order kinetic model

In surface adsorption studies, the pseudo-first-order is an old kinetic model and can give information about the adsorption kinetics of pollutants.[28] Pseudo-first-order rate equations were typically used to describe the adsorbate performance from the tested dye solution. The linear model of this kinetic model is provided using the following equation: [29]

$$\ln(q_e - q_t) = \ln q_e - k_1 t \tag{7}$$

where q_e / mg g^{-1} is the amount of dye adsorbate on the adsorbent surface at equilibrium, q_t / mg g^{-1} is the amount of dye adsorbed at time t / min and k_1 / min^{-1} is the rate constant. Fig. 12 shows the pseudo-first-order model of the adsorption of MG dye onto *E. caeruleum* ash by charting ln $(q_e$–$q_t)$ *versus* contact time. According to Table II, k_1 and q_e were calculated and R^2 for this kinetic model was 0.90.
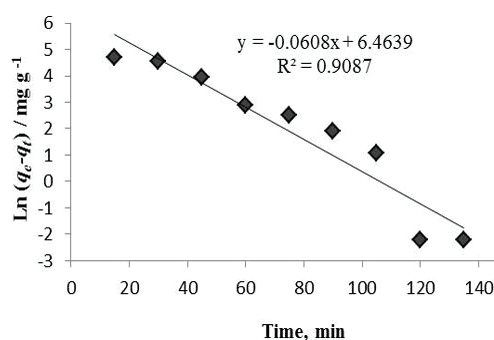
Fig. 12. Pseudo-first-order model of MG adsorption onto *Eryngium caeruleum* ash.

TABLE II. Adsorption kinetic models of MG adsorption onto *Eryngium caeruleum* ash

Adsorption kinetic model	Constant	MG dye
Pseudo-first-order	q_e / mg g^{-1}	641.55
	k_1 / min^{-1}	0.06
	R^2	0.90
Pseudo-second-order	q_e / mg g^{-1}	243.90
	k_1 / min^{-1}	0.004
	R^2	0.97
Elovich kinetic	α / g mg^{-1}	14.09
	β / mg g^{-1} min^{-1}	0.017
	R^2	0.92
Intraparticle-diffusion	K_{id} / mg g^{-1}min$^{-1/2}$	15.47
	C / mg g^{-1}	23.8
	R^2	0.88

Pseudo-second-order kinetic model

The pseudo-second-order model is another model applied for analysing the adsorption kinetics. The linear equation for the model is as follows:[30]

$$\frac{t}{q_t} = \frac{1}{k_2 q_e^2} + \frac{t}{q_e} \tag{8}$$

where k_2 / g mg^{-1} min^{-1} is the constant rate and t / min is the contact time. Fig. 13 shows the charting of t/q_t *versus* contact time and according to Table II, R^2 for this kinetic model obtained 0.97. The data indicate that the second-order kinetic

equation can provide a suitable description of the MG adsorption mechanism on the surface of the adsorbent.
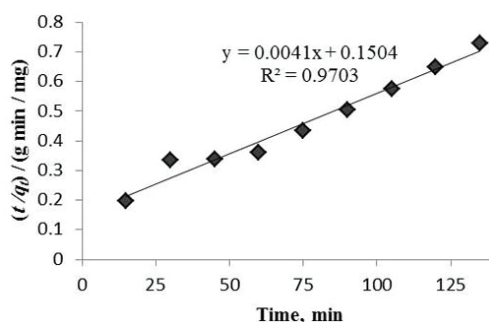
Fig. 13. Pseudo-second-order model of MG adsorption onto *Eryngium caeruleum* ash.

Elovich kinetic model

Elovich is a kinetic equation that has been used to evaluate boron adsorption. This model has the following linear formula:[31]

$$q_t = \frac{1}{\beta}\ln(\alpha\beta) + \frac{1}{\beta}\ln t \tag{9}$$

where α is the chemisorption rate at zero coverage and β is associated with both chemical adsorption activation energy and the extent of surface coverage. Fig. 14 shows the Elovich model of MG dye adsorption onto *E. caeruleum* ash by charting q_t *versus* $\ln t$. According to Table II, R^2 for the Elovich kinetic model is 0.92, which shows that this kinetic model has a suitable correlation coefficient.
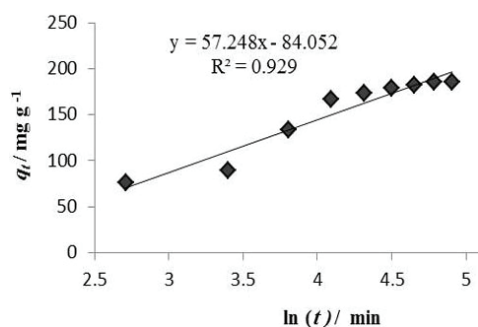
Fig. 14. Elovich kinetic model of MG adsorption onto *Eryngium caeruleum* ash.

Intraparticle-diffusion kinetic model

Fig. 15 shows the intraparticle diffusion model of MG dye adsorption onto *E. caeruleum* ash by charting q_t *versus* $t^{0.5}$. This is a kinetic model based on diffusion, which has the following equation:[32]

$$q_t = k_{id}t^{0.5} + C \tag{10}$$

where K_{id} / mg g^{-1} min$^{-1/2}$ the constant rate, q_t / mg g^{-1} is the fraction adsorbate uptake at time and C / mg g^{-1} is the intercept that gives information about the thickness of the boundary layers surrounding the adsorbent. According to Table II, R^2 for this kinetic model is 0.88.
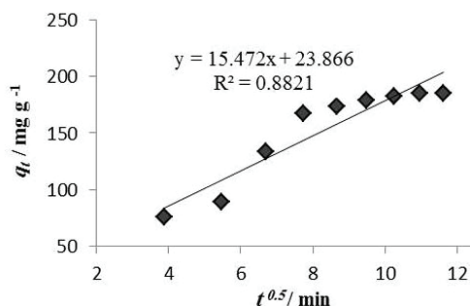
Fig. 15. Intraparticle diffusion model of MG adsorption onto *Eryngium caeruleum* ash.

Thermodynamic study

In this study, the thermodynamic equations were used to investigate the effect of temperature on the adsorption of MG on the adsorbent surface. In fact, to increase the efficiency of the adsorption process, thermodynamic studies were performed. Thermodynamic parameters can be obtained using the following formulas:[33]

$$\Delta G^o = -RT \ln K_d \qquad (11)$$

$$\ln K_d = \frac{\Delta S^o}{R} - \frac{\Delta H^o}{RT} \qquad (12)$$

where T / K is is the absolute solution temperature and K_d is the equilibrium constant. The spontaneity or non-spontaneity of the adsorption system is inferred from the change in Gibbs energy. According to Table III, by increasing the temperature in the range of 273–303 K, it was found that the values of $\Delta G°$ decreased from –0.978 to –0.198 kJ mol^{-1}. Therefore, at higher temperatures, the adsorption of the MG dye is spontaneous and more favourable.[23] According to the intercept and slope of the plot in Fig. 16, the parameters of the thermodynamic process, namely $\Delta H°$ and $\Delta S°$ were calculated and the positive value for $\Delta H°$ indicates an endothermic adsorption process. Considering that $\Delta S° > 0$, the

TABLE III. Thermodynamic study of MG adsorption onto *Eryngium caeruleum* ash

T / K	K_d	$\Delta G°$ / kJ mol^{-1}	$\Delta H°$ / kJ mol^{-1}	$\Delta S°$ / J mol^{-1} K^{-1}	R^2
273	1.538718291	–0.978136222	136.02	497.817	0.9661
283	5.207006369	–3.882234294			
293	28.2106599	–8.135515677			
303	669.7222222	–16.39171195			
313	2014.166667	–19.79805951			

affinity of the adsorbent for MG dye decreased and it was found that the randomness of the solid / solution interface increased during adsorption.
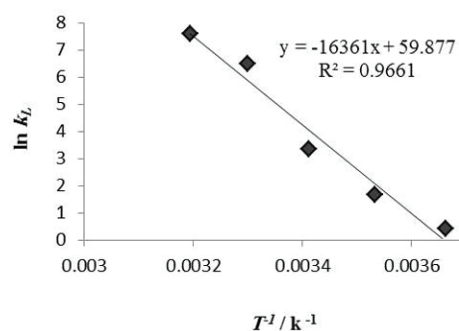
Fig. 16. Thermodynamic study of MG dye adsorption onto *Eryngium caeruleum* ash.

Comparison of the various adsorbents to remove MG dye

Table IV shows various adsorbents used for MG dye removal and it was concluded that the *E. caeruleum* ash adsorbent has been able to allocate the maximum adsorption capacity, compared to other adsorbents, which indicates that this adsorbent is suitable to remove MG dye from an aqueous solution.

TABLE IV. Comparison of the various adsorbents to remove MG dye

Adsorbent	Adsorption capacity mg g^{-1}	pH	Ref.
Almond gum	172.41	7	34
Sulfuric acid-treated coffee husk (ACH)	264.82	6.8	35
Activated carbon from apricot stone (ASM)	88.5	10	36
Elaeagnus Stone Activated Carbon (EAC)	432.90	7	37
Nanochitosan from shrimp shells (STP)	317.73	6	38
Carbonised pomegranate peel (CPP)	31.45	6	24
Carica papaya wood	52.63	10	39
Activated carbon from pistachio shell (PisAC)	76.92	7	40
Eryngium caeruleum ash	476.19	7	This study

CONCLUSIONS

Recently, researchers have been interested in finding cost-effective adsorbents for wastewater treatment. The structural and morphological characteristics of *Eryngium caeruleum* ash were investigated using FT-IR and SEM. Various experimental parameters like initial concentration of the dye, equilibrium contact time, temperature, dosage of the adsorbent and pH of dye solution, were investigated. The optimum efficiency for MG removal using *E. caeruleum* ash was observed at pH 7, dosage of 0.01 g, contact time of 120 min, initial MG concentration of 100 ppm and temperature of 40 °C. The adsorption process of MG dye onto the adsorbent was fitted with the pseudo-second-order kinetics model and

the Langmuir isotherm model and the q_{max} has been attained at 476.19 mg g^{-1}. The adsorption procedure, supported due to the negative $\Delta G°$ and positive $\Delta H°$ values, was identified as spontaneous, chemisorptive and endothermic. According to this study, *E. caeruleum* ash, in addition to being low-cost, easy to access, easy to prepare and preventing the spread of pollution in the environment, is also environmentally friendly. Therefore, this adsorbent can remove malachite green dye from aqueous solutions.

И З В О Д

УКЛАЊАЊЕ МАЛАХИТ-ЗЕЛЕНЕ БОЈЕ ПЕПЕЛОМ *Eryngium caeruleum*

SHAGHAYEGH AZIZI и HASSAN ZAVVAR MOUSAVI

Department of Analytical Chemistry, Faculty of Chemistry, University of Guilan, P. O. Box 41335-1914, Rasht, Iran

Малахит зелена боја је успешно уклоњена из воденог раствора употребом пепела *Eryngium caeruleum* као адсорбента. Испитиван је утицај ефективних фактора на процес уклањања боје, као што су време контакта, почетна концентрација боје, количина адсорбенса, температура и pH. Добијени резултати показују да су оптимални услови за адсорпцију малахит зелене боје: pH 7, време контакта 120 min, количина адсорбенса 0,01 g, почетна концентрација боје 100 mg mL^{-1}. Такође, резултати су у складу са Лангмуировом изотермом ($R^2 = 0,98$), ($q_{max} = 476,19$ mg g^{-1}), и кинетиком псеудо-другог реда ($R^2 = 0,97$). Ендотермна и спонтана адсорпција су имплициране позитивним $\Delta H°$ и $\Delta S°$ вредностима, као и негативним $\Delta G°$. Добијени резултати указују да за уклањање малахит зелене боје из водених раствора може да се примени јефтин и еколошки прихватљив адсорбенс пепео *E. caeruleum*.

(Примљено 15. априла, ревидирано 28. августа, прихваћено 27. септембра 2024)

REFERENCES

1. M. Zarrabi, R. Alizadeh, S. Mahboob, *Sep. Purif. Technol.* **211** (2019) 738 (https://doi.org/10.1016/j.seppur.2018.10.026)
2. M. M. Hassan, C. M. Carr, *Chemosphere* **209** (2018) 201 (https://doi.org/10.1016/j.chemosphere.2018.06.043)
3. M. Imran, D.E. Crowley, A. Khalid, S. Hussain, M.W. Mumtaz, M. Arshad, *Rev. Environ. Sci. Biotechnol.* **14** (2015) 73 (https://doi.org/10.1007/s11157-014-9344-4)
4. K. Tewari, G. Singhal, R. K. Arya, *Rev. Chem. Eng.* **34** (2018) 427 (https://doi.org/10.1515/revce-2016-0041)
5. K. Jain, A. S. Patel, V. P. Pardhi, S. J. S. Flora, *Molecules* **26** (2021) 1797 (https://doi.org/10.3390/molecules26061797)
6. D. A. Yaseen, M. Scholz, *Int. J. Environ. Sci. Technol.* **16** (2019) 1193 (https://doi.org/10.1007/s13762-018-2130-z)
7. D. Ma, H. Yi, C. Lai, X. Liu, X. Huo, Z. An, L. Li, Y. Fu, B. Li, M. Zhang, L. Qin, S. Liu, L. Yang, *Chemosphere* **275** (2021) 130104 (https://doi.org/10.1016/j.chemosphere.2021.130104)

8. F. E. Titchou, H. Zazou, H. Afanga, J. El Gaayda, R. Ait Akbour, P. V. Nidheesh, M. Hamdani, *Chem. Eng. Process. – Process Intensif.* **169** (2021) 108631 (https://doi.org/10.1016/j.cep.2021.108631)
9. A. Khaligh, H. Zavvar Mousavi, A. Rashidi, H. Shirkhanloo, *J. Serb. Chem. Soc.* **83** (2018) 651 (https://doi.org/10.2298/JSC170827112K)
10. A. A. Fodeke and O. O. Olayera, *J. Serb. Chem. Soc.* **84** (2019) 1143 (https://doi.org/10.2298/JSC190209042F)
11. W. Wei, L. Yang, W. H. Zhong, S. Y. Li, J. Cui, Z. G. Wei, *Dig. J. Nanomater. Biostruct.* **19** (2015) 1343 (https://www.chalcogen.ro/1343_Wei.pdf)
12. S. Farch, M. M. Yahoum, S. Toumi, H. Tahraoui, S. Lefnaoui, M. Kebir, M. Zamouche, A. Amrane, J. Zhang, A. Hadadi, L. Mouni, *Separations* **10** (2023) 60 (https://doi.org/10.3390/separations10010060)
13. A. B. D. Nandiyanto, W. C. Nugraha, I. Yustia, R. Ragadhita, M. Fiandini, M. Saleh, D. R. Ningwulan, *J. Adv. Res. Appl. Mech.* **106** (2023) 1 (https://doi.org/10.37934/aram.106.1.113)
14. A. B. D. Nandiyanto, R. Oktiani, R. Ragadhita, *Indones. J. Sci. Technol.* **4** (2019) 97 (https://doi.org/10.17509/ijost.v4i1.15806)
15. J. Coates, *Encycl. Anal. Chem.* **12** (2000) 10815 (https://doi.org/10.1002/9780470027318.a5606)
16. E. Smidt, M. Schwanninger, *Spectrosc. Lett.* **38** (2005) 247
17. (https://doi.org/10.1081/SL-200042310)
18. R. Bagheri, M. Ghaedi, A. Asfaram, E. A. Dil, H. Javadian, *Polyhedron* **171** (2019) 464 (https://doi.org/10.1016/j.poly.2019.07.037)
19. M. Messaoudi, M. Douma, N. Tijani, Y. Dehmani, L. Messaoudi, *Desalin. Water Treat.* **240** (2021) 191 (https://doi.org/10.5004/dwt.2021.27688)
20. U. Jinendra, B. M. Nagabhushana, D. Bilehal, *Desalin. Water Treat.* **209** (2021) 392 (https://doi.org/10.5004/dwt.2021.26536)
21. N. Khamis Soliman, A. F. Moustafa, A. A. Aboud, K. S. A. Halim, *J. Mater. Res. Technol.* **8** (2019) 1798 (https://doi.org/10.1016/j.jmrt.2018.12.010)
22. N. M. Mahmoodi, Z. Mokhtari Shourijeh, *Desalin. Water Treat.* **57** (2016) 20076 (https://doi.org/10.1080/19443994.2015.1109562)
23. Y. Miyah, A. Lahrichi, M. Idrissi, K. Anis, R. Kachkoul, N. Idrissi, S. Lairini, V. Nenov, F. Zerrouq, *J. Mater. Environ. Sci.* **8** (2017) 3570 (https://www.jmaterenvironsci.com/Document/vol8/vol8_N10/377-JMES-Myah.pdf)
24. D. R. Rout, H. M. Jena, *Mater. Today* **47** (2021) 1173 (https://doi.org/10.1016/j.matpr.2021.03.406)
25. F. Gündüz, B. Bayrak, *J. Mol. Liq.* **243** (2017) 790 (https://doi.org/10.1016/j.molliq.2017.08.095)
26. D. C. Roy, M. M. Sheam, M. R. Hasan, A. K. Saha, A. K. Roy, M. E. Haque, M. M. Rahman, T. Swee-Seong, S. K. Biswas, *bioRxiv* (2020) 2020 (https://doi.org/10.1101/2020.03.29.014274)
27. S. Archana, B. K. Jayanna, A. Ananda, M. S. Ananth, A. M. Ali, H. B. Muralidhara, K. Y. Kumar, *J. Indian Chem. Soc.* **99** (2022) 100249 (https://doi.org/10.1016/j.jics.2021.100249)
28. Y. Dehmani, O. El Khalki, H. Mezougane, S. Abouarnadasse, *Chem. Data Collect.* **33** (2021) 100674 (https://doi.org/10.1016/j.cdc.2021.100674)
29. D. R. Rout, H. M. Jena, *Environ. Sci. Pollut. Res.* **30** (2023) 22992 (https://doi.org/10.1007/s11356-022-23774-3)

30. J. U. Ani, S. C. Agbo, O. A. Odewole, F. K. Ojo, O. L. Alum, K. G. Akpomie, A. C. Ofomatah, H. O. Chukwuemeka-Okorie, O. D. Onukwuli, *IOP Conf. Ser.: Earth Environ. Sci*. **1178** (2023) 012023 (https://doi.org/10.1088/1755-1315/1178/1/012023)

31. S. Ukachuku, E. D. Dikio, *World News Nat. Sci.* **49** (2023) 1 (http://www.worldnewsnaturalsciences.com/wp-content/uploads/2023/05/WNOFNS-49-2023-1-13.pdf)

32. E. H. Gürkan, B. İlyas, Y. Tibet, *Int. J. Environ. Anal. Chem*. **103** (2023) 1343 (https://doi.org/10.1080/03067319.2021.1873314)

33. S. S. Madan, K. L. Wasewar, C. Ravi Kumar, *Adv. Powder Technol*. **27** (2016) 2112 (https://doi.org/10.1016/j.apt.2016.07.024)

34. A. I. Abd-Elhamid, H. F. Aly, H. A. Soliman, A. A. El-Shanshory, *J. Mol. Liq*. **265** (2018) 226 (https://doi.org/10.1016/j.molliq.2018.05.127)

35. F. Bouaziz, M. Koubaa, F. Kallel, R. E. Ghorbel, S. E. Chaabouni, *Int. J. Biol. Macromol*. **105** (2017) 56 (https://doi.org/10.1016/j.ijbiomac.2017.06.106)

36. T. K. Murthy, B. S. Gowrishankar, M. C. Prabha, M. Kruthi, R. H. Krishna, *Microchem. J.***146** (2019) 192 (https://doi.org/10.1016/j.microc.2018.12.067)

37. M. Abbas, *Adsorpt. Sci. Technol*. **38** (2020) 24 (https://doi.org/10.1177/0263617420904476)

38. Ü. Geçgel, O. Üner, G. Gökara, Y. Bayrak, *Adsorpt. Sci. Technol*. **34** (2016) 512 (https://doi.org/10.1177/0263617416669727)

39. S. Salamat, M. Hadavifar, H. Rezaei, *J. Environ. Chem. Eng.* **7** (2019) 103328 (https://doi.org/10.1016/j.jece.2019.103328)

40. S. Rangabhashiyam, S. Lata, P. Balasubramanian, *Surf. Interfaces* **10** (2018) 197 (https://doi.org/10.1016/j.surfin.2017.09.011)

41. H. Mahadevan, P. V. M. Nimina, K. A. Krishnan, *Sustain. Water Resour. Manage*. **8** (2022) 38 (https://doi.org/10.1007/s40899-022-00612-5).

Enhancing fire resistance in wood with high-water retention silica gel: A promising flame-retardant solution

ZHONGBIN FEI, YINGNAN ZHANG, ZHI WANG, YILING DUAN and BIN ZHANG*

International Center for Chemical Process Safety, Nanjing Tech University, Nanjing, 211816, China

Abstract: This study aims to evaluate water retention and flame-retardant properties of silica gel prepared using anionic polyacrylamide (HPAM), gluconate-delta-lactone (GDL) and aluminum citrate (AlCit). Silica gel samples were synthesized with sodium silicate (8 wt. %), sodium bicarbonate (4 wt. %) and varying concentrations of HPAM (0.2–0.8 wt. %) and GDL (0.1–0.3 wt. %). The prepared gels were characterized using XPS, XRD, FTIR and TGA. Optimal water retention capacity was achieved with 0.4 wt. % HPAM and 0.2 wt. % GDL. Compared to traditional gels, silica gel has more surface water molecules due to the additional hydrophilic groups and the amorphous nature of silica. At high temperatures, silica forms a layer with the charcoal from treated wood combustion, inhibiting oxygen penetration and minimizing further combustion. After combustion at 500 °C, the mass loss of wood treated with silica gel is 36–53 % less than untreated wood, indicating greater weight retention and demonstrating silica gel's effectiveness in preventing continued burning.

Keywords: polyacrylamide; microscopic process; combustion morphology; mass loss; amorphous silica.

INTRODUCTION

Wood plays a vital role in human life due to its unique properties such as porosity, anisotropy, wet swelling, dry shrinkage, combustion and biodegradability.[1] The wood processing industry in China encompasses several key sectors, including sawn timber processing, wood chip processing, veneer processing, other wood processing, wood-based panel production and wood products manufacturing, with products like construction timber and wooden furniture. In 2022, China's timber output reached 106.93 million m³, comprising 92.44 million m³ of logs and 14.49 million m³ of fuelwood.

However, wood's flammability poses risks in building, furniture and décorative items, leading to fire spread and the production of smoke and gases such as carbon monoxide, which can be fatal. Treating wood with a fire retardant is crucial to reduce its combustibility.[2] One of the oldest flame retardants, borates, is still in use due to its low toxicity and volatility. However, boron compounds' tendency to leach from wood surfaces and interiors under specific conditions poses challenges.[3] Surface coatings and fixation of pure boron compounds have shown limited effectiveness in reducing leaching.[4] Additionally, metal salts can be used to reduce smoke production and flammability by promoting the formation of charcoal and reducing tar products.[5] However, these salts may also leach from treated wood, affecting their long-term efficacy.[6]

Alkaline silicates like sodium silicate and potassium silicate, which form glass when applied to wood, have been used to retard fire.[7,8] Research suggests that these silicates can react with cell walls and limit leaching.[9] When ignited, these silicates create a protective glass layer, improving wood's thermal stability and fire resistance.[10]

Silica gel, an example of a silicate fire retardant, offers benefits such as good water retention, cooling ability, non-toxicity, thermal and chemical stability and low cost.[11–13] Silica gel can be used in inorganic and organic forms, with each having its advantages and drawbacks. Inorganic silica gel is inexpensive but has poor water absorption, while organic polymer gels offer excellent moisture retention and durability against heat but are expensive.[14] In the field of fire protection, gel-based fire-retardant materials are commonly used in coal mines but are not often utilized for wood fire protection.[15–18] Xue *et al*. have explored the use of gel-stabilized foam, created using water glass and sodium bicarbonate, to extinguish coal mine fires.[19] However, the water retention of this foam has not been extensively studied. Fan *et al*.[13] have modified water glass gels with polymers to produce plastic gels with improved water absorption and thermal resistance. The outcomes demonstrated that the plastogel, with improved water retention, cools the coal body and prevents its oxidative breakdown. Additionally, silica foam has been developed to adhere to the surface of solid combustible objects, providing a strong fire-retardant effect, although its rapid self-hardening time limits its practical application.[20,21] To enhance wood's resistance to leaching and fire, Zhu *et al*. added nanosilica sol to fire retardants containing phosphorus.[22] Despite these advancements, the flame-retardant mechanisms of these materials, including cooling, shielding and insulating, require further investigation.

In this study, considering the chemical stability of polyacrylamide (HPAM), its non-reactivity with the substances separated during the gelation process and its stability against pH and temperature variations, HPAM was chosen to be added to silica gel prepared with aluminum citrate and water glass solution to investigate its impact on water retention. Sodium polyacrylate molecules can

interweave into the silicate hydrogel through intermolecular interactions, forming an inorganic–organic interpenetrating network gel system. Various analytical approaches were used to examine the flame-retardant mechanism of silica gel, including analysis of elemental composition, functional groups and silica gel treated with wood components. The combustion morphology and mass loss of silica gel-treated wood were also examined to understand its macroscopic mechanism.

EXPERIMENTAL

Preparation of materials

Anionic polyacrylamide (HPAM, Shanghai Bidet Medical Technology Co., ltd., China), gluconate-delta-lactone (GDL, Sahn Chemical Technology Shanghai Co., ltd., China), aluminum citrate (AlCit, Beijing Enokai Technology Co., ltd., China), inorganic salt sodium silicate solution (Sahn Chemical Technology Shanghai Co., ltd., China), sodium bicarbonate (McLean Reagent Chemistry Co., ltd., Shanghai, China) and deionized water mixed reaction made up the majority of the silica gel used in this study.

In Table I, one can see the ratios of different ingredients required to make silica gel for the tests.

TABLE I. Quantities of HPAM and GDL for the synthesis of silica gels (m(AlCit) = 1.0 g, m(Na$_2$SiO$_3$) = 8.0 g, m(NaHCO$_3$) = 4.0 g and m(deionized water) = 87g)

No.	GDL, g	HPAM, g
1	0.1	0.2
2	0.1	0.4
3	0.1	0.6
4	0.1	0.8
5	0.2	0.2
6	0.2	0.4
7	0.2	0.6
8	0.2	0.8
9	0.3	0.2
10	0.3	0.4
11	0.3	0.6
12	0.3	0.8

The process of preparing silica gel is outlined as follows: HPAM solutions were mixed with GDL (0.1, 0.2 and 0.3 wt. %) and AlCit (1.0 wt. %) at different concentrations (0.2, 0.4, 0.6 and 0.8 wt. %). Sodium silicate and sodium bicarbonate concentrations of 8 and 4 wt. %, respectively, were chosen based on previous studies on silica gel gelation.[23] The solution was stirred using a magnetic stirrer to ensure homogeneity. Sodium silicate was then added to the mixture to initiate the gelation process. The synthesized silica gel was vacuum-dried at 100 °C to remove excess water.

Characterizations and calculation

The water retention capacity of the silica gel was determined by placing the gel in a 100 °C oven and weighing it hourly over a 12-h period. This process was repeated for each sample

set, with the changes in mass being monitored hourly. The average water retention capacity was then calculated based on these measurements.

The following formula can be used to determine the water retention capacity of silica gel:[24]

$$W = 100 \frac{M_1 - M_2}{M_1} \tag{1}$$

where W is the water retention percentage of silica gel, M_1 is the initial weight of silica gel and M_2 is the gel weight after every hour of drying.

XPS was used to analyze surface elements and their chemical states. The experiment used a homogeneous AlKα X-ray source at 1486.6 eV, with working pressure and analysis chamber vacuum levels set at 10^{-9} mbar and 5×10^{-7} Pa, respectively.

XRD diffractometer analyzed phase proportion, with a range of 5 to 90° (2θ), step size of 0.02° and settings of 40 kV, 40 mA and 5 °/min scanning speed.

Wood@gel samples were prepared by mixing silica gel with 100–200 mesh wood.[19] Firstly, selected pine wood measuring 1 cm×1 cm×10 cm was dried in a vacuum drying oven at 70 °C for 12 h. The dried wood was then submerged in silica gel for ten minutes to enhance its fire resistance. For fire resistance testing, the samples were burned for one minute under the flame of an alcohol lamp. The percentage of weight loss was calculated to assess the fire resistance.

Tensor 37 infrared spectrometer was used to analyze functional group differences, with a scan range of 400 to 4000 cm^{-1} and an estimated accuracy of 4 cm^{-1}.

The Mettler simultaneous thermal analyzer measured dimensions during degradation. TGA applied 20 ml/min of air, heating from 30 to 800 °C at 10.0 °C/min using a 10.0±0.5 mg sample in a 70 μL alumina crucible.

The total weight loss percentage (W) is calculated according to Eq. (1), with M_1 and M_2 representing the sample's mass before and after the combustion test, respectively.

<div align="center">RESULTS AND DISCUSSION</div>

Principles of silica gel generation

Silicic acid was created by the progressive combining of H$^+$ with the ions that were negative in the sodium silicate solution and by adding NaHCO$_3$. The silicic acids polymerize with each other, as shown in Fig. 1a, to form polysilicic acid, which then transforms into silica gel with a spatially organized structure consisting of Si–O–Si linkages. During silica gel formation, intermolecular interactions between HPAM molecules and Si–O bonds can lead to the formation of a gel system with an organic–inorganic interpenetrating mesh structure (Fig. 1b). This increases the tensile strength of the silica gel. Additionally, the –COO– group of HPAM can coordinate with the polynucleated hydroxyl-bridged composite ions created by aluminum (Fig. 1b), which helps to form a strong network structure in the system and enhances the ability of silica gel to retain water.[17]

Water retention rate

Figs. 2a–c indicate that silica gels, prepared with a 0.4 wt% concentration of HPAM, demonstrated the highest water retention capacity when varying concen-
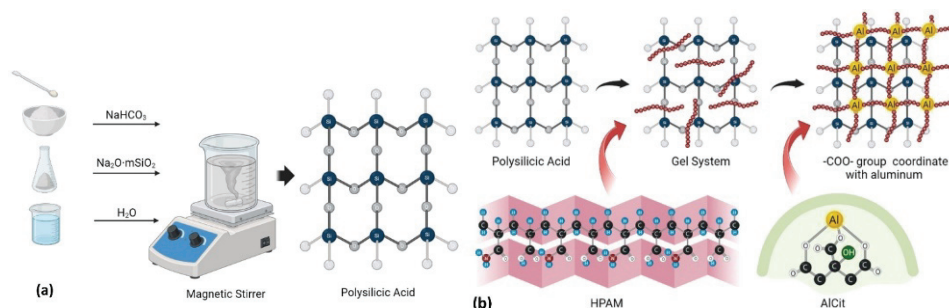
Fig. 1. The principle of silica gel generation: a) formation and structure of polysilicic acid; b) structural formation process of multinuclear hydroxyl-bridged composite ionic coordination networks.

trations of GDL (0.1, 0.2 and 0.3 wt. %) were utilized. Furthermore, at HPAM and GDL concentrations of 0.4 and 0.2 wt. %, respectively, the silica gel exhibited superior water retention as shown in Fig. 2d.
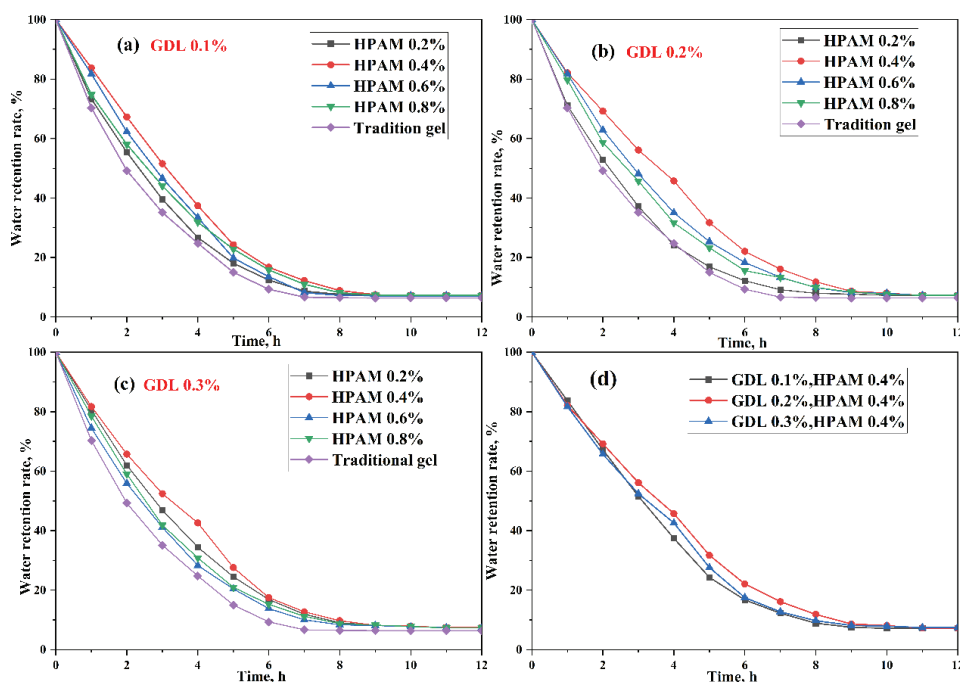
Fig. 2. Variation in silica gel water retention rates through heating time.

HPAM contributes to water retention through its ability to form a three-dimensional network that traps water molecules. At 0.4 wt. %, HPAM provides an optimal balance between viscosity and gel strength, ensuring sufficient network formation without overly increasing the viscosity, which could impede water

mobility within the gel. GDL acts as a gelling agent and pH adjuster. At 0.2 wt. %, GDL hydrolyzes to gluconic acid, gradually lowering the pH and facilitating the gelation process by promoting the cross-linking of HPAM chains. This concentration of GDL ensures a controlled and gradual gelation process, leading to a stable gel network.

The active hydrolysis and deprotonation of some $-CONH_2$ and $-COOH$ groups in HPAM result in increased electrostatic repulsion and elongation of the polymer chain. The hydrolysis of HPAM converts amide groups ($-CONH_2$) to carboxylic acid groups ($-COOH$), while deprotonation removes H^+ from carboxylic acid groups, forming carboxylate anions ($-COO-$). $-COO-$ forms strong hydrogen bonds with water, enhancing the stability of the polymer chain contacts. Therefore, the addition of the appropriate amount of HPAM contributes to the silica gel's excellent water retention properties.

XPS analysis

The sample with the best water retention (HPAM and GDL concentration of 0.4 and 0.2 wt. %) was analyzed using XPS. The results are displayed in Fig. 3a, revealing the composition of silica gel in terms of 1s and 2p electronic states. The 1s orbitals include O, Na and C, while Si and Al are present in the 2p orbitals. The Si 2p peak at 103.08 eV indicates that Si exists in the form of silica in the solution.

The C 1s spectrum of silica gel, illustrated in Fig. 3b, displays peaks corresponding to various groups. The spectrum shows an overlap of peaks for C–C and C–H, with the highest peak representing C–O, followed by C=O and O=C–O. Previous studies have indicated that hydrophilic functional groups such as C–O and C=O, as well as hydrophobic functional groups like C–C and C–H, are the primary functional groups in silica gel.[25] With 97 % or more of its functional groups being hydrophilic, the gel exhibits high hydrophilicity, enhancing its fire prevention effectiveness. The 97 % hydrophilic content was determined through XPS analysis of the C 1s spectrum. By integrating the peak areas for hydrophilic (C–O, C=O, O=C–O) and hydrophobic (C–C, C–H) groups, it was found that hydrophilic groups accounted for 97 % or more of the total peak area, indicating the gel's predominant hydrophilicity.

XRD analysis

Fig. 3c depicts the results of the X-ray diffraction analysis of the silica gel, with a broad peak at 22° indicating its typical amorphous state, consistent with the JCPDS phase identification card (PDF#27-0605).[26,27]

Studies have shown that when silica gel is exposed to humid air, the hydroxyl groups of water molecules react with silica particles on its outermost layer, producing Si–OH groups.[28] The surface of SiO_2 has a high affinity for water

molecules due to the hydrophilic nature of hydroxyl groups. Additionally, the substantial surface area and small pores of silica facilitate the coverage of the entire outer layer by water molecules.[29] Consequently, the water present in silica gel is a combination of chemically and physically adsorbed water.
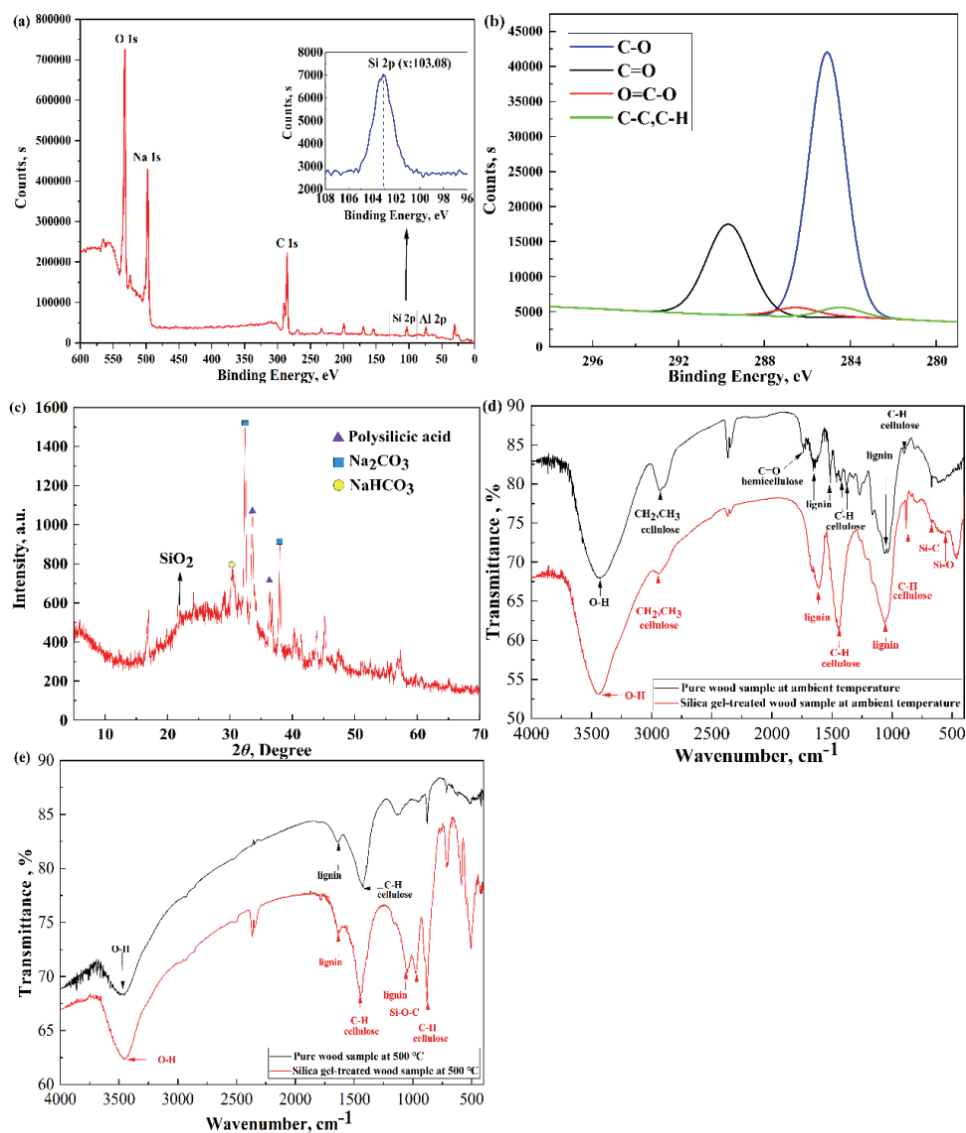

Fig. 3. Characterization of the microstructure of the samples: a) XPS wide energy scan spectrum of silica gel; b) C 1s XPS curve of silica gel; c) XRD graph of silica gel; d) FTIR testing of pure wood sample and silica gel-treated wood sample at ambient temperature; e) FTIR testing of pure wood sample and silica gel-treated wood sample at 500 °C.

Furthermore, Fig. 3c reveals the presence of polysilicic acid (PDF#27-0606) and Na_2CO_3 (PDF#08-0448) in the produced silica gel. The presence of Na_2CO_3 indicates the polymerization and reaction mechanism of silica gel discussed earlier in the preparative synthesis section. In this process, H^+ in the $NaHCO_3$ (PDF#15-0700) solution is absorbed by sodium silicate to produce polysilicate and sodium carbonate. Polysilicate helps the wood surface form a heat-stabilizing layer at high temperatures, thereby enhancing the wood's fire resistance. Therefore, silica gel is considered an effective fire retardant due to its ability to form such a protective layer:

$$SiO_3^{2-} + HCO_3^- \rightarrow nSiO_2 + H_2O + CO_3^{2-} \qquad (2)$$

FTIR analysis

Hemicellulose, cellulose and lignin are the primary components of wood.[30] There are four sets of experimental samples: unignited natural wood, unignited natural wood treated with silica gel, wood ignited by a 500 °C heat source and wood treated with silica gel and then ignited by a 500 °C heat source. Fig. 3d shows the FTIR spectrum of unignited natural wood and unignited natural wood treated with silica gel. In the spectrum of unignited natural wood, the peaks at 2930 cm^{-1} correspond to CH_2 and CH_3 groups. The C–H groups are distributed in three peaks at 1427, 1378 and 898 cm^{-1}, which are the main absorption peaks associated with cellulose. The peak at 1738 cm^{-1} indicates the C=O stretching vibration, characteristic of hemicellulose. The three major absorption peaks of lignin are observed at 1634, 1510 and 1053 cm^{-1}, representing the vibrations of the C–O stretching bond.

In comparison, the FTIR spectrum of the silica gel–treated wood shows additional peaks at 553 and 669 cm^{-1}. The peak at 553 cm^{-1} indicates the presence of silica gel in the wood, while the peak at 669 cm^{-1} corresponds to the Si–C stretching vibration, suggesting a chemical connection between silica gel and wood components. These additional peaks are not present in the untreated wood spectrum. The presence of Si–O and Si–C bonds in the treated wood leads to the formation of thick, highly heated charred layers, acting as a barrier that retards the burning process by limiting the dispersion of flammable volatile components and heat transfer.[31]

Fig. 3e displays the FTIR results of wood samples ignited by a 500 °C heat source, including the both untreated and silica gel-treated samples. In the spectrum of untreated wood ignited at 500 °C, only the 1427 cm^{-1} cellulose absorption peak remains, while the peaks of hemicellulose and lignin vanish or are reduced. This indicates that lignin pyrolysis is essentially complete at 500 °C, with the system continuing to pyrolyze and deoxygenate, forming charcoal progressively.

In comparison, the FTIR spectrum of the silica gel-treated wood heated at 500 °C shows that the cellulose retains an absorption peak at 898 cm^{-1}, demon-

strating improved thermal resilience. The lignin peak at 1510 cm^{-1} is only partially lost and new peaks at 715 and 976 cm^{-1}, characteristic of the Si–C and the Si–O–C bonds, respectively. In addition to the Si–O and the Si–C bonds described above, the thermal stability of Si–O–C has been also demonstrated in the literature.[32] Hence, the presence of these bonds indicates the formation of charred layers at high temperatures, effectively halting the decomposition and burning of wood. Therefore, silica gel exhibits excellent fire-retardant properties, as the treated wood still contains cellulose and lignin that are not completely broken down 500 ℃.

TGA-DTG analysis

To evaluate the thermal resistance, charring prospects and decomposition rate of wood, TGA analysis can be employed. TGA analysis was conducted to investigate the thermal stability, charring ability and degradation rate of wood, silica gel and wood@gel in an air atmosphere (Fig. 4). The thermogravimetric (TG) and differential thermogravimetric (DTG) analyses in Fig. 4 reveal three phases in the thermal degradation of wood. The initial stage (30–130 ℃) involves the evaporation of water molecules, causing a 6 % mass loss. In the second charring stage (160–360 ℃, peak at 317 ℃), the weight decreases significantly from 94 to 33 % as hemicellulose and cellulose decompose into char residues, releasing CO_2, CO, CH_4, CH_3OH and C_2H_5OH.[2] The third stage (360–500 ℃, peak at 437 ℃) involves calcination, with a residual percentage of 4.9 % due to the decomposition of lignin and oxidation of char residue from the second stage.[33]

The wood@gel sample exhibits a 5 % mass loss in the first stage (30–130 ℃) due to water evaporation. In the second stage (130–500 ℃), wood@gel shows a high residual carbon rate of 56 %, attributed to the oxidized breakdown of cellulose and hemicellulose. Compared to pure wood, wood@gel loses weight more slowly in this phase, indicating the protective effect of silica gel. The maximal breakdown temperature of wood@gel in the second stage is 263 ℃, according to the DTG curve (Fig. 4b) and the third stage breakdown can reach 580 ℃, suggesting silica gel's involvement in wood decomposition. In contrast, the dehydration of surface Si–OH groups on silica gel is principally responsible for the third stage mass loss of wood@gel, which results in a residual carbon rate that is 41 % greater than that of pure wood. The preservation of cellulose and delay of pyrolysis reaction in wood are attributed to the charred layer produced by silica gel during combustion, as noted by Rowell, Miyafuji and Saka, which obstructs blazing and smoldering combustion by limiting oxygen and combustible product access.[34,35]

The flame-retardant mechanism of wood@gel involves the formation of multi-coordination organosilicon compounds with polyhydroxy cellulose at high temperatures, hindering thermal movement between cellulose macromolecular

chains, reducing the pyrolysis rate and enhancing thermal stability.[36] Additionally, the creation of a protective carbonized layer with Si–O, Si–O–C and Si–C linkages between the silicon-containing compound and wood improves thermal stability.
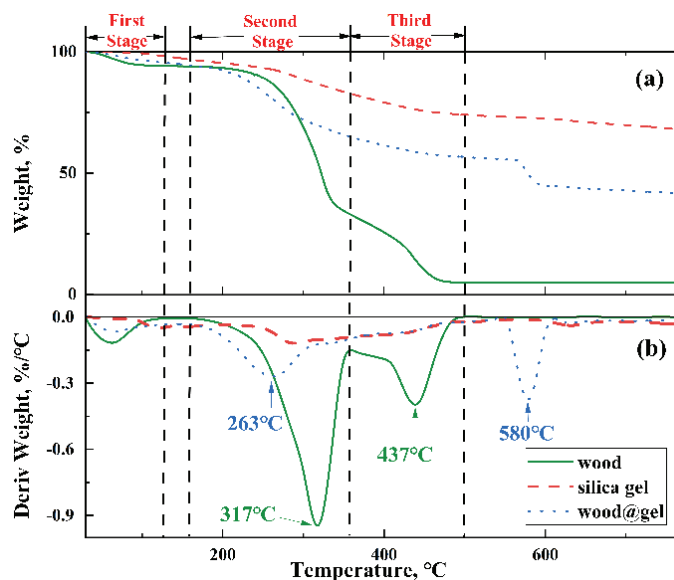
Fig. 4. Wood, silica gel and wood@gel samples' TG (a) and DTG (b).

Fire resistance analysis

Using natural wood (sample 1#) and wood treated with silica gel (sample 2#), we investigated silica gel's ability to delay flames on wood. Both samples were exposed to the flame of an alcohol lamp as described in the fire resistance analysis section. The results depicted in Fig. 5 indicate that sample 1# ignited after 6 seconds and even though the alcohol lamp was removed after 60 s, it took 197 s for the flame to extinguish. This prolonged burning was mainly due to the complete decomposition of the active ingredients present in wood, such as cellulose, hemicellulose and other wood elements. Conversely, under the same flame conditions, sample 2# did not exhibit any combustion phenomena for 60 s after ignition, as shown in Fig. 5. The presence of silica gel on the wood's surface led to the development of a protective charred coating that effectively prevented further burning.

Table II presents the mass loss of samples before and after combustion. Samples 1# and 2# experienced total mass losses of 76 and 23 %, respectively. The addition of silica gel reduced the mass loss rate by 70 % in sample 2#, attributed to the formation of a protective layer via Si–O, Si–O–C and Si–C linkages on its external layer during burning. This coating enhances the wood's fire resistance.
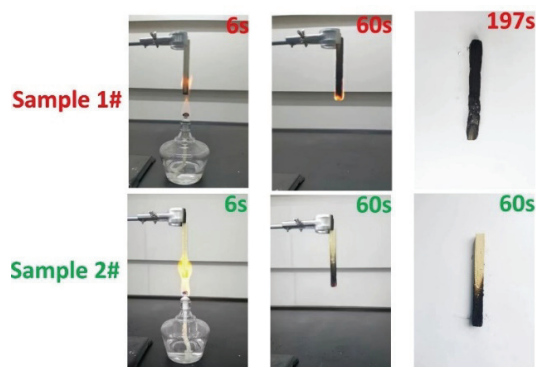
Fig. 5. Experiment testing the resistance to fire.

TABLE II. Burning mass reduction velocity at the fire resistance test

Sample	1#			2#		
Pre-burning, g	4.72	4.84	4.80	4.95	4.97	4.99
Post-burning, g	1.10	1.24	1.09	3.90	3.73	3.84
Mass loss rate, %	76.69	74.38	77.29	21.21	24.95	23.05
Average mass loss rate, %		76.12			23.07	

CONCLUSION

In this investigation, various ratios of HPAM and GDL were utilized to assess the water retention and flame-retardant properties of silica gel on wood. Maximum water retention was observed at 0.4 wt. % HPAM and 0.2 wt. % GDL. To better understand these properties, we conducted combustion experiments and microscopic mechanism studies.

The combustion experiments show that silica gel forms a barrier that isolates oxygen and heat from reaching the wood surface. Additionally, silicon increases the thermal stability of the carbon layer during the wood carbonization process, acting as a flame retardant. Microscopic mechanism studies show that hydrophilic groups C–O and C=O on the surface of silica gel contribute to its excellent hydrophilicity. After the wood combustion, the formation of Si–O, Si–O–C and Si–C bonds on the surface increases the thermal stability of the carbon layer, revealing the flame-retardant mechanism of the carbon layer. The results demonstrated silica gel reduces mass loss in treated wood at high temperatures by 36 % (TG analysis) and 53 % (fire resistance testing) respectively, showing its efficacy as a fire retardant.

И З В О Д

ПОВЕЋАЊЕ ОТПОРНОСТИ ДРВЕТА НА САГОРЕВАЊЕ ПОМОЋУ СИЛИКА ГЕЛА СА ВЕЛИКИМ ЗАДРЖАВАЊЕМ ВОДЕ: ОБЕЋАВАЈУЋЕ РЕШЕЊЕ ЗА УСПОРАВАЊЕ САГОРЕВАЊА

ZHONGBIN FEI, YINGNAN ZHANG, ZHI WANG, YILING DUAN и BIN ZHANG

International Center for Chemical Process Safety, Nanjing Tech University, Nanjing, 211816, China

У овом раду је испитивано задржавање воде и могућност успоравања сагоревања силика гела припремљеног коришћењем анјонског полиакриламида (HPAM), глуконат--делта-лактона (GDL) и алуминијум-цитрата (AlCit). Узорци силика гела су синтетисани коришћењем натријум-силиката (8 mas. %), натријум-хидрогенкарбоната (4 mas. %) и различитих количина HPAM (0,2–0,8 mas. %) и GDL (0,1–0,3 mas. %). Гелови су окарактерисани следећим техникама: XPS, XRD, FTIR и TGA. Оптимално задржавање воде је постигнуто при 0,4 mas. % HPAM и 0,2 mas % GDL. Овај гел садржи, у поређењу са традиционалним геловима, више површинске воде захваљујући већем броју хидрофилних група и аморфној природи. На високим температурама силика гел формира слој са угљеником који настаје сагоревањем дрвета, спречавајући продирање кисеоника, што минимизира даље сагоревање. Након сагоревања на 500 °C, губитак масе дрвета третираног силика гелом је 36–53 % мањи у поређењу са нетретираним дрветом, што указује на ефикасност силика гела у спречавању даљег сагоревања.

REFERENCES

1. T. Farid, M. I. Rafiq, A. Ali, W. Tang, *EcoMat* **4** (2022) e12154 (https://doi.org/10.1002/eom2.12154)
2. S. He, W. Wu, M. Zhang, H. Qu, J. Xu, *J. Therm. Anal. Calorim.* **128** (2017) 825 (https://doi.org/10.1007/s10973-016-5947-z)
3. E. Baysal, M. K. Yalinkilic, M. Altinok, A. Sonmez, H. Peker, M. Colak, *Constr. Build. Mater.* **21** (2007) 1879 (https://doi.org/10.1016/j.conbuildmat.2006.05.026)
4. I. Ratajczak, B. Mazela, *Holz Als Roh Werkst.* **65** (2007) 231 (https://doi.org/10.1007/s00107-006-0154-4)
5. Q. Fu, D. S. Argyropoulos, D. C. Tilotta, L. A. Lucia, *J. Anal. Appl. Pyrolysis* **81** (2008) 60 (https://doi.org/10.1016/j.jaap.2007.08.003)
6. H. Yamaguchi, *Wood Sci. Technol.* **36** (2002) 399 (https://doi.org/10.1007/s00226-002-0149-1)
7. A. M. Pereyra, C. A. Giudice, *Fire Saf. J.* **44** (2009) 497 (https://doi.org/10.1016/j.firesaf.2008.10.004)
8. G. Canosa, P. V. Alfieri, C. A. Giudice, *J. Fire Sci.* **29** (2011) 431 (https://doi.org/10.1177/0734904111404652)
9. S. Nami Kartal, W. J. Hwang, A. Yamamoto, M. Tanaka, K. Matsumura, Y. Imamura, *Int. Biodeterior. Biodegrad.* **60** (2007) 189 (https://doi.org/10.1016/j.ibiod.2007.03.002)
10. S. Hribernik, M. S. Smole, K. S. Kleinschek, M. Bele, J. Jamnik, M. Gaberscek, *Polym. Degrad. Stabil.* **92** (2007) 1957 (https://doi.org/10.1016/j.polymdegradstab.2007.08.010)
11. S. G. Hu, S. Xue, *J. Coal Sci. Eng. China* **17** (2011) 256 (https://doi.org/10.1007/s12404-011-0306-y)
12. M. Wu, Y. Liang, Y. Zhao, W. Wang, X. Hu, F. Tian, Z. He, Y. Li, T. Liu, *Colloids Surfacs,. A* **629** (2021) 127443 (https://doi.org/10.1016/j.colsurfa.2021.127443)

13. Y. Fan, Y. Zhao, X. Hu, M. Wu, D. Xue, *Fuel* **263** (2020) 116693 (https://doi.org/10.1016/j.fuel.2019.116693)
14. S. Hu, S. Xue, *J. Coal. Sci. Eng. China* **17** (2011) 256 (https://doi.org/10.1007/s12404-011-0306-y)
15. B. Qin, G. Dou, Y. W, H. Wang, L. Ma, D. Wang, *Fuel* **190** (2017) 129-135 (https://doi.org/10.1016/j.fuel.2016.11.045)
16. P. Qian, Z. Qin, H. Guo, C. Geng, N. Yan, X. Cui, *Ind. Saf. Environ. Prot.* **38** (2012) 13 (https://caod.oriprobe.com/articles/30918095/ Sodium_Silicate_polyelectrolyte_Composite_Gel_Mate.htm)
17. X. Ren, X. Hu, D. Xue, Y. Li, Z. Shao, H. Dong, W. Cheng, Y. Zhao, L. Xin, W. Lu, *J. Hazard. Mater.* **371** (2019) 643 (https://doi.org/10.1016/j.jhazmat.2019.03.041)
18. K. Wang, W. Lu, Y. Du, Q. Zhang, J. Xu, *Min. Saf. Environ. Prot.* **43** (2016) 8 (http://www.cnki.net/kcms/detail/50.1062.TD.20160202.1908.006.html)
19. D. Xue, X. Hu, W. Cheng, J. Wei, Y. Zhao, L. Shen, *Fuel* **264** (2020) 116903 (https://doi.org/10.1016/j.fuel.2019.116903)
20. D. S. Kuprin, *J. Sol-Gel Sci. Technol.* **81** (2017) 36 (https://doi.org/10.1007/s10971-016-4285-8)
21. A. V. Vinogradov, D. S. Kuprin, I. M. Abduragimov, G. N. Kuprin, E. Serebriyakov, V. V. Vinogradov, *ACS Appl. Mater. Interfaces* **8** (2016) 294 (https://doi.org/10.1021/acsami.5b08653)
22. X. Zhu, Y. Wu, C. Tian, Y. Qing, C. Yao, *J. Nanomater.* **2014** (2014) 1 (https://doi.org/10.1155/2014/867106)
23. Y. Zhang, M. Jing, M. Zhang, S. Hou, B. Zhang, *Fire Technol.* **58** (2022) 3597 (https://doi.org/10.1007/s10694-022-01334-y)
24. Y. Liu, M. Wang, S. Zhao, Y. Liu, J. Yang, *J. Shandong Univ. Sci. Technol.(Nat. Sci.)* **37** (2018) 26 (https://kns.cnki.net/kcms/detail/37.1357.N.20180509.1327.012.html)
25. W. Xia, J. Yang, C. Liang, *Appl. Surf. Sci.* **293** (2014) 293 (https://doi.org/10.1016/j.apsusc.2013.12.151)
26. M. A. Abou Rida, F. Harb, *J. Met. Mater. Miner.* **24** (2014) 37 (https://www.jmmm.material.chula.ac.th/index.php/jmmm/article/view/108)
27. S. He, Y. Huang, G. Chen, M. Feng, H. Dai, B. Yuan, X. Chen, *J. Hazard. Mater.* **362** (2019) 294 (https://doi.org/10.1016/j.jhazmat.2018.08.087)
28. R. L. DeRosa, P. A. Schader, J. E. Shelby, *J. Non-Cryst. Solids* **331** (2003) 32 (https://doi.org/10.1016/j.jnoncrysol.2003.08.078)
29. X. Chen, G. Zhu, J. Wang, Q. Chen, *Bull. Chin. Ceram. Soc.* **36** (2017) 4044 (http://gsytb.jtxb.cn/EN/Y2017/V36/I12/4044)
30. D. C. O. Marney, L. J. Russell, R. Mann, *Fire Mater.* **32** (2008) 357 (https://doi.org/10.1002/fam.973)
31. Y. Zhang, M. Jing, M. Zhang, S. Hou, Y. Gong, J. Jiang, B. Zhang, *Silicon* **14** (2022) 12633 (https://doi.org/10.1007/s12633-022-01975-2)
32. Y. Yang, CN 107805447 A (2017)
33. M. Uddin, K. Kiviranta, S. Suvanto, L. Alvila, J. Leskinen, R. Lappalainen, A. Haapala, *Fire Saf. J.* **112** (2020) 102943 (https://doi.org/10.1016/j.firesaf.2019.102943)
34. R. M. Rowell, *The chemistry of solid wood*, American Chemical Society, Washington, DC, 1984, pp. 531–574 (https://doi.org/10.1021/ba-1984-0207)
35. H. Miyafuji, S. Saka, *J. Wood Sci.* **47** (2001) 483 (https://doi.org/10.1007/BF00767902)
36. D. H. Blount, US 4380592 A (1983).

Efficiency of physical–chemical treatment of wastewater of the paper and cardboard factory

LARYSA SABLII[1], OLEKSANDR OBODOVYCH[2] and VITALII SYDORENKO[2]*

[1]*Department of Bioenergy, Bioinformatics and Environmental biotechnology, National Technical University of Ukraine "Igor Sikorsky Kyiv Polytechnic Institute", Prospect Beresteiskyi 37, 03056, Kyiv, Ukraine and* [2]*Department of Heat and Mass Transfer in Disperse Systems, Institute of Engineering Thermophysics of NAS of Ukraine, Akademika Bulakhovskoho 2, 03164 Kyiv, Ukraine*

Abstract: The purpose of the work is to study the wastewater treatment of a cardboard and paper factory in the Khmelnytskyi region using physicochemical methods, namely coagulation and oxidation, to increase the efficiency of removing organic pollutants according to *COD* and *BOD* indicators. The use of coagulation and chlorination methods, before biological treatment in aeration tanks, was proposed. Alumofloc 18 % was used as a coagulant, PAA was used as a flocculant and sodium hydroxide was used as an alkalizing reagent. The study was conducted on a mixture of industrial and sewage wastewater with *COD* and BOD_5 – 3200 and 1575 mg L^{-1}, respectively, and on industrial wastewater with *COD* and BOD_5 – 4480 and 1960 mg L^{-1}, respectively. The effects of reducing *COD* and BOD_5 indicators in the first case after coagulation were 30 and 40 %, after chlorination – 37.82 and 43.18 %, respectively, and in the second after coagulation – 28.58 and 47.25 %, respectively. The effects of wastewater treatment of a cardboard and paper factory using coagulation and oxidation methods will allow for a reduction in the concentration of organic substances according to *COD* and *BOD* indicators before the biological treatment of wastewater in aeration tanks and also will ensure an increase in the efficiency of biological treatment.

Keywords: liquid waste; organic pollutants; coagulation; alumofloc; chlorination.

INTRODUCTION

Wastewater from cardboard and paper factories cause great damage to environment and water body. Such waters are a stable colloidal system. Organic substances presented in wastewater cause complex changes in water bodies.[1] They disrupt the established abiotic factors and are involved in chemical and

---

biochemical processes. As a result, non-negotiable changes occur in the composition of biocenoses and the river water quality decreases significantly. Wastewater contains cellulose fibers, paper, fillers, dyes, latexes, emulsions, adhesives, *etc*. They have a high content of suspended solids and organic substances, as well as specific smell. Sources of organic substances are products of cellulose destruction, formed during bleaching and processing. These are substances such as aliphatic (alcohols, amines, acids, aldehydes, *etc*.) and terpene hydrocarbons, aromatic hydrocarbons of the phenolic series, low molecular weight alcohols, fatty acids, *etc*.[2] Due to the significant content of organic substances, wastewater is characterized by high *COD* values ranging from 800 to 2000 mg L^{-1} and *BOD*$_5$ values are within 500–800 mg L^{-1}. The *BOD*$_5$/*COD* ratio has average values, which indicate the possibility of applying a biological method of wastewater treatment. *BOD*$_5$/*COD* has a value in the range from 0.2 to 0.7. Suspended solids range from 900 to 3000 mg L^{-1}. Therefore, factory wastewater requires mechanical pretreatment, as a result of which coarse and suspended solids and some colloidal particles are removed.[3] The presence of low concentrations of phosphorus and nitrogen compounds in wastewater indicates that they should be added to water for biological processes.

Today, the most widespread methods of wastewater treatment in cardboard and paper factories are physico-chemical, namely reagent treatment, coagulation, flocculation, chemical, electrochemical oxidation[4] and biological. The use of reagent methods requires the purchase of chemical reagents, namely coagulants based on iron, aluminum, expensive flocculants or strong oxidizers as ozone[5,6] or hydrogen peroxide (Fenton method),[4] which does not ensure high purification efficiency in conditions of multicomponent pollution. Adsorption methods[7] can be used for wastewater treatment but require sophisticated equipment.

The most accessible and effective both from the point of view of high efficiency of the treatment, low costs for construction and operation and the impact on the environment and natural water bodies is the biological method,[8–11] namely the aerobic[12,13] and anaerobic[14–20] methods.

At a cardboard and paper factory in the Khmelnytskyi region, wastewater is treated at a wastewater treatment plant, which includes grit traps, primary radial sedimentation tanks, aeration tanks with activated sludge regenerators, secondary radial sedimentation tanks and bioponds (Fig. 1).

The productivity of the treatment plant is 7000 m^3 per day. Aeration tanks are designed for 14 h of aeration and 12 h of regeneration. The main drawback of the treatment plant is the insufficient efficiency of wastewater treatment from organic pollutants according to *COD* and *BOD* indicators, which necessitated research to find and use methods of pretreatment of factory wastewater using physical and chemical treatment.
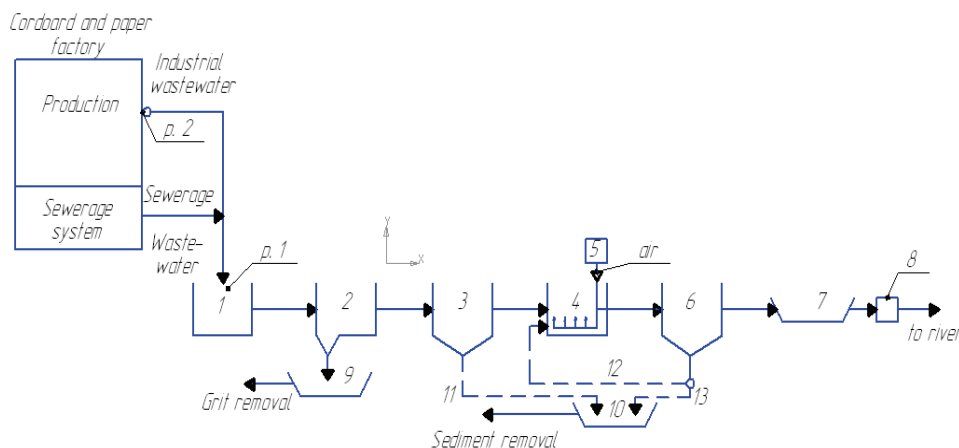
Fig. 1. Block diagram of waste water removal and treatment of cardboard and paper factory: 1 – Inlet chamber; 2 – grit traps; 3 – primary sedimentation tanks; 4 – aeration tanks; 5 – air blower; 6 – secondary sedimentation tanks; 7 – biopounds; 8 – disinfection; 9 – grit beds; 10 – sludge beds; 11 – sediment; 12 – recirculated activated sludge; 13 – surplus activated sludge. p.1 – sampling site of the mixture of industrial and sewerage wastewater from the inlet chamber; p.2 – sampling site of industrial wastewater in the well at the outlet of industrial wastewater from the workshop.

The purpose of the work is to study the wastewater treatment of a cardboard and paper factory using physicochemical methods, namely, coagulation and oxidation, for increasing the efficiency of removing organic pollutants according to *COD* and *BOD* indicators.

EXPERIMENTAL

A series of samples of the following wastewater were selected for analysis:

1) a mixture of industrial and sewage wastewater from the inlet chamber of the wastewater treatment plant of the cardboard and paper factory (Table I);

2) wastewater directly from production (Table II).

Samples were taken at points p.1 and p.2, shown in the block diagram shown in Fig. 1. Coagulation and chlorination of samples were carried out in laboratory conditions. Samples were taken at the indicated points three times: at 9 a.m., 2 p.m. and 7 p.m.

The analysis results of the samples taken at sampling site p.1 and p.2 were averaged according to the indicators. The average values are shown in the Tables I and II. In the first case (Table I), the following indicators were determined: pH, suspended solids, *COD*, BOD_5 of untreated wastewater, water after coagulation, as well as chlorinated coagulated water. In the second case (Table II), the same indicators were determined for the untreated and water after coagulation.

Reagents with the following doses were used for the study for coagulation: alumofloc 18 % – 0.6 mL L^{-1}; sodium hydroxide – 55 mg L^{-1} and PAA flocculant – 2 mg L^{-1}. The volume of sediment after coagulation and settling for 2 h was 20 %.

For chlorination active chlorine – 42 mg L^{-1} was used. The duration of settling after coagulation and chlorination was 2 h. Coagulation was successful in both cases. In the water

obtained after settling, in the first case suspended solids decreased from 127 to 15 mg L^{-1} and in the second – from 162 to 20 mg L^{-1}. The results of the conducted analyses according to average values are summarized in Tables I and II.

The dissolved oxygen concentration in both cases was close to zero (0–0.1 mg L^{-1}), so the oxidation of water impurities with the participation of dissolved oxygen was not considered.

The error, of the results of experimental measurements, was not higher than 5 %.

To increase the efficiency of removing pollutants from wastewater of a cardboard and paper factory during primary sedimentation, it is possible to apply pre-reagent treatment of wastewater with the help of a coagulant, for example alumofloc. This reagent forms colloidal particles of aluminum hydroxide in water, capable of coagulation and forming flakes. Suspended particles (cellulose fibers, paper particles, fillers, *etc*.) colloidal and dissolved organic substances (hydrocarbons, fatty acids, *etc*.) contained in wastewater are adsorbed on the surface of the flakes, thus forming aggregates that settle in sedimentation tanks. As a result of coagulation, the concentration of suspended substances in wastewater and the concentration of organic substances according to *COD* and *BOD*$_5$ indicators are reduced to a greater extent than with simple settling.

In order to increase the efficiency of removal of organic substances from wastewater, the chlorination was used for pretreatment. The action of active chlorine consists in the chemical oxidation of organic substances, which are contained in large quantities in wastewater of the cardboard and paper factory, namely aliphatic (alcohols, amines, acids, aldehydes, ketones, *etc*.) and terpene hydrocarbons, aromatic hydrocarbons of the phenolic series, low molecular weight alcohols, fatty acids, *etc*.

These substances are determined by *COD* and *BOD*$_5$ indicators. Moreover, most of these substances are difficult to oxidize biologically (during wastewater treatment in aeration tanks), so pretreatment is needed.

The purpose of oxidation is to decompose hard-to-oxidize substances into biodegradable substances for microorganisms in the biological treatment. When oxidized with chlorine, simpler compounds are formed. For example, acids or ketones are formed when alcohols are oxidized and acids are formed when aldehydes are oxidized. The formed reaction products are biologically degradable with the participation of active sludge of aeration tanks, which increases the efficiency of biological wastewater treatment. For example, when ketones are oxidized with chlorine, mixtures of organic acids are formed, which are easily decomposed by activated sludge microorganisms.

When ketones are oxidized, C–C bonds between the carbon atoms of the carbonyl group and the carbon radical are broken with the formation, for example, of a mixture of formic, acetic, propionic, or other biodegradable acids.

RESULTS AND DISCUSSION

Rows 5 to 10 of Tables I and II show the results of some calculations that characterize the efficiency of wastewater treatment using the applied coagulation and chlorination methods.

Studies of the wastewater treatment in the factory using the coagulation method showed the following.

In a case of an industrial and sewage wastewater mixture (Table I) in the mixture of wastewater from the inlet chamber of the wastewater treatment plant,

after coagulation, BOD_5 decreases by 40 % and COD by 30 %. The BOD_5/COD ratio for the next biological treatment in the aeration tanks of the wastewater treatment plant should be greater than 0.5. In this case, as the results showed, coagulation worsened the ratio from 0.49 to 0.42.

TABLE I. Change in indicators of the mixture of industrial and sewage wastewater of the cardboard and paper factory after coagulation and chlorination

Ser. no	Indicator	Unit	Value		
			Initial	After coagulation	After coagulation and chloration
1	pH	–	6.3	7.1	7.25
2	Suspended solids	mg L^{-1}	127	15	15
3	COD	mgO$_2$ L^{-1}	3200	2240	1990
4	BOD_5	mgO$_2$ L^{-1}	1575	945	895
5	COD/BOD_5 ratio	–	2.03	2.37	2.22
6	BOD_5/COD ratio	–	0.49	0.42	0.45
7	$COD – BOD_5$ ("pure" COD)	mg O$_2$ L^{-1}	1625	1295	1095
8	Decrease of the BOD_5	mg O$_2$ L^{-1}		630 (40 %)	50 (43.18 %)
				680 (43.17 %)[a]	
9	Decrease of the COD	mg O$_2$ L^{-1}		960 (30 %)	250 (37.82 %)
				1210 (37.81 %)[a]	
10	Decrease of "pure" COD	mg O$_2$ L^{-1}		330 (20.3 %)	200 (12.4 %)
				530 (32.62 %)[a]	

[a]Estimated differences in the values of the indicators of the untreated wastewater and water after coagulation and chlorination

The difference between COD and BOD_5 ("pure" COD) is:
$$3200 – 1575 = 1625 \text{ mg O}_2 \text{ L}^{-1};$$
$$2240 – 945 = 1295 \text{ mg O}_2 \text{ L}^{-1}.$$

The difference of "pure" COD of wastewater from the inlet chamber of the wastewater treatment plant before and after coagulation is: $1625 – 1295 = 330$ mg O$_2$ L^{-1}.

The "pure" COD of wastewater (without taking into account its BOD_5) after coagulation decreased by only 330 mg O$_2$ L^{-1} or 20.3 %.

As a result of chlorination, the following indicators were obtained.

After coagulation and chlorination, BOD_5 decreases by 43.18 % and COD – by 37.82 %, in wastewater from the inlet chamber of the wastewater treatment plant. Chlorination (separately, after coagulation) decreased BOD_5 by 3.18 % and COD by 7.82 %.

Chlorination, in comparison with coagulation, additionally reduced BOD_5 by 5.3 % and COD by 11.17 %.

The BOD_5/COD ratio in the case of using coagulation and chlorination decreased from 0.49 to 0.45.

"Pure" COD (minus BOD_5) will be:

$$3200 - 1575 = 1625 \text{ mg O}_2 \text{ L}^{-1};$$
$$2240 - 945 = 1295 \text{ mg O}_2 \text{ L}^{-1};$$
$$1990 - 895 = 1095 \text{ mg O}_2 \text{ L}^{-1}.$$

TABLE II. Change in indicators of industrial wastewater cardboard and paper factory after coagulation

Ser. no	Indicator	Unit	Value	
			Initial	After coagulation
1	pH	–	6.5	7.2
2	Suspended solids	mg L^{-1}	162	20
3	COD	mgO$_2$ L^{-1}	4480	3200
4	BOD_5	mgO$_2$ L^{-1}	1960	1034
5	COD/BOD_5 ratio	–	2.28	3.09
6	BOD_5/COD ratio	–	0.43	0.32
7	$BOD – COD_5$ ("pure" COD)	mg O$_2$ L^{-1}	2520	2166
8	Decrease of the BOD_5	mg O$_2$ L^{-1}	926 (47.25 %)	
9	Decrease of the COD	mg O$_2$ L^{-1}	1280 (28.58 %)	
10	Decrease of the "pure" COD	mg O$_2$ L^{-1}	354 (14.05 %)	

The difference of "pure" COD of wastewater from the inlet chamber of the wastewater treatment plant before and after coagulation and chlorination will be:

$$1625 - 1095 = 530 \text{ mg O}_2 \text{ L}^{-1}.$$

After coagulation and chlorination, the "pure" COD of wastewater (excluding its BOD_5) decreased by only 530 mg O$_2$ L^{-1} or 32.62 %.

The difference between "pure" COD of wastewater from the inlet chamber of the wastewater treatment plant before and after coagulation will be:

$$1625 - 1295 = 330 \text{ mg O}_2 \text{ L}^{-1}.$$

The "pure" COD of wastewater (without taking into account its BOD_5) after coagulation decreased by only 330 mg O$_2$ L^{-1} or by 20.3 %.

The difference between the "pure" COD of wastewater from the inlet chamber of the wastewater treatment plant between coagulated and chlorinated wastewater will be:

$$1295 - 1095 = 200 \text{ mg O}_2 \text{ L}^{-1}.$$

The "pure" COD of wastewater (excluding its BOD_5) between coagulated and chlorinated wastewater decreased by only 200 mg O$_2$ L^{-1} or 12.4 %.

In the case of production wastewater from a cardboard and paper factory (Table II), the BOD_5 indicator after coagulation decreases by 47.25 % and the COD by 28.58 %. In this case, coagulation decreases the BOD_5/COD ratio from 0.43 to 0.32.

"Pure" COD (minus BOD_5) will be:

$$4480 - 1960 = 2520 \text{ mg O}_2 \text{ L}^{-1};$$
$$3200 - 1034 = 2166 \text{ mg O}_2 \text{ L}^{-1}.$$

The difference of "pure" COD of industrial wastewater before and after coagulation will be:

$$2520 - 2166 = 354 \text{ mg O}_2 \text{ L}^{-1}.$$

The "pure" COD (excluding BOD_5) decreased by only 354 mg O$_2$ L^{-1} or 14.05 % after coagulation.

As can be seen from Tables I and II (rows 7 and 8), the coagulation and settling allow a reduction of BOD_5 in the first and second cases by 40 (Table I) and 47.25 % (Table II) and COD by 30 % (Table I) and 28.58 % (Table II), respectively. These indicators indirectly indicate percentages of organic pollutants (according to BOD_5) and the total amount of organic matter (according to COD) that are in wastewater in suspended and colloidal states. At the same time, it is worth noting that coagulation reduces BOD_5 more effectively than COD, which indicates that most of the hard-to-oxidize compounds are dissolved.

CONCLUSION

As a result of studies of the coagulation process for the treatment of wastewater from a cardboard and paper factory, a decrease in the indicators of suspended solids, COD and BOD was obtained.

The BOD_5/COD ratio was less than 0.5 and this must be taken into account when adjusting the composition of wastewater (by changing the ratio of easily and hard-oxidizing substances due to the detection and reduction of chemical components coming from production).

It was determined that 60–70 % of organic substances, according to the COD indicator, are in a dissolved state. During the coagulation of wastewater, the efficiency of purification according to the BOD_5 indicator was determined to be 40–47 %. It has been determined that as a result of chlorination, the maximum reduction of "pure" COD is achieved; therefore, the possibility and expediency of chlorination of water after the secondary settling tank in increased doses, should be considered in the wastewater treatment technology of the cardboard and paper factory.

It should be noted that the use of reagents in the doses adopted in the study is unlikely to be economically justified, but it will be advisable to arrange an oxidizer-biocoagulator in front of the primary settling tank, in which activated sludge is used instead of reagents.

И З В О Д

ЕФИКАСНОСТ ФИЗЧКО-ХЕМИЈСКИХ МЕТОДА У ПРЕЧИШЋАВАЊУ ОТПАДНИХ ВОДА
ФАБРИКЕ КАРТОНА И ПАПИРА

LARYSA SABLII[1], OLEKSANDR OBODOVYCH[2] и VITALII SYDORENKO[2]

¹Department of Bioenergy, Bioinformatics and Environmental biotechnology, National Technical University of Ukraine "Igor Sikorsky Kyiv Polytechnic Institute", Prospect Beresteiskyi 37, 03056, Kyiv, Ukraine и ²Department of Heat and Mass Transfer in Disperse Systems, Institute of Engineering Thermophysics of NAS of Ukraine, Akademika Bulakhovskoho 2, 03164 Kyiv, Ukraine

Сврха рада је проучавање пречишћавања отпадних вода фабрике картона и папира у Khmelnytskyi региону коришћењем физичко–хемијских метода, односно коагулације и оксидације, како би се повећала ефикасност уклањања органских загађивача према *COD* и *BOD* индикаторима. Предложена је употреба метода коагулације и хлорисања пре биолошког третмана у аерационим резервоарима. Алумофлок 18 % је коришћен као коагулант, РАА је коришћен као флокулант, а натријум-хидроксид је коришћен као алкализирајући реагенс. Студија је спроведена на мешавини индустријских и канализационих отпадних вода са *COD* и *BOD*$_5$ – 3200 и 1575 mg L^{-1}, редом, и на индустријским отпадним водама са *COD* и *BOD*$_5$ – 4480 и 1960 mg L^{-1}, редом. Ефекти смањења *COD* и *BOD*$_5$ индикатора у првом случају након коагулације били су 30 и 40 %, након хлорисања – 37,82 и 43,18 %, редом, а у другом случају након коагулације – 28,58 и 47,25 %, редом. Ефекти пречишћавања отпадних вода из фабрике картона и папира методама коагулације и оксидације омогућиће смањење концентрације органских материја према *COD* и *BOD* индикаторима пре биолошког третмана у аерационим резервоарима и обезбедиће повећање ефикасности биолошког третмана.

(Примљено 6. децембра 2023, ревидирано 25. јануара, прихваћено 19. фебруара 2024)

REFERENCES

1. *The Global Paper Packaging Market: Growth, Trends, Competitive Landscape and Forecasts Report*, Globe Newswire, Dublin, 2020
2. M. A. Hubbe, J. R. Metts, D. Hermosilla, M. A. Blanco, L. Yerushalmi, F. Haghighat, P. Lindholm-Lehto, Z. Khodaparast, M. Kamali, A. Elliott, *BioRes*. **11** (2016) 7953 (https://doi.org/10.15376/biores.11.3.Hubbe)
3. O. Ashrafi, L. Yerushalmi, F. Haghighat, *J. Environ. Manage.* **158** (2015) 146 (https://doi.org/10.1016/j.jenvman.2015.05.010)
4. K. Eskelinen, H. Särkkä, N. A. Kurniawan, M. E. T. Sillanpää, *Desalination* **255** (2010) 179 (https://doi.org/10.1016/j.desal.2009.12.024)
5. N. Kishimoto, T. Nakagawa, H. Okada, H. Mizutani, *J. Water Environ. Technol.* **8** (2010) 99 (https://doi.org/10.2965/jwet.2010.99)
6. W. De los Santos Ramosa, T. Poznyaka, I. Chairez, I. Córdova, *J. Hazard. Mater.* **169** (2009) 428 (https://doi.org/10.1016/j.jhazmat.2009.03.152)
7. S. Kakkar, A. Malik, S. Gupta, *J. Appl. Nat. Sci.* **10** (2018) 695 (https://doi.org/10.31018/jans.v10i2.1769)
8. C. Ram, P. Rani, K.A. Gebru, *Phys. Sci. Rev.* **5** (2020) 8 (https://doi.org/10.1515/psr-2019-0050)
9. P. Singh, A. Srivastava, *Int. J. Pharm. Biol. Sci.* **5** (2014) 773 (https://api.semanticscholar.org/CorpusID:98160371)

10. M. Cabrera, A. Zaki, in *Biological Wastewater Treatment and Resource Recovery*, F. Robina, A. Zaki, Eds., InTech, Rijeka, 2017, p. 256 (https://doi.org/10.5772/62795)
11. A. Schnell, P. V. Hodson, P. Steel, H. Melcer, J. H. Carey, *Water Res.* **34** (2000) 501 (https://doi.org/10.1016/S0043-1354(99)00161-X)
12. C. W. Bryant, *Water Sci. Technol.* **62** (2010) 1248 (https://doi.org/10.2166/wst.2010.934)
13. C. V. Dubeski, R. M. Branion, K. V. Lo, *J. Environ. Sci. Health* **36** (2001) 1245 (https://doi.org/10.1081/ese-100104875)
14. M. Tielbaard, T. Wilson, E. Feldbaumer, W. Driessen, in *Proceedings of TAPPI International Environmental Conference* (2002), TAPPI Press, Atlanta, GA, 2002, pp. 621–634
15. L. Habets, W. Driessen, *Water Sci. Technol*. **55** (2007) 223 (https://doi.org/10.2166/wst.2007.232)
16. N. B. Golub, M. V. Potapova, Yu. V. Karpenko, *IBB* **3** (2019) 96 (https://doi.org/10.20535/ibb.2019.3.2.166429)
17. N.B. Golub, M.V. Shinkarchuk, O.A. Kozlovets, B. V. Morgun, O. R. Lakhneko, A. I. Stepanenko, M. V. Borisjuk, *Water Air Soil Pollut*. **231** (2020) 445 (https://doi.org/10.1007/s11270-020-04805-6)
18. R. Chhotu, R. Pushpa, G. A. Kibrom, M. G. M. Abrha, ,*Phys. Sci. Rev.* **5** (2020) 20190050 (https://doi.org/10.1515/psr-2019-0050)
19. M. A. Hubbe, J. R. Metts, D. Hermosilla, M. A. Blanco, L. Yerushalmi, F. Haghighat, P. Lindholm – Lehto, Z. Khodaparast, M. Kamali, A. Elliott, *BioRes.* **11** (2016) 7953 (https://doi.org/10.15376/biores.11.3.hubbe)
20. S. R. Hassan, N. Q. Zaman, I. Dahlan, *Prep. Biochem. Biotechnol*. **50** (2019) 234 https://doi.org/10.1080/10826068.2019.1692214).

Journal of the Serbian Chemical Society

Refinement technique for nanocellulose extraction from corn cobs as a green material for environmental sustainability

ISMAIL IBRAHIM AL-KHATEEB[1]*, YUSRA M. AL-OBAIDI[2] and SABRI M. HUSSAIN[2]

[1]*Dijlah University College, Baghdad, Iraq and* [2]*Chemistry Department, Science College, Anbar University, Ramadi, Iraq*

Abstract: Corn cob and other types of agricultural biomass waste are abundant and have several potential uses as renewable materials. A unique extraction approach for producing nanocellulose materials with precise control, scalability and promising practical applications has been presented. Nanocrystalline cellulose was produced from corn cobs by mechanical treatment with ultrasonic technology, room temperature extraction for 30 min and sulfuric acid concentrations ranging from 30 to 60 %. Nanocellulose has been effectively extracted from maize cobs with comparatively high yields and crystallinities ranging from 63.55 to 71.76 %. The TEM data demonstrate the production of fiber nanoparticles with a size range of 15.3–2.1 nm. Simultaneously, SEM results match TEM findings. SEM pictures indicate smaller nanoparticles as sonication duration rises, but particle size does not vary with acid content. XRD analysis indicates an increase in the amount of crystalline cellulose in nanocellulose, demonstrating a notable transformation of cellulose. Nanocellulose and cellulose had similar FTIR spectra, distinct from the basic material of corn cobs. The FTIR analysis showed that the NaOH and subsequent bleaching treatments eliminated most hemicellulose and nearly all lignin throughout the conversion process. This work introduces a method for extracting nanocellulose from corncob waste utilizing standard ultrasonic technology under moderate conditions, at a cheap cost, in an ecologically responsible manner, with a high yield while maintaining its integrity.

Keywords: acid-hydrolysis; isolation; nano; sonication.

INTRODUCTION

Cellulose is the most abundant polymer in most plant biomasses.[1] Regardless, cellulose has numerous beneficial properties, such as being renewable, recyclable, eco-friendly, inexpensive and with many mechanical powers.[2] Leftovers from plants like corn cobs, rice straw, *etc*., have been selected for manufacturing cellulose nanoparticles.[3] Nanocellulose (NC) is one of the most durable and rigid

---

257

organic molecules. It has a very large surface area, is hydrophilic and is adjustable to surface activation. Among the new materials to emerge this century, nanocelluloses (NC) and their derivatives have several promising uses in areas such as membrane technology, composites, healthcare, functional additives, water purification and industrial implementations.[4–13] Pollution by chemical compounds is a global environmental concern based on the magnitude of the negative impact they have on the environment, plants and human health.[14]

Corn cobs from corn production are non-edible agricultural residues that can be utilized to produce green fuel and chemicals. The demand for corn grain will increase as the population increases, resulting in the increase in corn cobs.[15]

Corn cobs are a rich source of cellulose with a range of 28–45 % and hemicellulose of about 38.78 %, but they also contain an adequate quantity of lignin (9.4 %).[12,16] Meanwhile, corn cob cellulose has a hydrophilic feature due to the presence of hydroxyl groups in each polymer module.[12] There may be advantages to the presence of lignin in lignocellulose nanofibrils – as residues in cellulose and nanocellulose packages – such as its potential antioxidant and UV absorption properties.[17]

This research seeks to highlight the novel approach employed in our previous study, which effectively minimizes the need for labor and financial resources, intending to utilize it for the extraction of nanocellulose from an alternative crop. Furthermore, we emphasize the significance of producing cellulose from agricultural byproducts, such as maize, to help preserve the environment.

EXPERIMENTAL

Samples and reagents

The plant material was sourced from Turkey and included cobs of *Zea mays* subsp. *Mays* L. The corncobs were initially washed with distilled water, followed by vacuum filtration to collect water. The samples were allowed to air dry at a temperature of 25 °C before being further dried at 100 °C using an oven with a suction system for 48 h. Once pulverized, the substance was enclosed in a plastic container for preservation.

We obtained analytical-grade sulfuric acid, sodium hydroxide and sodium hypochlorite from Sigma–Aldrich.

Preparations of nanocellulose from corn cobs

Reducing acid concentrations, eliminating dialysis and utilizing the freeze-drying process improve the hydrolysis method for NC preparations when compared to methods suggested by other researchers.[18] The dried corn cob powder was bleached at 80 °C for 4 h with 0.1% sodium hypochlorite. The bleached fiber is washed and filtered with purified water before being dried. A bleached fiber of ten grams comes from the bleaching phase and remains hydrolyzed in 100 mL of sulfuric acid at numerous meditations (30, 40, 50 and 60 %) using an energetic exciting. In order to terminate the reaction, deionized water was mixed with the solution of 100 mL and the pH was adjusted to 7 through 1 % NaOH. A postponement is collected, filtered and sonicated through ultra-sonication (UP400S) for different durations of time (30, 60, 120 min). The NC fibers are then dried, converted to powder and stored for future use.

Characterization of nanocellulose

In order to determine the characteristics of NC, the following equipment was utilized.

Transmission electron microscope (TEM). A FEI technical G2 Split Biotic transmission electron microscope at 120 kV was used to examine the surface morphology required for the synthesis of nanofiber and nanoparticles prepared from corn cobs.

Field emission scanning electron microscope (FEI-SEM). The morphologies and diameter of NC particles and fibers prepared from corn cobs were examined using FEI SEM (model Quanta 200FEG), configured to operate at (120 kV) at various magnification levels.

The X-Ray diffraction. X-ray diffraction was assessed using Micro Max 007HF DW. The diffracted power of the CuKα radiation ($\lambda = 0.154$ nm, 45 kV and 45 mA) was evaluated in the 2θ range from 50 to 70°; the maximum power was 1.2 kW.

Following Eq. (1),[18] the empirical crystallinity index (*CrI*) was determined. The formula for calculating the crystallinity index is as follows:

$$CrI = 100 \frac{I_{200} - I_{am}}{I_{200}} \tag{1}$$

At a 2θ angle of approximately 22.5°, the greatest peak intensity is denoted by I_{200}, whereas I_{am} represents the lowest diffraction at a 2θ angle of around 18°.

Fourier transform infrared (FTIR) spectroscopy. FTIR (models Vertex 70 and Hyperion scan optical microscopes) was used to characterize the structure and functional groups that were present in all samples. FTIR spectra were generated from KBr pellets, which were made by mixing KBr powder and samples homogeneously in a mass ratio of 99:1 by scanning within the range of 1400–400 cm^{-1}.

RESULTS AND DISCUSSION

TEM images

The sonication and hydrolysis treatment of H_2SO_4 prepared from corn cobs led to the production of nanocellulose as nanorod-like and spherical nanoparticles, which were specified by applying various morphological techniques for nanomaterials.

The TEM images showed a rod-like shape with an average diameter of 38.5–74 nm. However, very interesting nanoparticles with a diameter of 2–17 nm were indicated in Fig. 1 for a sample sonicated for 120 min and 30 % H_2SO_4. Increasing the concentration of acid to 40 % with an ultrasonic treatment of 120 min led to the production of nanoparticles with a non-uniform shape and a diameter of 11–70 nm. The result in Fig. 2 clarifies the aggregation of nanoparticles with an average diameter of 42.3 nm for 120 min of sonication and 50 % acid. Aspherical nanoparticles with an average diameter of 25–40 nm was obtained for sonication for 120 min with 60 % acid (Fig. 3).

After analyzing nanocellulose using transmission electron microscopy (TEM), it has been shown that the treatment, including 30 % H_2SO_4 for 120 min, is more favorable compared to other methods. This finding is distinct from previously published research. The research findings indicate that nanocellulose, ranging in

size from 8.3 to 17 nm, was produced from rice husk.[19] On the other hand, a dendritic structure was formed from cotton, which was used as a plant source.[20]
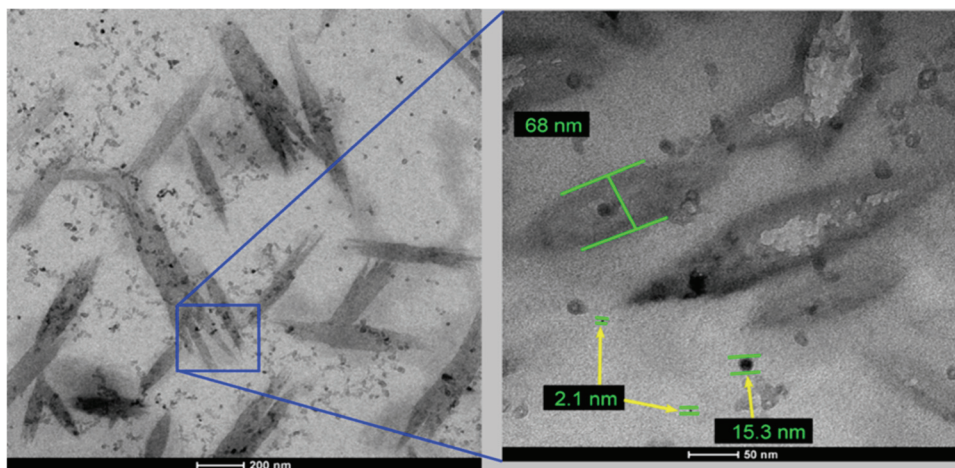

Fig. 1. TEM images of nanocellulose prepared by corn cobs sonicate for 120 min at 30 % acid.
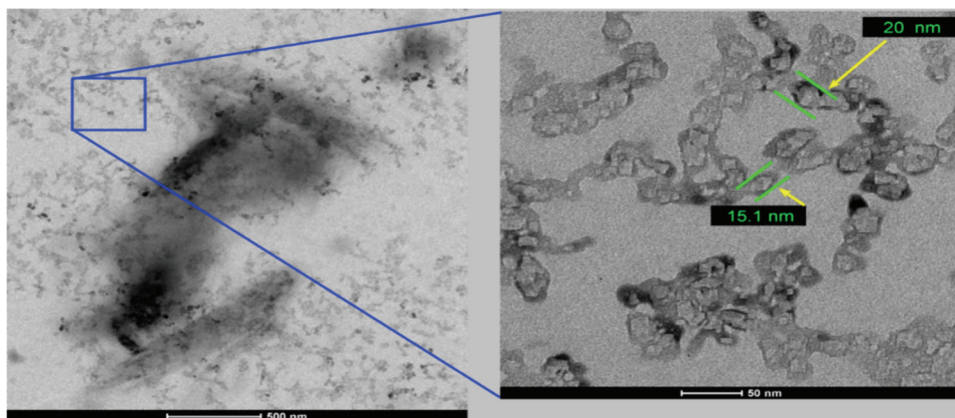

Fig. 2. TEM images of nanocellulose prepared by corn cobs sonicate for 120 min at 50 % acid.

SEM micrographs

SEM images of unsonicated samples of corn cobs were reviewed in Fig. 4. The surface of natural fibers demonstrates microscale fibers and microstructures. A sample sonicated for 30 min with 30 % acid comprises nanostructure fibers with an average diameter of 25 to 40 nm, accompanied by large amorphous regions. Increasing the sonication time to 60 min led to the detection of nano whiskers with an average diameter of 17–32 nm. The amorphous zones approximately vanished except for a few regions (Fig. 5). A sonicated sample for 120 min and 30 % acid proved long nano whiskers with an average diameter between 16 and 27 nm. These
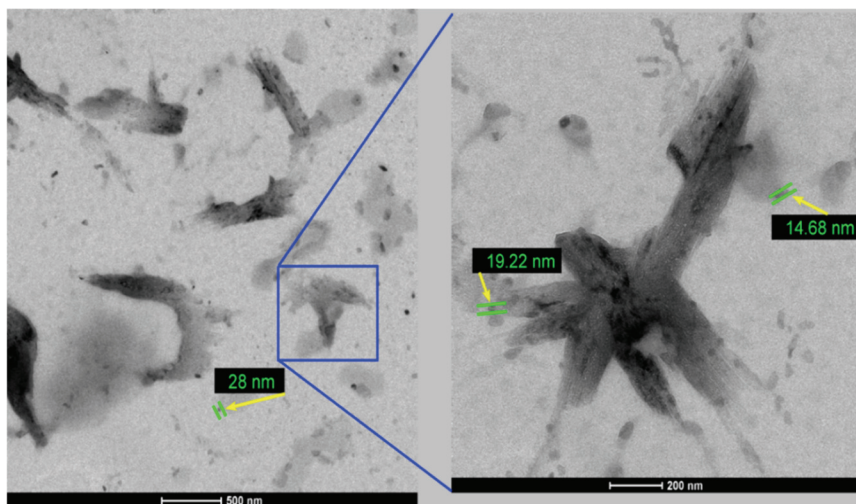
Fig. 3. TEM images of nanocellulose prepared by corn cobs sonicate for 120 min at 60 % acid.
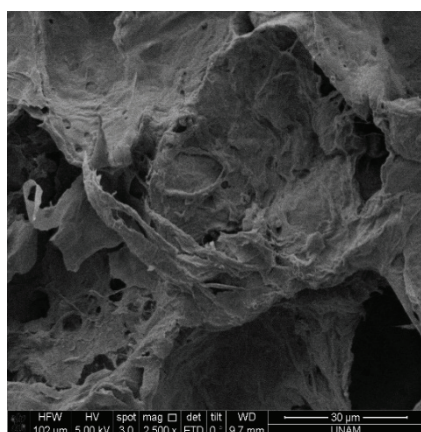

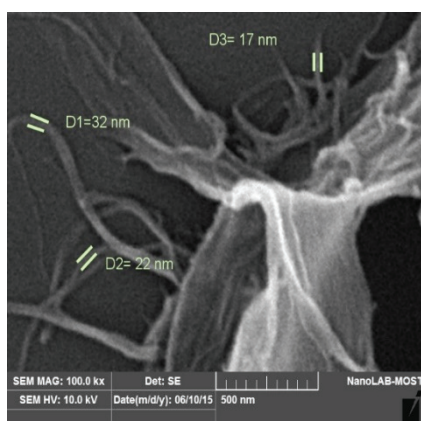Fig. 4. SEM image for corn cobs.

Fig. 5. SEM image of nanocellulose prepared by corn cobs sonicate for 60 min at 30 % acid.

whiskers are separated into complex, smaller sub-whiskers. Amorphous regions disappeared completely, as illustrated in Fig. 6. The sonication process of 30 min with 40 % acid led to the incorporation of condensed and fine nano-web-like tiny fibers with an average diameter of 27 nm, as indicated in Fig. 7. When the sonic-ation time increased to 60 min, it was observed that nanofiber structures originated with a 35 nm average diameter. With a sonication time of 120 min, it was verified that separated nanofibers arise with an average diameter of 38 nm. With 30 min of sonication and 50 % acid, the nanostructures that appeared in the samples consisted of a nanonetwork with a 56 nm average diameter. While sonication time reached 60 min and 50 % acid, the results showed nanofibers with an average diameter of 42 nm.
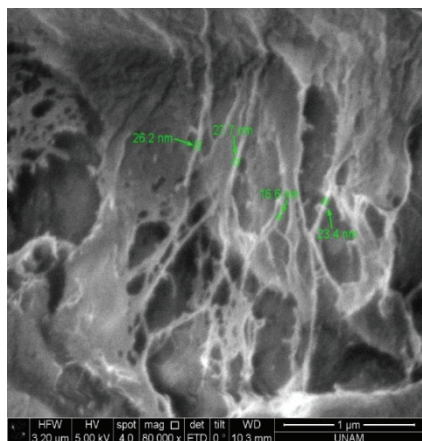

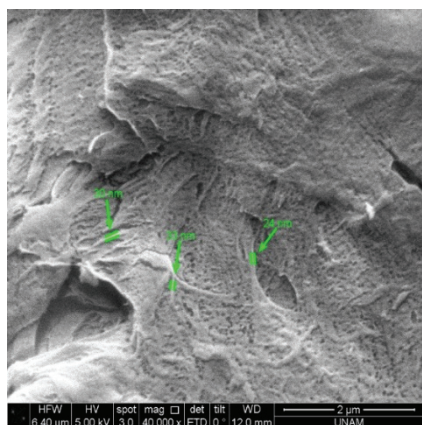Fig. 6. SEM image of nanocellulose prepared by corn cobs sonicate for 120 min at 30 % acid.

Fig. 7. SEM image of nanocellulose prepared by corn cobs sonicate for 30 min at 40 % acid.

It was indicated that branched nanofibers occurred at 120 min of sonication time and 50 % acid with an average diameter of 31 nm (Fig. 8). With 30 min of sonication time and 60 % acid, the results indicated a 34.5 nm average diameter.

When the sonication time reached 60 min with 60 % acid, the results revealed nano whiskers with an average diameter of 32 nm. Finally, at 120 min of sonication time and 60 % acid, a network of nanofibers existed in the sample with 46 nm average diameters (Fig. 9). SEM findings reflected a disappearance of amorphous regions from nanocellulose patterns.
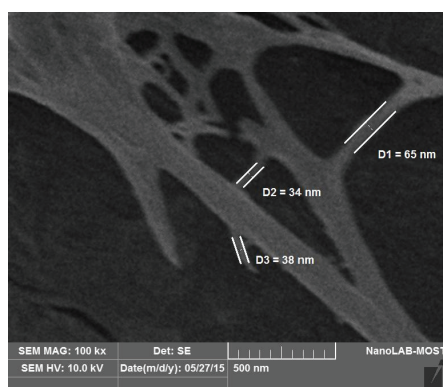

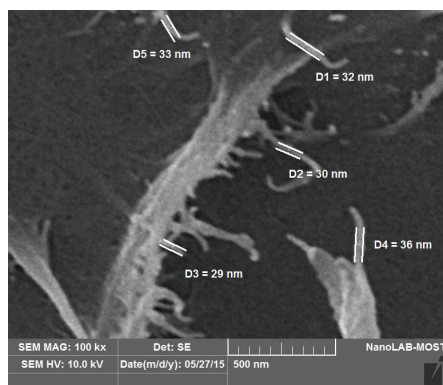Fig. 8. SEM image of nanocellulose prepared by corn cobs sonicate 120 min at 50 % acid.

Fig. 9. SEM image of nanocellulose prepared by corn cobs sonicate 120 min at 60 % acid.

The SEM results reveal that the diameters of nanocellulose vary based on the plant source and extraction process. The diameters are generally lower when derived from corn cobs than when derived from cotton.[20,21]

X-Ray diffraction

To evaluate the crystallinity index and percentage of crystallin, the X-ray diffraction crystallinity index and the percentage of crystallin in untreated corn cobs and NC derived from corn cobs (Figs. 10 and 11). The NC specimens demonstrated three peaks at 2θ 18, 22 and 34°. The findings demonstrate that the percentage of crystalline material rose from 46.68 % in the untreated samples to 71.76 % when the amount of acid was injected and the duration of sonication was

increased (Table I). These findings exhibit a comparatively elevated level in comparison to the findings of other studies.[22]
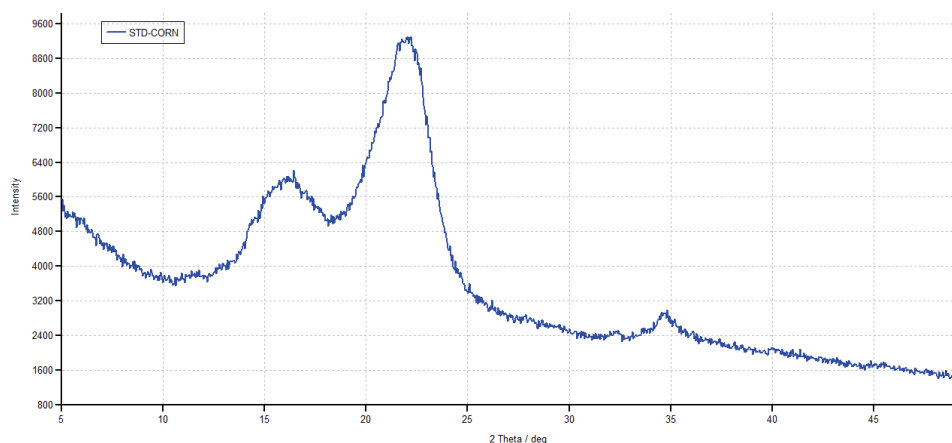

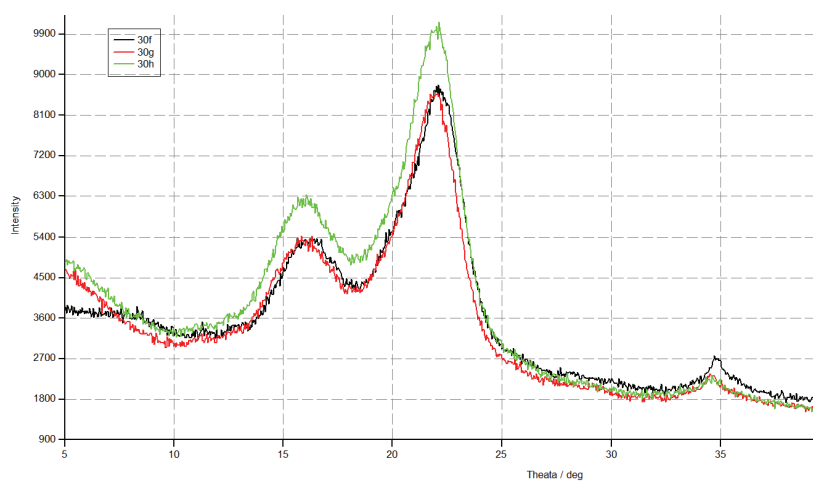Fig. 10. X-ray diffraction pattern of untreated corn cobs.

Fig. 11. X-ray diffraction patterns comparisons of nanocellulose prepared from corn cobs at different sonication time (30, 60 and 120 min) at 30 % acid.

The micro-jet produced by ultrasonic cavitation broke down the cellulose surfaces and fibrillations were acquired; therefore, the surface expanse increased, accelerating the oxidization response[23] because of the mechanical potential required under ultrasonic strength for the insolvent to crystallize the configuration of the thin layer of cellulose tissue better than internal celluloses and reducing the crystallinity index. Furthermore, the confined tremendousness temperatures and compression circumstances (5000 K and 500 atm) with an aggressing shockwave established by cavitation may set up in the step downcast of the crystallized

arrangement of cellulose.[24] The deflection peak located at 2θ 22.5° for the sample that exhibited an advanced crystallinity index demonstrated that it remained strong and had enormous values compared to the peaks created by others. This nanocrystal forms the base of the nano whiskers web that increases the rheology and elasticity of nanocellulose. These interpretations point out preferable crystalline fields and are assured by the increase in the crystallinity index.[25]

TABLE I. Crystallinity percentages and crystallinity indexes of nanocellulose at different acid concentrations and sonication times

Treatment		Crystallinity index	Crystallinity, %
Acid, %	Sonication, min		
–	Unsonicated sample	65.22	46.68
30	30	51.26	67.23
	60	51.44	67.31
	120	51.23	67.22
40	30	58.49	70.67
	60	54.55	68.75
	120	53.74	68.37
50	30	59.18	71.01
	60	60.64	71.76
	120	58.06	70.45
60	30	56.09	69.49
	60	50.37	66.83
	120	42.65	63.55

FTIR Determinations

FTIR spectroscopic analysis assessed the absorption frequencies to categorize the arranged NC. The robust comprehensive range from 3400 to 3300 cm^{-1} is assigned to O–H extending,[26] while the peaks nearby are 2900 cm^{-1} allocated to C–H extending vibrations. This peak is reduced in concentration (Figs. 12 and 13) compared to that in non-sonicated raw substance varieties. The carbonyls assemble absorption peaks were noticed at 1650 cm^{-1}; at the same time, the peaks at 1730 cm^{-1} in the range referred to C=O extending of the acetyl chain with uranid esters series of hemicelluloses or to esters connection of carboxylic groups in lignans and hemicellulose.[27,28]

At the same time, the peaks of 1280 cm^{-1} belong to the C–O stretch of aryls set in lignan;[29] this peak completely vanished from the spectra of synthesized NC. This outcome proposed that all hemicelluloses and lignans be extracted from NC, particularly with the highest level of acid absorption and sonicate times. Additionally, the highest points at 1431, 1373 and 1317 cm^{-1} are correlated with the twisty vibration of the –CH$_2$, C–H and C–O sets of the perfumed circle, respectively. This peak is seen in Fig. 13. The peak positioned at 1031 to 1162.9 cm^{-1} qualified for the distortion of the C–H shocking vibrations and the C–O–C pyranoses minimum

circle.[30,31] Lastly, the peak of absorbances detected at 896 cm^{-1} is allocated to the identical C–O–C extending at (l-4)-glycosidic linkage that becomes less intense for NC varieties matched to the unsolicited samples.[32]
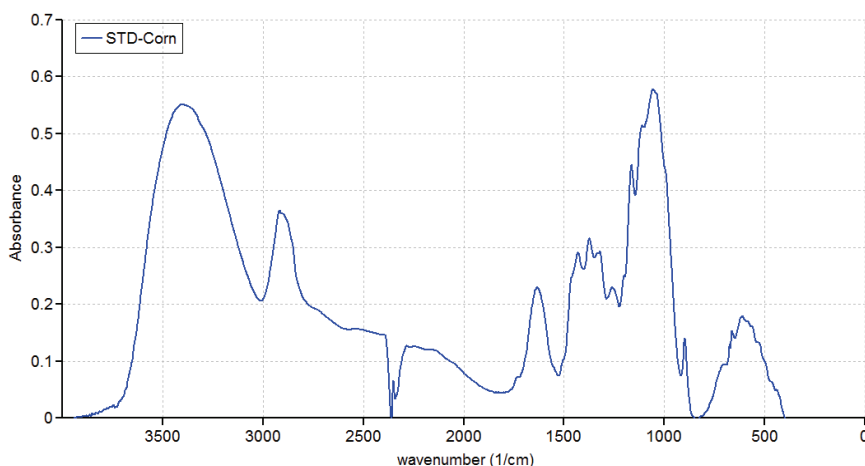
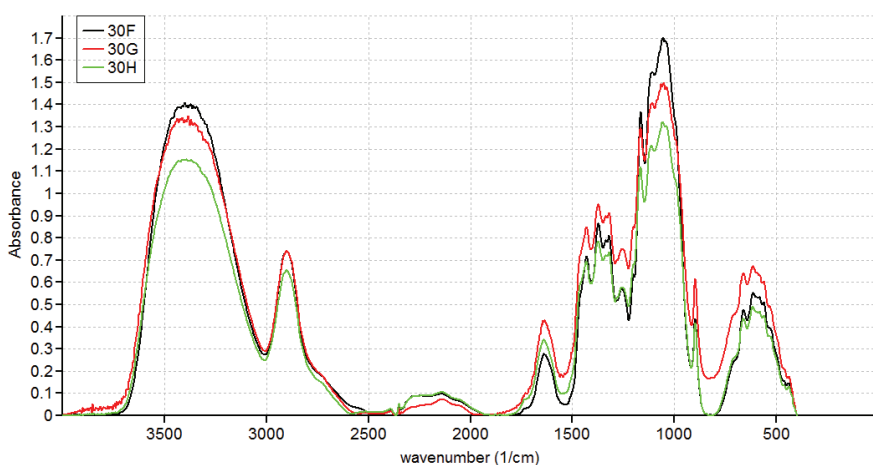

Fig. 12. FTIR Spectrum of corn cobs raw material.

Fig. 13. FTIR variety patterns comparisons of nanocellulose prepared from corn cobs at different sonification time (30, 60 and 120 min) at 30 % acid.

Following the completion of this procedure, both hemicellulose and lignin were eliminated, which supports the notion that the current approach is quite beneficial for the extraction of nanocellulose.

CONCLUSION

This paper has effectively demonstrated, for the first time, the use of the sonication technique coupled with the hydrolysis method in synthesizing cellulose

nanoparticles. The results specify that the X-ray diffraction, TEM, SEM and FTIR spectroscopy methods assure the formation of cellulose nanoparticles by this technology. Though the preferable outcomes under sonication's usage come from the remediation of 30 % acid sonicate for 120 min, these approaches designate that cellulose nanoparticles have a worthy prospect in the future for manufacturing purposes and corrective objectives. The FTIR analysis showed that the NaOH and subsequent bleaching treatments eliminated most hemicellulose and nearly all lignin throughout the conversion process. Though cellulose nanoparticles of honestly definite dimension result from this procedure, the precise cause of the modifications in the size of nanoparticles synthesized using corn cobs addressed under the two different conditions studied here (sonication time and acid concentration) must be further inspected.

ИЗВОД

УНАПРЕЂЕНА ТЕХНИКА ЕКСТРАКЦИЈЕ НАНОЦЕЛУЛОЗЕ ИЗ ОКЛАСАКА КУКУРУЗА КАО ЗЕЛЕНОГ МАТЕРИЈАЛА ЗА ЕКОЛОШКУ ОДРЖИВОСТ

ISMAIL IBRAHIM AL-KHATEEB[1], YUSRA M. AL-OBAIDI[2] и SABRI M. HUSSAIN[2]

[1]*Dijlah University College, Baghdad, Iraq u* [2]*Chemistry Department, Science College, Anbar University, Ramadi, Iraq*

Окласак кукуруза, као и друга отпадна пољопривредна биомаса су присутни у великој количини и имају значајну потенцијалну примену као обновљиви материјали. Представљен је јединствен приступ екстракцији за производњу наноцелулозних материјала са прецизном контролом, скалабилношћу и обећавајућим практичним применама. Нанокристална целулоза је добијена из окласака кукуруза методом која укључује механичку обраду ултразвучном технологијом и екстракцију на собној температури у трајању од 30 min и при концентрацији сумпорне киселине у распону од 30 до 60 %. Наноцелулоза је ефикасно екстрахована из окласака кукуруза у релативно високим приносима и са степеном кристалиничности у распону од 63,55 до 71,76 %. ТЕМ подаци показују да се добијају наночестице у облику влакана, са распоном величина од 15,3 до 2,1 nm. SEM резултати одговарају ТЕМ налазима. SEM слике указују да се мање наночестице добијају са повећањем трајања ултразвучне обраде, док величина честица не варира са променом садржаја киселине. XRD анализа указује на повећање количине кристалне целулозе у наноцелулози, показујући значајну трансформацију целулозе. Наноцелулоза и целулоза су имале сличне FTIR спектре, који су се разликовали од основног материјала из окласака кукуруза. FTIR анализа је показала да су NaOH и накнадни третмани бељења елиминисали већину хемицелулозе и скоро сав лигнин током процеса конверзије. Овај рад приказује методу екстракције наноцелулозе из отпадних окласака кукуруза, уз примену стандардне ултразвучне технологије под умереним условима, по јефтиној цени на еколошки одговоран начин, са високим приносом уз очување интегритета наноцелулозе.

(Примљено 5. јануара, ревидирано 15. јануара, прихваћено 21. маја 2024)

REFERENCES

1. Y. Mahmoud, Z. Safidine, N. Belhanecche-Bensemra, *J. Serb. Chem. Soc.* **86** (2021) 521 (https://doi.org/10.2298/JSC200806011M)

2. C. Chang, I. Wang, K. Hung, Y. Perng, *J. Taiwan Sci.* **25** (2010) 251 (https://doi.org/10.7075/TJFS.201009.0251)
3. A. Mandal, D. Chakrabarty, *Carbohydrate Polym.* **86** (2011) 1291 (https://doi.org/10.1016/j.carbpol.2011.06.030)
4. A. Al-Rawi, I. Al-Khateeb, T. Zaidan, *Environ. Nanotech. Monit. Manage.* **16** (2021) 100529 (https://doi.org/10.1016/j.enmm.2021.100529).
5. Z. Raji, A. Karim, A. Karam, S. Khalloufi, *Waste* **1** (2023) 775 (https://doi.org/10.3390/waste1030046)
6. K. Staszak, K. Wieszczycka, *Membranes* **13** (2023) 114 (https://doi.org/10.3390/membranes13010114).
7. A. Etale, A. Onyianta, S. Turner, S. Eichhorn, *Chem. Rev.* **123** (2023) 2016 (https://doi.org/10.1021/acs.chemrev.2c00477)
8. R. Castro-Muñoz, L. González-Melgoza, O. García-Depraect, *Chemosphere* **270** (2021) 129421 (https://doi.org/10.1016/j.chemosphere.2020.129421)
9. A. Sharma, Anjana; H. Rana, S. Goswami, *J. Polymers Environ.* **30** (2022) 1 (https://doi.org/10.1007/s10924-021-02185-4)
10. A. Mautner, *Polym. Int.* **69** (2020) 741 (https://doi.org/10.1002/pi.5993)
11. N. Camparotto, G. Paixão, G. de Vargas Brião, R. Oliveira, P. Prediger, M. Vieira, *Environ. Toxic. Pharm.* **99** (2023) 104105 (https://doi.org/10.1016/j.etap.2023.104105)
12. T. Sen, *Molecules* **21**(2023) 5575 (https://doi.org/10.3390/molecules28145575)
13. M. Vukčević, M. Maletić, B. Pejić, N. Karić, K. Trivunac, A.P. Grujić, *J. Serb. Chem. Soc.* **88** (2023) 669 (https://doi.org/10.2298/JSC221213015V)
14. N. Shahi, B. Min, B. Sapkota, V. Rangari. *Sustainability* **12** (2020) 6015 (https://doi.org/10.3390/su12156015)
15. M. Klaas, C. Greenhalf, M. Ouadi, H. Jahangiri, A. Hornung, C. Briens, F.Berruti, *Results Engineering* **7** (2020) 100165 (https://doi.org/10.1016/j.rineng.2020.100165)
16. J. Kevin, B. Shinners, N. Binversie, *Biomass Bioenergy* **31** (2007) 576 (https://doi.org/10.1016/j.biombioe.2007.02.002)
17. S. Guo, X. Li , Y. Kuang, O. Rojas, *Carbohydrate Polym.* **253** (2021) 117223 (https://doi.org/10.1016/j.carbpol.2020.117223)
18. Y. Vishnoi, A. K. Trivedi, M. K. Gupta, H. Singh, S. M. Rangappa, S. Siengchin, *Heliyon* **10** (2023) e23846 (https://doi.org/10.1016/j.heliyon.2023.e23846)
19. S. Varshney, V. Mulpuru, N. Mishra, M. K. Gupta, *Mater. Technol.* **37** (2022) 2608 (https://doi.org/10.1080/10667857.2022.2051939)
20. I. Al-Khateeb, S. Hussin, Y. Al-Obaidi, *Int. J. Mater. Chem. Phys.* **1** (2015) 99 (http://files.aiscience.org/journal/article/html/70130018.html)
21. H. A, Silvérioa, W. P. F. Netoa, N. O, Dantas, D. Pasquini, *Ind. Crops Prod.* **44** (2013) 427 (https://doi.org/10.1016/j.indcrop.2012.10.014)
22. D. Sartika, A. P. Firmansyah, I. Junais, I. W. Arnata, F. Fahma, A. Firmanda, *Int. J. Biol. Macromol.* **240** (2023) 124327 (https://doi.org/10.1016/j.ijbiomac.2023.124327)
23. L. Wu, F. Tian, J. Sun, *J. Appl. Polym. Sci.* **138** (2020) e50206 (https://doi.org/10.1002/app.50206)
24. K. Seena, P. Thomas, S. Begum, C. Midhun, Dominic, Nisa V. Salim, N. Hameed, Sanjay M. Rangappa, S. Siengchin, J. Parameswaranpillai, *J. Appl. Polym. Sci.* **138** (2020) e50213 (https://doi.org/10.1002/app.50213)

25. H. Kargarzadeh, I. Ahmad, I. Abdullah, *Cellulose* **19** (2012) 855 (https://doi.org/10.1007/s10570-012-9684-6)

26. A. Ali, S. Mazumdar, R. Dutta, *Cellulose Chem. Technol.* **57** (2023) 699 (https://doi.org/10.35812/CelluloseChemTechnol.2023.57.63)

27. T. Wang, Y. Zhao, *Carbohydr. Polym.* **253** (2021) 117225 (https://doi.org/10.1016/j.carbpol.2020.117225)

28. H. Dai, S. Ou, Y. Huang, H. Huang, *Cellulose* **25** (2018) 1743 (https://doi.org/10.1007/s10570-018-1671-0)

29. L. Zaini, M. Jonoobi, P. Tahir, S. Karimi, *J. Biomater. Nanobiotech.* **4** (2013) 37 (http://dx.doi.org/10.4236/jbnb.2013.41006)

30. A. Görgüç, E. Gençdağ, K. Demirci, B. Bayraktar, A. Zungur-Bastıoğlu, F. Yılmaz, *Mater. Chem. Phys.* **310** (2023) 128482 (https://doi.org/10.1016/j.matchemphys.2023.128482)

31. T. Kim, Q. Doan, K. Chiang, *Sustain. Environ. Res.* **32** (2022) 26 (https://doi.org/10.1186/s42834-022-00136-9)

32. Y. Wang, X. Wei, J. Li, Q. Wang, F. Wang, L. Kong, *J. Mater. Sci. Chem. Engineering* **1** (2013) 49 (http://dx.doi.org/10.4236/msce.2013.15010).